

**Exploring the anticancer potential of  
bisbenzylisoquinoline alkaloid- phaeanthine and its  
targeted delivery through a nanocarrier system**

by

**ALISHA VALSAN C.**

**10BB18A39030**

A thesis submitted to the  
Academy of Scientific & Innovative Research  
for the award of the degree of  
**DOCTOR OF PHILOSOPHY**  
in  
**SCIENCE**

Under the supervision of  
**Dr. K. V. RADHAKRISHNAN**



**CSIR-National Institute for Interdisciplinary  
Science and Technology (CSIR-NIIST),  
Thiruvananthapuram – 695 019**



**Academy of Scientific and Innovative Research  
AcSIR Headquarters, CSIR-HRDC Campus  
Sector 19, Kamla Nehru Nagar,  
Ghaziabad, U. P. – 201 002, India**

**January 2024**

**Dedicated to those who made me  
believe in myself.....**

# CSIR-National Institute for Interdisciplinary Science and Technology



(NIIST)


Council of Scientific and Industrial Research (CSIR)  
Industrial estate P.O., Thiruvananthapuram- 695019  
Kerala, India

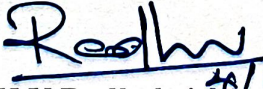


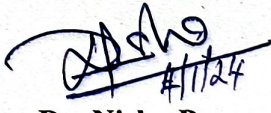
4<sup>th</sup> January 2024

## CERTIFICATE

This is to certify that the work incorporated in this Ph.D. thesis entitled, *Exploring the anticancer potential of bisbenzylisoquinoline alkaloid- phaeanthine and its targeted delivery through a nanocarrier system*", submitted by *Ms. Alisha Valsan C.* to the Academy of Scientific and Innovative Research (AcSIR) in fulfillment of the requirements for the award of the Degree of *Doctor of Philosophy in Sciences*, embodies original research work carried out by the student. We further certify that this work has not been submitted to any other University or Institution in part or full for the award of any degree or diploma. Research materials obtained from other sources and used in this research work have been duly acknowledged in the thesis. Images, illustrations, figures, tables, etc., used in the thesis from other sources, have also been duly cited and acknowledged.

  
Alisha Valsan C.

  
Dr. K.V. Radhakrishnan  
(Supervisor)

  
Dr. Nisha P.  
(Co-Supervisor)

## STATEMENTS OF ACADEMIC INTEGRITY

I Alisha Valsan C., a Ph.D. student of the Academy of Scientific and Innovative Research (AcSIR) with Registration No. 10BB18A39030 hereby undertake that, the thesis entitled *“Exploring the anticancer potential of bisbenzylisoquinoline alkaloid- phaeanthine and its targeted delivery through a nanocarrier system”* has been prepared by me and that the document reports original work carried out by me and is free of any plagiarism in compliance with the UGC Regulations on *“Promotion of Academic Integrity and Prevention of Plagiarism in Higher Educational Institutions (2018)”* and the CSIR Guidelines for *“Ethics in Research and in Governance (2020)”*.

January 4 2024


Thiruvananthapuram



Alisha Valsan C

---

It is hereby certified that the work done by the student, under my supervision, is plagiarism-free in accordance with the UGC Regulations on *“Promotion of Academic Integrity and Prevention of Plagiarism in Higher Educational Institutions (2018)”* and the CSIR Guidelines for *“Ethics in Research and in Governance (2020)”*.



Dr. K. V. Radhakrishnan  
(Supervisor)

January 4 2024

Thiruvananthapuram



Dr. Nisha P.  
(Co-supervisor)

January 4 2024

Thiruvananthapuram

## DECLARATION

I, Alisha Valsan C., AcSIR Registration No. 10BB18A39030 declare that my thesis entitled, “*Exploring the anticancer potential of bisbenzylisoquinoline alkaloid- phaeanthine and its targeted delivery through a nanocarrier system*” is plagiarism-free in accordance with the UGC Regulations on “Promotion of Academic Integrity and Prevention of Plagiarism in Higher Educational Institutions (2018)” and the CSIR Guidelines for “*Ethics in Research and in Governance (2020)*”.

I would be solely held responsible if any plagiarised content in my thesis is detected, which is violative of the UGC regulations 2018.

January 4 2024

Thiruvananthapuram



**Alisha Valsan C.**

## ACKNOWLEDGMENTS

*I have immense pleasure in expressing my deep gratitude to Dr. K. V. Radhakrishnan and Dr. Nisha P., my thesis supervisor and co-supervisor for all the support and encouragement provided during these years.*

*My heartfelt gratitude to Dr. Kaustabh Kumar Maiti, for his unwavering support throughout these years, in guiding the work, giving the relevant suggestions, for correcting and modifying both the manuscript and thesis. Words cannot adequately convey how much he had helped me completing this thesis.*

*I wish to thank Dr. C. Anandharamakrishnan and Dr. A. Ajayaghosh, present and former Director of the CSIR-National Institute for Interdisciplinary Science and Technology, Thiruvananthapuram, for providing me with the necessary facilities for carrying out the work.*

*I would like extend my sincere thanks to:*

- ✓ *Dr. P. Jayamurthy, Dr. V. Karunakaran, Dr. C. H. Suresh, and Dr. R. Luxmi Varma; present and former AcSIR co-ordinators.*
- ✓ *Dr. Kaustabh Kumar Maiti, Dr. Rajeev K. Sukumaran and Dr. P. Jayamurthy; Doctoral Advisory Committee members for their valuable suggestions and discussions during DAC meetings*
- ✓ *Dr. K V Radhakrishnan, Dr. P. Sujatha Devi, and Dr. R. Luxmi Varma, present and former Head of the Division, Chemical Sciences and Technology Division (CSTD).*
- ✓ *Dr. A. Kumaran, Dr. L. Ravishankar, Dr. B.S. Sasidhar, Dr. Sunil Varughese and Dr. Jubi John; Scientists in organic chemistry are greatly acknowledged. And a special mention to Dr. Jubi John for the support and help.*
- ✓ *Mr. Kiran Mohan for TEM analysis, Mrs. Saumini Matthew for NMR, Mrs. Viji S., for mass spectral analyses*
- ✓ *Dr. Vishnupriya Murali, Mr. Shamjith and Ms. Vidyalekshmi M S for all the suggestions and help in completing the works and clarifying my doubts at any time.*
- ✓ *Dr. Meenu M. T, Dr. Prabha B, Dr. Vishnu K. Omanakuttan, Dr. Biji M. for all the help.*
- ✓ *A special thanks to Ms. Anuja for being there for me every time especially when I am low and confused*

- ✓ *Anaga, Anusha, Priya, and Vimal for the love and companionship*
- ✓ *Dr. Manu M. Joseph, Dr. Greeshma Gopalan, Dr. Sasikumar, Dr. Sharathna, Dr. Neethu, Dr. Santhi, Dr. Arya J.S, Dr. Varsha K. Karunankaran, Mr. Madhukrishnan, Dr. Hridhya, Ms. Aswathy, Dr. Rajimol, Ms. Shamna, Ms. Deepika, Ms. Chandana, Ms. Reshma, Ms. Kavya, Dr. Deepa all other KVR and KKM group members for their love.*
- ✓ *SA 2020 members and Team CSTD- Throwball for making my 5 years at NIIST wonderful.*
- ✓ *My teachers at St. Thomas college, Thrissur and St. Marys' college, Thrissur for their constant support and motivation in pursuing PhD. A special thanks to Dr. Geethu, DR. Joby Paul. Dr. Reji Raphael, Dr. Rekha. Dr. Sr. Sandra, Dr. Anto, Dr. Vimala, Dr. Anu D. Alappat.*
- ✓ *Mr. Sanu Thankachan for motivating me to join for a PhD.*
- ✓ *CSIR for the financial assistance*

*I express profound gratitude to my parents, my "achan" and "amma," for their unwavering love and support. They have been the pillars celebrating even the smallest triumphs in my life, whether in sports, NCC, or academics. I extend my love and gratitude to my sister Aleena, brother-in-law "chettan," nephew "appoos," and niece "aami" for their affectionate support. Special thanks to my husband, Vipin, for being my constant source of support and encouragement. I am also thankful to my in-laws for their continuous love and support over the years. Above all, I express my gratitude to the Almighty for the abundant blessings bestowed upon me.*

**ALISHA VALSAN C.**

## TABLE OF CONTENTS

<b>Certificate</b>	<b>i</b>
<b>Statement of Academic integrity</b>	<b>ii</b>
<b>Declaration</b>	<b>iii</b>
<b>Acknowledgement</b>	<b>iv</b>
<b>Table of contents</b>	<b>vi</b>
<b>List of abbreviations</b>	<b>xiv</b>
<b>Preface</b>	<b>xix</b>

### CHAPTER 1

<b>An overview of bisbenzylisoquinoline alkaloids in cancer therapy: Recent advances &amp; opportunities</b>	<b>1-48</b>	
1.1	Introduction	1
1.2	Cancer prevalence	4
1.2.1	Cervical cancer	6
1.3	Natural products in cancer drug discovery	8
1.4	Genus <i>Cyclea</i>	10
1.4.1	<i>Cyclea</i> species reported in India	11
1.5	Anticancer potential of bisbenzylisoquinoline (BBIQ) alkaloids	14
1.5.1	Tetrandrine	16
1.5.2	Berbamine	22
1.5.3	Fangchinoline	29
1.5.4	Cycleanine & Curine	33



1.6	Limitations of chemotherapeutic drugs	34
1.7	Advantages of drug delivery systems for better therapeutic outcome	35
1.8	Conclusion	36
1.9	Objectives of the current investigation	37
1.10	References	38
<b>CHAPTER 2</b>		
	<b>Exploring the cytotoxic potential of phaeanthine: a bisbenzylisoquinoline alkaloid isolated from <i>Cyclea peltata</i> induces mitochondria-mediated apoptosis in cervical cancer cells</b>	49-85
2.1	Introduction	50
2.2	Results and Discussions	52
2.2.1	Extraction, isolation & characterization of phytomolecules from <i>Cyclea peltata</i>	52
2.2.2	Primary cytotoxicity screening of isolated phytomolecules	57
2.2.3	Computational screening of PHA	59
2.2.4	Molecular dynamic simulation of Akt-PHA complex	59
2.2.5	Apoptotic evaluation of PHA	60
2.2.6	Evaluation of caspase mediated apoptosis	61
2.2.7	Assessment of mitochondrial membrane potential induced by PHA	61
2.2.8	Evaluation of cyt c dynamics by PHA	63
2.2.9	PHA induced DNA condensation and DNA fragmentation	64

2.2.10	Cellular internalization and DNA fragmentation by SERS modality	64
2.2.11	inhibition of clonogenic potential by PHA in HeLa cells	66
2.2.12	Induction of cell cycle arrest by PHA	66
2.2.13	PHA modulated expression of various proteins involved in apoptosis	68
2.3	Conclusion	72
2.4	Experimental Section	72
2.4.1	General experimental procedures	72
2.4.2	Extraction, isolation and characterization of phytomolecules	73
2.4.2.1	Collection of plant material	73
2.4.2.2	Extraction and isolation procedures of <i>C.peltata</i>	73
2.4.2.3	Spectral data	73
	Phaeanthine	73
	Cycleanine	74
	<i>N</i> -methylcorydaldine	74
2.4.3	Cell culture methods	75
2.4.4	Cell viability assay	75
2.4.5	Molecular docking	75
2.4.6	Molecular dynamic simulation	76
2.4.7	Apoptotic assays	76
2.4.8	Caspase fluorometric assay	77

2.4.9	Mitochondrial membrane potential assay	77
2.4.10	Cytochrome C release	77
2.4.11	DNA condensation and fragmentation studies	77
2.4.12	Internalization & fragmentation by SERS	78
2.4.13	Colony formation assay	78
2.4.14	Cell cycle analysis	79
2.4.15	Protein expression studies	79
2.4.16	Apoptotic antibody array assay	79
2.5	References	80
<b>CHAPTER 3</b>		87-121
<b>CHAPTER 3A</b>		
<b>Mechanistic insights into the antimetastatic effects of phaeanthine in triple-negative breast cancer cell</b>		87-105
3A.1	Introduction	88
3A.2	Results and Discussion	90
3A.2.1	Cytotoxicity induced by PHA in MDA-MB-231 cells	91
3A.2.2	Apoptosis induction by PHA	91
3A.2.3	Annexin V apoptosis assay	92
3A.2.4	Caspase activation by PHA	93
3A.2.5	Inhibition of clonogenic potential by PHA	94
3A.2.6	Cell cycle arrest induced by PHA	94
3A.2.7	PHA inhibited migration & invasion of MDA-MB-231 cells	94
3A.2.8	PHA induced reversal of EMT	97

3A.2.9	PHA induced downregulation of major integrins	98
3A.2.10	PHA modulated the expression of MMPs	99
3A.2.11	PHA modulated the expression of major regulatory proteins	100
3A.3	Conclusion	102
3A.4	Experimental section	102
3A.4.1	Cell culture methods	102
3A.4.2	Cytotoxicity assay	102
3A.4.3	Apoptosis assay	103
3A.4.4	Annexin V apoptosis assay	103
3A.4.5	Caspase fluorometric assay	103
3A.4.6	Colony formation assay	103
3A.4.7.	Cell cycle analysis	104
3A.4.8	Wound healing assay	104
3A.4.9	Adhesion, migration and invasion assay	104
3A.4.10	Protein expression studies	105
 <b>CHAPTER 3B</b>		
<b>Mechanistic insights into the anti-angiogenic effects of Phaeanthine in EA.hy926 cells</b>		107-121
3B.1	Introduction	107
3B.2	Results and discussion	110
3B.2.1	Cytotoxicity evaluation of PHA	110
3B.2.2	Effect of PHA on wound healing in EA.hy926 cells	111

3B.2.3	Effect of PHA on migration & invasion of endothelial cells	112
3B.2.4	Effect of PHA on tube formation of endothelial cells	113
3B.3	Conclusion	115
3B.4	Experimental section	115
3B.4.1	Cell culture methods	115
3B.4.2	Cytotoxicity assay	115
3B.4.3	Wound healing assay	116
3B.4.4	Migration and invasion assay	116
3B.4.5	Tube formation assay	116
3B.5	References	117

## **CHAPTER 4**

<b>Development of MSN-based nano delivery system for the combination-therapy of phaeanthine &amp; 2-deoxy-D-glucose against cervical cancer cells</b>		123-150
4.1	Introduction	124
4.2	Results and discussion	127
4.2.1	Cytotoxicity of PHA & 2-DG	127
4.2.2	Establishing the synergistic combination of PHA & 2-DG	127
4.2.3	Fabrication of chitosan coated MSN-Mn nanoparticles for pH responsive release of PHA & 2-DG	132
4.2.4	Synthesis of EGFR targeting peptide-LARLLT by SPPS	134

4.2.5	Targetability of the synthesized peptide in cervical cancer cells	135
4.2.6	Drug loading and cellular internalization assessment of the targeted nanodelivery system (TNDS)	136
4.2.7	Evaluating the pH and GSH responsive release of cargo from the TNDS by SERS modality	137
4.2.8	Cytotoxicity evaluation of TNDS	139
4.2.9	Apoptosis inducing potential of TNDS	141
4.2.10	Glycolytic inhibition and alterations induced by the TNDS	142
4.3	Conclusion	143
4.4	Experimental section	144
4.4.1	Synthesis of MSN-Mn & APTES functionalization of the nanoparticles	144
4.4.2	Chitosan coating of MSN-Mn	144
4.4.3	Synthesis of EGFR targeting peptide-LARLLT by SPPS	145
4.4.4	Rhodamine B conjugation with peptide sequence	146
4.4.5	Drug loading and internalization	146
4.4.6	Cytotoxicity and synergy combination evaluation	146
4.4.7	Apoptotic evaluation	146

4.4.7	Glycolytic inhibition analysis	147
4.5	References	147
	Abstract	151
	List of publications	153
	List of conference presentations	154
	Attachment of the photocopy of publications	

## List of abbreviations

2-DG	2-deoxy-D-glucose
5-FU	5- Fluorouracil
AGE	Agarose gel electrophoresis
Ala	Alanine
Apaf	Apoptotic protease activating factor-1
APTES	(3-Aminopropyl)triethoxysilane
Arg	Arginine
ATCC	American type culture collection
ATP	Adenosine triphosphate
AuNPs	Gold nanoparticles
Bax	BCL-2 associated X-protein
BCA assay	Bicinchoninic acid assay
Bcl-2	B-cell lymphoma-2
Berb	Berbamine
b-FGF	Basic fibroblast growth factor
Bid	BH3 interacting domain death agonist
CAM	Cell adhesion molecule
CD40	Cluster of differentiation 40
Cdc25c	Cell division cycle 25c
CDKs	Cyclin dependent kinases
CI	Combination index
COX	Cyclooxygenases



CS	Chitosan
CTAB	Cetyl trimethyl ammonium bromide
Cyt c	Cytochrome c
DBBI	Di bisbenzylisoquinoline alkaloid
DCM	Dichloromethane
DIC	N, N '-diisopropylcarbodiimide
DIPEA	N,N-Diisopropylethylamine
DLS	Dynamic light scattering
DMEM	Dulbecco's modified eagle medium
DMF	Dimethylformamide
DMSO	Dimethyl sulfoxide
ECM	Extracellular matrix
EDC	Ethylene dichloride
EDX	Energy dispersive X-ray spectroscopy
EGFR	Epidermal growth factor receptor
EMT	Epithelial mesenchymal transition
Fang	Fangchinoline
FBS	Fetal bovine serum
FDA	Food and Drug Administration
FGF	Fibroblast growth factor
FITC	Fluorescein isothiocyanate
Fmoc	Fluorenylmethoxycarbonyl
GAPDH	Glyceraldehyde 3-phosphate dehydrogenase
GSH	Glutathione
HBSS	Hanks' balanced salt solution

HIF-1 $\alpha$	Hypoxia inducible factor-1 alpha
HMPB	4-Hydroxymethyl-3-methoxyphenoxybutyric acid
HPLC	High performance liquid chromatography
HPV	Human papillomavirus
HRMS	High resolution mass spectroscopy
HSP 60	Heat shock protein 60
IC <sub>50</sub>	Half maximal inhibitory concentration
ICAM	Intracellular adhesion molecule
ICMR	Indian Council of Medical Research
IGF-2	Insulin like growth factor-2
I $\kappa$ B $\alpha$	Inhibitor of NF- $\kappa$ B, alpha
JNK	c-Jun-N-terminal kinases
Leu	Leucine
LOX	Lipoxygenases
MAPK	Mitogen activated protein kinase
Mcl-1	Myeloid cell leukemia-1
MDR	Multi Drug Resistance
MDS	Molecular dynamic simulation
MET	Mesenchymal epithelial transition
MMP	Matrix metalloproteinase
Mn	Manganese
MSN	Mesoporous silica nanoparticles
mTOR	Mammalian target of rapamycin
MTT	3-[4,5-dimethylthiazol-2-yl]-2,5-diphenyltetrazolium
NaOH	Sodium hydroxide

NCRP	National Cancer Registry Programme
NF- $\kappa$ B	Nuclear factor kappa-light-chain-enhancer of activated B cells
NHS	N-hydroxy succinimide
NMR	Nuclear magnetic resonance
NPs	Nanoparticles
PAGE	Poly acrylamide gel electrophoresis
PARP	Poly ADP ribose polymerase
PCNA	Proliferating cell nuclear antigen
PD-1	Programmed cell death protein 1
PDGF	Platelet derived growth factor
PDI	Polydispersity index
PEG	Poly ethylene glycol
p-gp	p-glycoprotein
PHA	Phaeanthine
PI	Propidium iodide
PS	Phosphatidyl serine
RB	Retinoblastoma
RBCs	Red blood cells
RhoB	Rhodamine B
RIPA buffer	Radio-immuno precipitation assay buffer
RMSD	Root mean square deviation
RMSF	Root mean square fluctuation
ROS	Reactive oxygen species
SD	Standard deviation
SERS	Surface enhanced raman spectroscopy

SHP-1	Src homology 2 domain-containing protein tyrosine phosphatase 1
SMAC	Second mitochondria-derived activator of caspase
SPPS	Solid phase peptide sythesis
STAT	Signal transducer and activator of transcription
tBu	Tert butyl
TEM	Transmission electron microscopy
TEOS	Tetraethyl orthosilicate
Tet	Tetrandrine
TFA	Trifluoro acetic acid
TGF- $\beta$	Transforming growth factor- beta
Thr	Threonine
TLC	Thin layer chromatography
TME	Tumor microenvironment
TNBC	Triple negative breast cancer
TNDS	Targeted nano delivery system
TNF- $\alpha$	Tumor necrosis factor- alpha
TP53	Tumor protein P53
VEGF	Vascular endothelial growth factor
WBCs	White blood cell
XIAP	X-linked inhibitor of apoptosis protein
$\zeta$ potential	Zeta potential

## PREFACE

Cancer, with its intricate and relentless nature, remains a formidable adversary in the realm of human health, necessitating continuous exploration and innovation in therapeutic approaches. As the conventional armamentarium of cancer therapies encounters challenges, there is a growing impetus to explore alternative treatments rooted in nature's pharmacopeia. This thesis delves into the realm of anticancer studies, focusing on a natural compound, Phaeanthine, isolated from *Cyclea peltata* and its targeted delivery through a sophisticated nanocarrier system developed from MSN-Mn.

The introductory **chapter 1** provides a comprehensive review of the challenges posed by cancer and the evolving landscape of therapeutic strategies. It navigates through the rationale for exploring natural compounds, with special focus on Bisbenzylisoquinoline alkaloids (BBIQs). BBIQ play a significant role in cancer therapy, owing to their diverse pharmacological properties that exhibit potential anti-cancer effects. These natural compounds, often derived from plant sources, have garnered attention from researchers and clinicians alike for their ability to target various aspects of cancer development and progression.

**Chapter 2** sets the stage by screening the isolated natural compounds isolated from *Cyclea peltata*, an intriguing source in the rich tapestry of botanical resources and a well-known medicinal plant in the traditional systems of medicine and the results implicated phaeanthine (PHA) as the potent lead against cervical cancer cell, HeLa. This chapter encompasses a detailed exploration of PHA's inherent anticancer potential, elucidating its ability to induce mitochondrial-mediated apoptosis and downregulate critical signalling pathways, with a particular emphasis on its impact on cervical cancer cells.

Building upon the promising anticancer properties of PHA, **Chapter 3** delves into its potential as an anti-metastatic and anti-angiogenic agent. The study extends its reach to highly metastatic model of TNBC- MDA-MB-231, unraveling PHA's efficacy in impeding the metastatic cascade, regulating key molecular players, and by reversing the EMT, a key event in the migration of cancer cells. PHA also found to potentially inhibit the process of angiogenesis by regulating the migration and invasion of endothelial cells and it could inhibit the tube formation of the cells at a very low concentration compared to its IC<sub>50</sub> value.

**Chapter 4** marks a pivotal turn as it introduces the innovation of a nanocarrier system for targeted delivery of PHA. By encapsulating PHA within a nanodelivery system composed of chitosan-coated mesoporous silica nanoparticles doped with manganese (MSN-Mn), the study seeks to enhance the compound's efficiency and precision. The nanoconstruct is further refined with the co-loading of 2-deoxy-D-glucose (2-DG) and conjugation with an Epidermal Growth Factor Receptor (EGFR) targeting hexapeptide sequence for specific delivery to cancer cells. The developed targeted nanodelivery system releases the cargo drug only when it is incorporated into the tumor cells, where the acidic pH within the cell milieu, will swells the chitosan coating and exposes the MSN-Mn and the high GSH concentration will trigger the degradation of MSN-Mn and releases the cargo into the cancer cells. This ensures the safety of the normal cells by targeting specifically the tumor cells.

This preface serves as an invitation to journey through the pages of this thesis, where the synergy between natural compounds and cutting-edge nanotechnology converges in the pursuit of advancing anticancer therapeutics. The exploration contributes not only to the scientific discourse but also to the broader mission of alleviating the burden imposed by cancer on global health.

---

## **An overview of bisbenzylisoquinoline alkaloids in cancer therapy: Recent advances and opportunities**

---

### **Abstract**

Cancer, ranked as the second leading cause of global mortality, demands significant attention for the development of more effective therapeutic drugs, emphasizing the limitations of current medications. Many of the conventional treatments are associated with numerous side effects like hypertension, reduction in WBCs, and many other physiological changes. There is a growing demand for drugs derived from natural pharmacophores due to their widespread availability, diverse structural variations, and minimal side effects.<sup>1</sup> A substantial body of evidence indicates that between 1981 and 2019, a total of 247 anticancer drugs were developed, with a majority originating from natural sources—either in their unaltered state, synthetic form or designed to mimic natural pharmacophores. Only 12% of these drugs are entirely synthetic. Given the indeterminate nature of cancer etiology, the importance of drugs capable of targeting multiple pathways cannot be overstated. Within the realm of natural compounds from plants, alkaloids, particularly bisbenzylisoquinoline (BBIQ) alkaloids, play a crucial role. BBIQ alkaloids, such as berberine, tetrandrine, chelidoniumine, and berbamine, exhibit remarkable effectiveness against a wide spectrum of cancers by modulating various signaling pathways. Several BBIQ alkaloids, including those mentioned, are currently undergoing clinical trials for cancer treatment. Therefore, exploring the potential of these types of alkaloids in cancer therapy is imperative in the face of the escalating incidence of cancer cases in our contemporary era.

### **1.1 Introduction**

Cancer ranks as the second most prevalent cause of death on a global scale. In 2020 alone, there were approximately 19.3 million new cases of cancer worldwide, resulting in nearly 10 million deaths<sup>2</sup> Extensive research over the decades has illuminated the complexity of cancer, highlighting it not as a singular ailment but rather as a compilation of diverse conditions and related diseases. The onset of cancer entails intricate genomic alterations triggered by a myriad of factors.<sup>3</sup> Several factors contribute to the transformation of a normal cell into a malignant tumor. According to Hanahan and Weinberg, there are six

alterations in cell physiology and conditions that collectively lead to the conversion of a healthy cell into an aggressive tumor: self-sufficiency in growth signals, insensitivity to growth inhibitory signals, evasion of programmed cell death (apoptosis), unrestricted replicative potential, sustained angiogenesis, and tissue invasion and metastasis.<sup>3</sup>

The overall cancer incidence is 2 to 3 fold higher in transitioning countries than in transitioned countries. The global cancer burden is expected to be 28.4 million cases in 2040, a 47 % rise from 2020 with a larger increase of incidence in transitioning (64 % to 95 %) versus transitioned (32 % to 56 %) countries. The death rates for cancers, especially breast and cervical cancers among women were considerably higher in transitioning versus transitioned countries.<sup>2</sup> WHO's International agency for research on cancer provided the data global cancer incidences of 18.1 million new cases, among the total cases around half of them were reported from Asia alone, that is exactly a number of 8,75,1000 (48.4 %) cases.(Figure 1.1.a)

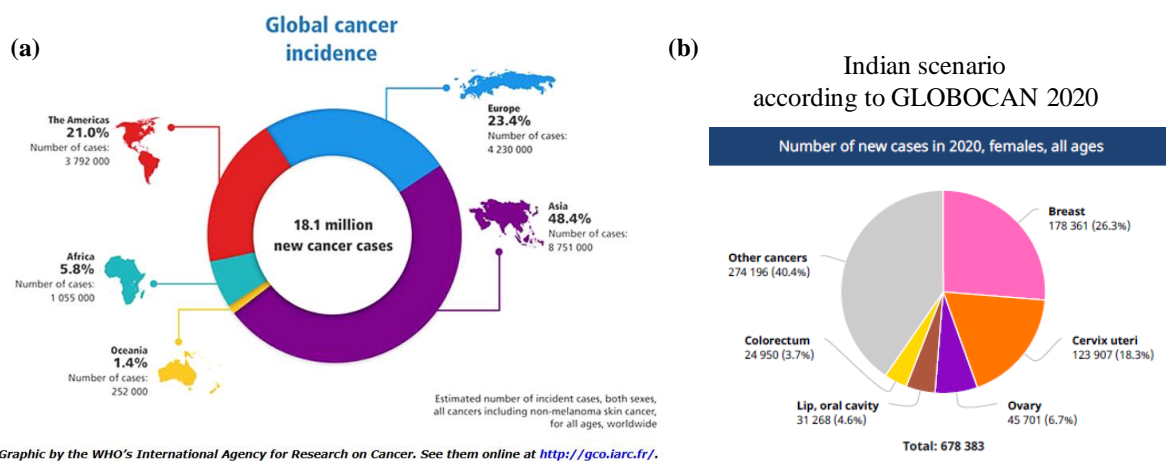


**Figure 1.1.** (a) Global cancer incidence,2020 (WHO's International Agency for Research on cancer), (b) Cancer incidence among Female population in India, according to Globocan 2020.

The cancer scenario in India is similar to the situation around the world. The report from NCRP (National Cancer Repository Program by ICMR), 2020 highlights that India's cancer burden could increase from 1.39 million in 2020 to 1.57 million in 2025. According to Globocan 2020, breast cancer is the leading cancer among women in India with accounting nearly 26.3 % of the total incidence of cancer, followed by the cancer of cervix uteri with 18.3 % of the cases. (Figure 1.1.b) The highest incidence of cancer in India was observed in North eastern region and followed by south coastal region.<sup>4</sup>



The higher mortality and morbidity in transitioning countries and local areas are due to the lack of proper preventive measures and diagnosis of cancer conditions in their early stages. Even though the developed nations managed to reduce the incidence of some of the cancers like, cervical cancer because of early detection, these advances in diagnosis facilities are lacking in lower-income countries. So, more therapies with lower costs are needed to be affordable by the transitioning countries. Affordable treatments are necessary to eradicate cancer on a global basis. For this, drugs of natural origin have vital importance due to its easier availability, more structural diversity, and vast biological properties. Hence natural products are crucial in the current pharmacopoeia.

From time immemorial, humans have depended on nature for many purposes, especially in finding a cure for enormous diseases. There is much evidence of using plants for medicinal purposes millions of years ago. Ancient civilizations utilized plants for curing many diseases. The presence of pollen grains from the grave of Neanderthals emphasized the use of medicinal plants long years ago.<sup>5</sup> One of the main reasons these natural compounds show diverse biological activities may be the co-evolution within the biological communities. The secondary metabolites are produced in self-defence to protect themselves from external stress features like herbivory, microbial attack, physiological stress, etc.<sup>5</sup> There have been many attempts and success stories in developing new drug entities of natural origin and even their semi-synthetically modified forms. The drugs from natural products can be of different types, such as microbially derived drugs; dactinomycin, bleomycin, and doxorubicin, fungal derived ones like penicilium, cyclosporine and lovastatin, animal derived drugs like exenatide, ziconitide and batroxobin and the plant derived drugs like vinblastine, irinotecan, topotecan, etoposide and paclitaxel.<sup>6,7</sup> There are around 247 anticancer drugs in market till 2019 of which only 29 (15.7 %) is of purely synthetic origin. Rest of the drugs are either purely natural origin or with natural pharmacophore, semi synthetically modified or the ones which mimic the natural products or the botanical formulations.<sup>7</sup>

The biologically active drug leads from plants of menispermaceae family is of eternal importance, because of its structural diversity and complexity of the chemical constituents of the family. The Menispermaceae family known as the moonseed family, is one of the widely exploited groups in terms of its chemical treasure. Bisbenzylisoquinoline alkaloids along with aporphines and protoberberines constitute the major chemical markers of the family. The presence of these alkaloids is reported in almost all species studied so

far.<sup>8</sup> The majority of these alkaloids were derived from the benzyltetrahydroisoquinoline nucleus. These group of alkaloids are also present in other families like Ranunculaceae, Berberidaceae, Monimiaceae, Annonaceae, Lauraceae and Nelumbonaceae, etc.<sup>8,9</sup>

The Bisbenzylisoquinoline alkaloids have an imperative role in the medicinal chemistry with a special focus on cancer studies. Some of the BBIQs are under clinical trials as cancer drugs, and many others show better anticancer potential. Berberine, Cephranthine, protopine, tetrandrine, Chelidonine are some of the BBIQs under clinical trials. This group of alkaloids is known as bisbenzylisoquinoline alkaloids because they are made of two benzylisoquinoline residues connected to each other by ether bridges or by direct carbon-carbon bonds.<sup>8</sup>

## **1.2 Cancer Prevalance**

Cancer stands as the second leading cause of global mortality, claiming nearly 10 million lives and registering an estimated 19.3 million new cases in 2020 alone. Projections indicate a concerning trajectory, with the anticipated global cancer burden reaching 28.4 million cases in 2040—an alarming 47% surge from 2020 incidents. Tumors are intricate tissues comprising diverse cell types, engage in complex interactions, fostering heterotypic relationships.

In the year 2000, Hanahan and Weinberg delineated six fundamental characteristics of cancer, representing acquired traits that transform normal cells into malignant neoplasms. (Figure 1.2) These characteristics include the ability to sustain proliferative signaling, evade growth suppressors, resist cell death, activate invasion and metastasis, enable replicative immortality, and induce angiogenesis. The acquisition of these traits empowers a normal cell to evolve into a cancerous entity capable of unrestrained proliferation and the formation of widespread tumors.

A prominent attribute of cancer cells lies in their capacity for persistent proliferation. While normal cells meticulously regulate cell numbers through controlled proliferative signaling cascades, cancer cells disrupt these mechanisms, leading to uncontrolled proliferation. Cancer cells demonstrate autocrine proliferative stimulation, generating their own growth factors and receptors to drive their proliferation. The overexpression of cell surface receptor proteins further amplifies downstream signaling, contributing to hyper responsive proliferation. There is evidence to suggest that cancer cells

impede negative feedback mechanisms, disrupting the homeostatic regulation of cell proliferation.

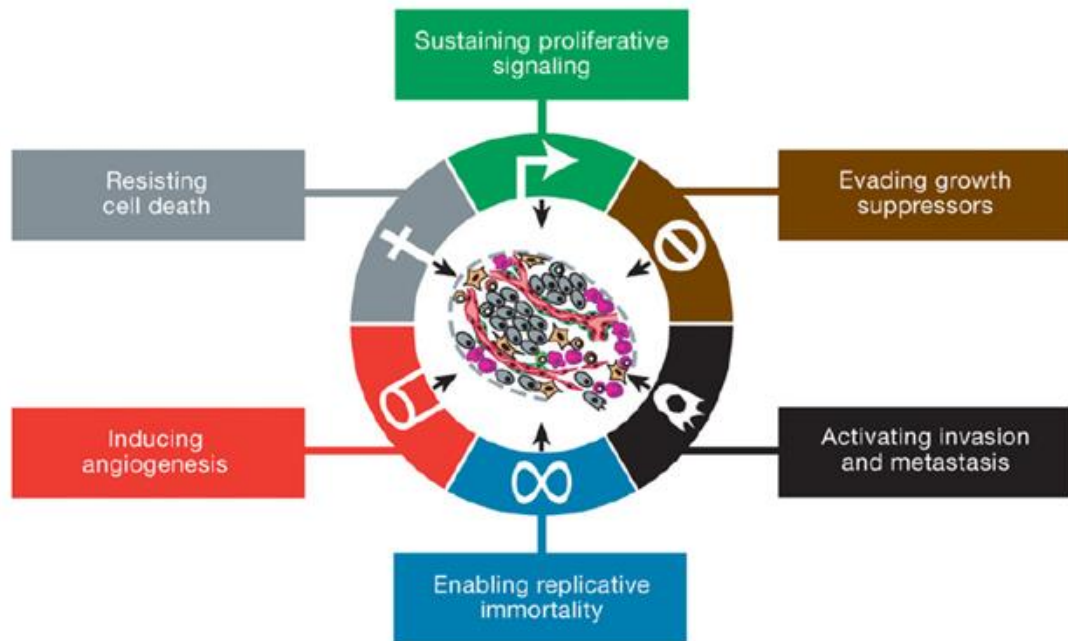


**Figure 1.2.** Hallmarks of cancer (adapted from *Cell*- 2011,144(5), 646-74)

Evading growth suppressors is another distinctive feature of cancer cells. Tumor suppressor proteins, such as retinoblastoma-associated (RB) and TP53, play critical roles in regulating proliferation. Dysfunctional RB pathways result in persistent proliferation, while TP53 proteins can halt the cell cycle and induce apoptosis in response to defects. Cancer cells, adept at evading these growth suppressors, proliferate continuously without hindrance. The programmed cell death mechanism, apoptosis, acts as a natural barrier against uncontrolled division and compromised genetic machinery. However, cancer cells prioritize resistance to apoptosis. They manipulate the genetic system by activating anti-apoptotic genes and downregulating pro-apoptotic genes, subverting the body's natural defense mechanism and facilitating their sustained survival.

Cancer cells possess a distinct feature that sets them apart from normal cells - their ability to replicate indefinitely and form macroscopic tumors. Unlike normal cells, which are typically limited in the number of successive cell growth and division cycles they can undergo, cancer cells exhibit continuous replication without impediment. Evidence suggests that this unlimited replicative potential is closely tied to telomeres, protective

structures at the ends of chromosomes. Telomerase, a specialized DNA polymerase, plays a crucial role in this process by adding repeated telomere sequences to chromosome ends, enabling cancer cells to evade the usual constraints on cell division. Notably, the levels of telomerase are significantly elevated in the majority of cancer cells, contributing to their unbridled replicative capacity. This understanding has opened avenues for research on potential therapeutic interventions targeting telomerase to selectively inhibit the proliferation of cancer cells while sparing normal cells.

Neovascularization associated with tumors, achieved through angiogenesis, serves to fulfil the nutritional and oxygen needs of cancer cells. As tumors progress, there is a consistent activation of an angiogenic switch, leading to the development of new vessels within the vasculature, thereby promoting the expansion of tumor growth.<sup>10</sup> Cancer cells gain the ability to detach from the primary tumor mass and infiltrate nearby tissues. This dynamic process involves alterations in cell adhesion, rearrangements of the cytoskeleton, and the activation of signalling pathways that enhance cell motility. The acquisition of invasive properties is pivotal for cancer cells to overcome the physical barriers presented by the extracellular matrix, enabling them to invade neighboring blood vessels or lymphatic channels. This crucial step facilitates the entry of cancer cells into the circulatory system, allowing for dissemination to distant sites. An understanding of the molecular mechanisms governing migration, invasion, and subsequent stages of the metastatic cascade is essential for the development of targeted therapies designed to inhibit these processes. By disrupting key events in metastasis, researchers aim to devise strategies that restrict the spread of cancer, ultimately leading to improved patient outcomes.

### **1.2.1 Cervical cancer**

A decade ago, cervical cancer held the third-highest prevalence globally among women. Yet, in 42 countries with limited resources, it emerged as the most commonly diagnosed cancer in women. The acknowledgment that persistent infection with carcinogenic human papillomavirus (HPV) types is the primary trigger for cervical cancer development has paved the way for new approaches in both primary and secondary prevention. Embracing these preventive measures has the potential to significantly reduce the incidence and mortality rates associated with cervical cancer.<sup>11</sup>

Substantial evidence indicates that licensed HPV vaccines, encompassing HPV16 and HPV18 antigens in both bivalent and quadrivalent formulations, exhibit high efficacy

in protecting against infection and precancerous cervical lesions linked to these specific HPV types, particularly when individuals have not been previously exposed. These two HPV types collectively contribute to 70–75% of all cervical cancers and 40–60% of their precursors. In recent years, an additional monovalent vaccine has obtained licensing, offering protection against seven carcinogenic HPV types, which, when combined, contribute to the majority of cervical cancers. While these vaccines are accessible, it's important to note that they are primarily preventive in nature and come with a significant cost barrier. This expense poses challenges, particularly for individuals in transitioning countries, where the incidence of cervical cancer is notably high. The financial burden associated with these vaccines makes them less accessible to a broader population, especially among women in regions facing economic challenges.

Several drugs, including bevacizumab, pembrolizumab, bleomycin sulfate, and topotecan hydrochloride, are commonly employed in the treatment of cervical cancer. Bevacizumab, functioning as an angiogenesis inhibitor, is a monoclonal antibody that impedes the formation of new blood vessels. Bleomycin sulfate disrupts cancer cells by damaging their DNA. In 2021, the FDA approved pembrolizumab, used in conjunction with chemotherapy, for advanced cervical cancer treatment. This drug inhibits the interaction between PD-1 (a protein expressed on cytotoxic T-cells) and PD-L1 proteins on specific cancer cells, removing an impediment on the immune system and enabling T-cells to target the cancer.<sup>12</sup>

Despite their efficacy, these drugs come with side effects. For instance, bevacizumab injection may result in nosebleeds, bleeding from the gums, or changes in urine or bowel movements. Bleomycin carries a risk of severe lung problems, especially in older patients or those receiving higher doses. Topotecan injection can reduce white blood cell count, raising the risk of infection, and may also cause thrombocytopenia, increasing the likelihood of bleeding problems.<sup>1</sup>

Considering the associated adverse effects, exploring alternative options, such as natural products, becomes imperative in addressing the challenges of treating this formidable disease.

### 1.3 Natural products in cancer drug discovery

Throughout history, Nature has addressed humanity's fundamental needs, including the provision of medicines to treat a wide range of diseases. Plants, in particular, have played a pivotal role in shaping advanced traditional medical systems. While Egyptian medicine traces back to 2900 BCE, the most well-known record is the "Ebers Papyrus," dating from 1500 BCE, which meticulously documents over 700 drugs, predominantly of plant origin. Records from Mesopotamia around 2600 BCE document the usage of approximately 1000 plant-derived substances, many of which continue to be utilized for treating various ailments, from coughs and colds to parasitic infections and inflammation. The Chinese "Materia Medica" boasts extensive documentation over the centuries, with the first record dating back to around 1100 BCE in the form of "Wu Shi Er Bing Fang," featuring 52 prescriptions. This was followed by notable works such as the Shennong Herbal (circa 100 BCE; 365 drugs) and the Tang Herbal (659 CE; 850 drugs). Similarly, documentation of the Indian Ayurvedic system predates 1000 BCE, with texts such as Charaka and Sushruta samhitas detailing 341 and 516 drugs, respectively.<sup>13</sup> The historical use of plants in the treatment of cancer has a rich tradition, with some plant-derived compounds forming the basis of modern anticancer drugs. However, it is essential to approach claims about the efficacy of such treatments with a degree of skepticism due to the vague definition of cancer in folklore and traditional medicine.

Plant-derived compounds have played a significant role in the development of anticancer drugs, with vinca alkaloids like vinblastine and vincristine being prime examples. These alkaloids, isolated from the Madagascar periwinkle (*Catharanthus roseus*), were initially investigated due to the plant's historical use in diabetes treatment. This unique discovery pathway highlights the interconnectedness of traditional medicinal knowledge and contemporary drug development. Etoposide and teniposide, both effective anticancer agents, are derived from epipodophyllotoxin, a natural product found in Podophyllum species. These plants have a historical context in traditional American and Asian medicine, treating conditions like skin cancers and warts. This historical association between traditional uses and the identification of potent anticancer compounds underscores the significance of exploring diverse sources and traditional knowledge in the search for new therapeutic agents.

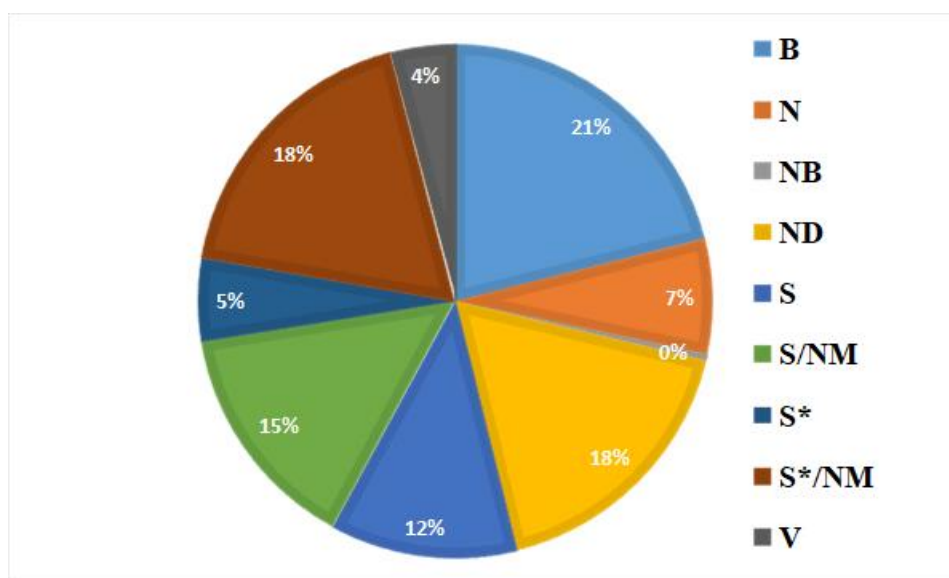


**Figure 1.3.** All anticancer drugs 01 JAN 1981–30 SEP 2019, n = 247; B (Biological macromolecule), N (Unaltered natural product), NB (Botanical drug), ND (Natural product derivative), S (Synthetic drug), S/NM (Synthetic drug-mimic of natural product), S\* (Synthetic drug with natural pharmacophore), S\*/NM (Synthetic drug with natural pharmacophore-mimic of natural product)) and V (Vaccine)-[Adapted from -*J. Nat. Prod.* 2020, 83, 3, 770-803]

In examining specific plant-derived anticancer drugs, paclitaxel from *Taxus brevifolia* has demonstrated efficacy against various cancers. Pharmacophore designs based on taxol, such as Baccatin, have shown promising antineoplastic activity. Vinca alkaloids (vincristine, vinblastine, leurosine, leurosidine) from *Catharanthus roseus* are commercially utilized to prevent microtubule assembly, and controlling cancer cell division. Synthetic analogues of these vinblastine like alkaloids like 5'-noranhydrovinblastine and vindesine and the semisynthetic agent vinflurine exhibit improved activity and lower toxicity.

Colchicine and demecolcine from *Colchicum autumnale* have been employed for treating solid tumors and chronic myelocytic leukemia by disrupting tubulin's dynamic equilibrium. Podophyllotoxin type lignans from Podophyllum species, including etoposide, a topoisomerase II inhibitor, demonstrate substantial anticancer properties. Ellipticine type alkaloids, such as ellipticine and its analogues, inhibit DNA, RNA, and protein synthesis. Jatropane diterpenoids from *Jatropha gossypifolia* exhibit potent antileukemic activity.

Camptothecin from *Camptotheca accuminata* serves as a potent DNA topoisomerase I inhibitory agent, with derivatives like Topotecan and Camptostar used to

treat various cancer types. Overall, the diverse array of plant-derived anticancer compounds underscores the need for continual scientific research to comprehend their mechanisms, optimize their use, and explore new candidates for cancer treatment.<sup>14</sup>

Discovering potential anticancer chemotherapeutic agents from plant sources hinges on maximizing the exploration of botanical diversity. It is imperative to investigate plant origins in new and previously unexplored areas to uncover novel compounds or analogs with heightened anticancer efficacy and reduced toxicity. An essential aspect is the advancement in high throughput isolation techniques, allowing for the swift and automated separation and purification of compounds from crude natural product extracts. The integration of highly automated separation methods expedites the identification and characterization process, significantly enhancing efficiency. Moreover, the amalgamation of modern techniques with high throughput screening systems is poised to yield a greater number of lead structures. This synergy facilitates the rapid testing of a large pool of compounds to evaluate their biological activity, promising an increase in the discovery of potential anticancer agents in the foreseeable future.

#### 1.4 Genus *Cyclea*

The genus *Cyclea* belongs to the family Menispermaceae and was created in 1840 by Arnotti. The species of this genus are mainly climbing shrubs, leaves are often peltate and palmately nerved. The inflorescence is axillary, terminal, and on old stems. The plants are unisexual, male flowers: sepals usually 4 or 5, usually connate, petals 4 or 5, stamens 4 or 5 connate into a peltate synandrium, anthers dehiscing transversely. Female flowers: sepals and petals 1 or 2, stigma short, 3 or many lobed. Fruits are drupe, obovate or globose, and endocarp is bony and horseshoe-shaped.<sup>15</sup>

The genus comprises around 55 species and the major ones are: *Cyclea debiliflora* Miers, *Cyclea acuminatissima* Merr., *Cyclea apoensis* Yamam., *Cyclea atjehensis* Forman, *Cyclea bicristata* (Griff.) Diels, *Cyclea caudata* Merr., *Cyclea densiflora* (Yamamoto) Y.C.Tang & Lo, *Cyclea fansipanensis* Gagnep., *Cyclea aphylla* Gagnep., *Cyclea hainanensis* Merr., *Cyclea longgangensis* J.Y.Luo, , *Cyclea elegans* King, *Cyclea laxiflora* Miers, *Cyclea adagascariensis* Baker, *Cyclea meeboldii* Diels, *Cyclea peltata* (Lam.) Hook.f. & Thomson, *Cyclea merrillii* Diels, *Cyclea kinabaluensis* Forman, *Cyclea barbata* Miers, *Cyclea migoana* Yamam., *Cyclea fissicalyx* Dunn, *Cyclea ochiaiana* (Yamam.) S.F.Huang & T.C.Huang, *Cyclea pendulina* Miers, *Cyclea peregrina* Miers, *Cyclea*



*polypetala* Dunn, *Cyclea gracillima* Diels, *Cyclea racemosa* Oliv., *Cyclea robusta* Becc., *Cyclea scyphigera* Suess. & Heine, *Cyclea sutchuenensis* Gagnep., *Cyclea tonkinensis* Gagnep., *Cyclea varians* Craib, *Cyclea hypoglauca* Diels, *Cyclea cauliflora* Merr., *Cyclea villosum* Miers, *Cyclea wallichii* Diels, *Cyclea insularis* (Makino) Hatus., *Cyclea wattii* Diels.<sup>15</sup>

#### 1.4.1 *Cyclea* species reported in India

Eight species of *Cyclea* have been reported from India, of which only three are widely explored in terms of the phytochemical studies.

The species reported from India are:

- *Cyclea barbata* Miers
- *Cyclea bicristata* (Griff.) Diels
- *Cyclea debiliflora* Miers
- *Cyclea fissicalyx* Dunn
- *Cyclea meeboldii* Diels
- *Cyclea peltata* (Lam.) Hook.f. & Thomson
- *Cyclea pendulina* Miers
- *Cyclea wattii* Diels

*Cyclea barbata* Miers: Its habitat is in evergreen and semi-evergreen forests, and is distributed to the Indo-malesian region. The leaves of this plant are known as green jelly leaves and are a common ingredient in many Asian countries in the preparation of dessert gels and also in medicinal preparations.<sup>16</sup> In 1993, Lin et al., carried out the phytochemical screening and antimalarial studies of *C.barbata*. They have isolated 5 BBIQ alkaloids, namely, (+)-tetrandrine, (-)-limacine, (+)-thalurugin, (+)-homoaromaline, and (-)-cyclopeltine from the roots of the plant.<sup>17</sup> In the same year, they have reported the presence of some other alkaloids such as (-)-2'-norlimacine, (+)-cycloabarbamine, (+)-tetrandrine-2'- $\beta$ -N-oxide, (+)-berbamine, (-)-repandine, (+)-cycleanorine, (+)-daphnandrine, (-)-Curine, (+)-Curine, (+)-Coclaurine, and (-)-N-methylcoclaurine from the roots of the same plant.<sup>18</sup>

*Cyclea bicristata* (Griff.) Diels: Its general habitat is subtropical evergreen forests at an altitude of upto 1500 m. The works of literature suggests that, no data is available on this

plant's phytochemical screening or any other studies. (Sci-finder-0 hit, key words: *Cyclea bicristata*- phytochemistry)

*Cyclea debiliflora* Miers: The habitat is in dry deciduous forests at an altitude of about 600-1200 m. The species distribution is restricted to India, especially in Meghalaya and is identified as possibly extinct (P-Ex).<sup>19</sup>

*Cyclea fissicalyx* Dunn: This species is found in western ghats, especially in the evergreen forest areas and is in endangered conservation status. Any works regarding its phytochemical isolation or other aspects are not available so far. (Sci-finder-0 hit, key words: *Cyclea fissicalyx*- phytochemistry)

*Cyclea meeboldii* Diels: *C.meeboldii* is found in the evergreen subtropical forest at an altitude of about 1500 m, especially in Nagaland & Mizoram in India, China & Myanmar. No further studies are reported for this plant. (Sci-finder-0 hit, key words: *Cyclea meeboldii*- phytochemistry)

*Cyclea peltata* (Lam.) Hook.f. & Thomson: A well-known plant in Indian Ayurvedic classic as Rajapatha, has been a part of many ayurvedic formulations. It is a well-explored plant and possess many pharmacological properties. The isolation of compounds from the plant was first reported in 1961, by S. Kupchan et al. have isolated 4 compounds from the roots of the plant, namely, *d*-tetrandrine, *dl*- tetrandrine, *d*- isochondrodendrine and fangchinoline.<sup>20</sup> After that, in 1973, the same group isolated 5 more BBIQ alkaloids from the roots: cycleapeltine, cycleadrine, cycleacurine, cycleanorine and cycleahomine chloride.<sup>21</sup> Tetrandrine and fangchinoline are well-known anticancer molecules effective against a wide array of cancers.

*Cyclea pendulina* Miers: This species of cyclea is endemic to Andaman & Nicobar Islands, India. Furthermore, it grows primarily in the wet tropical biome. No literature is available on this plant's chemical characterisation and its biological activities. (Sci-finder-0 hit, key words: *Cyclea pendulina*- phytochemistry)

*Cyclea wattii* Diels: This species is a liana & grows primarily in the temperate biome. The native range of this species is from Assam to China. Wang et al., in 2010 isolated 5 compounds from the plant's roots, including 2 new bisbenzylisoquinoline alkaloids, Wattisine A, Wattisine B, Curine, Steponine, and  $\alpha$  – cyclanoline Wattisine A

showed very excellent cytotoxicity against HCT-8, and Bel-7402 with an IC<sub>50</sub> value of 1.74  $\mu$ M and 7.29  $\mu$ M, respectively.<sup>22</sup>

**Table 1.1** Bisbenzylisoquinoline alkaloids isolated from *Cyclea* species reported in India

Sl. number	Species	Alkaloid	References
1.	<i>Cyclea barbata</i>	(+) – Tetrandrine	17
2		(-) – Limacine	
3		(+) –Thalrugosine	
4		(+) – homoaromaline	
5		(-) – Cycleapeltine	
6		(-) – 2'- norlimacine	18
7		(+) – Cycleabarbatine	
8		(+) – tetrandrine-2'- $\beta$ -N-oxide	
9		(+)- Berbamine	
10		(-) – Repandine	
11		(+) – Cycleanorine	
12		(+) – Daphnandrine	
13		(-) – Curine	
14		(+) – Curine	
15		(+) – Coclaurine	
16		(-) – N- methylcoclaurine	
17	<i>Cyclea peltata</i>	(+) – tetrandrine	20
18		( $\pm$ ) - tetrandrine	
19		(+) – isochondrodendrine	
20		fangchinoline	
21		Cycleapeltine	21
22		Cycleadrine	
23		Cycleacurine	
24		Cycleanorine	
25		Cycleahomine chloride	
26		Phaeanthine	
27	Cycleanine		
28	<i>Cyclea wattii</i>	Wattisine A	22

30		Wattisine B	
31		Curine	
32		Steponine	
33		$\alpha$ - cyclanoline	

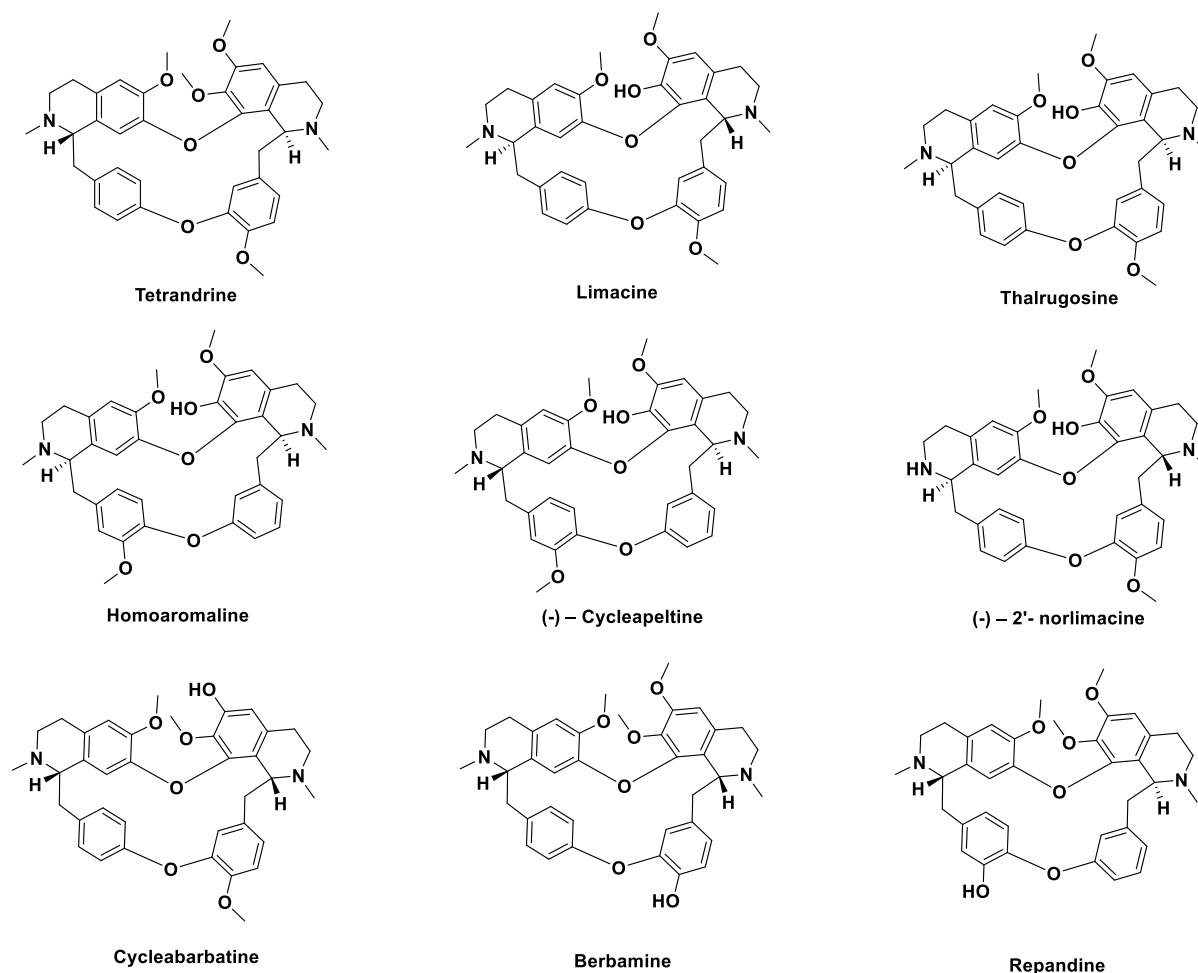


**Figure 1.4.** Bisbenzylisoquinoline alkaloids isolated from *Cyclea* species

### 1.5 Anti-cancer potential of Bisbenzylisoquinoline (BBIQ) alkaloids

Aforementioned, the menispermaceae family is rich in alkaloids of various groups BBIQs, aporphines and protoberberine types, and here, the emphasis will be on the BBIQ alkaloids because of its enormous potential in curing the cancer by regulating multiple signalling pathways. Bisbenzylisoquinoline alkaloids are of prime importance in the medicinal chemistry field. Their complex structure may be attributed to a wide variety of biological activities. Many BBIQ alkaloids are under clinical trials and used as drugs against many diseases. The pharmacological activities are not only restricted to cancer

treatments but also to treat many ailments such as diabetes, malaria, vascular diseases, hypertension, fungal infections, and schizophrenia, and also act as a calcium channel blocker.<sup>24-30</sup>

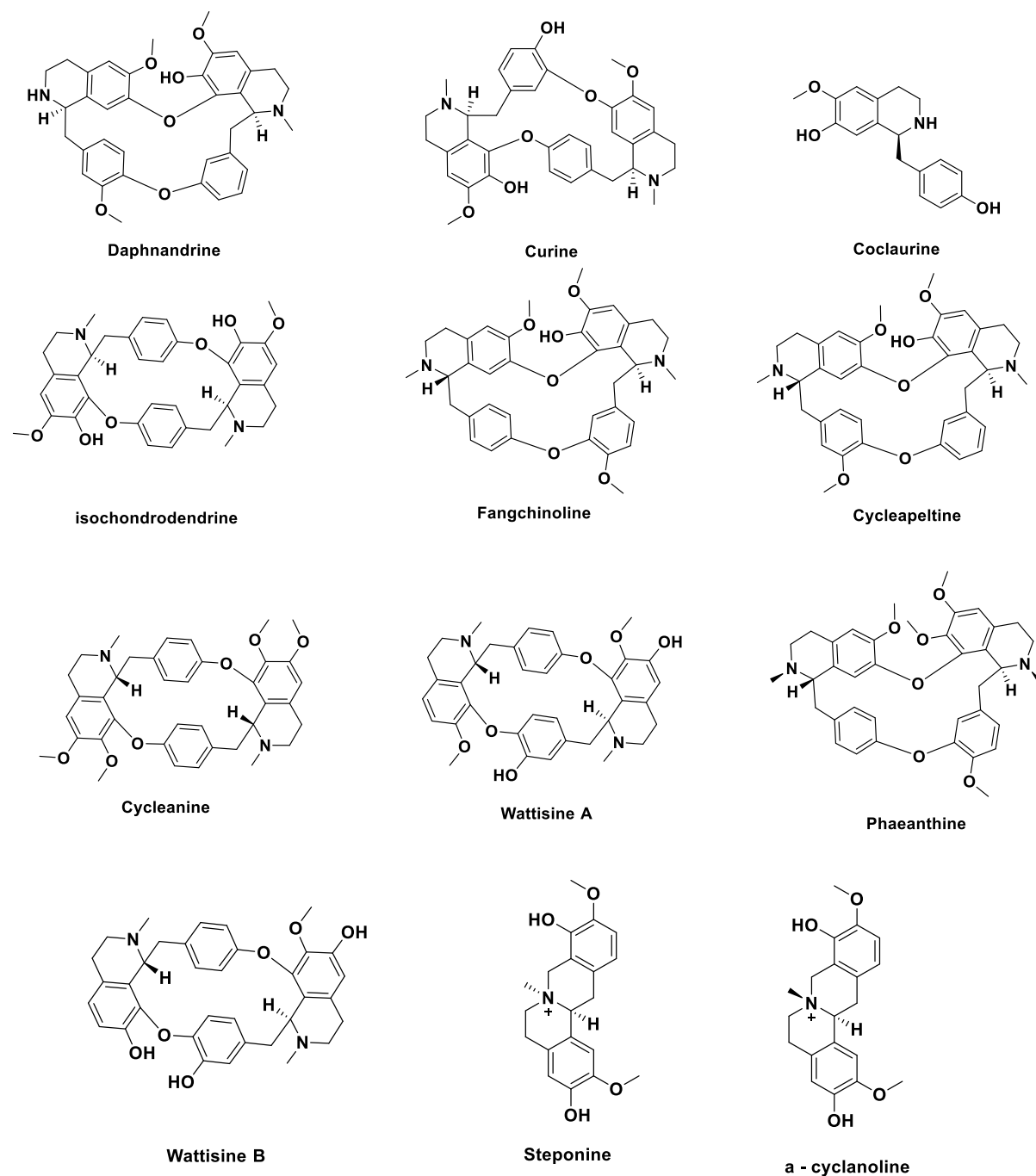


**Figure 1.5.** Bisbenzylisoquinoline alkaloids isolated from *Cyclea* species

Here, the importance of 25 bisbenzylisoquinoline alkaloids isolated from the *Cyclea* species reported in India will be emphasized. (Figure 1.4 and 1.5) The following sections will discuss the anti-cancer studies of Tetrandrine, berbamine, curine, cycleanine and

fangchinoline. The rest of the BBIQ alkaloids have not been explored in the area of cancer research to date.

### 1.5.1 Tetrandrine

Against breast cancer: Tetrandrine (Tet) is effective against triple-negative breast cancer cell MDA-MB 231, Tet induced ROS generation and led to cell death and induced autophagy.<sup>31,32</sup> They revealed that, Tet acts as a potent inhibitor of (exp)P-gp mediated Multidrug resistance (MDR). They also found that, it could have potentiated the cytotoxicity of doxorubicin, a 20.4-fold reversal in the presence of 2.5  $\mu\text{M/L}$  of Tet. Fu *et al.*, in 2002 carried out the *in vivo* studies in the MCF-7/adr cell xenograft model. Tet also found to be effective in lowering the membrane fluidity.<sup>33</sup> The effect of Tet was also studied by Yao *et al.*, (2017) in synergy with arsenite in MCF-7 cells, the treatment could upregulate the expression of FOXO3a, and decrease the cyclin D1 level, thereby inducing G0/G1 phase cell cycle arrest.<sup>34</sup>

In 2014 the efficacy of Tet against renal cancer was studied by Chen *et al.*, against 786-O and 769-P cell lines. They proved that, Tet treatment induced activation of caspases and upregulated the expression of cell cycle regulatory proteins p21 & p27.<sup>35</sup> The effect of Tet on lung cancer was studied. Lee *et al.*, performed the studies in lung adenocarcinoma cells, A549, the compound induced cell cycle arrest at G1 phase, induced caspase 3 activation and decreased cellular tubulin level<sup>36</sup>. In another study by Lin *et al.*, in 2016 the anti-cancer effect of a novel derivative of Tet, H1 was evaluated on non-small cell lung cancer cells. Tet induced DR-5 dependent apoptosis and activated endoplasmic reticulum stress mediated cell death mechanism to inhibit the cancer growth.<sup>37</sup> Cho *et al.*, in 2009 studied the effect of Tet on proliferation of lung carcinoma cells, they found that Tet could suppressed the cell proliferation of A549 cells by downregulating Akt & ERK phosphorylation and the inhibition of ERK using PD98059 synergistically enhanced the TET-induced apoptosis of A549 cells.<sup>38</sup>

Tet against Hepatic Cancers: The anti-tumor capabilities of Tet were investigated in various hepatic cancer cells, specifically in HepG2 and Huh7 cells. Studies conducted by different research groups over various time periods demonstrated that Tet could trigger caspase 3 activation, PARP cleavage, p53-independent apoptosis, heightened expression of p21/WAF1 proteins, and enhanced Fas/Apo-1. The compound induced G1 phase cell cycle arrest, and Tet also led to the downregulation of surviving, a protein associated with

proliferation and survival. Additionally, the treatment increased the generation of reactive oxygen species (ROS).<sup>39-43</sup>

Zhao *et al.*, in 2004 investigated the impact of Tet on hepatic stellate cells (T-HSC/CI-6) and found that Tet triggered the activation of caspase 3. In a separate study conducted by Hsu *et al.*, in 2007 on HSC-T6 cells, the compound demonstrated inhibitory effects on NF- $\kappa$ B transcription, phosphorylation of I $\kappa$ B $\alpha$ , and expression of ICAM-1 mRNA. These findings suggest that Tet has the potential to regulate hepatic fibrosis.<sup>44,45</sup> And in another study by Qi *et al.*, using rat hepatocytes (HL-7702) Tet could promote mitochondrial dysfunction through ROS generated by CYP450.<sup>46</sup> The synergistic action of Tet with sorafenib was also explored by Wan *et al.*, in curing the hepatic cancer, the combination lead to the accumulation of ROS and subsequently activated apoptotic pathway.<sup>43</sup>

Against Colon cancer: In the study conducted by Chen *et al.*, Tet induced dephosphorylation of Akt, and induced the nuclear translocation of GSK3 $\beta$  and upregulation of p27<sup>kip1</sup>. The compound also induced G1 phase cell cycle arrest and downregulated the PI3K/Akt/GSK3 $\beta$  signaling pathway in human colon cancer cell HT-29.<sup>47</sup> In mouse colon cancer cell CT-26, Wu *et al.*, carried out studies to demonstrate the effect of Tet and they found that Tet increased the expression of ERK1/2 and p38 MAPK.<sup>48</sup> In a separate study by He *et al.*, in 2011 Tet in combination with 5-FU was able to decrease the proliferation of colorectal cancer cells, SW480 and HCT116 by decreasing  $\beta$ -catenin level of cells and also reduced the migration and invasion of the cancer cells.<sup>49</sup> Therefore, Tet can be used as an effective agent against colon cancer.

The anti-angiogenesis potential of Tet was studied by Xiao *et al.*, in mouse endothelial cells (EOMA), treatment with the compound induced G1/S phase cell cycle arrest, downregulated the expression of cyclin D, cyclin E, and other CDKs. Tet induced intracellular ROS accumulation. So, Tet can be a potent lead for inhibiting the tumor vascular growth.<sup>50</sup> Apoptosis induced by Tet in human bladder cancer was studied by Li *et al.*, (2011) in bladder cancer cells 5637 and T24 cells. Compound induced apoptosis by the activation of caspase 9, caspase 8 and caspase 3, also induced the cleavage of PARP. Tet treatment lead to the release of cyt c from mitochondria to the cytosol.<sup>51</sup> The role of Tet in inhibiting the growth of gastric cancer cell BGC-823 was studied by Qin *et al.*, in 2013 and they found that the compound upregulated the expression of Bax, Bak, Bad, caspase 3,

Caspase 9 and Apaf-1, and induced the release of cyt c. Tet also downregulated the anti-apoptotic proteins Bcl-2 and Bcl-xl, thereby inducing apoptosis.<sup>52</sup> Similarly, a study in the same cell line by another group Li. *et al.*, reported the production of intracellular ROS and apoptosis induction by the co-delivery of paclitaxel and tetrandrine in a nanosystem.<sup>53</sup>

The effect of Tet against the leukemic cell, U 937 was explored by two different groups. Jang *et al.*, in 2004 reported that the Tet induced the activation of JNK, ROS mediated caspase activation, and also induced the activation of PKC- $\delta$ , while Liang *et al.*, found that Tet induced non  $\text{Ca}^{2+}$  dependent apoptosis, thereby inducing cell death and inhibiting the growth of leukemic cells.<sup>54,55</sup> In a study by Liu *et al.*, in 2015 reported that Tet suppressed the proliferation of human prostate cancer cells DU145 and PC-3 by inhibiting the PI3K-Akt signalling pathway, and the compound inhibited the migration and invasion of the cancer cells.<sup>56</sup> Wu *et al.*, in 2014 reported that the compound inhibited the proliferation and invasion of glioma U87 cells mainly by inhibiting the ADAM17 expression, which is a crucial component in the proteolytic cleavage of collagen IV of the ECM and also by downregulating the PI3K/Akt signalling.<sup>57</sup> The antitumor effects of Tet on the proliferation of rat glioma cells, RT-2 were evaluated by Chen *et al.*, in 2009. Treatment decreased the expression of VEGF and inhibited the angiogenesis in subcutaneous gliomas.<sup>58</sup> The *in vitro* and *in vivo* analysis on the effect of Tet in reversing the multi-drug resistance was studied by Fu *et al.*, and they found Tet as a potent P-gp inhibitor and also Tet increased the accumulation of vincristine in MDR KBc200 cells. The studies were carried out in human epidermoid carcinoma KBv200 cells and KBv200 cell xenograft model in nude mice.<sup>59</sup> The synergistic effect of Tet with cisplatin was studied by Zhang *et al.*, and the treatment could significantly enhanced the cytotoxicity in ovarian cancer cells, NIH:OVCAR-3 and A 2780, mainly by modulating the wnt/cadherin pathway.<sup>60</sup>

**Table.1.2.** Anticancer studies of Tetrandrine

Compound/ Combination	Type of study	Cancer type/ cells	Molecular mechanism	References
Tetrandrine	<i>In vitro</i>	Pancreatic cancer(PANC-1) TNBC (MDA MB 231 )	Elevated ROS levels Upregulation of caspase 8,9 and 3	31



Tetrandrine	<i>in vitro</i>	Cervical (HeLa), breast (MCF-7, MDA MB 231)	Apoptosis induced caspase activation via ROS	32
Tetrandrine	<i>In vitro &amp; in vivo</i>	Human breast adenocarcinoma	Potent inhibitor of P-gp mediated MDR  Lowered cell membrane fluidity	33
Tetrandrine + arsenite	<i>In vitro</i>	Human breast cancer (MCF-7)	Upregulated FOXO3a, downregulated cyclin D1 & survivin  G0/G1 phase arrest and induced autophagy	34
Tetrandrine	<i>In vitro</i>	Renal cell carcinoma (786-O, 769-P)	Activation of caspases, upregulation of cell cycle regulatory proteins p21 & p27	35
Tetrandrine	<i>In vitro</i>	Human lung adenocarcinoma (A549)	Induces cell cycle arrest at G1 phase, activation of caspase 3, decrease in cellular tubulin level	36
Tetrandrine H1 (derivative)	<i>In vitro</i>	Non-small cell lung cancer	DR-5 dependent apoptosis, activated ER stress by enforcing the expression of Bip/GRP78, IRE1 $\alpha$ , peIF2 $\alpha$ and CHOP	37
Tetrandrine	<i>In vitro</i>	Lung carcinoma (A549)	Downregulated Akt & ERK phosphorylation	38
Tetrandrine	<i>In vitro</i>	Hepatoma cell line (HepG2)	Activation of caspase 3, cleavage of PARP	39
Tetrandrine	<i>In vitro</i>	Hepatocellular carcinoma (Huh-7)	P53 independent intrinsic apoptosis pathway, induces G1 phase cell cycle arrest, downregulated the expression of survivin	40

Tetrandrine	<i>In vitro</i>	Hepatic stellate cells (T-HSC/ CI-6)	Activation of caspase 3	44
Tetrandrine	<i>In vitro &amp; in vivo</i>	Hepatic stellate cells (HSC-T6)	Inhibited NF- $\kappa$ B transcription, I $\kappa$ B $\alpha$ phosphorylation & ICAM-1 mRNA expression	45
Tetrandrine	<i>In vitro</i>	Rat hepatocytes (HL-7702)	Promotes mitochondrial dysfunction through ROS generated by CYP450	46
Tetrandrine	<i>In vitro &amp; in vivo</i>	Human hepatocellular carcinoma (Huh7 & HepG2)	Apoptosis by activating ROS and repressing Akt signaling	41
Tetrandrine	<i>In vitro</i>	Human hepatoblastoma (HepG2)	Induced G1 phase arrest Increase expression of p53, p21/WAF1 protein Enhanced Fas/Apo-1 its ligands mFasL & sFasL	42
Tetrandrine + Sorafenib	<i>In vitro &amp; in vivo</i>	Hepatoma cells (BEL7402, FHCC98) Hepatoblastoma cell (HepG2) Colon cancer cell (HCT116, RKO, DLD1)	Induced mitochondria mediated apoptosis Enhanced accumulation of intracellular ROS	43
Tetrandrine	<i>In vitro</i>	Human colon cancer (HT-29)	Induced dephosphorylation of Akt, Activation of nuclear translocation of GSK3 $\beta$ and upregulation of p27 <sup>kip1</sup> G1 cell cycle arrest	47

			Inhibits PI3K/AKT/GSK3 $\beta$ pathway Induce cyclin D1 phosphorylation	
Tetrandrine	<i>In vitro</i>	Mouse Colon cancer (CT-26)	Increase the expression of ERK1/2 & p38MAPK	48
Tetrandrine + 5-FU	<i>In vitro &amp; in vivo</i>	Colorectal cancer (SW480, HCT116)	Decreased $\beta$ -catenin level	49
Tetrandrine	<i>In vitro &amp; in vivo</i>	Mouse Endothelial cell (EOMA)	Induced G1/S phase, downregulated cyclin D, Cyclin E and CDKs Induced Intracellular ROS accumulation	50
Tetrandrine	<i>In vitro</i>	Human bladder cancer cells (5637, T24)	Induced apoptosis by activation of caspase 9, caspase 8 and caspase 3 PARP cleavage	51
Tetrandrine	<i>In vitro &amp; in vivo</i>	Human gastric cancer (BGC-823)	Upregulated Bax, Bak, Bad, Caspase 3 & 9, apaf 1 Induced release of Cyt c Downregulated Bcl-2, Bcl-xl	52
Tetrandrine + Paclitaxel (NanoParticle)	<i>In vitro</i>	Gastric carcinoma (BGC-823)	Induced intracellular ROS production. Inhibition of ROS dependent Akt pathway	53
Tetrandrine	<i>In vitro</i>	Leukemia (U 937)	Activation of JNK, ROS mediated caspase activation, PKC- $\delta$ activation	54
Tetrandrine	<i>In vitro</i>	Leukemic cell (U937)	Induced nuclear condensation Induced non Ca <sup>2+</sup> dependent apoptosis	55

Tetrandrine	<i>In vitro</i>	Human prostate cancer (PC-3, DU 145)	Activated caspase cascade, inhibited PI3K-Akt signal pathway	56
Tetrandrine	<i>In vitro</i>	Glioma (U87)	Downregulating ADAM 17 and PI3K-Akt signalling	57
Tetrandrine	<i>In vitro &amp; in vivo</i>	Rat Glioma (RT-2)	Decreased expression of VEGF Inhibited angiogenesis in subcutaneous gliomas	58
Tetrandrine	<i>In vitro &amp; in vivo</i>	Human epidermoid carcinoma (KB & KBv200)	Reversed the resistance to vincristine in KBv200 Inhibited azidopine photo affinity labelling of P-gp & increase accumulation of vincristine in MDR KBv200	59
Tetrandrine + Cisplatin	<i>In vitro &amp; in vivo</i>	Ovarian cancer (NIH:OVCAR-3 & A 2780)	Modulate the Wnt/ $\beta$ -catenin signalling pathway	60

### 1.5.2 Berbamine

Berbamine (Berb) is another well explored BBIQ used in the cancer therapy as the compound can stimulate normal haematopoiesis and can enhance the immune functions in cancer patients. In leukemic cells NB4, the study conducted by Ying *et al.*, in 2007, Berb induces the activation of caspase 3 and downregulated the transcription of the proliferative and survival protein, survivin mRNA. Thereby inducing apoptosis in human acute promyelocytic leukemia.<sup>61</sup> In imatinib resistant human leukemic cell, K562-r, Berb treatment increased chemosensitivity of the resistant cells to imatinib by downregulating *mdr-1* mRNA and P-gp expression. The compound treatment induced apoptosis by inhibiting the anti-apoptotic proteins, Bcl-2 and Bcl-xl and also upregulated Bax and led to the release of cytochrome c into cytosol. The findings were from the study conducted by Wei *et al.*, in 2009.<sup>62</sup> In another study conducted by Liang *et al.*, in 2011, Berb induced G1 phase cell cycle arrest in chronic myeloid leukemic cell, KU812 and the expression of

smad-3 protein was upregulated and downregulated the anti-apoptotic proteins Bcl-2 and Bcl-xl, thereby controlling the leukemic proliferation.<sup>63</sup>

Berbamine against Liver cancer: The effect of Berb against hepatoma cell SMMC7721 was evaluated by Wang *et al.*, the compound induced G0/G1 phase cell cycle arrest. The proliferation was inhibited by apoptosis, which is evident from the upregulation of caspase3 and 9 also led to the depolarization of mitochondrial membrane.<sup>64</sup> The *in vitro* and *in vivo* studies conducted by Wang *et al.*, in 2009 revealed the inhibition in the proliferation of hepatocellular carcinoma with Berb treatment. The *in vitro* studies were carried in HepG2 cells. Treatment induced the upregulation of Fas, p53, caspase 3,8 and 9. In HepG2 human HCC xenograft model of nude mice, treatment caused the reduction in tumor volume. Thus, they found that Berb can effectively inhibit the cancer growth.<sup>65</sup> Berbamine improved the responsiveness of sorafenib in hepatocellular carcinoma cells HepG2 and SK-HEP-1. It induced Src phosphorylation in Na<sup>+</sup>/K<sup>+</sup> ATPase dependent manner and activated the p38 MAPK and EGFR-ERK pathways. This was evident from the study conducted by Yang *et al.*, in 2021.<sup>66</sup> In another study by Yu *et al.*, in hepatocellular carcinoma cell, SMMC-7721, Berb increased the expression of Cx32 expression and thereby increasing the gap junctions. The enhanced gap junction and inhibition on the PI3K/Akt signalling pathway inhibited invasion and migration of the liver cancer cells.<sup>67</sup> The *in vitro* and *in vivo* analysis of Berb on the liver cancer revealed the target as Ca<sup>2+</sup>/calmodulin-dependent protein kinaseII, thereby suppressing the tumor growth. This study by Meng *et al.*, also revealed that the treatment with Berb downregulated the self-renewal abilities of liver cancer initiating cells.<sup>68</sup> So, Berbamine is found to be very effective against liver cancer and even it suppresses the survival of liver cancer initiating cells.

Hu *et al.*, in 2019 conducted experiments in Pancreatic cancer cells Panc-1 and Miapaca-2 and concluded that Berbamine enhanced the efficacy of EGFR target inhibitor, Gefitinib by inhibiting the STAT3 phosphorylation.<sup>69</sup> In another study, the combination therapy of Berbamine with Gemcitabine, in pancreatic cancer cells Bxpc-3 and Panc-1, Jin *et al.*, found that the combination treatment upregulated the pro apoptotic proteins Bax, Bid, p21 and TGF- $\beta$  receptor II and downregulated the expression of Smad-7, c-Myc and cyclin D1. Therefore Berb can activate the TGF- $\beta$ /smad signalling pathway to control the proliferation of cancer cells.<sup>70</sup>

In a study conducted by Zhu *et al.*, Berb reduced the STAT3 phosphorylation in Head and neck squamous cell carcinoma, along with radiation. The combination also decreased the Bax/Bcl-2 ratio. The *in vivo* experiments, also showed the efficacy of Berb + radiation in controlling the growth of tumor.<sup>71</sup> Berb's efficacy in inhibiting the growth of glioblastoma cells (U87MG) was studied *in vitro* and *in vivo* by Kim *et al.*, in 2021. The compound reduced the expression of VEGF/VEGFR2, CaMKII $\gamma$  signalling pathways. Also it reduced the *in vivo* neovascularisation and tumor growth in CAM model.<sup>72</sup> In another study by Liang *et al.*, berbamine has been identified as a NF- $\kappa$ B inhibitor in myeloma cells. Berb treatment induced cell cycle arrest at G1 phase. It also induced the upregulation of A20 protein, and downregulated the IKK $\alpha$ , P-I $\kappa$ B $\alpha$ , thereby blocking the NF- $\kappa$ B pathway. It inhibited the nuclear localization of p65 in human myeloma cells (KM3 cells).<sup>73</sup> In gastric cancer cells, SGC-7901 and BGC-823, Li *et al.*, conducted experiments and found that the compound induced G0/G1 phase cell cycle arrest and inhibited the expression of BRD4. Thus being a BRD4 inhibitor, Berb induced the apoptosis and inhibited the proliferation.<sup>74</sup>

The effect of Berb against lung cancer was also explored. In a study by Hou *et al.*, they evaluated the efficacy of the compound in controlling the growth of lung cancer through both *in vitro* and *in vivo* studies. Compound induced dose dependent cell inhibitory effect in A549 cells and in nude mice with prolonged survival time.<sup>75</sup> Berb downregulated the anti-apoptotic protein Bcl-2 and upregulated the pro apoptotic protein Bax, thereby inducing the cell death and controlling the tumor growth in A549 cells in the studies conducted by Duan *et al.*, in 2010.<sup>76</sup> Liu *et al.*, in 2021 analyzed that Berb inhibited the PI3K/Akt and MDM2-p53 signalling pathway in lung cancer cells, A549 & PC9. In the same study, they conducted *in vivo* experiments in xenograft mouse models, and concluded that the compound treatment significantly reduced the tumor volume. These studies suggests Berb as a potential candidate against lung cancer.<sup>77</sup>

Wang *et al.*, conducted experiments in human breast cancer cells (MDA MB 231 & MDA MB 435S), and found that Berb could reduce the Bcl-2/Bax ratio and VEGF secretion. It also decreased the activation of pro MMP-2 and Pro MMP-2. The treatment also reduced the Akt and NF- $\kappa$ B signalling pathway, thereby inhibiting the proliferation and metastasis of the highly metastatic breast cancer cells.<sup>78</sup> In another study by Liu *et al.*, in Triple negative cancer cells (MDA MB 231 & MCF-7), the compound downregulated the proliferative signalling pathway by downregulating the expression of PI3K, Akt, P-Akt, COX-2, LOX, MDM2 and mTOR.<sup>79</sup> based on the evidences from the studies conducted by

Han *et al.*, in bladder cancer cells (5637 & T24), cell cycle arrest at S phase was induced by Berb, it also suppressed the proliferative pathway NF- $\kappa$ B signalling. Treatment induced the ROS mediated apoptosis, thereby inhibiting the tumor cell growth.<sup>80</sup>

The effect of Berb on the proliferation of ovarian cancer cell, SKOV3 was studied by Zhang *et al.*, in 2018 and found that it could suppress the proliferation by activating the caspase cascade and inhibited the Wnt/ $\beta$ -catenin signalling. Treatment induced the cell cycle arrest at G0/G1 phase and downregulated the Bcl-2 protein expression.<sup>81</sup> Zhang and his team in 2018 studied the efficacy of Berb against colorectal cancer cells and found that Berb induced the cell cycle arrest at G0/G1 phase and induced mitochondrial membrane depolymerisation and upregulated the p53, caspase-3, caspase-9, Bax and Cleaved PARP. Thereby, inducing the apoptosis of the colorectal cancer cells (HCT116 and SW480).<sup>82</sup> In another study by Mou *et al.*, in colorectal cancer cell, HT29, Berb induced the activation of caspase 3 & 9 and increased the Bax/Bcl-2 ratio. Also, it triggered the autophagic vesicle development by increased expression of LC3B-1, ATG-5, ATG-12 and Beclin-1. The compound could inhibit the MEK/ERK signalling pathway in HT 29 cells.<sup>83</sup> Berb inhibited the proliferation of prostate cancer cells PC-3 and LNCaP by inducing apoptosis as evident from the studies by Zhao *et al.*, in 2016. An increase in Bax/Bcl-2 and the activation of caspase 3 and 9 were observed. Also, the treatment induced the mitochondrial swelling, vacuolization and formation of fused cristae. Thereby inducing mitochondrial mediated apoptosis both *in vitro* and *in vivo* model.<sup>84</sup>

**Table.1.3.** Anticancer studies of Berbamine

Compound/ Combination	Type of study	Cancer type/ cells	Molecular mechanism	References
Berbamine	<i>In vitro</i>	Leukemic cells (NB4 cells)	Activated caspase 3 ↓ Survivin mRNA	61
Berbamine	<i>In vitro &amp; in vivo</i>	Human leukemia cells (K562-r cells)	Increased chemosensitivity of the cells to imatinib ↓ <i>mdr-1</i> mRNA & P-gp protein, Bcl-2, Bcl-xl ↑ Bax, cytoplasmic cyt c	62

Berbamine	<i>In vitro</i>	Chronic myeloid leukemia (KU812)	Induced G1 phase arrest Upregulated transcription of Smad 3, p21 ↓ Bcl-2 & Bcl-xL	63
Berbamine	<i>In vitro</i>	Human hepatoma cells (SMMC7721)	Cell cycle arrest at G0/G1 phase Induced loss of mitochondrial membrane potential ↑ Caspase 3 & caspase 9	64
Berbamine	<i>In vitro &amp; in vivo</i>	Hepatocellular carcinoma (HepG2)	↑ Fas & p53 , Caspase 3,8,9 Depolarization of mitochondrial membrane	65
Berbamine + Sorafenib	<i>In vitro</i>	Hepatocellular carcinoma (HepG2 & SK-HEP-1)	Induces Src phosphorylation in Na <sup>+</sup> /K <sup>+</sup> ATPase-dependent manner Activation of p38 MAPK & EGFR-ERK pathways	66
Berbamine	<i>In vitro</i>	Human liver cancer (SMMC-7721)	Increased the Cx32 expression Increased gap junction function Decreased expression of PI3K & P-Akt	67
Berbamine	<i>In vitro &amp; in vivo</i>	Liver cancer (HepG2, PLC/PRF/5, SK-Hep-1, and SNU398)	Targeted CAMKII Downregulated self-renewal abilities of liver cancer initiating cells	68
Berbamine + Gefitinib	<i>In vitro</i>	Pancreatic cancer cells (Panc-1 & Miapaca-2)	Inhibits STAT3 phosphorylation	69



Berbamine + Gemcitabine	<i>In vitro</i>	Pancreatic cancer cells (Bxpc-3 & Panc-1)	Upregulation of Bax, Bid, p21 & TGF- $\beta$ receptor II Downregulation of Bcl-2, Bcl-xL, Smad 7, c-Myc & Cyclin D1 Activated TGF- $\beta$ / smad signaling pathway	<sup>70</sup>
Berbamine + Radiation	<i>In vitro &amp; in vivo</i>	Head & neck squamous cell carcinoma (FaDu & KB)	Reduction in STAT3 phosphorylation $\downarrow$ Bax/Bcl-2 ratio	<sup>71</sup>
Berbamine	<i>In vitro &amp; in vivo</i>	Glioblastoma cells (U87MG), endothelial (HUVEC)	$\downarrow$ VEGF/VEGFR2, CaMKII $\gamma$ , TrKB, HIF-1 $\alpha$	<sup>72</sup>
Berbamine	<i>In vitro</i>	Human Myeloma cells (KM 3 cells)	Cell cycle arrest at G1 phase $\uparrow$ A20 protein $\downarrow$ IKK $\alpha$ , P-I $\kappa$ B $\alpha$ , NF- $\kappa$ B downstream targets Inhibition of p65 nuclear localization	<sup>73</sup>
Berbamine	<i>In vitro</i>	Gastric cancer cells (SGC-7901, BGC-823)	Induces G0/G1 phase cell cycle arrest BRD4 inhibitor	<sup>74</sup>
Berbamine	<i>In vitro &amp; in vivo</i>	Lung cancer (A549)	Induced dose dependent cell inhibitory effect	<sup>75</sup>
Berbamine	<i>In vitro</i>	NSCLC (A549)	Downregulated Bcl-2 Upregulated Bax	<sup>76</sup>
Berbamine	<i>In vitro &amp; in vivo</i>	Lung cancer cells (A549 & PC9)	Inhibited PI3K/Akt & MDM2-p53 signaling pathway Downregulated c-Maf	<sup>77</sup>

Berbamine	<i>In vitro</i>	Human breast cancer (MDA MB 231 & MDA MB 435 S)	Reduces Bcl-2/Bax ratio Reduced VEGF secretion Decreases pro MMP-9/pro MMP-2 activation Suppresses Akt & NF- $\kappa$ B by reducing the phosphorylation of C-Met & Akt	78
Berbamine	<i>In vitro</i>	TNBC (MDA MB 231 & MCF-7 )	Downregulated PI3K, Akt, P- Akt, COX-2, LOX, MDM2 & mTOR Upregulated p53	79
Berbamine	<i>In vitro &amp; in vivo</i>	Bladder cancer cell (5637 & T24)	cell cycle arrest at S phase Suppresses NF- $\kappa$ B pathway Induced ROS mediated apoptosis Upregulated p21 & p27 Downregulated cyclin D, cyclin A2, CDK-2, p65, P- p65, P-I $\kappa$ B $\alpha$	80
Berbamine	<i>In vitro &amp; in vivo</i>	Ovarian cancer cells (SKOV3 cells)	Cell cycle arrest at G0/G1 phase Increased cleaved caspase-3, and Caspase-9 and Bax Downregulated Bcl-2 Inhibited Wnt/ $\beta$ -catenin signalling	81
Berbamine	<i>In vitro &amp; in vivo</i>	Colorectal cancer (HCT116, SW480)	Cell cycle arrest at G0/G1 phase Decreased mitochondrial membrane potential Upregulated p53, Caspase-3, caspase-9, Bax, PARP Decreased Bcl-2 expression	82

Berbamine	<i>In vitro</i>	Colon cancer (HT29)	Activation of capase 3 & 9 Increased Bax/ Bcl-2 ratio Triggered autophagic vesicle development Increased LC3B-1, ATG-5, ATG-12 & Beclin-1 Blocked MEK/ERK signalling pathway	<sup>83</sup>
Berbamine	<i>In vitro &amp; in vivo</i>	Prostate cancer (PCa, LNCaP)	Induced mitochondrial swelling, vacuolization & formation of fused cristae Increased Bax, active capase 9 & caspase 3	<sup>84</sup>

### 1.5.3 Fangchinoline

Fangchinoline (Fang) is an emerging anti-cancer candidate in terms of its antineoplastic potential. There are a few reports on its cancer inhibiting studies. In lung cancer cell, A549 Guo and his team conducted studies in 2015 and found that the compound Fang inhibited the phosphorylation of FAK at Tyr397 position, which makes the compound a potent kinase inhibitor of FAK and controlling the growth and proliferation of cancer cells.<sup>85</sup> *Jung et al.*, studied the effect of Fang against multiple myeloma and it was found to be very effective in inhibiting the proliferation of myeloma by modulating the oncogenic STAT3 signaling pathway. Fang attenuated the DNA binding ability of STAT3 and its translocation into the nucleus in U266 cells. Increased SHP-1 levels and induced apoptosis also effectively reduced the tumor progression in xenograft mouse model.<sup>86</sup> In bladder cancer cells, T24 and 5637, *Fan et al.*, conducted studies with Fang and concluded that it induced concentration dependent cell death and the proliferative biomarker protein, PCNA was downregulated. The treatment induced both apoptosis and autophagy in bladder cancer cells. Fang also inhibited the mTOR and decreased the intracellular ATP levels, thus posing a challenge for the energy requirement of cancer cells.<sup>87</sup> The *in vitro* studies by *Wang et al.*, in 2011 with Fang in different hepatocellular carcinoma cells (HepG2 and PLC/PRF/5 cells), revealed the involvement of autophagy mediated cell death. Compound induced

nuclear translocation of p53 and selective transactivation of *sestrin2*, and finally mTOR independent autophagic cell death.<sup>88</sup>

The effect of Fang against breast cancer was well explored by various groups in triple negative breast cancer cells, MDA MB 231 and MCF-7. Fang treatment induced G1 phase cell cycle arrest, reduced the expression of major proteins involved in the regulation of cell cycle, and activated various caspases involved in the process of apoptosis. They found that the compound enhanced the mitochondrial cyt c release, and inhibited the Akt/GSK-3 $\beta$ / cyclin D1 signaling pathways. Also downregulated the expression of MMP-2, MMP-9 and NF- $\kappa$ B levels.<sup>89-92</sup> These findings suggest that, the fangchinoline as a potent drug candidate against breast cancer.

In human chronic myeloid leukemic cell KBM5 and Multiple myeloma cell U266, studies by Jung *et al.*, revealed that Fang downregulated the expression of NF- $\kappa$ B and the activation of AP-1. It attenuated the IKK phosphorylation. Treatment increased TNF- $\alpha$  induced apoptosis.<sup>93</sup> The *in vitro* and *in vivo* assessment conducted by Bao *et al.*, in 2021 in the conjunctival melanoma (CM) cells, revealed the fang inhibited the proliferation of CM cells, compound downregulated the expression of c-Myc by binding to the FUBP2. Also they found that treatment reduced the expression levels of BRCA1 and RAD51.<sup>94</sup> Jung and his team members in 2022 conducted studies in human colon cancer cells, HCT116 and SNU-1040, and found that Fang restricted the epithelial-mesenchymal transition. The treatment suppressed the expression of fibronectin, vimentin, MMP-2, MMP-9, N-cadherin, Twist and snail levels. And they observed an enhanced the expression of occluding & E-cadherin, also downregulated the mTOR and Wnt/ $\beta$ -catenin signalling pathways, thereby controlling the metastasis and spread of colon cancer.<sup>95</sup> Tian *et al.*, found that Fang could inhibited the expression of PI3K and repressed the migratory and invasive potential in gastric cancer cell, SGC-7901.<sup>96</sup> In human prostate cancer cells, PC-3 and LnCaP, Li *et al.*, 2015 carried out studies and revealed that fangchinoline treatment induced the G0/G1 phase cell cycle arrest. The *in vivo* studies in tumor bearing nude mice, reduced the tumor growth and volume upon treatment with Fang also caused decrease in proteasome activities. They also recorded that treatment induced the accumulation of ubiquitinated proteins Ub-I $\kappa$ B $\alpha$ , Ub-p27 and Ub-Bax.<sup>97</sup> All these data, shed light on how this compound can be utilized against broad spectrum of cancers.

**Table.1.4.** Anticancer studies of Fangchinoline

<b>Compound/ Combination</b>	<b>Type of study</b>	<b>Cancer type/ cells</b>	<b>Molecular mechanism</b>	<b>References</b>
Fangchinoline	<i>In vitro</i> & <i>in vivo</i>	Lung cancer (A549)	Inhibited phosphorylation of FAK (Tyr397) & its downstream pathways	85
Fangchinoline	<i>In vitro</i> & <i>in vivo</i>	Multiple myeloma (U266)	Inhibited STAT3 Attenuated DNA binding ability of STAT3 & its translocation into the nucleus Increased SHP-1 levels Increased ROS production & altered GSSH/GSH ratio	86
Fangchinoline	<i>In vitro</i>	Bladder cancer (T24 & 5637)	Downregulated PCNA expression Increased cleavage of caspase-3 Upregulated LC3-II/LC3-I ratio Downregulated p62 levels Inhibited mTOR & reduced intracellular ATP levels	87
Fangchinoline	<i>In vitro</i>	Hepatocellular carcinoma (HepG2 & PLC/PRF/5 cells)	Induced autophagy Induced nuclear translocation of p53, selective transactivation of <i>sestrin2</i> and mTOR independent autophagic cell death	88
Fangchinoline	<i>In vitro</i>	Breast cancer cells (MDA MB 231 & MCF-7)	Induced G1 phase arrest Reduced cyclin D1, cyclinD3 & cyclin E levels	89

			Increased CDK inhibitors, p21/WAF1 & p27/KIP1 Inhibited kinase activities of CDK2, CDK4 & CDK6	
Fangchinoline	<i>In vitro</i>	Breast adenocarcinoma (MDA MB 231)	Activation of Caspase-3,8,9 Enhanced mitochondrial cyt c release Increased Bax Decreased Bcl-2 & P-Akt	<sup>90</sup>
Fangchinoline	<i>In vitro</i>	Breast cancer (MDA MB 231)	Inhibition on Akt/ GSK-3 $\beta$ / Cyclin D1 signaling pathways Increased Bax/Bcl-2 ratio Cell cycle arrest at G1 phase Decreased PCNA & cyclin D1 Reduced the phosphorylation of Akt & GSK-3 $\beta$	<sup>91</sup>
Fangchinoline	<i>In vitro</i>	Breast cancer (MDA MB 231)	Downregulated MMP-2, MMP-9 and NF- $\kappa$ B levels Increased I $\kappa$ B levels	<sup>92</sup>
Fangchinoline	<i>In vitro</i>	Human chronic myeloid leukaemia (KBM5), Multiple myeloma (U266)	Downregulated NF- $\kappa$ B & AP-1 activation Attenuated IKK phosphorylation Increased TNF- $\alpha$ induced apoptosis	<sup>93</sup>
Fangchinoline	<i>In vitro &amp; in vivo</i>	Conjunctival melanoma (CM- AS16, CRMM1, CRMM2, CM2005- 1)	Suppressed homologous recombination directed by DNA repair by binding with FUBP2 Downregulated BRCA1& RAD51	<sup>94</sup>

Fangchinoline	<i>In vitro</i>	Human colon cancer (HCT-116 & SNU-1040)	Suppressed fibronectin, vimentin, MMP-2, MMP-9, N-cadherin, Twist & Snail levels Enhanced occludin & E-cadherin Downregulated c-Met/PI3K/Akt/ mTOR & Wnt/ $\beta$ -catenin cell signaling	<sup>95</sup>
Fangchinoline	<i>In vitro</i>	Gastric cancer (SGC 7901)	Inhibits expression of PI3K Represses migratory & invasive potential	<sup>96</sup>
Fangchinoline	<i>In vitro</i> & <i>In vivo</i>	Human prostate cancer (PC-3 & LnCaP)	Cell cycle arrest at G0/G1 phase Induced proteasome inhibition Induced accumulation of ubiquitinated proteins Ub-I $\kappa$ B $\alpha$ , Ub-p27, Ub-Bax	<sup>97</sup>

#### 1.5.4 Cycleanine & Curine

Cycleanine and curine were not that much explored as compared to that of Tetrandrine, Berbamine and Fangchinoline. A very few works are reported on the anticancer efficacy of these compounds. In a computational study, by Nwaeful *et al.*, in 2022, the impact of cycleanine in cancer research was explored. They investigated cycleanine as a PARP1 inhibitor or activator of pro-caspase 3. The compound established stable intermolecular interactions at the active sites of PARP-1, thereby inhibiting the PARP-1. The compound also acted as an allosteric activator of procaspase-3.<sup>98</sup> Also in another study by Uche *et al.*, Cycleanine inhibited the proliferation of ovarian cancer cells, Ovar-8, A2780, Ovar-4 and Igrov-1. Compound induced activation of caspase 3/7 and cleavage of PARP.<sup>99</sup>

Gong *et al.*, in 2017 studied the effect of curine in various cell lines and found that (-) Curine induced cell cycle arrest at G1 phase in hepatocellular carcinoma cells HepG2 and Huh-7. The compound induced cell death irrespective of the p53 status of the cell, they found that it also downregulated the expression of cyclin D1 and upregulated p21 levels.<sup>100</sup>

The effect of curine against leukemic cells, HL-60 was studied by Dantas *et al.*, in 2015 and they revealed that compound induced plasma membrane damage and phosphatidyl serine externalization. Curine treatment led to the depolarisation of the mitochondrial membrane.<sup>101</sup>

## 1.6 Limitations of chemotherapeutic drugs

Despite the improved effectiveness and enhanced survival provided by modern anti-cancer treatments, the side effects and long-term consequences of chemotherapy continue to be a significant worry for both patients and clinicians. Existing drugs or alternative strategies designed to mitigate the adverse effects of chemotherapy are often only partially effective. Moreover, they may not adequately address potential long-term consequences or could even introduce additional side effects, further contributing to patient discomfort. Nausea and vomiting are the most feared side effects for patients undergoing chemotherapy gastrointestinal side effects are also common, and which can be distressing and potentially fatal for cancer patients. Many drugs cause local ulceration and pain by inducing oral and gastrointestinal mucositis which will in turn cause anorexia, malabsorption, weight loss and fatigue. Some drugs are even known to cause central and peripheral nephrotoxicity.<sup>102</sup> Some key limitations include:

1. **Non-Specificity:** Chemotherapeutic drugs often lack specificity, affecting both cancerous and normal rapidly dividing cells. This leads to numerous side effects, such as nausea, hair loss, and compromised immune function.
2. **Resistance Development:** Cancer cells can develop resistance to chemotherapy over time, rendering initially effective treatments ineffective. This resistance may occur due to genetic mutations, drug efflux pumps, or changes in the tumor microenvironment.
3. **Toxicity:** Chemotherapy can cause systemic toxicity, affecting healthy tissues and organs. This can result in severe adverse effects, impacting the patient's quality of life and leading to treatment interruptions or dose reductions.
4. **Limited Efficacy in Advanced Stages:** Chemotherapy may be less effective in advanced stages of cancer when the disease has metastasized or when tumors have become resistant to treatment. This often necessitates the exploration of alternative treatment modalities.



5. **Impact on Normal Cell Division:** Since chemotherapeutic drugs target rapidly dividing cells, they may affect normal tissues with high cell turnover rates, such as the bone marrow and gastrointestinal lining. This can lead to conditions like anemia, thrombocytopenia, and gastrointestinal issues.
6. **Immunosuppression:** Chemotherapy can suppress the immune system, making patients more susceptible to infections. This may result in prolonged recovery periods and increased vulnerability to opportunistic diseases.

Understanding and addressing these limitations is crucial for advancing cancer treatment strategies and improving patient outcomes. Researchers are continually working to develop targeted therapies, immunotherapies, and combination treatments to overcome these challenges in the field of oncology.

### **1.7 Advancement of drug delivery system for better therapeutic outcome**

Advancing drug delivery systems is essential for achieving better therapeutic outcomes in medical treatments. By improving the precision, efficiency, and targeted delivery of drugs, advancement to maximize the therapeutic effects can be fulfilled while minimizing side effects. This involves the development of innovative technologies and formulations that can enhance drug absorption, prolong drug release, and optimize drug distribution to specific target tissues or cells.

The goal is to overcome challenges such as poor drug solubility, limited bioavailability, and non-specific distribution. Novel drug delivery systems may include biocompatible nanoparticles, liposomes, micelles, and other carrier systems designed to encapsulate and transport drugs to the desired site of action. Additionally, controlled-release formulations help maintain therapeutic drug levels in the body over an extended period, reducing the need for frequent dosing.

Advancements in drug delivery systems not only improve treatment efficacy but also enhance patient compliance and overall quality of life. These innovations contribute to the evolution of personalized medicine, tailoring treatments to individual patient needs and characteristics. Overall, the continuous progress in drug delivery systems holds the promise of revolutionizing medical therapeutics and optimizing patient outcomes.

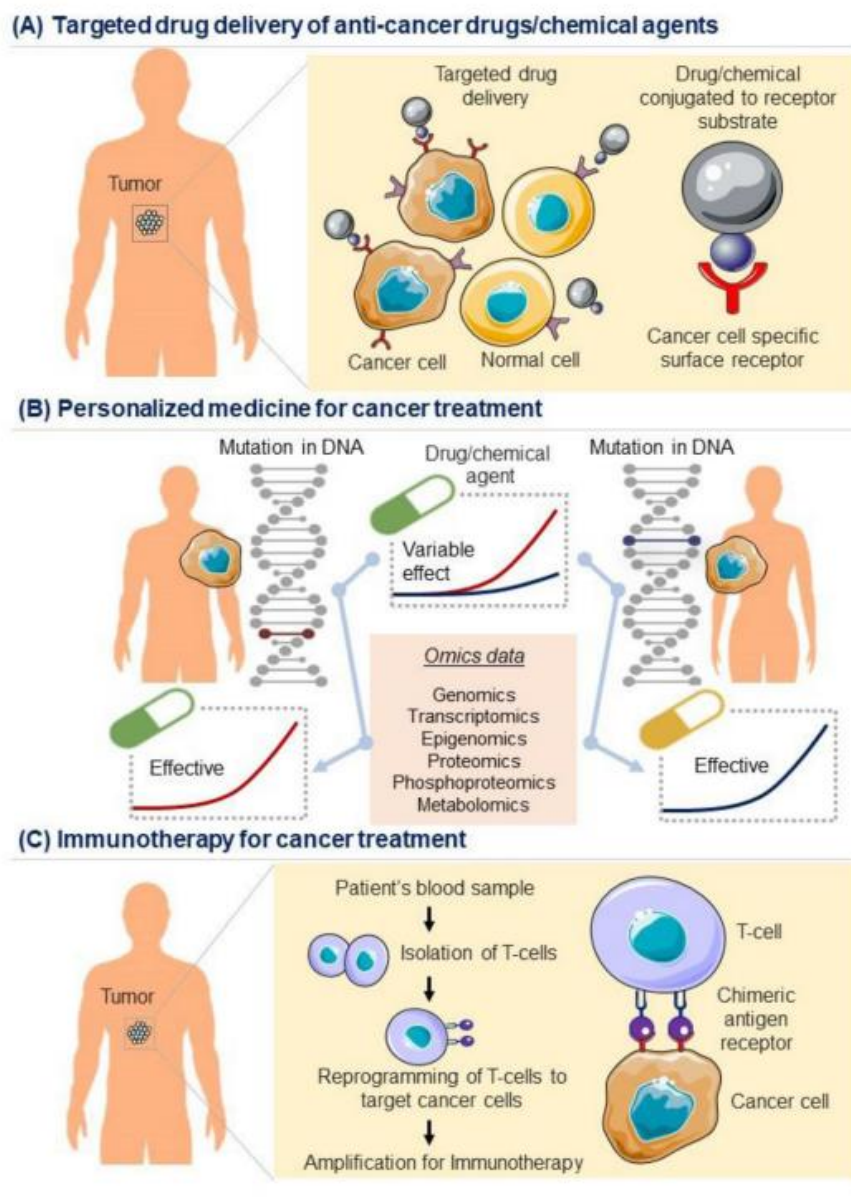


Figure 1.6 Illustration depicting targeted approaches for cancer therapy (adapted from *Genes & Diseases* (2023) 10, 1367e1401)

## 1.8 Conclusion

The projected global cancer burden for 2040 stands at 28.4 million cases, indicating a substantial 47% increase from the 2020 cancer incidence. The escalating daily occurrence of cancer and the adverse effects associated with current medications underscore the urgency of the development of more therapeutic drugs characterized by reduced side effects and enhanced efficacy. Prioritizing the exploration of natural sources for drug development necessitates the screening of various hits. Establishing a sustainable

infrastructure for disseminating cancer prevention measures and providing cancer care in transitioning countries is paramount for comprehensive global cancer control efforts. In this context, bisbenzylisoquinoline alkaloids emerged as crucial players in cancer treatment, with several from this group currently undergoing clinical trials and they act by interrupting and regulating multiple signalling pathways. Notably, the Menispermaceae family is a prolific source of these alkaloids, prompting the selection of the readily available plant, *Cyclea peltata*, for the study aimed at developing a drug entity with less side effects. The pursuit of such research not only holds promise for expanding our therapeutic arsenal but also contributes to the broader goal of fostering global cancer prevention and care initiatives.

### 1.9 Objectives of the current investigation

With recent advancements in the area of natural product-based drug development especially for cancer therapy, a thorough literature survey regarding the anticancer studies of natural products was done and it shed light on the importance of a group of compounds, bis benzylisoquinoline alkaloids (BBIQ), which occupy a key position in the area of drug development. One of the objectives of this work was a detailed literature analysis of the anticancer studies trailing from BBIQ alkaloids. Menispermaceae family members are a rich resource of such compounds, a commonly available plant from this family is selected for the analysis, ie., *Cyclea peltata*.

The primary focus of this thesis revolves around the scientific validation, *via* the development of an anticancer lead derived from bisbenzylisoquinoline alkaloids found in *Cyclea peltata*. This plant is well-recognized in traditional medicinal practices like Ayurveda and has been extensively used in various formulations, such as Pushyanuga churna, for treating ailments related to the women's reproductive system, especially for reducing the water stagnation in uterine cancer situations. Despite its historical use in addressing issues like as an effective candidate for curing such ailments of the reproductive system, the anticancer potential particularly against cervical cancer, remains largely unexplored. The goal of this research is to investigate the potential of *Cyclea peltata*, specifically focusing on the BBIQ alkaloids present in the plant, as a treatment for the most common cancer affecting the women's reproductive system, ie., cervical cancer. The apoptosis-inducing potential of the most active compound from the plant and the pathway by which the compound can act will be evaluated. In continuation with the above objective,

the antimetastatic and antiangiogenic potential of the potent molecule, phaeanthine will be analyzed in a highly metastatic model and in endothelial cells respectively.

The last decades of advances in the area of nanomedicine and nanotechnology, paved the way forward in the application of these in cancer medicine. Keeping this in mind, the objective of the next chapter was to fabricate a targeted nanodelivery system (TNDS) to improve the therapeutic efficacy of the active lead molecule. For the effective delivery, the nanosystem was conjugated with a peptide, which will target a receptor protein on the surface of the cancer cells. This will enable a targeted delivery leaving the normal cells unharmed. In order to improve the therapeutic efficacy of the TNDS, the molecule Phaeanthine will be co-loaded with another drug molecule, a glycolytic inhibitor, 2-deoxy-D-glucose. The efficacy of the TNDS was studied in cervical cancer cell, HeLa.

### 1.10 References

- (1) Bethesda (MD). *MedlinePlus [Internet]. Bethesda (MD): National Library of Medicine (US); [updated Jun 24; cited 2023 Spetember 10]. Available from: <https://medlineplus.gov/>.*
- (2) Sung, H.; Ferlay, J.; Siegel, R. L.; Laversanne, M.; Soerjomataram, I.; Jemal, A.; Bray, F. Global Cancer Statistics 2020 : GLOBOCAN Estimates of Incidence and Mortality Worldwide for 36 Cancers in 185 Countries. *CA. Cancer J. Clin.* **2021**, 71 (3), 209–249. <https://doi.org/10.3322/caac.21660>.
- (3) Douglas Hanahan and Robert A. Weinberg. The Hallmarks of Cancer. *Cell* **2000**, 100 (7), 57–70. [https://doi.org/10.1016/S0092-8674\(00\)81683-9](https://doi.org/10.1016/S0092-8674(00)81683-9).
- (4) ICMR-NCDIR, B. *Report of National Cancer Registry Program; 2020.*
- (5) Zhang, L.; Demain, A. L. Natural Products and Drug Discovery. *Nat. Prod. Drug Discov. Ther. Med.* **2005**, 3–29. [https://doi.org/10.1007/978-1-59259-976-9\\_1](https://doi.org/10.1007/978-1-59259-976-9_1).
- (6) Cragg, G. M.; Newman, D. J. Discovery and Development of Antineoplastic Agents from Natural Sources. *Cancer Invest.* **1999**, 17 (2), 153–163.
- (7) Newman, D. J.; Cragg, G. M. Natural Products as Sources of New Drugs over the Nearly Four Decades from 01/1981 to 09/2019. *J. Nat. Prod.* **2020**, 83, 770–803. <https://doi.org/10.1021/acs.jnatprod.9b01285>.
- (8) Barbosa-Filho, J.; Vasconcelos Leitão da-Cunha, E.; Gray, A. I. *Alkaloids of the Menispermaceae; 2000; Vol. 54.* [https://doi.org/10.1016/S0099-9598\(00\)54002-4](https://doi.org/10.1016/S0099-9598(00)54002-4).

- (9) Itoh, A.; Saitoh, T.; Tani, K.; Uchigaki, M.; Sugimoto, Y.; Yamada, J.; Nakajima, H.; Ohshiro, H.; Sun, S.; Tanahashi, T. Bisbenzylisoquinoline Alkaloids from *Nelumbo Nucifera*. *Chem. Pharm. Bull.* **2011**, *59* (8), 947–951. <https://doi.org/10.1248/cpb.59.947>.
- (10) Hanahan, D.; Weinberg, R. A. Hallmarks of Cancer: The next Generation. *Cell* **2011**, *144* (5), 646–674. <https://doi.org/10.1016/j.cell.2011.02.013>.
- (11) Arbyn, M.; Weiderpass, E.; Bruni, L.; Sanjosé, S. De; Saraiya, M.; Ferlay, J.; Bray, F. Estimates of Incidence and Mortality of Cervical Cancer in 2018 : A Worldwide Analysis. *lancet Glob. Heal.* **2019**, *4* (19), 1–13. [https://doi.org/10.1016/S2214-109X\(19\)30482-6](https://doi.org/10.1016/S2214-109X(19)30482-6).
- (12) Food and Drug administration. *FDA approves pembrolizumab combination for the first-line treatment of cervical cancer.* [https://www.fda.gov/drugs/resources-information-approved-drugs/fda-approves-pembrolizumab-combination-first-line-treatment-cervical-cancer#:~:text=On October 13%2C2021%2C the Food and Drug Administration,PD-L1 %28CPS ≥1%29%2C as determined by an FDA-appro](https://www.fda.gov/drugs/resources-information-approved-drugs/fda-approves-pembrolizumab-combination-first-line-treatment-cervical-cancer#:~:text=On%20October%2013%2C2021%2C%20the%20Food%20and%20Drug%20Administration,PD-L1%20CPS%20%26gt;=1%29%2C%20as%20determined%20by%20an%20FDA-appro).
- (13) Cragg, G. M.; Grothaus, P. G.; Newman, D. J. Impact of Natural Products on Developing New Anti-Cancer Agents †. **2009**, 3012–3043.
- (14) Mukherjee, A. K.; Basu, S.; Sarkar, N.; Ghosh, A. C. Advances in Cancer Therapy with Plant Based Natural Products. *Curr. Med. Chem.* **2001**, *8*, 1467–1486.
- (15) WFO. *Cyclea Arn. ex Wight.* <http://www.worldfloraonline.org/taxon/wfo-4000010244>.
- (16) Yuliarti, O.; Chong, S. Y.; Goh, K. K. T. Physicochemical Properties of Pectin from Green Jelly Leaf (*Cyclea Barbata* Miers). *Int. J. Biol. Macromol.* **2017**, *103*, 1146–1154. <https://doi.org/10.1016/j.ijbiomac.2017.05.147>.
- (17) Lin, L. Z.; Shieh, H. L.; Angerhofer, C. K.; Pezzuto, J. M.; Cordell, G. A.; Xue, L.; Johnson, M. E.; Ruangrunsi, N. Cytotoxic and Antimalarial Bisbenzylisoquinoline Alkaloids from *Cyclea Barbata*. *J. Nat. Prod.* **1993**, *56* (1), 22–29. <https://doi.org/10.1021/np50091a004>.
- (18) Guinadeau, H.; Lin, L.-Z.; Ruangrunsi, N.; Cordell, G. A. Bisbenzylisoquinoline Alkaloids from *Cyclea Barbata*. *J. Nat. Prod.* **1993**, *56* (11), 1989–1992. <https://doi.org/10.1016/bs.alkal.2018.07.001>.
- (19) Lasushe, K.; Hussain, A.; Prakash, P.; Lal, K.; Choudhury, H.; Deori, C.; Roy, Di. K.; Singh, B.; Upadhaya, K. A Comprehensive Checklist of Threatened Plants of Meghalaya , Northeast India. *J. Asia-Pacific Biodivers.* **2022**, *15* (3), 435–441. <https://doi.org/10.1016/j.japb.2022.03.008>.
- (20) Kupchan, S. M.; Yokoyama, N.; Thyagarajan, B. S. Menispermaceae Alkaloids II- The Alkaloids of *Cyclea Peltata* Diels. *J. Pharm. Sci.* **1961**, *50* (2), 164–167.

- (21) Kupchan, S. M.; Liepa, A. J.; Baxter, R. L.; Hintz, H. P. J. New Alkaloids and Related Artifacts from Cycled Peltata. *J. Org. Chem.* **1973**, *38* (10), 1846–1852. <https://doi.org/10.1021/jo00950a016>.
- (22) Wang, J. Z.; Liu, X. Y.; Wang, F. P. Two New Curine-Type Bisbenzylisoquinoline Alkaloids from the Roots of *Cyclea Wattii* with Cytotoxic Activities. *Chem. Pharm. Bull.* **2010**, *58* (7), 986–988. <https://doi.org/10.1248/cpb.58.986>.
- (23) Valsan, A.; Meenu, M. T.; Murali, V. P.; Malgija, B.; Joseph, A. G.; Nisha, P.; Radhakrishnan, K. V.; Maiti, K. K. Exploration of Phaeanthine: A Bisbenzylisoquinoline Alkaloid Induces Anticancer Effect in Cervical Cancer Cells Involving Mitochondria-Mediated Apoptosis. *ACS Omega* **2023**, *8* (16), 14799–14813. <https://doi.org/10.1021/acsomega.3c01023>.
- (24) Sheng, W. D.; Jiddawi, M. S.; Hong, X. Q.; Abdulla, S. M. Treatment of Chloroquine-Resistant Malaria Using Pyrimethamine in Combination with Berberine, Tetracycline or Cotrimoxazole. *East Afr. Med. J.* **1997**, *74* (5), 283–284.
- (25) Dai, G. Z.; Zeng, B.; Zhang, Y. L.; Lu, Y. X. Intravenous Tetrandrine in Terminating Acute Episodes of Paroxysmal Supraventricular Tachycardia. *Chin. Med. J. (Engl.)* **1990**, *103* (6), 460–463.
- (26) Li, D.; Lu, H.; Li, X.; Quan, Q.; Lu, W. Calcium Channel Blockers in Cirrhotic Patients with Portal Hypertension. *Chin. Med. J. (Engl.)* **1995**, *108* (11), 803–808.
- (27) Ferrier, I. N.; Johnstone, E. C.; Crow, T. J. Clinical Effects of Apomorphine in Schizophrenia. *Br. J. Psychiatry* **1984**, *144*, 341–348.
- (28) Yin, J.; Xing, H.; Ye, J. Efficacy of Berberine in Patients with Type 2 Diabetes Mellitus. *Metab. Clin. Exp.* **2008**, *57*, 712–717. <https://doi.org/10.1016/j.metabol.2008.01.013>.
- (29) Jian-ping, S. H. I.; Hong, Z.; Zhi-dong, Z. Synergistic Effects of Tetrandrine on the Antifungal Activity of Topical Ketoconazole Cream in the Treatment of Dermatophytoses : A Clinical Trial. *Chin. J. Integr. Med.* **2011**, *17* (7), 499–504. <https://doi.org/10.1007/s11655-010-0782-3>.
- (30) Court, J. M. Stitute for Aboriginal Development in Alice Springs . It Is Privately. **2015**, *88* (100), 2015.
- (31) Bhagya, N.; Chandrashekar, K. R.; Prabhu, A.; Rekha, P. D. Tetrandrine Isolated from *Cyclea Peltata* Induces Cytotoxicity and Apoptosis through ROS and Caspase Pathways in Breast and Pancreatic Cancer Cells. *Vitr. Cell. Dev. Biol. - Anim.* **2019**, *55* (5), 331–340. <https://doi.org/10.1007/s11626-019-00332-9>.
- (32) Wang, H.; Liu, T.; Li, L.; Wang, Q.; Yu, C.; Liu, X.; Li, W. Tetrandrine Is a Potent Cell Autophagy Agonist via Activated Intracellular Reactive Oxygen Species. *Cell Biosci.* **2015**, *5* (4), 1–9. <https://doi.org/10.1186/2045-3701-5-4>.

- (33) Fu, L. W.; Zhang, Y. M.; Liang, Y. J.; Yang, X. P.; Pan, Q. C. The Multidrug Resistance of Tumour Cells Was Reversed by Tetrandrone in Vitro and in Xenografts Derived from Human Breast Adenocarcinoma MCF-7 / Adr Cells. *Eur. J. Cancer* **2002**, *38*, 418–426.
- (34) Yao, M.; Yuan, B.; Wang, X.; Sato, A.; Sakuma, K.; Kaneko, K.; Komuro, H.; Okazaki, A.; Hayashi, H. Synergistic Cytotoxic Effects of Arsenite and Tetrandrone in Human Breast Cancer Cell Line MCF-7. *Int. J. Oncol.* **2017**, *51*, 587–598. <https://doi.org/10.3892/ijo.2017.4052>.
- (35) Chen, T.; Ji, B.; Chen, Y. Tetrandrone Triggers Apoptosis and Cell Cycle Arrest in Human Renal Cell Carcinoma Cells. *J. Nat. Med.* **2014**, *68* (1), 46–52. <https://doi.org/10.1007/s11418-013-0765-0>.
- (36) Lee, J. H.; Kang, G. H.; Kim, K. C.; Kim, K. M.; Park, D. Il; Choi, B. T.; Kang, H. S.; Lee, Y. T.; Choi, Y. H. Tetrandrone-Induced Cell Cycle Arrest and Apoptosis in A549 Human Lung Carcinoma Cells. *Int. J. Oncol.* **2002**, *21* (6), 1239–1244. <https://doi.org/10.3892/ijo.21.6.1239>.
- (37) Lin, Y.; Wang, Y.; Liu, X.; Yan, J.; Su, L.; Liu, X. A Novel Derivative of Tetrandrone (H1) Induces Endoplasmic Reticulum Stress-Mediated Apoptosis and Prosurvival Autophagy in Human Non-Small Cell Lung Cancer Cells. *Tumor Biol.* **2016**, *37* (8), 10403–10413. <https://doi.org/10.1007/s13277-016-4950-0>.
- (38) Cho, H. S.; Chang, S. H.; Chung, Y. S.; Shin, J. Y.; Park, S. J.; Lee, E. S.; Hwang, S. K.; Kwon, J. T.; Tehrani, A. M.; Woo, M.; Noh, M. S.; Hanifah, H.; Jin, H.; Xu, C. X.; Cho, M. H. Synergistic Effect of ERK Inhibition on Tetrandrone-Induced Apoptosis in A549 Human Lung Carcinoma Cells. *J. Vet. Sci.* **2009**, *10* (1), 23–28. <https://doi.org/10.4142/jvs.2009.10.1.23>.
- (39) Yoo, S. M.; Oh, S. H.; Lee, S. J.; Lee, B. W.; Ko, W. G.; Moon, C. K.; Lee, B. H. Inhibition of Proliferation and Induction of Apoptosis by Tetrandrone in HepG2 Cells. *J. Ethnopharmacol.* **2002**, *81* (2), 225–229. [https://doi.org/10.1016/S0378-8741\(02\)00082-X](https://doi.org/10.1016/S0378-8741(02)00082-X).
- (40) Yu, V. W. L.; Ho, W. S. Tetrandrone Inhibits Hepatocellular Carcinoma Cell Growth through the Caspase Pathway and G2/M Phase. *Oncol. Rep.* **2013**, *29* (6), 2205–2210. <https://doi.org/10.3892/or.2013.2352>.
- (41) Liu, C.; Gong, K.; Mao, X.; Li, W. Tetrandrone Induces Apoptosis by Activating Reactive Oxygen Species and Repressing Akt Activity in Human Hepatocellular Carcinoma. *Int. J. Cancer* **2011**, *129*, 1519–1531. <https://doi.org/10.1002/ijc.25817>.
- (42) Kuo, P.; Lin, C. Tetrandrone-Induced Cell Cycle Arrest and Apoptosis in Hep G2 Cells. *Life Sci.* **2003**, *73*, 243–252. [https://doi.org/10.1016/S0024-3205\(03\)00266-2](https://doi.org/10.1016/S0024-3205(03)00266-2).
- (43) Wan, J.; Liu, T.; Mei, L.; Li, J.; Gong, K.; Yu, C.; Li, W. Synergistic Antitumour

- Activity of Sorafenib in Combination with Tetrandrine Is Mediated by Reactive Oxygen Species (ROS)/Akt Signaling. *Br. J. Cancer* **2013**, *109* (2), 342–350. <https://doi.org/10.1038/bjc.2013.334>.
- (44) Zhao, Y. Z.; Kim, J. Y.; Park, E. J.; Lee, S. H.; Woo, S. W.; Ko, G.; Sohn, D. H. Tetrandrine Induces Apoptosis in Hepatic Stellate Cells. *Phyther. Res.* **2004**, *18* (4), 306–309. <https://doi.org/10.1002/ptr.1435>.
- (45) Hsu, Y. C.; Chiu, Y. T.; Cheng, C. C.; Wu, C. F.; Lin, Y. L.; Huang, Y. T. Antifibrotic Effects of Tetrandrine on Hepatic Stellate Cells and Rats with Liver Fibrosis. *J. Gastroenterol. Hepatol.* **2007**, *22* (1), 99–111. <https://doi.org/10.1111/j.1440-1746.2006.04361.x>.
- (46) Qi, X. M.; Miao, L. L.; Cai, Y.; Gong, L. K.; Ren, J. ROS Generated by CYP450, Especially CYP2E1, Mediate Mitochondrial Dysfunction Induced by Tetrandrine in Rat Hepatocytes. *Acta Pharmacol. Sin.* **2013**, *34* (9), 1229–1236. <https://doi.org/10.1038/aps.2013.62>.
- (47) Chen, X. L.; Ren, K. H.; He, H.; Shao, R.; Chen, X.; Ren, K.; He, H.; Shao, R. Involvement of PI3K / AKT / GSK3  $\beta$  Pathway in Tetrandrine-Induced G 1 Arrest and Apoptosis. *Cancer Biol. Ther.* **2008**, *7* (7), 1073–1078. <https://doi.org/10.4161/cbt.7.7.6142>.
- (48) Wu, J.; Chen, Y.; Chen, J.; Lin, T.; Tseng, S. Tetrandrine Induces Apoptosis and Growth Suppression of Colon Cancer Cells in Mice. *Cancer Lett.* **2010**, *287*, 187–195. <https://doi.org/10.1016/j.canlet.2009.06.009>.
- (49) He, B. C.; Gao, J. L.; Zhang, B. Q.; Luo, Q.; Shi, Q.; Kim, S. H.; Huang, E.; Gao, Y.; Yang, K.; Wagner, E. R.; Wang, L.; Tang, N.; Luo, J.; Liu, X.; Li, M.; Bi, Y.; Shen, J.; Luther, G.; Hu, N.; Zhou, Q.; Luu, H. H.; Haydon, R. C.; Zhao, Y.; He, T. C. Tetrandrine Inhibits Wnt/ $\beta$ -Catenin Signaling and Suppresses Tumor Growth of Human Colorectal Cancer. *Mol. Pharmacol.* **2011**, *79* (2), 211–219. <https://doi.org/10.1124/mol.110.068668>.
- (50) Xiao, W.; Jiang, Y.; Men, Q.; Yuan, L.; Huang, Z.; Liu, T.; Li, W.; Liu, X. Tetrandrine Induces G1/S Cell Cycle Arrest through the ROS/Akt Pathway in EOMA Cells and Inhibits Angiogenesis in Vivo. *Int. J. Oncol.* **2015**, *46* (1), 360–368. <https://doi.org/10.3892/ijo.2014.2735>.
- (51) Li, X.; Su, B.; Liu, R.; Wu, D.; He, D. Tetrandrine Induces Apoptosis and Triggers Caspase Cascade in Human Bladder Cancer Cells. *J. Surg. Res.* **2011**, *166* (1), e45–e51. <https://doi.org/10.1016/j.jss.2010.10.034>.
- (52) Qin, R.; Shen, H.; Cao, Y.; Fang, Y.; Li, H.; Chen, Q.; Xu, W. Tetrandrine Induces Mitochondria-Mediated Apoptosis in Human Gastric Cancer BGC-823 Cells. *PLoS One* **2013**, *8* (10), 2–11. <https://doi.org/10.1371/journal.pone.0076486>.



- (53) Li, X.; Lu, X.; Xu, H.; Zhu, Z.; Yin, H.; Qian, X.; Li, R.; Jiang, X.; Liu, B. Paclitaxel/Tetrandrine Coloaded Nanoparticles Effectively Promote the Apoptosis of Gastric Cancer Cells Based on “Oxidation Therapy.” *Mol. Pharm.* **2012**, *9* (2), 222–229. <https://doi.org/10.1021/mp2002736>.
- (54) Jang, B. C.; Lim, K. J.; Paik, J. H.; Cho, J. W.; Baek, W. K.; Suh, M. H.; Park, J. B.; Kwon, T. K.; Park, J. W.; Kim, S. P.; Shin, D. H.; Song, D. K.; Bae, J. H.; Mun, K. C.; Suh, S. Il. Tetrandrine-Induced Apoptosis Is Mediated by Activation of Caspases and PKC- $\delta$  in U937 Cells. *Biochem. Pharmacol.* **2004**, *67*, 1819–1829. <https://doi.org/10.1016/j.bcp.2004.01.018>.
- (55) Liang, L. Y.-; Yu-Jen, C.; Tsu-Yen, W.; Wang, S.-Y.; Chang, K.-H.; Chung, C.-H.; Chen, M.-L. Induction of Apoptosis in Human Leukemic U937 Cells by Tetrandrine. *Anticancer. Drugs* **1998**, *9*, 77–81.
- (56) Liu, W.; Kou, B.; Ma, Z. K.; Tang, X. S.; Lv, C.; Ye, M.; Chen, J. Q.; Li, L.; Wang, X. Y.; He, D. L. Tetrandrine Suppresses Proliferation, Induces Apoptosis, and Inhibits Migration and Invasion in Human Prostate Cancer Cells. *Asian J. Androl.* **2015**, *17*, 850–853. <https://doi.org/10.4103/1008-682X.142134>.
- (57) Wu, Z.; Wang, G.; Xu, S.; Li, Y.; Tian, Y.; Niu, H.; Yuan, F.; Zhou, F.; Hao, Z.; Zheng, Y.; Li, Q.; Wang, J. Effects of Tetrandrine on Glioma Cell Malignant Phenotype via Inhibition of ADAM17. *Tumor Biol.* **2014**, *35* (3), 2205–2210. <https://doi.org/10.1007/s13277-013-1293-y>.
- (58) Chen, Y.; Chen, J.; Tseng, S. Tetrandrine Suppresses Tumor Growth and Angiogenesis of Gliomas in Rats. *Int. J. Cancer* **2009**, *124*, 2260–2269. <https://doi.org/10.1002/ijc.24208>.
- (59) Fu, L.; Liang, Y.; Deng, L.; Ding, Y.; Chen, L.; Ye, Y.; Yang, X.; Pan, Q. Characterization of Tetrandrine , a Potent Inhibitor of P-Glycoprotein-Mediated Multidrug Resistance. *cancer Chemother. Pharmacol.* **2004**, *53*, 349–356. <https://doi.org/10.1007/s00280-003-0742-5>.
- (60) Zhang, Y.; Wang, C.; Wang, H.; Wang, K.; Du, Y.; Zhang, J. Combination of Tetrandrine with Cisplatin Enhances Cytotoxicity through Growth Suppression and Apoptosis in Ovarian Cancer in Vitro and in Vivo. *Cancer Lett.* **2011**, *304* (1), 21–32. <https://doi.org/10.1016/j.canlet.2011.01.022>.
- (61) Xiao-ying, Z.; Zhi-wen, H.; Dong, W.; Rong-zhen, X. Berbamine Selectively Induces Apoptosis of Human Acute Promyelocytic Leukemia Cells via Survivin Mediated Pathway. *Chin. Med. J. (Engl).* **2007**, *120* (9), 802–806.
- (62) Wei, Y. L.; Xu, L.; Liang, Y.; Xu, X. H.; Zhao, X. Y. Berbamine Exhibits Potent Antitumor Effects on Imatinib-Resistant CML Cells in Vitro and in Vivo. *Acta Pharmacol. Sin.* **2009**, *30* (4), 451–457. <https://doi.org/10.1038/aps.2009.19>.

- (63) Liang, Y.; Qiu, X.; Xu, R. Z.; Zhao, X. Y. Berbamine Inhibits Proliferation and Induces Apoptosis of KU812 Cells by Increasing Smad3 Activity. *J. Zhejiang Univ. Sci. B* **2011**, *12* (7), 568–574. <https://doi.org/10.1631/jzus.B1000230>.
- (64) Wang, G. yu; Zhang, J. wei; Lü, Q. hua; Xu, R. zhen; Dong, Q. hua. Berbamine Induces Apoptosis in Human Hepatoma Cell Line SMMC7721 by Loss in Mitochondrial Transmembrane Potential and Caspase Activation. *J. Zhejiang Univ. Sci. B.* **2007**, *8* (4), 248–255. <https://doi.org/10.1631/jzus.2007.B0248>.
- (65) Wang, G. Y.; Lv, Q. H.; Dong, Q.; Xu, R. Z.; Dong, Q. H. Berbamine Induces Fas-Mediated Apoptosis in Human Hepatocellular Carcinoma HepG2 Cells and Inhibits Its Tumor Growth in Nude Mice. *J. Asian Nat. Prod. Res.* **2009**, *11* (3), 219–228. <https://doi.org/10.1080/10286020802675076>.
- (66) Yang, S.; Yang, S.; Zhang, H.; Hua, H.; Kong, Q.; Wang, J.; Jiang, Y. Targeting Na<sup>+</sup>/K<sup>+</sup>-ATPase by Berbamine and Ouabain Synergizes with Sorafenib to Inhibit Hepatocellular Carcinoma. *Br. J. Pharmacol.* **2021**, *178*, 4389–4407. <https://doi.org/10.1111/bph.15616>.
- (67) Yu, B. Bin; Liu, L. L.; Yan, J. D.; Cao, J. B.; Cao, Y. Effect of Berbamine on Invasion and Metastasis of Human Liver Cancer SMMC-7721 Cells and Its Possible Mechanism. *Anticancer. Drugs* **2022**, *33* (1), e178–e185. <https://doi.org/10.1097/CAD.0000000000001179>.
- (68) Meng, Z.; Li, T.; Ma, X.; Wang, X.; Ness, C. Van; Zhou, H.; Tang, J.; Lou, G.; Wang, Y.; Wu, J.; Yen, Y. Berbamine Inhibits the Growth of Liver Cancer Cells and Cancer Initiating Cells by Targeting Ca<sup>2+</sup> /Calmodulin-Dependent Protein Kinase II. *Mol. Cancer Ther.* **2014**, *12* (10), 1–18. <https://doi.org/10.1158/1535-7163.MCT-13-0314>.
- (69) Hu, B.; Cai, H.; Yang, S.; Tu, J.; Huang, X.; Chen, G. Berbamine Enhances the Efficacy of Gefitinib by Suppressing STAT3 Signaling in Pancreatic Cancer Cells. *Onco. Targets. Ther.* **2019**, *12*, 11437–11451. <https://doi.org/10.2147/OTT.S223242>.
- (70) Jin, X.; Wu, Y. Berbamine Enhances the Antineoplastic Activity of Gemcitabine in Pancreatic Cancer Cells by Activating Transforming Growth Factor- $\beta$ /Smad Signaling. *Anat. Rec.* **2014**, *297*, 802–809. <https://doi.org/10.1002/ar.22897>.
- (71) Zhu, H.; Ruan, S.; Jia, F.; Chu, J.; Zhu, Y.; Huang, Y.; Liu, G. In Vitro and in Vivo Superior Radiosensitizing Effect of Berbamine for Head and Neck Squamous Cell Carcinoma. *Onco. Targets. Ther.* **2018**, *11*, 8117–8125. <https://doi.org/10.2147/OTT.S171212>.
- (72) Kim, Y. J.; Han, J. M.; Jung, H. J. Antiangiogenic and Antitumor Potential of Berbamine, a Natural CaMKII $\gamma$  Inhibitor, against Glioblastoma. *Biochem. Biophys. Res. Commun.* **2021**, *566*, 129–134. <https://doi.org/10.1016/j.bbrc.2021.06.025>.

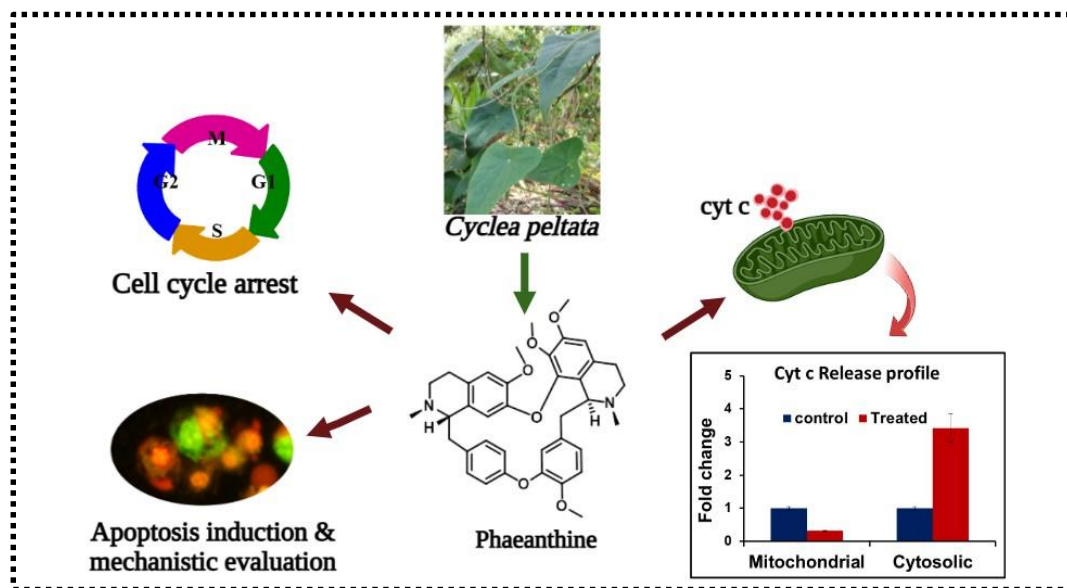
- (73) Liang, Y.; Xu, R. Z.; Zhang, L.; Zhao, X. Y. Berbamine, a Novel Nuclear Factor B Inhibitor, Inhibits Growth and Induces Apoptosis in Human Myeloma Cells. *Acta Pharmacologica Sinica*. 2009, pp 1659–1665. <https://doi.org/10.1038/aps.2009.167>.
- (74) Li, H.; Luo, K.; Yang, Z.; Chen, M.; Yang, X.; Wang, J.; Ying, Y.; Wu, D.; Wang, Q. Berbamine Suppresses the Growth of Gastric Cancer Cells by Inactivating the BRD4/c-MYC Signaling Pathway. *Drug Des. Devel. Ther.* **2022**, *16*, 129–141. <https://doi.org/10.2147/DDDT.S338881>.
- (75) Hou, Z. B.; Lu, K. J.; Wu, X. L.; Chen, C.; Huang, X. E.; Yin, H. T. In Vitro and in Vivo Antitumor Evaluation of Berbamine for Lung Cancer Treatment. *Asian Pacific J. Cancer Prev.* **2014**, *15*, 1767–1769. <https://doi.org/10.7314/APJCP.2014.15.4.1767>.
- (76) Duan, H.; Luan, J.; Liu, Q.; Yagasaki, K.; Zhang, G. Suppression of Human Lung Cancer Cell Growth and Migration by Berbamine. *Cytotechnology* **2010**, *62*, 341–348. <https://doi.org/10.1007/s10616-009-9240-x>.
- (77) Liu, L.; Xu, Z.; Yu, B.; Tao, L.; Cao, Y. Berbamine Inhibits Cell Proliferation and Migration and Induces Cell Death of Lung Cancer Cells via Regulating C-Maf, PI3K/Akt, and MDM2-P53 Pathways. *Evidence-based Complement. Altern. Med.* **2021**, *2021*. <https://doi.org/10.1155/2021/5517143>.
- (78) Wang, S.; Liu, Q.; Zhang, Y.; Liu, K.; Yu, P.; Liu, K.; Luan, J.; Duan, H.; Lu, Z.; Wang, F.; Wu, E.; Yagasaki, K.; Zhang, G. Suppression of Growth, Migration and Invasion of Highly-Metastatic Human Breast Cancer Cells by Berbamine and Its Molecular Mechanisms of Action. *Mol. Cancer* **2009**, *8*, 81. <https://doi.org/10.1186/1476-4598-8-81>.
- (79) LIU, L.; YAN, J.; CAO, Y.; YAN, Y.; SHEN, X.; YU, B.; TAO, L.; WANG, S. Proliferation, Migration and Invasion of Triple Negative Breast Cancer Cells Are Suppressed by Berbamine via the PI3K/Akt/MDM2/P53 and PI3K/Akt/MTOR Signaling Pathways. *Oncol. Lett.* **2021**, *21* (70), 1–10. <https://doi.org/10.3892/ol.2020.12331>.
- (80) Han, C.; Wang, Z.; Chen, S.; Li, L.; Xu, Y.; Kang, W.; Wei, C.; Ma, H.; Wang, M.; Jin, X. Berbamine Suppresses the Progression of Bladder Cancer by Modulating the ROS/NF- $\kappa$ B Axis. *Oxid. Med. Cell. Longev.* **2021**, *2021*. <https://doi.org/10.1155/2021/8851763>.
- (81) Zhang, H.; Jiao, Y.; Shi, C.; Song, X.; Chang, Y.; Ren, Y.; Shi, X. Berbamine Suppresses Cell Proliferation and Promotes Apoptosis in Ovarian Cancer Partially via the Inhibition of Wnt/ $\beta$ -Catenin Signaling. *Acta Biochim. Biophys. Sin. (Shanghai)*. **2018**, *50* (6), 532–539. <https://doi.org/10.1093/abbs/gmy036>.
- (82) Zhang, H.; Jiao, Y.; Shi, C.; Song, X.; Chang, Y.; Ren, Y.; Shi, X. Berbamine Suppresses Cell Viability and Induces Apoptosis in Colorectal Cancer via Activating

- P53-Dependent Apoptotic Signaling Pathway. *Cytotechnology* **2018**, *70*, 321–329. <https://doi.org/10.1007/s10616-017-0146-8>.
- (83) Mou, L.; Liang, B.; Liu, G.; Jiang, J.; Liu, J.; Zhou, B.; Huang, J.; Zang, N.; Liao, Y.; Ye, L.; Liang, H. Berbamine Exerts Anticancer Effects on Human Colon Cancer Cells via Induction of Autophagy and Apoptosis, Inhibition of Cell Migration and MEK/ERK Signalling Pathway. *J. B.U.ON.* **2019**, *24* (5), 1870–1875.
- (84) Zhao, Y.; Lv, J. J.; Chen, J.; Jin, X. B.; Wang, M. W.; Su, Z. H.; Wang, L. Y.; Zhang, H. Y. Berbamine Inhibited the Growth of Prostate Cancer Cells in Vivo and in Vitro via Triggering Intrinsic Pathway of Apoptosis. *Prostate Cancer Prostatic Dis.* **2016**, 1–9. <https://doi.org/10.1038/pcan.2016.29>.
- (85) Guo, B.; Su, J.; Zhang, T.; Wang, K.; Li, X. Fangchinoline as a Kinase Inhibitor Targets FAK and Suppresses FAK-Mediated Signaling Pathway in A549. *J. Drug Target.* **2015**, *23* (3), 266–274. <https://doi.org/10.3109/1061186X.2014.992898>.
- (86) Jung, Y. Y.; Ha, I. J.; Um, J. Y.; Sethi, G.; Ahn, K. S. Fangchinoline Diminishes STAT3 Activation by Stimulating Oxidative Stress and Targeting SHP-1 Protein in Multiple Myeloma Model. *J. Adv. Res.* **2022**, *35*, 245–257. <https://doi.org/10.1016/j.jare.2021.03.008>.
- (87) Fan, B.; Zhang, X.; Ma, Y.; Zhang, A. Fangchinoline Induces Apoptosis, Autophagy and Energetic Impairment in Bladder Cancer. *Cell. Physiol. Biochem.* **2017**, *43*, 1003–1011. <https://doi.org/10.1159/000481698>.
- (88) Wang, N.; Pan, W.; Zhu, M.; Zhang, M.; Hao, X.; Liang, G.; Feng, Y. Fangchinoline Induces Autophagic Cell Death via P53/Sestrin2/AMPK Signalling in Human Hepatocellular Carcinoma Cells. *Br. J. Pharmacol.* **2011**, *164* (2 B), 731–742. <https://doi.org/10.1111/j.1476-5381.2011.01349.x>.
- (89) Xing, Z.; Zhang, Y.; Zhang, X.; Yang, Y.; Ma, Y.; Pang, D. Fangchinoline Induces G1 Arrest in Breast Cancer Cells through Cell-Cycle Regulation. *Phytotherapy Research.* 2013, pp 1790–1794. <https://doi.org/10.1002/ptr.4936>.
- (90) Xing, Z. B.; Yao, L.; Zhang, G. Q.; Zhang, X. Y.; Zhang, Y. X.; Pang, D. Fangchinoline Inhibits Breast Adenocarcinoma Proliferation by Inducing Apoptosis. *Chem. Pharm. Bull.* **2011**, *59* (12), 1476–1480. <https://doi.org/10.1248/cpb.59.1476>.
- (91) Wang, C. D.; Yuan, C. F.; Bu, Y. Q.; Wu, X. M.; Wan, J. Y.; Zhang, L.; Hu, N.; Liu, X. J.; Zu, Y.; Liu, G. L.; Song, F. Z. Fangchinoline Inhibits Cell Proliferation via Akt/GSK-3 $\beta$ /Cyclin D1 Signaling and Induces Apoptosis in MDA-MB-231 Breast Cancer Cells. *Asian Pacific J. Cancer Prev.* **2014**, *15* (2), 769–773. <https://doi.org/10.7314/APJCP.2014.15.2.769>.
- (92) Wang, B.; Xing, Z.; Wang, F.; Yuan, X.; Zhang, Y. Fangchinoline Inhibits Migration and Causes Apoptosis of Human Breast Cancer MDA-MB-231 Cells. *Oncol. Lett.*

- 2017, 14, 5307–5312. <https://doi.org/10.3892/ol.2017.6831>.
- (93) Jung, Y. Y.; Shanmugam, M. K.; Chinnathambi, A.; Alharbi, S. A.; Shair, O. H. M.; Um, J. Y.; Sethi, G.; Ahn, K. S. Fangchinoline, a Bisbenzylisoquinoline Alkaloid Can Modulate Cytokine-Impelled Apoptosis via the Dual Regulation of NF-KB and AP-1 Pathways. *Molecules* **2019**, 24 (17), 55–64. <https://doi.org/10.3390/molecules24173127>.
- (94) Bao, K.; Li, Y.; Wei, J.; Li, R.; Yang, J.; Shi, J.; Li, B.; Zhu, J.; Mao, F.; Jia, R.; Li, J. Fangchinoline Suppresses Conjunctival Melanoma by Directly Binding FUBP2 and Inhibiting the Homologous Recombination Pathway. *Cell Death Dis.* **2021**, 12 (380), 1–11. <https://doi.org/10.1038/s41419-021-03653-4>.
- (95) Jung, Y. Y.; Chinnathambi, A.; Alahmadi, T. A.; Alharbi, S. A.; Kumar, A. P.; Sethi, G.; Ahn, K. S. Fangchinoline Targets Epithelial–Mesenchymal Transition Process by Modulating Activation of Multiple Cell-Signaling Pathways. *J. Cell. Biochem.* **2022**, 123, 1222–1236. <https://doi.org/10.1002/jcb.30279>.
- (96) Tian, F.; Ding, D.; Li, D. Fangchinoline Targets PI3K and Suppresses PI3K/AKT Signaling Pathway in SGC7901 Cells. *Int. J. Oncol.* **2015**, 46, 2355–2363. <https://doi.org/10.3892/ijo.2015.2959>.
- (97) Li, D.; Lu, Y.; Sun, P.; Feng, L.-X.; Liu, M.; Hu, L.-H.; Wu, W.-Y.; Jiang, B.-H.; Yang, M.; Qu, X.-B.; Guo, D.-A.; Liu, X. Inhibition on Proteasome B1 Subunit Might Contributr to the Anti-Cancer Effects of Fangchinoline in Human Prostate Cancer. *PLoS One* **2015**, 10 (10), 1–21.
- (98) Nwaefulu, O. N.; Al-Shar'i, N. A.; Owolabi, J. O.; Sagineedu, S. R.; Woei, L. C.; Wai, L. K.; Islam, M. K.; Jayanthi, S.; Stanslas, J. The Impact of Cycleanine in Cancer Research: A Computational Study. *J. Mol. Model.* **2022**, 28 (11). <https://doi.org/10.1007/s00894-022-05326-1>.
- (99) Uche, F. I.; Drijfhout, F. P.; McCullagh, J.; Richardson, A.; Li, W. W. Cytotoxicity Effects and Apoptosis Induction by Bisbenzylisoquinoline Alkaloids from *Triclisia* Subcordata. *Phyther. Res.* **2016**, No. April, 1533–1539. <https://doi.org/10.1002/ptr.5660>.
- (100) Gong, S.; Xu, D.; Zou, F.; Peng, R. (–)-Curine Induces Cell Cycle Arrest and Cell Death in Hepatocellular Carcinoma Cells in a P53-Independent Way. *Biomed. Pharmacother.* **2017**, 89, 894–901. <https://doi.org/10.1016/j.biopha.2017.01.148>.
- (101) Dantas, B. B.; Faheina-Martins, G. V.; Couliadiati, T. H.; Bomfim, C. C. B.; Da Silva Dias, C.; Barbosa-Filho, J. M.; Araújo, D. A. M. Effects of Curine in HL-60 Leukemic Cells: Cell Cycle Arrest and Apoptosis Induction. *J. Nat. Med.* **2015**, 69 (2), 218–223. <https://doi.org/10.1007/s11418-014-0881-5>.
- (102) Nurgali, K.; Jagoe, R. T.; Abalo, R. Editorial: Adverse Effects of Cancer

Chemotherapy: Anything New to Improve Tolerance and Reduce Sequelae? *Front. Pharmacol.* **2018**, 9 (MAR), 1–3. <https://doi.org/10.3389/fphar.2018.00245>.

## Exploring the cytotoxic potential of phaeanthine: a bisbenzylisoquinoline alkaloid isolated from *Cyclea peltata* induces mitochondria-mediated apoptosis in cervical cancer cells



### Abstract

Pharmacophores obtained from natural product sources possess considerable structural diversity, variable physicochemical features, and relatively lesser toxicity than synthesized drug entities. In this context, phaeanthine, a bisbenzylisoquinoline alkaloid isolated from the rhizomes of *Cyclea peltata*, showed selective cytotoxicity towards cervical cancer cells (HeLa) with an  $IC_{50}$  of  $8.11 \pm 0.04 \mu\text{M}$ . Subsequent investigation with *in silico* molecular docking of phaeanthine displayed preferential binding to the apoptotic protein Akt as reflected by a docking score of  $-5.023$ . Interestingly, in the follow-up *in vitro* assessment of the compound co-related with mitochondria-mediated apoptosis specifically by downregulating the expression of Akt and p-Akt, including other anti-apoptotic proteins MCL-1, IGF-2, and XIAP. In the complementary *in-vitro* assessment, mitochondrial membrane polarization and dynamics of intercellular cytochrome c validated the intrinsic mechanism of

*the apoptotic phenomenon. This in-depth assessment of the anti-cancer potential of phaeanthine is the first comprehensive study evaluated against HeLa cells.*

## 2.1 Introduction

Cancer is the second leading cause of death globally, with an approximate number of 10 million deaths in 2020 alone and cervical cancer is the fourth most prevalent cancer worldwide, claiming one life every two minutes. It is also the leading cause of death in women cancer patients in 42 countries.<sup>1</sup> However, cervical cancer can be prevented by an early diagnosis because it has a long window to become metastatic. Due to this reason, developing more affordable therapeutic entities can greatly help in fighting this disease.

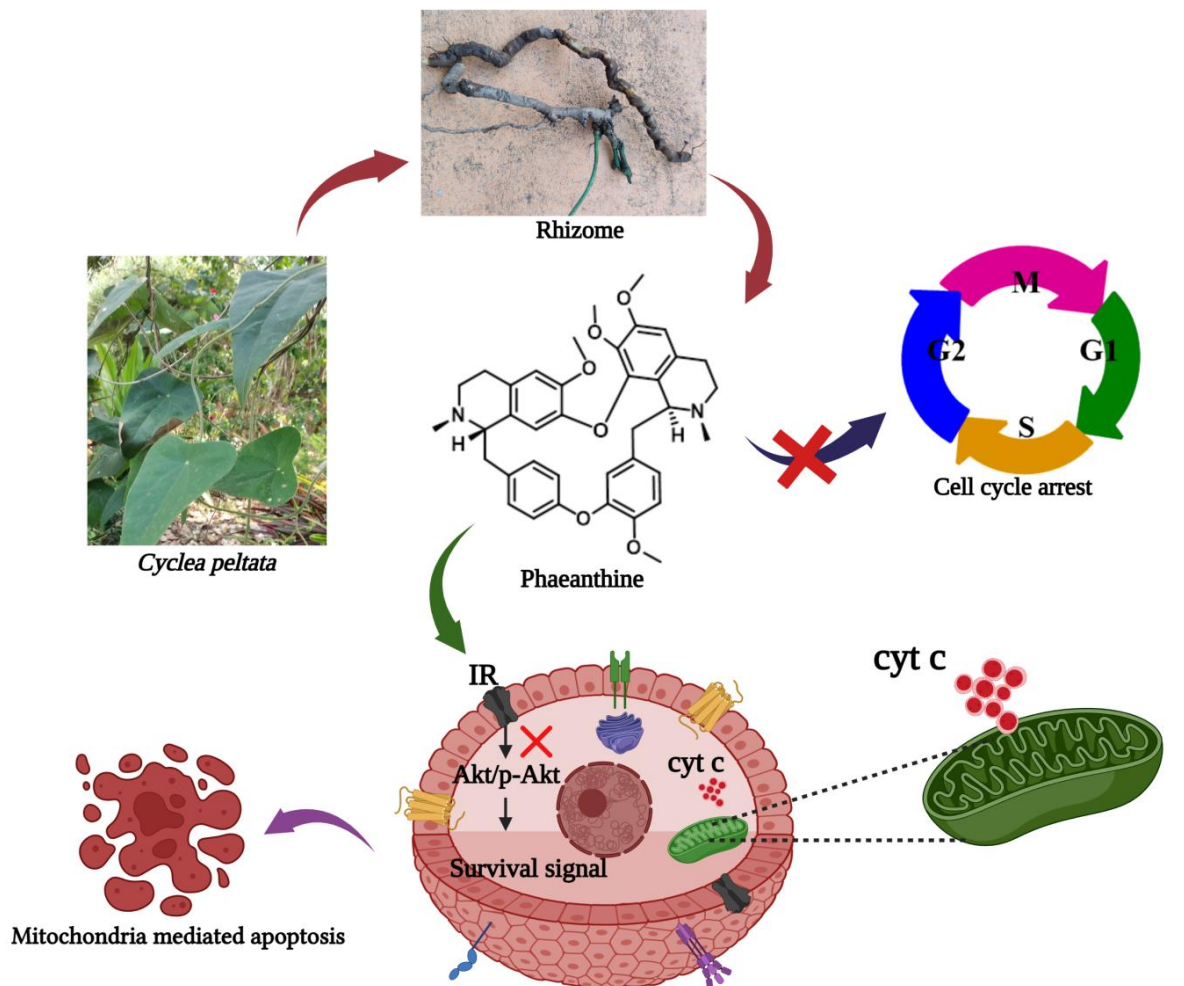
In ancient India, traditional medicines involved ayurvedic formulations developed from plants and herbs. With advancements in technology and knowledge, these formulations have been replaced by more precise and accurate treatment strategies using bioactive molecules. So, natural products and their synthetic analogs occupy a significant role in the current pharmacopeia.

For the present study, the plant *Cyclea peltata* (Lam) Hook.f & Thoms. has been chosen which belongs to the family Menispermaceae and it has frequently used in traditional systems but hitherto unexplored for its anticancer activity. The plant is known as Rajapata in Sanskrit and is reputedly a well-known drug quoted in most of the ancient ayurvedic classics like Charak Samhita (1000BC), Sushruta Samhita (1000BC), and Ashtangahridya (6AD). It has been widely used in many Ayurvedic formulations like Pushyanuga churna for overall wellness of a women's reproductive system and for treating many female reproductive disorders.<sup>2,3</sup> The plant enables to reduce the excess water stagnation with uterine tumours, ovarian cysts, and leucorrhoea.<sup>2</sup> and traditionally used by tribal communities in India to treat diarrhea, wounds, and certain skin diseases.<sup>4,5,6</sup> The plant is known to possess many pharmacological properties, including antidiabetic, anticancer potential at extract level,<sup>7,8</sup> nephroprotective activity,<sup>9</sup> hepatoprotective potential,<sup>10</sup> antibacterial activity,<sup>11,12</sup> gastric antisecretory and antiulcer property.<sup>13</sup> Additionally, *C. peltata* root extract is effective in neutralizing the venom of *Naja naja*,<sup>14</sup> also shows significant antipyretic and analgesic activity,<sup>15</sup> and the ethyl acetate extract is shown to have anti-inflammatory potential. In Swiss albino rats, the methanolic extract of



the plant reduced DAL-induced tumour development.<sup>8</sup> So, based on the available literature, it is clear that the plant possesses anti-tumour potential, but an in-depth evaluation of the key phytomolecule, phaeanthine, is not explored. Phaeanthine is a benzyloquinoline alkaloid that includes narcotics like codeine and morphine, muscle relaxants like papaverine and (+)-tubocurarine, antimicrobials like sanguinarine and berberine, and anticancer agent noscapine, among others. Phaeanthine has not been explored much in terms of its anti-cancer potential. Some other activities are reported for the compound, like antiplasmodial activity<sup>16</sup>, antiprotozoal activity<sup>17</sup> and acetylcholinesterase inhibitory potential<sup>18</sup>.

Considering the reports, it is planned to investigate the effect of phytomolecules isolated from the plant on anti-cancer profiling with a focus on the most common cancer of the female reproductive system, i.e., cervical cancer. The major phytomolecules from *C. peltata* rhizomes have been isolated and examined the anticancer potential in the present investigation. The acetone and ethanolic extract of the plant yielded mainly three compounds, phaeanthine, cycleanine, and *N*-methylcorydaldine. Initially, all the three compounds were screened for antiproliferative potential against cervical cancer cells, HeLa, among which phaeanthine was found to have appealing cytotoxicity features. *In silico* examination of phaeanthine demonstrated an excellent binding affinity with the proliferative protein Akt, compared to the other eight protein codes. Subsequently, the anti-cancer potential of phaeanthine has been evaluated with downstream *in vitro* assays to assess its ability to induce apoptosis, including FITC annexin V, caspase assays, and DNA fragmentation. Furthermore, clonogenic assay and changes in mitochondrial membrane potential were also performed. As a novel insight, surface enhanced Raman spectroscopy (SERS) was employed to scrutinize DNA fragmentation by identifying the signature Raman fingerprint of the phosphate backbone. Moreover, phaeanthine exhibited intrinsic mitochondria-mediated apoptosis and resulted in the downregulation of the expression of proliferative protein Akt and its phosphorylated form, p-Akt and other anti-apoptotic proteins Mcl-1, XIAP (Scheme 2.1). As per the literature reports, this is the first report on the anticancer potential of phaeanthine against cervical cancer cell; HeLa, and its apoptotic induction through mitochondria-mediated intrinsic pathway has also been established.



Created with BioRender.com

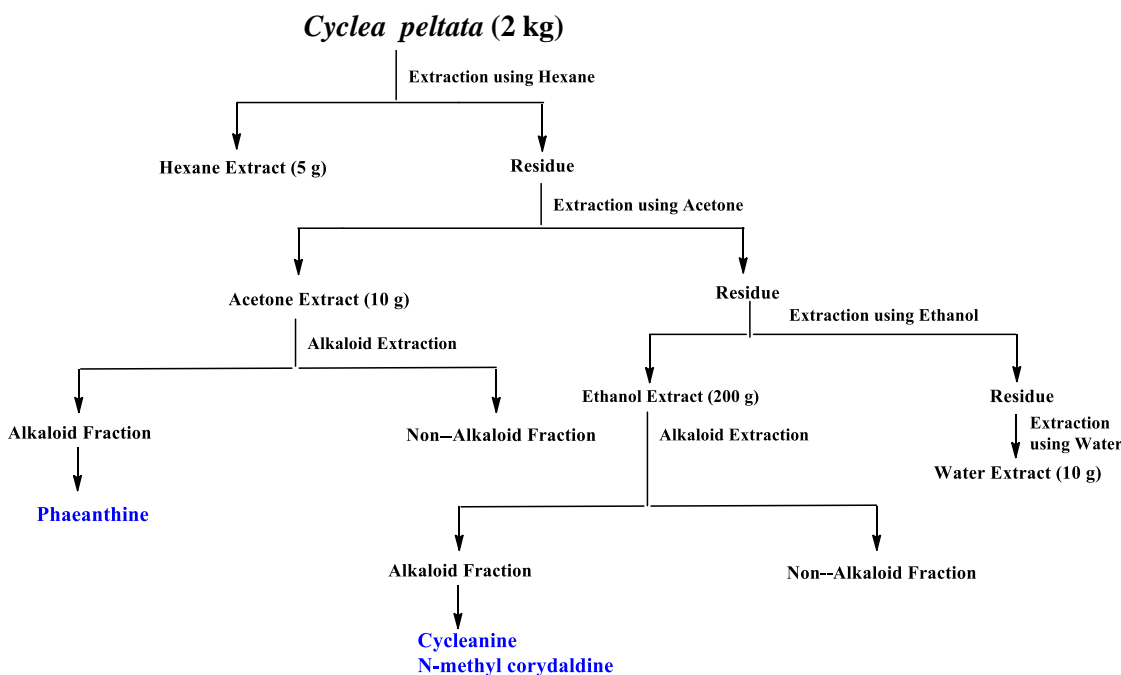
**Scheme 2.1.** Phaeanthine downregulates Akt signalling pathway and induces mitochondria-mediated cell death

## 2.2 Results and Discussion

### 2.2.1 Extraction, Isolation, and Characterization of Phytomolecules from *Cyclea peltata* rhizomes

The collected *C. peltata* rhizome was subjected to sequential extraction by hexane, acetone, ethanol, and water (Scheme 2.2). Since the acetone and ethanol extract responded to Dragondorff's test, we adopted a detailed acid-base extraction procedure. Three major compounds were isolated from the plant extract, which included 2 DBBI alkaloids

(Dibisbenzylisoquinoline) alkaloids. The compounds were identified as phaeanthine (80 mg - 0.004 % yield), cycleanine (50 mg - 0.0025 % yield), and *N*-methylcorydaldine (30 mg - 0.0015 % yield) based on extensive characterization using NMR technique ( $^1\text{H}$ ,  $^{13}\text{C}$ , 2D), and HRMS analysis, which were in good agreement with the reported data.<sup>17,19,20</sup> (Figure 2.1 -2.6)



**Scheme 2.2.** Extraction scheme of the rhizome of *Cyclea peltata*

The acetone extract of *C. peltata* was subjected to acid-base extraction procedure in order to get the alkaloid and non-alkaloid fraction. The alkaloid fraction showed a major spot in TLC, which on further purification led to the isolation of the compound and is confirmed as alkaloid by the Dragendorff's test. The  $^1\text{H}$  NMR spectrum showed six singlets signifying the presence of six methyl groups. The chemical shift values at  $\delta$  2.62 and 2.33 ppm direct the existence of two N-methyl groups with carbon peaks at  $\delta$  42.6 and 42.3 ppm. The position of six methyl groups was confirmed with the help of HMBC analysis. The ten aromatic protons resonated in between  $\delta$  7.35 and 6.00 ppm includes two 2H doublets with  $J = 8.0$  Hz, represents the presence of a para disubstituted benzene ring. The head-to-head confirmation of the compound was proved by the presence of a fragmentation peak at  $m/z$  312.1663 in the HRMS spectrum. Furthermore, from the detailed 2D NMR analysis, and HRMS analysis ( $m/z$

623.3252 (M+H)<sup>+</sup>), the structure of compound 8 was confirmed as tetrandrine, a well-reported compound from *C. peltata*. But the optical rotation showed a negative value (-353°, c = 0.2, Methanol), indicates the compound as the diastereoisomer of tetrandrine, named phaenthine, further confirmed with the melting point analysis (182-185 °C)

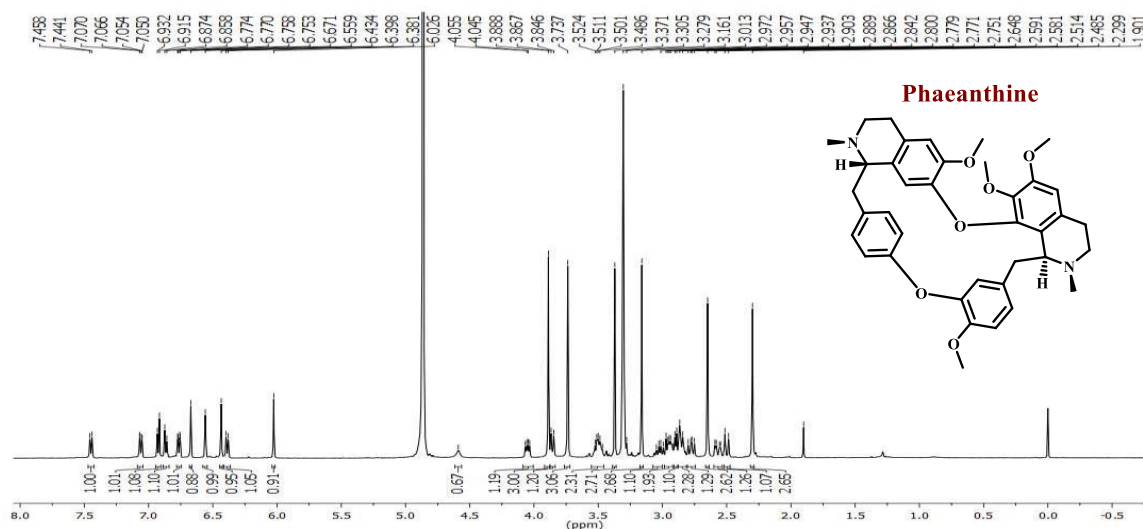


**Figure 2.1.** <sup>1</sup>H NMR spectrum of phaenthine

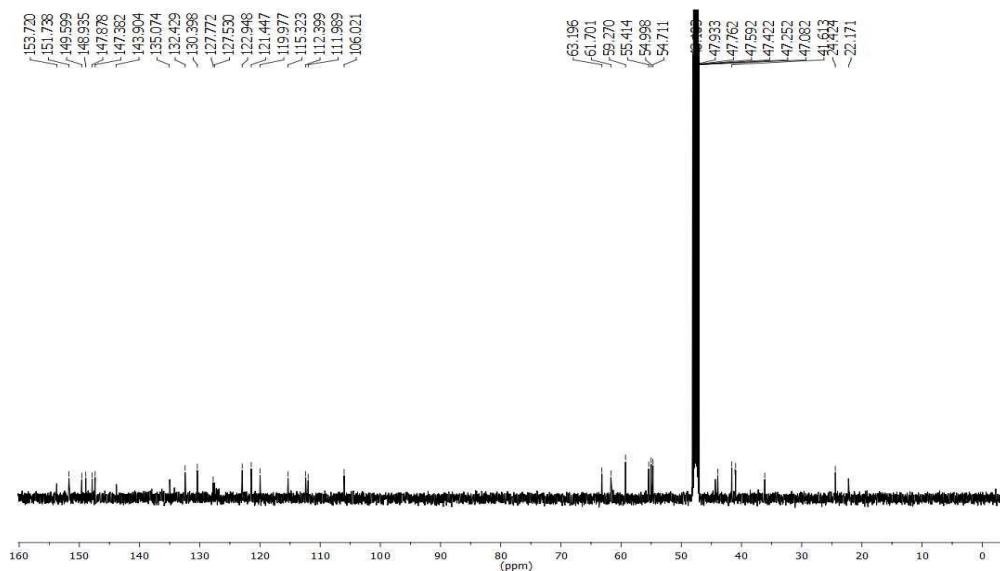


**Figure 2.2.** <sup>13</sup>C NMR spectrum of phaenthine

The ethanol extract was subjected to acid-base extraction, and the alkaloid fraction was checked for the TLC. The three major spots, were identified where all three spots gave an orange-red stain in Dragendorff's reagent, detected as alkaloids. As in the previous cases, the

$^1\text{H}$  NMR spectrum of cycleanine displayed ten aromatic protons in the range  $\delta$  7.29-5.93 ppm and six methyl groups at  $\delta$  3.86, 3.68, 3.30, 3.12, 2.55, and 2.27 ppm indicating the presence of DBBI structural backbone. The chiral carbons resonated as a multiplet in the range  $\delta$  3.84-3.80 ppm and as a doublet at  $\delta$  3.69 ppm with  $J = 11.0$  Hz with corresponding carbons at  $\delta$  63.9 and 61.5 ppm in the  $^{13}\text{C}$  NMR. The head-to-head confirmation of the compound was proved by the presence of a fragmentation peak at  $m/z$  312.1602 in the HRMS spectrum. From the literature analysis and HRMS analysis ( $623.31210$  ( $\text{M}+\text{H}$ ) $^+$ ), the structure of compound was confirmed as Cycleanine with optical rotation of  $-14.9^\circ$  ( $c = 0.2$ , Methanol) and melting point in the range  $116\text{-}120^\circ\text{C}$ .

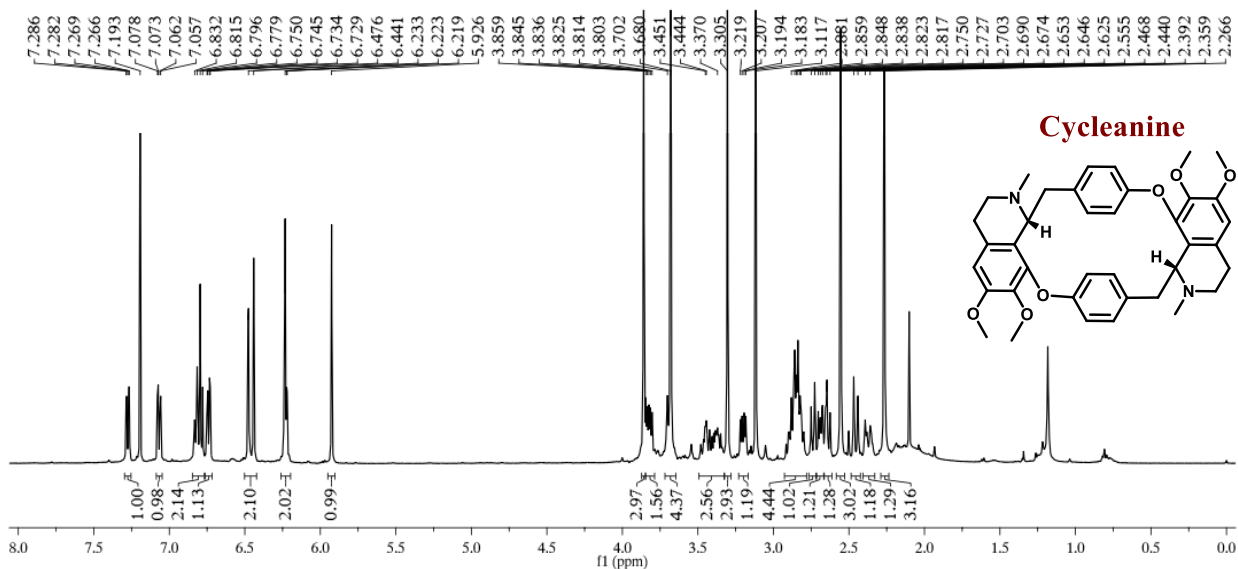


**Figure 2.3.**  $^1\text{H}$  NMR spectrum of cycleanine

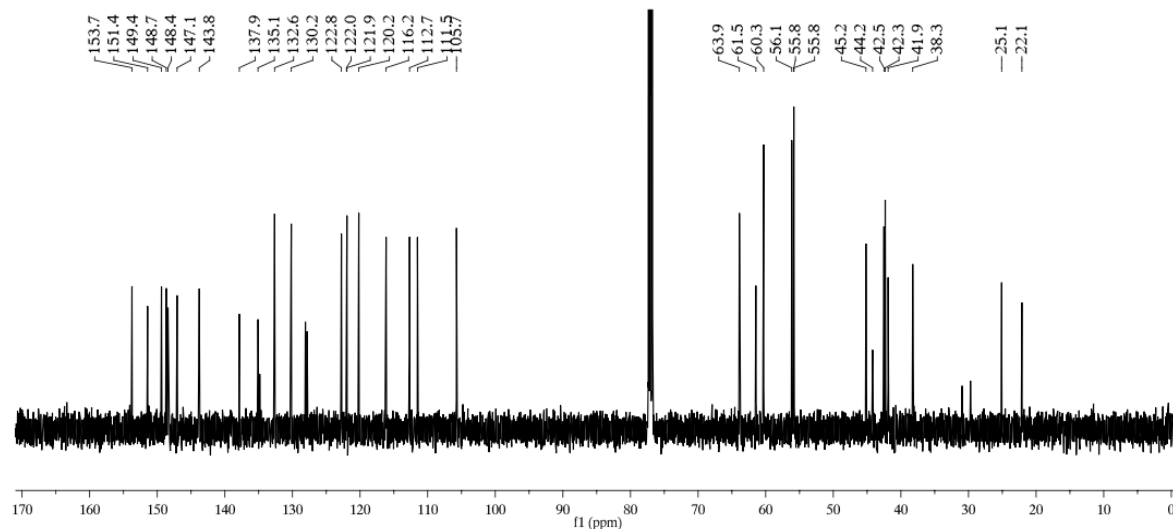


**Figure 2.4.**  $^{13}\text{C}$  NMR spectrum of cycleanine

The  $^1\text{H}$  NMR of the next compound showed two singlets at  $\delta$  7.53 and 6.56 ppm. The spectrum also possesses two sharp singlets at  $\delta$  3.85 and 3.84 ppm, indicating the presence of two methoxy groups. The sharp singlet at  $\delta$  3.07 ppm indicates a methyl group with a carbon peak at  $\delta$  35.3 ppm, may be attached to a nitrogen atom in the system. Two triplets  $\delta$  3.48 and 2.87 ppm with  $J = 7.0$  and 6.5 Hz showed a HOMOCOSY relation. The  $^{13}\text{C}$  NMR has twelve carbon peaks. Also, a signal at  $\delta$  165.0 ppm indicates the existence of an amide moiety. From the detailed 2D NMR analysis, the structure of the compound was identified as *N*-methylcorydaldine. Further, the structure was confirmed with the  $m/z$  value 222.1138 in the HRMS analysis.

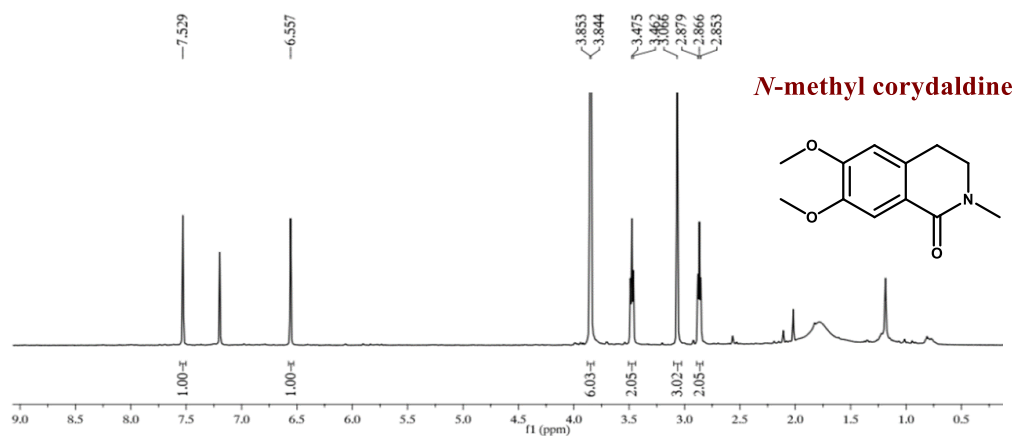


**Figure 2.5.**  $^1\text{H}$  NMR spectrum of *N*-methylcorydaldine

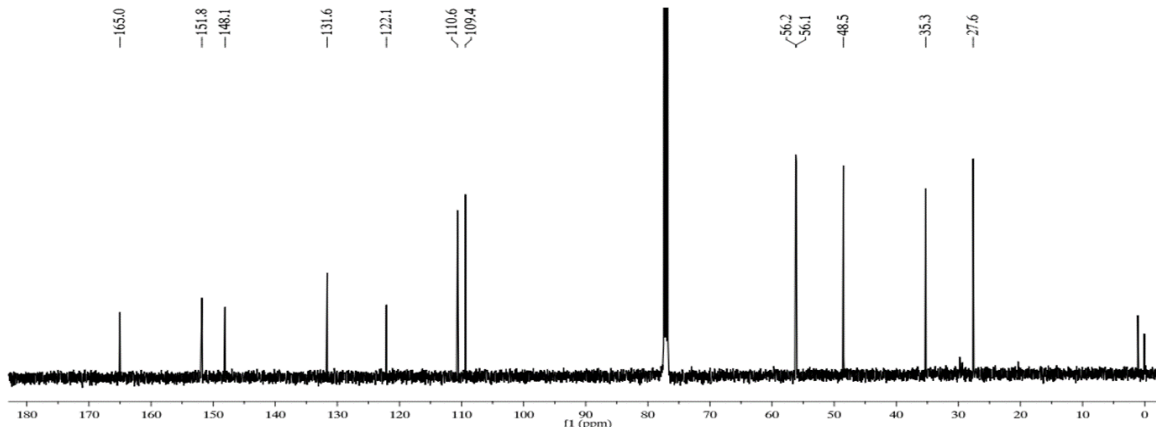


**Figure 2.6.**  $^{13}\text{C}$  NMR spectrum of *N*-methyl corydaldine

### 2.2.2 Primary Cytotoxicity Screening of Isolated Phytomolecules

Preliminary selection based on the cytotoxicity of the three isolated compounds was evaluated by MTT (3-[4,5-dimethylthiazol-2-yl]-2,5-diphenyltetrazolium) assay in HeLa cells. Among the three compounds, phaeanthine (PHA) showed a promising antiproliferative potential with an  $\text{IC}_{50}$  value of  $8.11 \pm 0.04 \mu\text{M}$  at 24 hours, whereas cycleanine showed an  $\text{IC}_{50}$  value of  $18.06 \pm 0.14 \mu\text{M}$ . Although, *N*-methylcorydaldine did not show any  $\text{IC}_{50}$  even when concentration was increased to  $100 \mu\text{M}$  (Figure 2.7.d). Since PHA exhibited pronounced inhibitory potential against HeLa cells at a lower concentration, its toxicity also checked against a normal non-tumorigenic breast epithelial cell line, MCF-10A. To our pleasant surprise, PHA did not show toxicity up to a moderate concentration, and its  $\text{IC}_{50}$  was found to be  $36.33 \pm 0.14 \mu\text{M}$ , which corresponded to a toxicity four times greater in HeLa cells. (Figure 2.7.e) Therefore, the downstream *in vitro* studies with PHA was extended as a potential phytomolecule.

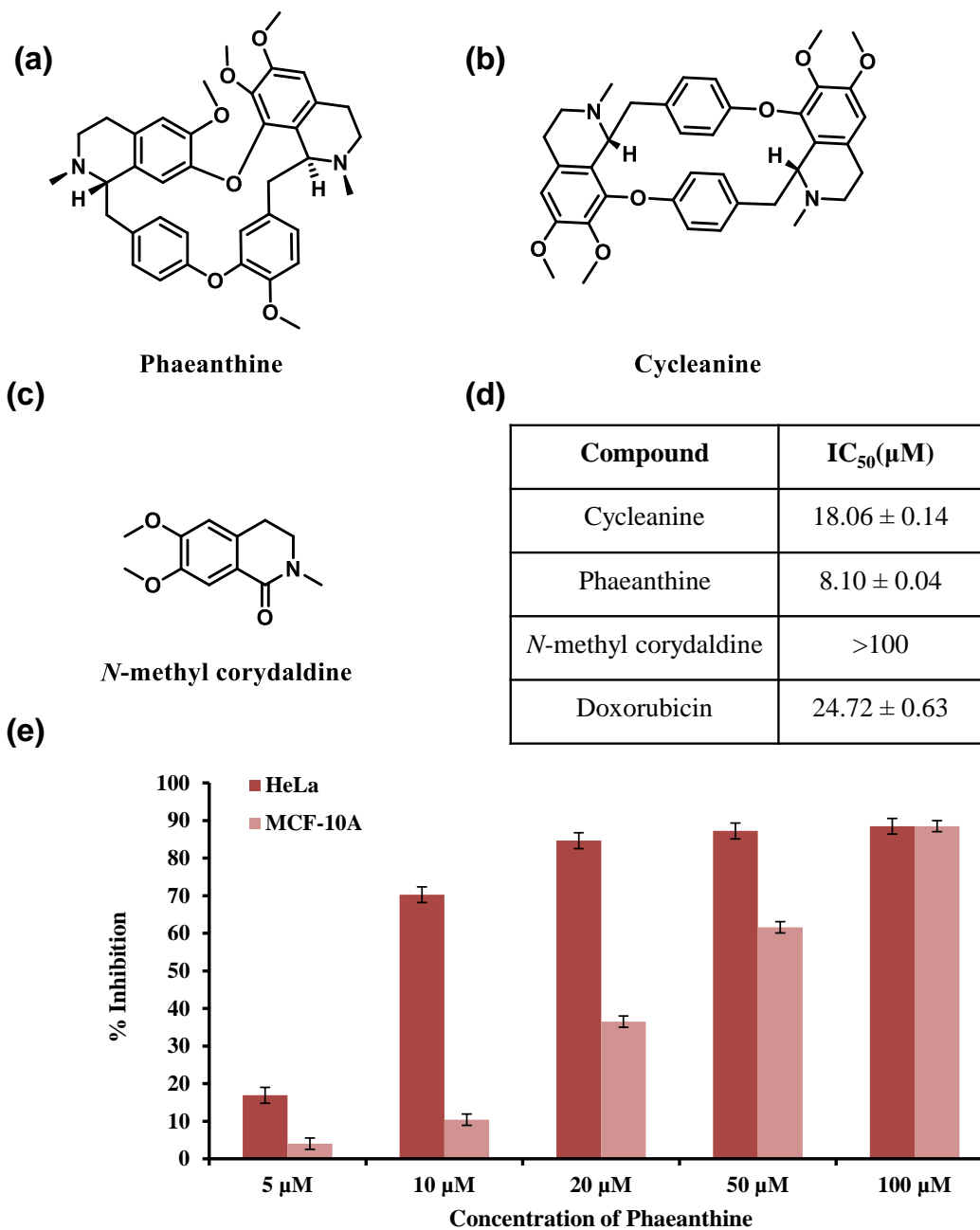


**Figure 2.7.** Chemical structure of the isolated compounds from *Cyclea peltata* rhizome (a) Phaeanthine, (b) Cycleanine, (c) *N*-methylcorydaldine (d) their IC<sub>50</sub> ( $\mu$ M) in HeLa cells for 24 hour incubation and (e) comparative % of inhibition of PHA on HeLa cell proliferation and MCF-10A (non-tumorigenic cell) cells for 24 hours of incubation



### 2.2.3 Computational Screening of PHA

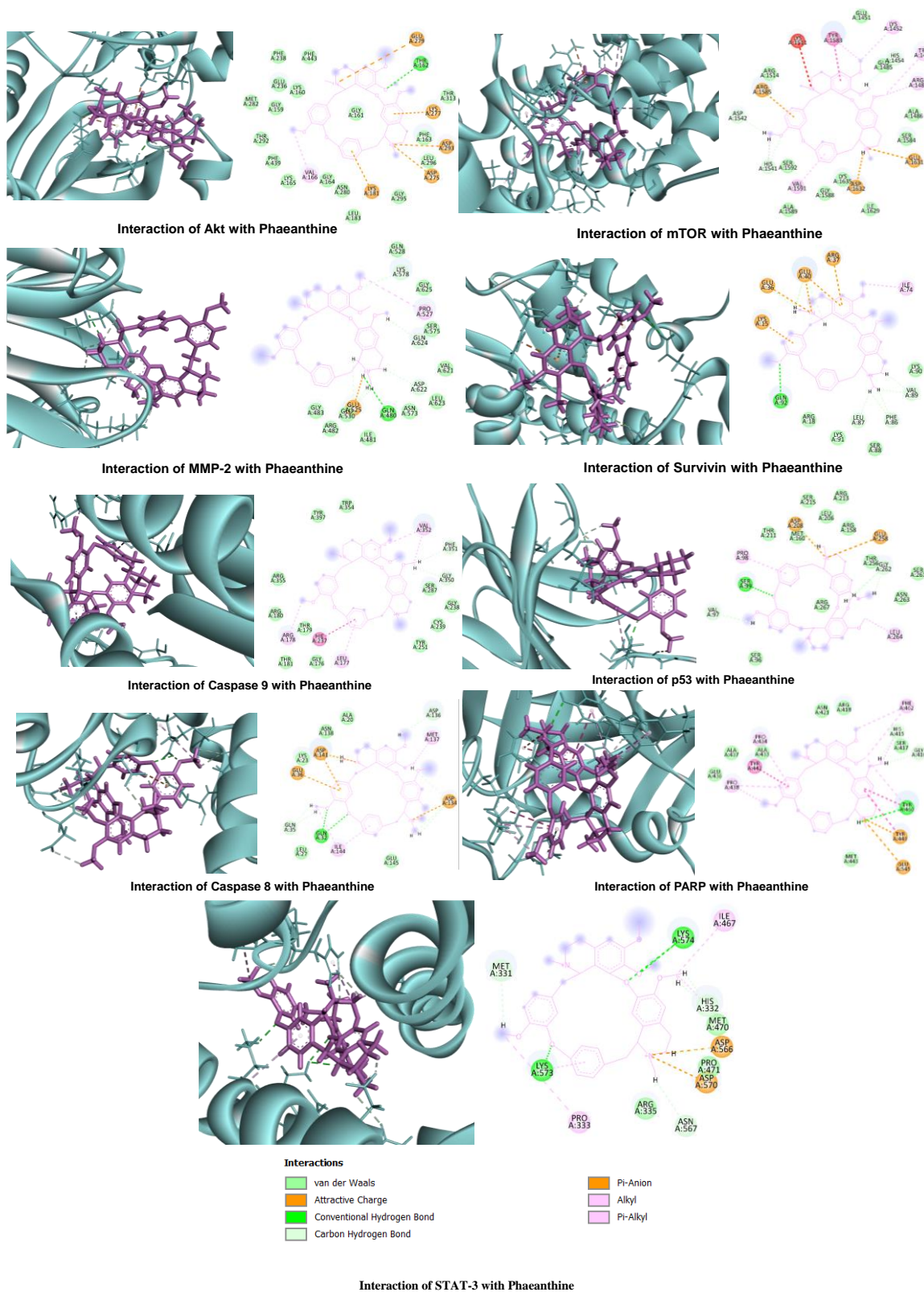
Next, the screening strategy was explored by employing computational tools where molecular docking was conducted with the selected proteins (Akt, MMP-2, mTOR, Survivin, Caspase -9, Caspase-8, p53, PARP, and STAT-3) involved in the apoptotic mechanism. Molecular docking studies among these proteins exhibited good binding affinity of PHA with the target Akt, possessing a docking score of -5.023 compared to other target proteins (Table 2.1 & Fig. 2.8). Hence, Akt was chosen for further molecular dynamic simulation studies. In the binding interaction between Akt and PHA, we observed that Thr162 donated hydrogen atoms to the ligand, leading to the formation of an H-bond with a distance of 2.31 Å. Apart from hydrogen bonds,  $\pi$ -cation interaction and salt bridges were also observed, which may contribute to the complex's stability. The intermolecular  $\pi$ -cation interaction was formed by the interaction of a cation from Lys277 with the polarizable  $\pi$  electron cloud of an aromatic ring in PHA. (Figure 2.9.a & b)

### 2.2.4 Molecular Dynamics Simulation of Akt- PHA Complex

To assess the stability and conformational flexibility of the Akt- PHA complex, molecular dynamics simulation was performed using Desmond (academic version) of Schrödinger Suite for 50 ns under OPLS-2005 force field. The Root Mean Square Deviation (RMSD), which gives insights into the conformational stability of the complex, was calculated throughout the 50 ns simulation time. The RMSD plot showed that the protein and protein-ligand complexes were stable till the end of the trajectory (Figure 2.9.c). Similarly, the Root Mean Fluctuation (RMSF) parameter to assess flexibility was also calculated, in which minor fluctuations of the residues were found and the residues at the N-terminal region were more fluctuated (Figure 2.9.d). In order to further decipher the changes in the position of ligand atoms, the ligand RMSF was calculated which showed minor fluctuations in ligand atoms. The H-bond interactions formed by the residue Thr162 were also confirmed by protein-ligand contacts in MD simulation (Figure 2.9.e). The  $\pi$ -cation hydrophobic contacts which formed over the simulation time with the residues Phe163, Val166, Phe238, Phe239, Phe439, Phe443, could also contribute to its stability. Ionic interactions, which do not involve a hydrogen bond, were also observed with the residues Glu193, Glu 236, and Asp293. Apart from these interactions, water bridges involving hydrogen-bonded interactions mediated by water

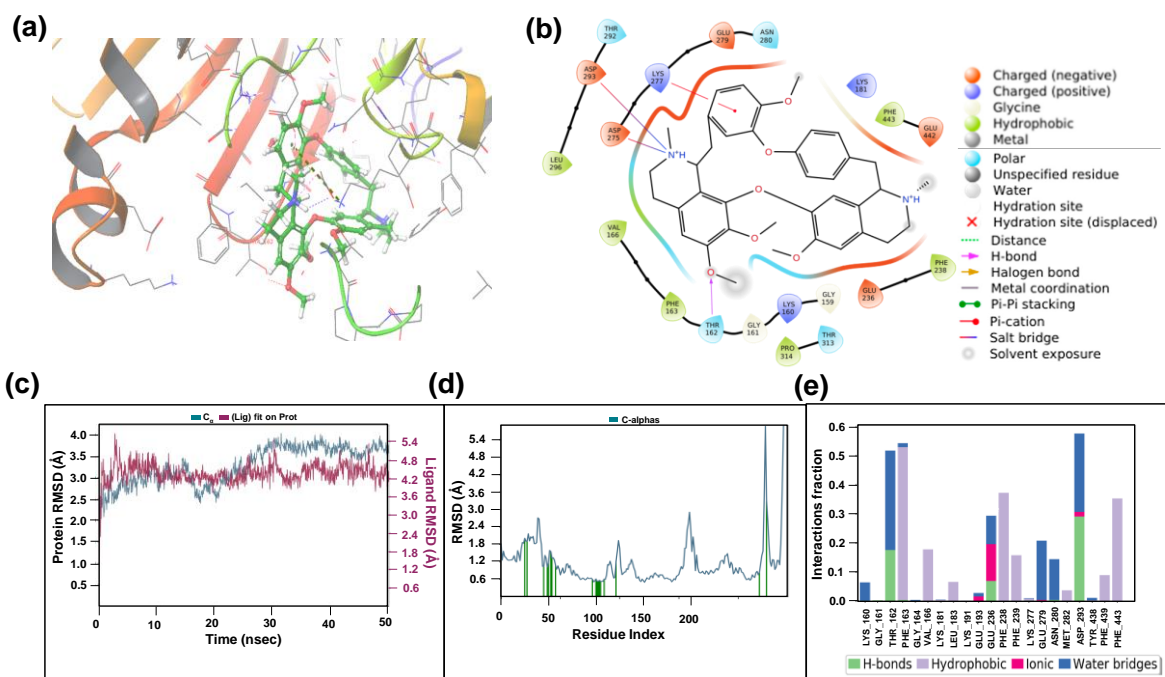
<b>Protein</b>	<b>PDB ID</b>	<b>Docking Score</b>	<b>Number of H-bonds</b>
Akt	1O6L	-5.023	1
MMP-2	1GEN	-3.226	1
mTOR	4JSP	-4.020	-
Survivin	1F3H	-2.763	-
Caspase-9	2AR9	-2.140	-
Caspase-8	4ZBW	-5.064	2
p53	1TUP	-2.091	1
PARP	5DSY	-4.218	1
STAT3	6NJS	-4.111	3

Table 2.1. Docking score of various proteins with Phaeanthine



**Figure 2.8.** Interaction of various proteins with Phaeanthine

molecules were observed. Overall, this suggests the stability of the Akt- PHA complex with the collaborative role of hydrogen bonding, hydrophobic interactions, and salt bridges.



**Figure 2.9.** (a)& (b) Interaction of PHA with Akt; results from MD simulation (c) RMSD Plot of Akt and PHA complex (d) RMSF plot of the protein. The green vertical line shows the residues interacting with the ligand. (e) Interactions between Akt and PHA over the 50 ns simulation time.

### 2.2.5 Apoptotic Evaluation of PHA

Firstly, live dead dual staining assay was conducted to differentiate the apoptotic cells where the fluorescent dyes (acridine orange and ethidium bromide) would label the viable and dead cells differently. HeLa cells were treated with PHA, which showed redder to orange-coloured cells than the control (green fluorescence) in a concentration-dependent manner (Figure 2.10.a). Next, APOP staining of cells was carried out to distinguish the apoptotic cells from healthy ones, where the dead cells resembled pink colour due to membrane damage by the treatment of PHA. At the same time, the untreated control did not show pink-coloured cells (Figure 2.10.b).

To corroborate the apoptosis-driven cell death by PHA, we also investigated the FITC annexin V apoptosis assay. HeLa cells were treated with two different concentrations of PHA (6  $\mu$ M

and 15  $\mu\text{M}$ ), where the percentage of apoptotic cells showed a considerable hike in the treated cells than that of the control. As shown in figure 3c, the percentage of apoptotic cells in the untreated control was 11.6%, which increased to 65.5% in cells treated with 6  $\mu\text{M}$  and 93.4% in 15  $\mu\text{M}$  PHA treated cells (Figure 2.10.c).

### 2.2.6 Evaluation of Caspase-Mediated Apoptosis

Cysteine-aspartic proteases or caspases regulate the cell death pathways involving mitochondria. The expression of caspase 3, 8, and 9 were evaluated by fluorometric assays. The expression of executioner caspase 3 upon treatment with PHA (15  $\mu\text{M}$ ) showed a hike of 2.6-fold fluorescence intensity compared to untreated cells. Likewise, in the case of caspase 9, cells treated with a higher concentration of compound (15  $\mu\text{M}$ ) showed a similar pattern with approximately 2.3 fold increases in the fluorescence intensity compared to control. But in case of caspase 8, a markable decrease in the fluorescence intensity was observed in the treated cells. At a 6  $\mu\text{M}$  concentration of PHA, a 2.25-fold decrease and at a higher (15  $\mu\text{M}$ ) concentration, decline in the fluorescence intensity (8.72 fold) than the control was observed (Figure 2.10.d). The up-regulation of caspase 9 and downregulation of caspase 8 substantiated the intrinsic or mitochondria-mediated apoptosis involved in the treatment of PHA in HeLa cells.

### 2.2.7 Assessment of Mitochondrial Membrane potential induced by PHA

A decrease in the mitochondrial membrane potential (MMP) could be considered a marker event in the early stages of apoptosis.<sup>21</sup> JC-1 is a cationic dye that can form aggregates at a high membrane potential in the mitochondrial matrix. This polymerization will yield red emission. But in mitochondrial membrane-compromised cells or an apoptotic cell, the MMP is very low. At this low MMP, JC-1 cannot form aggregate and will retain as a monomer and yield green fluorescence. So, this aggregate/monomer ratio can be used as a parameter to study apoptosis in cancer cells. The apoptotic cells will show a lower red/green or aggregate/monomer ratio. HeLa cells were treated with 5  $\mu\text{M}$  and 8  $\mu\text{M}$  of PHA for 24 hours of incubation which showed a higher green fluorescence than red, indicating the JC-1 retaining as monomer (Figure 2.11.a). The aggregate/monomer ratio is reduced compared to

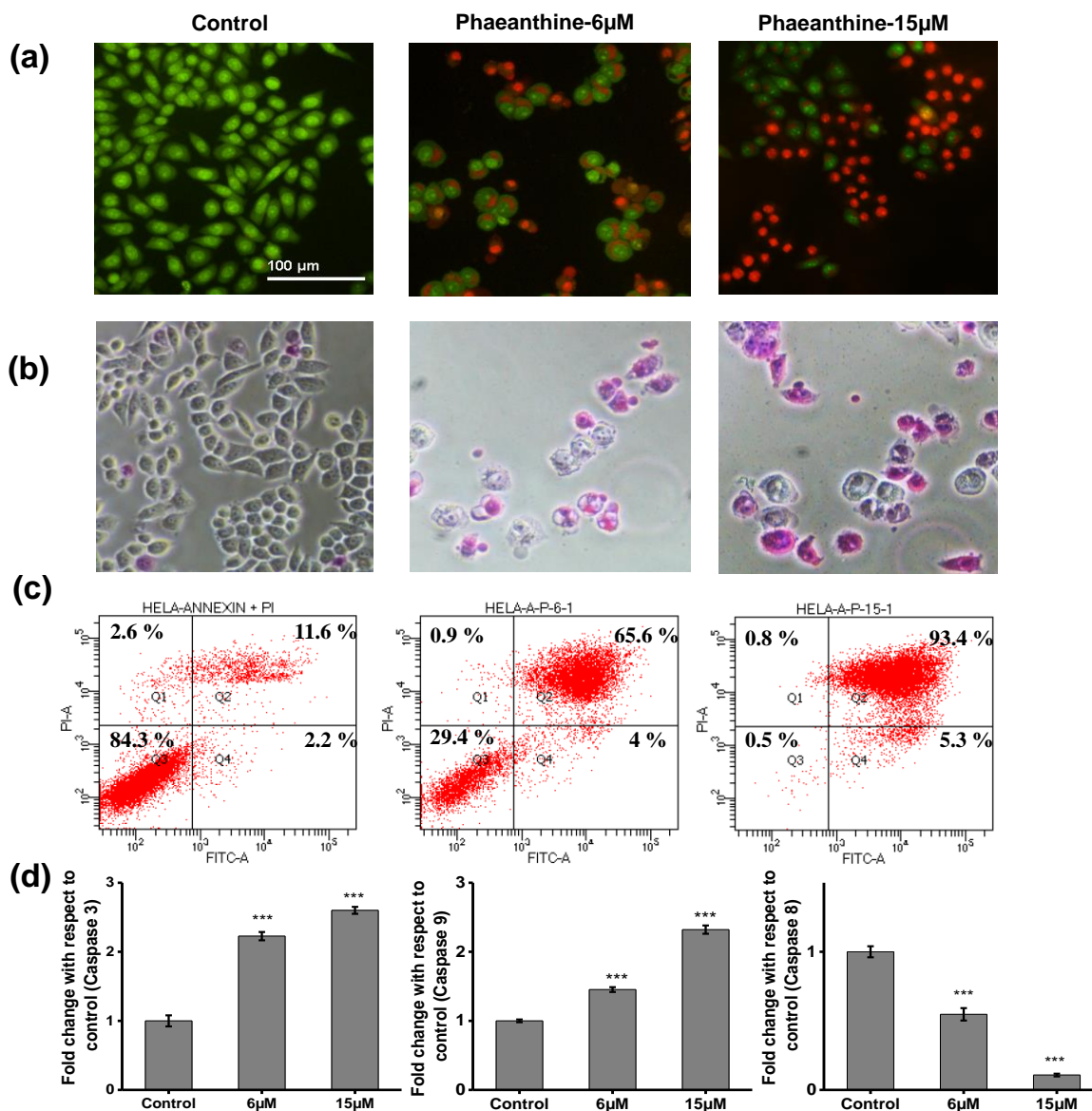


**Figure 2.10.** PHA induced apoptosis in HeLa cells. HeLa cells were treated/untreated with 6 and 15  $\mu$ M concentrations for 24 h to perform (a) Acridine orange-ethidium bromide dual staining assay, (b) APOP staining assay, (c) Annexin V apoptosis assay, (d) Caspase fluorometric assay- The assays were carried out in triplicates and the data are expressed as mean  $\pm$  SD. p values \*\*\*  $p < 0.001$ , \*  $p < 0.05$  were considered to be significant as compared to the control.

the untreated cells. The untreated cells showed an aggregate/monomer ratio of  $2.6034 \pm 0.30$ . In contrast, treated cells at 5  $\mu$ M concentration showed  $0.2830 \pm 0.03$  and at 8  $\mu$ M PHA treated cells have  $0.2013 \pm 0.05$  ratios (Figure 2.11.b). The decrease in the aggregate/monomer ratio

indicates the JC-1 aggregate formation is hindered upon the treatment, by the depolarisation of membrane potential.

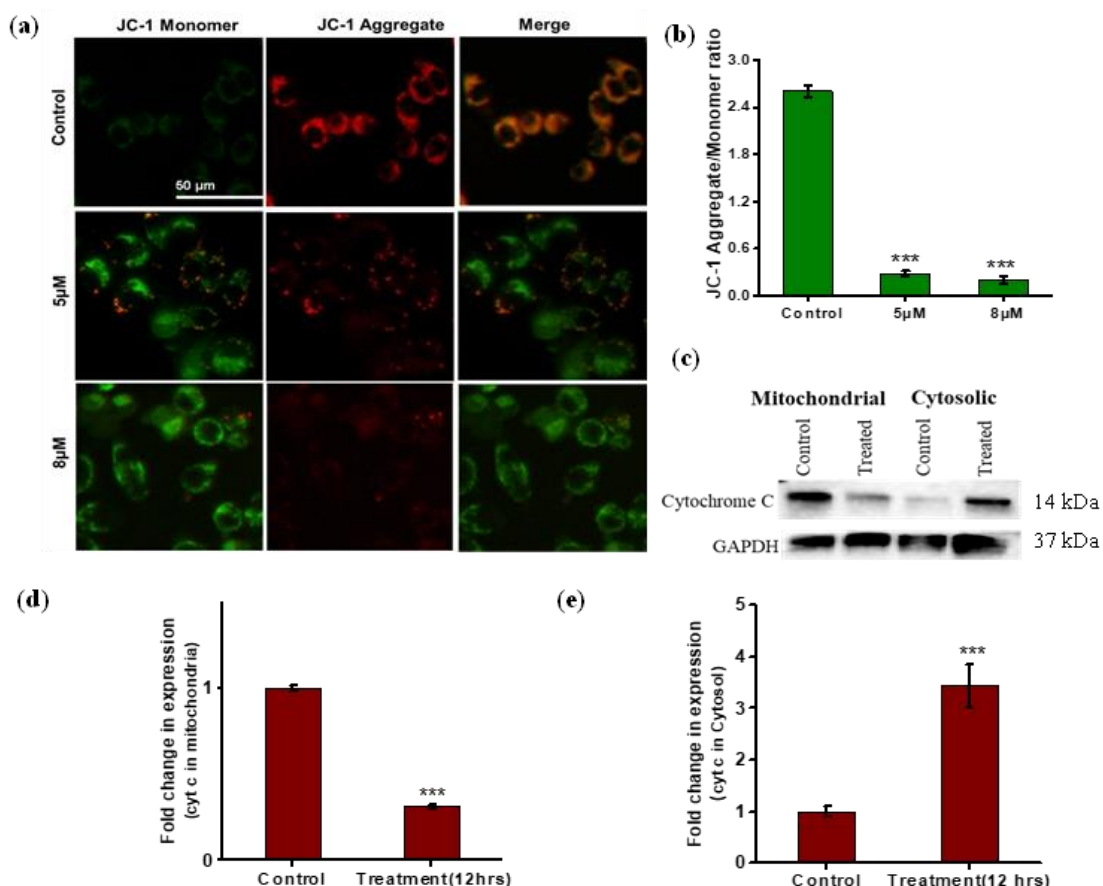


**Figure 2.11.** (a) Mitochondrial membrane potential evaluated by JC-1 dye (b) JC-1 aggregate/monomer ratio gets decreased with the treatment (at 5 and 8 µM of PHA), (c) Blot of mitochondrial and cytosolic cytochrome c, (d) expression of mitochondrial cytochrome c in control versus PHA treated cells, (e) expression of cytosolic cytochrome c in control versus PHA treated cells. The assays were carried out in triplicates, and the data are expressed as mean ± SD. p values \*\*\* p<0.001, was considered significant compared to the control.

### 2.2.8 Evaluation of Cytochrome C (cyt c) Dynamics by PHA

The extent of the intrinsic apoptotic pathway was well understood by the dynamics of cyt c, which triggers the mitochondria-dependent apoptosis pathways. The cyt c is located in normal healthy cells' inter mitochondrial membrane space. Upon receiving apoptotic stimuli, the outer membrane gets permeabilized and releases cyt c to the cytosol. So, the release of cyt c is a noticeable change during apoptosis or it represents mitochondria's involvement in

apoptotic cell death.<sup>22</sup> The expression of mitochondrial and cytosolic cyt c has been investigated and compared their expression between PHA treated and untreated cells (Figure 2.11.c). The results depicted the release of cyt c into the cytosol from mitochondria since the treated group showed membrane gets permeabilized and releases cyt c to the cytosol. So, the release of cyt c is an upregulation in cytosolic cyt c (Figure 2.11.d). Also, downregulated the mitochondrial cytochrome c protein expression compared to the control group (Figure 2.11.e).

### **2.2.9 PHA induced DNA condensation and DNA fragmentation**

DNA condensation and subsequent fragmentation is a hallmark of apoptosis. Therefore, the condensation pattern of DNA was studied using Hoechst nuclear staining assay. The nuclei of the untreated cells appeared round and uniformly stained, while the PHA treated cells showed intensely stained areas because of DNA condensation (Figure 2.12.a). Further, the agarose gel electrophoresis was carried out to confirm the DNA fragmentation pattern. The isolated DNA demonstrated a laddering pattern in the cells treated with a higher concentration of PHA (Figure 2.12.b).

### **2.2.10 Cellular Internalization and DNA Fragmentation by SERS Modality**

As a new insight, Raman fingerprints of PHA through surface enhanced Raman scattering (SERS) spectral analysis were evaluated for cellular internalization and DNA fragmentation (Figure 2.12.d). Cellular internalization of PHA was tracked in a time-dependent manner in HeLa cells. Cells were treated with PHA (6  $\mu\text{M}$ ) to monitor intracellular Raman fingerprints of PHA with 633 nm laser of confocal Raman microscope using colloidal gold nanoparticles (AuNPs: 40-45 nm) as SERS substrate. After 1 hour, it was observed the signature Raman peaks of PHA at 1000 and 1590  $\text{cm}^{-1}$  (aromatic ring vibrations)<sup>23,24</sup>, 1160  $\text{cm}^{-1}$ , 1212  $\text{cm}^{-1}$  (trisubstituted amine C-N stretch)<sup>25</sup>. Similarly, distinct peak patterns were observed at around 2 hours onwards till 4 hours, but after 8 hours, the PHA peaks were declined substantially, which may be due to its cellular metabolic decomposition.



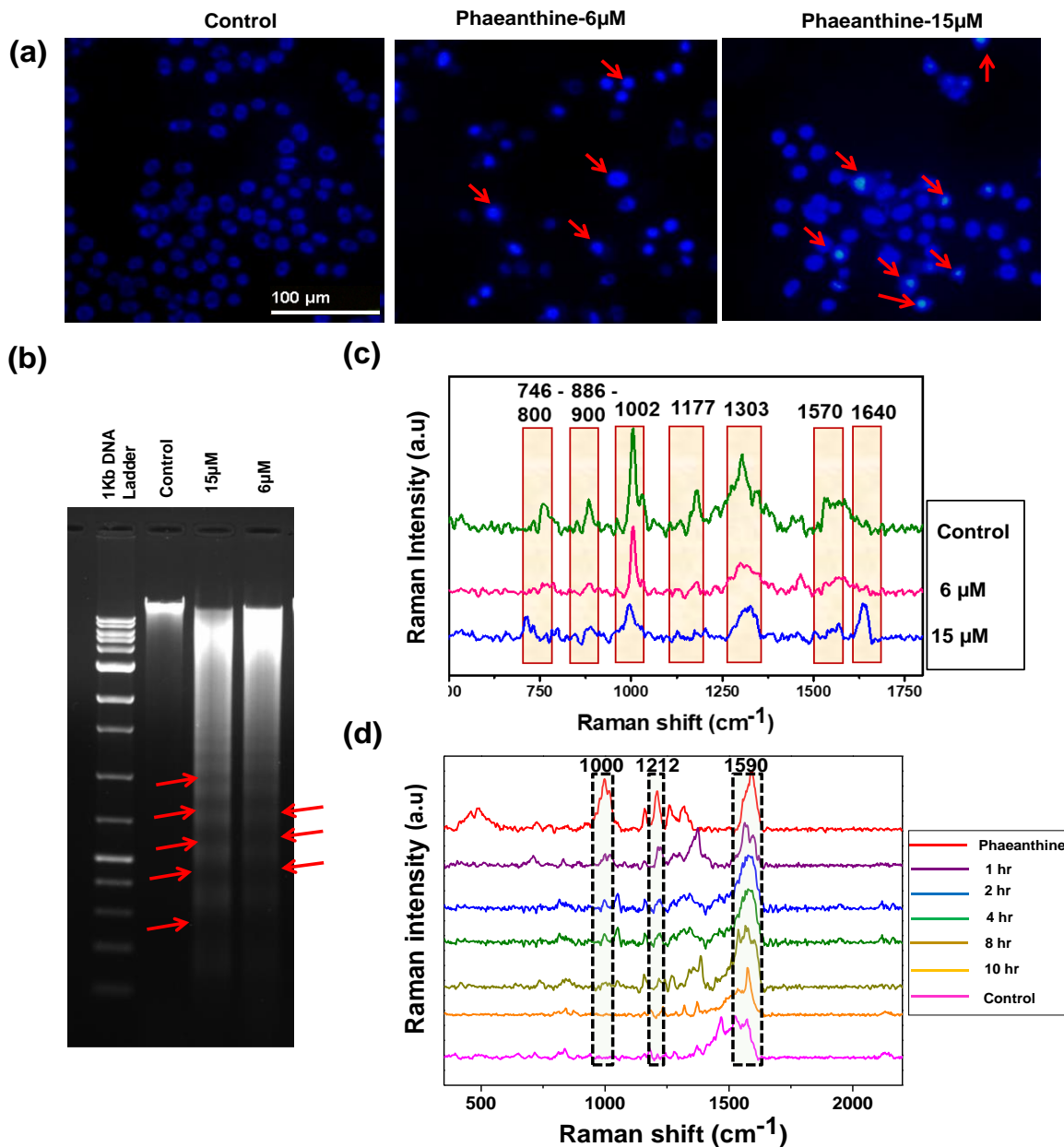


**Figure 2.12.** Nuclear fragmentation and condensation induced by PHA (a) Hoechst nuclear staining, (b) DNA laddering by AGE, (c) SERS analysis of DNA fragmentation, (d) Internalisation of PHA (6 µM) into cells monitored using SERS.

Next, the isolated DNA from the PHA treated and the untreated cells were mixed with AuNPs, and SERS fingerprints were assessed. The signature Raman peaks associated with various molecular vibrations from DNA were identified which complied perfectly with the literature report.<sup>26,27</sup> The DNA signature peaks from 746 to 800 cm<sup>-1</sup>, including ring breathing mode of pyrimidines, phosphodiester bond vibrations, especially -O-P-O stretching, as well as deoxyribose and phosphodiester bond peaks at 870 to 900 cm<sup>-1</sup> and aromatic ring vibrations at

1002  $\text{cm}^{-1}$  were found to be less intensified in the treated samples (Figure 2.12.c). Similar effect was observed for 1177/1180  $\text{cm}^{-1}$  cytosine guanine and 1303  $\text{cm}^{-1}$  adenine, cytosine peaks and DNA mode vibrations peaks at 1573-7  $\text{cm}^{-1}$ . We could observe enhanced peak intensity at 1620-1660  $\text{cm}^{-1}$  in higher dosage (15 $\mu\text{M}$ ) of PHA -treated cellular DNA indicating the base-pairing interactions and base-stacking effects due to H bond formation. This may be due to DNA fragmentation associated with the base-pairing regions, leading to the generation of the particular SERS peaks in the treated sample. Thus, the SERS analysis reconfirms the apoptosis associated DNA fragmentation in the PHA treated samples.

### **2.2.11 Inhibition of Clonogenic Potential by PHA in HeLa Cells**

Next, investigation on the inhibitory potential of PHA was assessed in the colony-forming capacity of HeLa cells. The compound at 0.5  $\mu\text{M}$  and 1  $\mu\text{M}$  effectively inhibited the clonogenic potential of HeLa cells. The survival fraction was getting substantially reduced in 1  $\mu\text{M}$  PHA treated colonies as compared to the control colonies (Figure 2.13.b). A very high clonogenic inhibitory potential at a significantly lower concentration (1  $\mu\text{M}$ ) reflects the inhibitory ability of the compound in a dose-dependent manner (Figure 2.13.a).

### **2.2.12 Induction of Cell Cycle arrest by PHA**

Flow cytometric analysis to investigate the cell cycle distribution was performed to further explore the mechanism of action of PHA. Malignancies are characterized by a dysregulation of the cell cycle, which allows them to proliferate uncontrollably. Many clinically used drugs are known to induce cell cycle arrest, thereby controlling tumour growth.<sup>28</sup> We have monitored the effect of PHA in regulating the cell cycle pattern upon treatment with 6 and 15  $\mu\text{M}$  concentrations for 24 hours of incubation. The percentage of cells at G1phase decreased to 51% and 41.2%, respectively, than the untreated control (59.1%). The

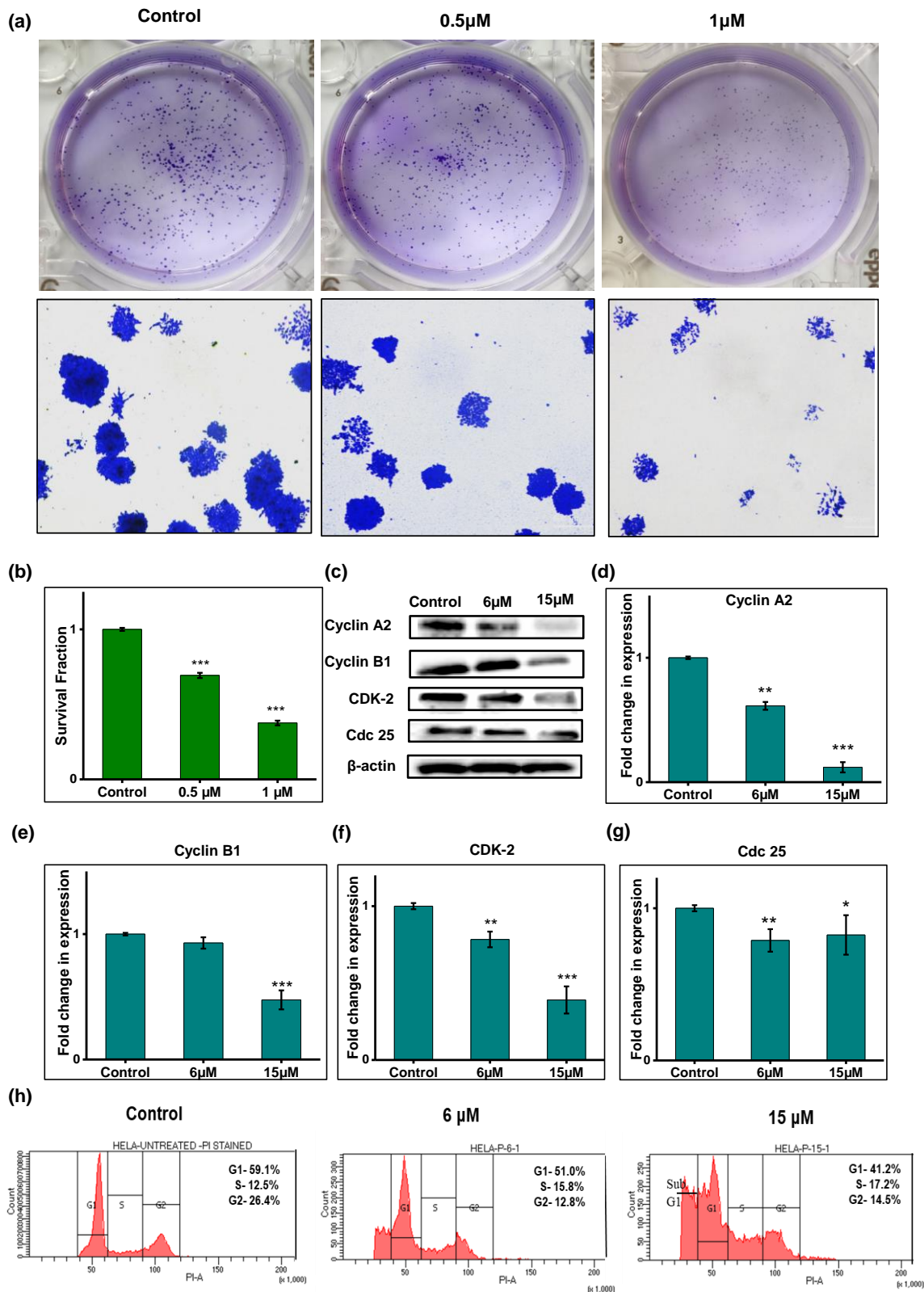


**Figure 2.13.** (a) Colony formation assay, (b) Survival fraction of the colonies, (c) Blot of cell cycle proteins, (d) Expression of Cyclin A2, Cyclin B1, CDK-2, and Cdc 25, (e) Cell cycle assay- Control denotes the untreated cells. The assays were carried out in triplicates and the data are expressed as mean  $\pm$  SD. p values \*\*\*\*  $p < 0.001$ , \*\*  $p < 0.01$ , \*  $p < 0.05$  were considered to be significant as compared to the control no Asterisk (\*) sign represent not significant p-value.

treated cells also showed an upsurge in the cells at the Sub G1 phase in a dose-dependent manner, indicating the apoptotic population of cells upon treatment (Figure 2.13.h). Further, we checked the expression of some of the key regulator proteins involved in the cell cycle regulation. Western blot analysis of various proteins like Cyclin A2, Cyclin B1, CDK 2, and Cdc25c was also carried out (Figure 2.13.c). A significant reduction in the expression of cyclins was observed, indicating the downregulation of cell cycle proteins, thereby arresting the cell cycle to prevent the proliferation of the cancer cells. Cyclin A2 is in a strategic position to control a large part of the cell cycle because of its presence during S, G2, and early mitosis.<sup>29</sup> Cells with repressed cyclin B1/Cdc2 activity are more likely to remain in the G2 phase, whereas cells with upregulated cyclin B1/Cdc2 activity are more likely to enter and complete mitosis.<sup>30</sup> So, the cyclin B1 downregulation will allow the cancer cells to remain in the G2 phase and arrest its entry to mitosis for proliferation. CDK2 helps in the S phase to G2 phase transition by binding to cyclin E and cyclin A during the initial and terminating stages of the S phase.<sup>31</sup> Cdc25c is involved in G2/M transition in cell cycle.<sup>32</sup> From the Western blotting of these proteins, we could observe the downregulation of all these four proteins involved in the cell cycle regulation (Figure 2.13.d, e, f, g). The results also indicate a possible chance of arrest at the G2 phase of the cell cycle, thereby regulating the proliferation of cells. PHA can control the cell cycle progression by downregulating the expression of crucial regulators like cyclins and CDKs. Targeting cell cycle regulators always makes a better therapeutic strategy.<sup>33</sup>

### 2.2.13 PHA Modulated Expression of Various Proteins Involved in Apoptosis

The promising apoptosis-inducing potential of PHA was re-confirmed based on the the expression studies of major proteins involved in the apoptotic pathway. Western blot analysis (Figure 2.14.a) and human apoptosis antibody array membrane assay (Figure 2.14.i & j) were performed to evaluate the expression of key players in the apoptosis pathways. The array membrane is comprised of antibodies of 43 key proteins involved in the process of cell death

via apoptosis. The expression studies finally revealed the alteration of various proteins. The proteins involved in promoting apoptosis, like Bax, cleaved PARP, Bid, p53, Caspase 3, p21, Hsp60 and p27 were upregulated. Treatment with PHA downregulated some of the anti-apoptotic proteins like Akt, p-Akt, Mcl-1, CD40, IGF-2, and XIAP. Bax and Bid are pro-apoptotic proteins and the activation of caspases and p53 promotes the apoptotic pathway. High levels of IGF-2 were found to be associated with an increased risk of developing cancer.<sup>34</sup> By downregulating the expression of IGF-2, PHA inhibits the binding of IGF-2 to the insulin receptor, thereby downregulating the Ras and Akt pathway, which ultimately inhibits the survival, proliferation, invasion, and angiogenesis of cancer cells.<sup>35</sup> The regulation of Akt signalling is an important phenomenon in cancer control. We observed a downregulation in the expression of total Akt and its phosphorylated form p-Akt, thereby inhibiting PI3K/Akt signalling for survival and proliferation with PHA treatment. CD40 is overexpressed in a wide variety of carcinomas, even a higher level of expression is observed in cervical carcinomas.<sup>36</sup> Activation of CD40 by CD40L results in the proliferation of cancer cells by upregulating MAPK, NF- $\kappa$ B, and JNK pathways.<sup>37</sup> So, PHA mediated downregulation of CD40 revealed an evident inhibition of the proliferative cells. X-linked inhibitor of apoptosis protein (XIAP) expression is observed to be elevated in cases of malignancies by inhibiting the activation of caspase 3 and 9 and inhibiting apoptosis-mediated cell death.<sup>38</sup> PHA induced a downregulation of XIAP which indicates the activation of initiator and executioner caspases, thereby initiating the cellular apoptotic death mechanism. It was observed the decrease in the expression of Mcl-1 protein with the treatment, Mcl-1 is usually found to inhibit the oligomerization of Bak and Bax and inhibits the release of cytochrome C from the mitochondrial membrane.<sup>39</sup> So, its downregulation will initiate apoptosis. So targeting Mcl-1 is a new strategy for cancer therapy.<sup>40</sup>

Bid is a proapoptotic protein which cleaves on activation and moves into the mitochondria to induce mitochondrial membrane permeabilization. This process is achieved by the oligomerization of Bax and Bak and, thus, the release of cyt c out of mitochondria.<sup>41</sup> Hsp60 plays a role in caspase-3 activation by functioning as a chaperone and promoting the protease-sensitive state of pro-caspase-3.<sup>42</sup> SMAC is another mitochondrial protein along with

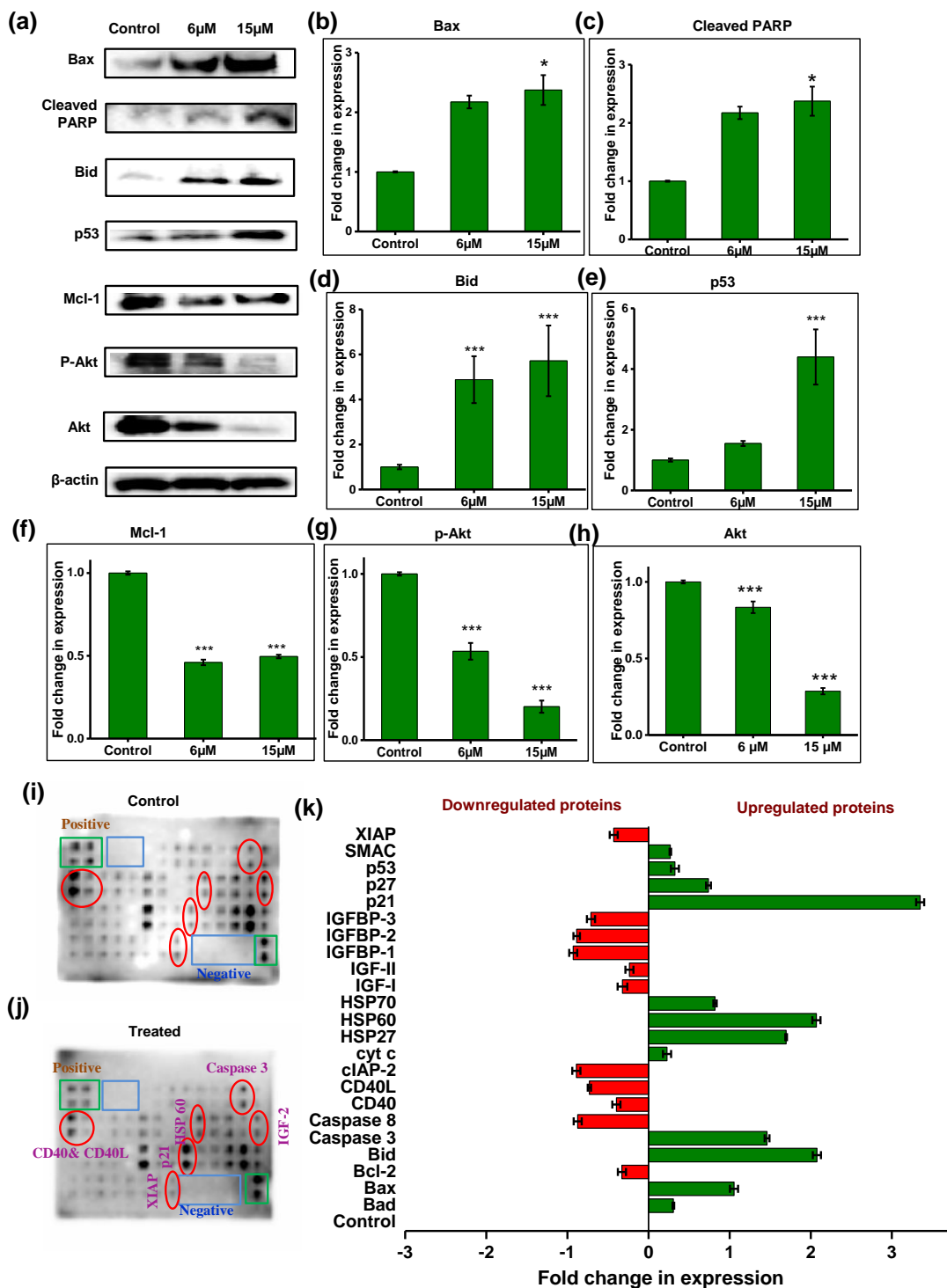


**Figure 2.14.** (a) Blot of apoptotic proteins, Fold change in expression of (b) Bax, (c) Cleaved PARP, (d) Bid, (e) p53, (f) Mcl-1 and (g) p-Akt (h) Akt, Apoptotic antibody array membrane analysis on HeLa cells (i) Untreated control and (j) treatment with PHA at a concentration of 8  $\mu$ M for 24 hours incubation and (k) fold change in expression of proteins in apoptotic array

membrane treated by PHA, The red colour bars indicates downregulated and the green represents upregulated proteins, the graph represents values as control intensity(1) subtracted from the normalised value of each protein. The assays were carried out in triplicates and the data are expressed as mean  $\pm$  SD .p values \*\*\*  $p < 0.001$ , \*  $p < 0.05$  were considered significant compared to the control and no Asterisk (\*) sign represents not significant p-value.

cyt c, which gets released into the cytosol upon receiving the death signal. SMAC eradicates the action of IAPs (Inhibitor of apoptosis proteins) and activates the caspase activation cascade with the help of cyt c and Apaf.<sup>43</sup> So, the upregulation of these proteins, namely, Bid, Hsp60, SMAC, and cyt c, specifies the involvement of mitochondria-mediated apoptosis in cancer cell death. Apart from these, the expression of proteins like p21, p27, and p53 also got elevated. These proteins are involved in cell cycle arrest and regulation<sup>44</sup>, thereby controlling the tumours further growth. From the above data a mechanism has been proposed for cell death in HeLa cells by PHA (Figure 2.15).

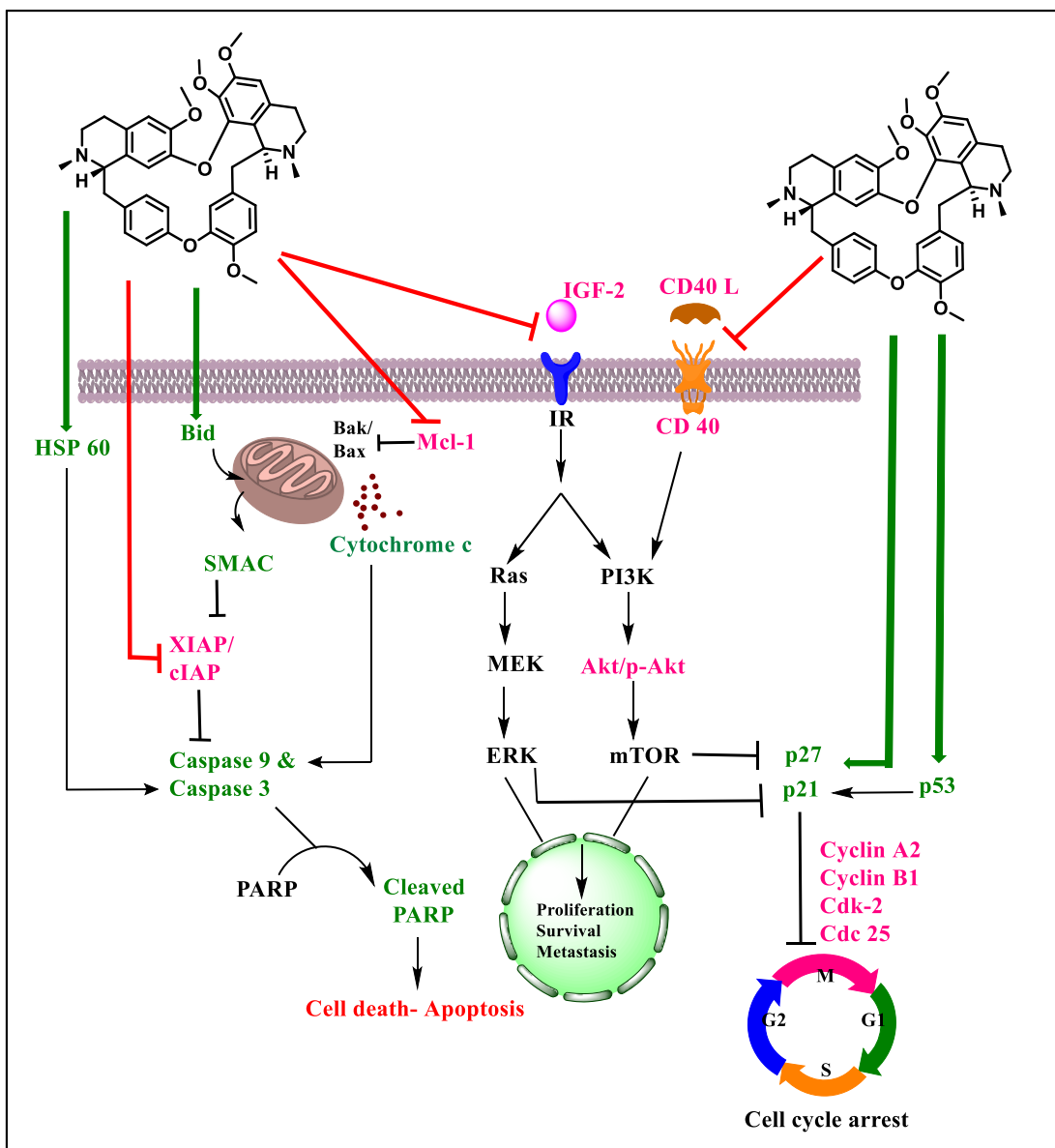


**Figure 2.15.** Proposed mechanism of action of PHA. Red arrows indicate inhibition, and green arrows represent activation of proteins. Green coloured and magenta coloured entries represent experimentally validated proteins that are upregulated and downregulated, respectively, while the black coloured entries are not currently evaluated.

### 2.3 Conclusion

In summary, three major alkaloids from the rhizome of *Cyclea peltata*, namely PHA, cycleanine, and *N*-methyl corydaldine were isolated successfully. Among the three, PHA



showed its highest potency in inhibiting cervical cancer cell proliferation. The selected compound, PHA, was found safer for the non-tumorigenic cell line, MCF-10A, especially at a moderate concentration, which was adequate for apoptotic induction in HeLa cells. *In silico* studies of the PHA revealed its good binding affinity with the anti-apoptotic and proliferative protein Akt, reflecting a docking score of -5.023. The *in silico* data was well complemented with *in vitro* assessment which confirmed mitochondria-mediated apoptosis by downregulating the expression of total Akt and its phosphorylated form, p-Akt, including other anti-apoptotic proteins like MCI-1, IGF-2, and XIAP. Furthermore, mitochondrial depolymerization and the release of cytochrome c into the cytosol resembled the mitochondria-mediated cell death by the treatment of PHA. As a new insight, the SERS fingerprint of PHA was utilized to track cellular internalization and investigated apoptotic events by Raman fingerprint analysis of cellular DNA and other biomolecules. Finally, the PHA triggered cell cycle arrest through downregulation of the expression of major regulatory proteins involved in cell cycle progression was studied as well. To the best of our knowledge, this is the first report on the detailed *in vitro* anticancer studies of PHA, and its inhibition on the Akt signalling pathway demonstrated in HeLa cells. These results can help in developing a better treatment strategy for cervical cancer from PHA, a natural pharmacophore.

## 2.4 Experimental Section

### 2.4.1 General Experimental procedures

All chemicals and solvents were purchased from Sigma- Aldrich, Merck, and Spectrochem and used without further purification. Analytical TLC was performed on a Merck 60 F<sub>254</sub> silica gel plate (0.25 mm thickness), and visualization was done with UV light (254 and 365 nm). Column chromatography was performed on Merck 60 silica gel (60–120 or 100–200 mesh). The 1D and 2D NMR spectra were recorded on a Bruker ADVANCE 500 MHz, using MeOD and CDCl<sub>3</sub> as solvents and the chemical shifts were expressed in ppm relative to the TMS peak. The melting point was recorded on Buchi melting point apparatus. The HRESIMS data were recorded at 60,000 resolutions using Thermo Scientific Exactive mass spectrometer. Specific rotation was measured on JASCO P-2000 polarimeter. HPLC of the compound PHA was done on Shimadzu HPLC-LC 20A series (in C18 column, Conditions:

0.25% acetic acid in water and methanol in the ratio 1:1, 145 kgf pressure and Flow rate:1.0 mL/min) and showed a purity of >98%.

## 2.4.2 Extraction, Isolation, and Characterization of Phytomolecules

### 2.4.2.1 Collection of plant material

*Cyclea peltata* rhizomes were collected from Wayanad, Kerala, India. A voucher specimen of the plant was deposited in the herbarium repository of M. S. Swaminathan Research Foundation (MSSRF), Kerala, India, with voucher number M.S.S.H. 2709.

### 2.4.2.2 Extraction and isolation procedure of *C. peltata*

The rhizomes of *Cyclea peltata* were thoroughly cleaned and dried in a hot air oven maintained at 50°C for three days. Approximately 2 kg of the plant material was coarsely crushed and subjected to repeated extraction using hexane, acetone, ethanol, and water, yielding 5 g of hexane extract, 20 g of acetone extract, 200 g of ethanol extract, and 10 g of water extract. Since the acetone and ethanol extract showed a positive result for Dragendorff's test for alkaloids, we adopted a detailed acid-base extraction procedure<sup>45</sup> to isolate the benzyloquinoline alkaloids from the ethanol extract. And the fractions were subjected to silica column chromatography to isolate the compounds.

### 2.4.2.3 Spectral data

#### Compound 1: Phaeanthine

**Molecular formula:** C<sub>38</sub>H<sub>42</sub>N<sub>2</sub>O<sub>6</sub>

**<sup>1</sup>H NMR** (500 MHz, MeOD):  $\delta_{\text{H}}$  7.45 (1H, d,  $J = 8.5$  Hz), 7.06 (1H, dd,  $J = 2.0$  Hz, 8.0 Hz), 6.92 (1H, d,  $J = 8.5$  Hz), 6.87 (1H, d,  $J = 8.0$  Hz), 6.76 (1H, dd,  $J = 2.0$  Hz, 8.5 Hz), 6.67 (1H, s), 6.56 (1H, s), 6.43 (1H, s), 6.39 (1H, d,  $J=8.5$  Hz), 6.03 (1H, s), 4.59 (1H, s), 4.07-4.03 (1H, m), 3.88 (3H, s), 3.86 (1H, d,  $J=10.5$  Hz), 3.73 (3H, s), 3.53-3.47 (2H, m), 3.37 (3H, s), 3.16 (3H, s), 3.06-3.01 (1H, m), 2.97-2.93 (2H, m), 2.90 (1H, d,  $J = 7.0$  Hz), 2.87-2.82 (2H, m), 2.80-2.75 (1H, m), 2.64 (3H, s), 2.57 (1H, dd,  $J = 5.0$  Hz, 17.0 Hz), 2.50 (1H, d,  $J = 14.5$  Hz), 2.30 (3H, s) ppm.

**$^{13}\text{C}$  NMR** (125 MHz, MeOD):  $\delta_{\text{C}}$  153.8, 151.7, 149.6, 149.0, 147.9, 147.4, 143.8, 135.0, 132.4, 130.4, 127.8, 127.6, 122.9, 121.4, 120.0, 115.3, 112.5, 112.0, 106.0, 63.2, 61.7, 59.3, 55.4, 55.0, 54.7, 44.3, 43.9, 41.6, 41.1, 41.0, 36.1, 24.4, 22.2 ppm.

**HRESI-MS**  $m/z$   $[\text{M}+\text{H}]^+$  623.3126 (calcd for  $\text{C}_{38}\text{H}_{43}\text{N}_2\text{O}_6$ , 623.3116). Specific rotation:  $[\alpha]_{\text{D}}^{25}$ :  $-353^\circ$ ,  $c = 0.2$ , MeOH, Melting point: 188-192  $^\circ\text{C}$

### Compound 2: Cycleanine

**Molecular formula:**  $\text{C}_{38}\text{H}_{42}\text{N}_2\text{O}_6$

**$^1\text{H}$  NMR** (500 MHz,  $\text{CDCl}_3$ ):  $\delta_{\text{H}}$  7.28 (1H, dd,  $J = 8.5$  Hz, 1.5 Hz), 7.07 (1H, dd,  $J = 8.0$  Hz, 2.5 Hz), 6.83-6.73 (2H, m), 6.74 (1H, dd,  $J = 8.0$  Hz, 2.5 Hz), 6.47 (1H, s), 6.44 (1H, s), 6.23-6.22 (2H, m), 5.93 (1H, s), 3.86 (3H, s), 3.84-3.80 (1H, m), 3.69 (1H, d,  $J = 11.0$  Hz), 3.68 (3H, s), 3.48-3.34 (2H, m), 3.30 (3H, s), 3.20 (1H, dd,  $J = 12.5$  Hz, 6.0 Hz), 3.12 (3H, s), 2.90-2.80 (4H, m), 2.74 (1H, d,  $J = 11.5$  Hz), 2.70-2.67 (1H, m), 2.65-2.62 (1H, m), 2.55 (3H, s), 2.45 (1H, d,  $J = 14.0$  Hz), 2.39-2.36 (1H, m), 2.27 (3H, s) ppm.

**$^{13}\text{C}$  NMR** (125 MHz,  $\text{CDCl}_3$ ):  $\delta_{\text{C}}$  153.7, 151.4, 149.4, 148.7, 148.4, 147.1, 143.8, 137.9, 135.1, 134.8, 132.6, 130.2, 128.1, 127.8, 122.8, 122.0, 121.9, 120.2, 116.1, 112.7, 111.5, 105.7, 63.9, 61.4, 60.3, 56.1, 55.8, 55.8, 45.2, 44.2, 42.5, 42.3, 41.9, 38.2, 25.1, 22.1 ppm.

**HRESI-MS**  $m/z$   $[\text{M}+\text{H}]^+$  623.3121 (calcd for  $\text{C}_{38}\text{H}_{43}\text{N}_2\text{O}_6$ , 623.3123), Specific rotation:  $[\alpha]_{\text{D}}^{25}$ :  $-14.9^\circ$ ,  $c = 0.2$ , MeOH, Melting point: 116-120  $^\circ\text{C}$

### Compound 3: *N*-methyl corydaldine

**Molecular formula:**  $\text{C}_{12}\text{H}_{15}\text{NO}_3$

**$^1\text{H}$  NMR** (500 MHz,  $\text{CDCl}_3$ ):  $\delta_{\text{H}}$  7.53 (1H, s), 6.56 (1H, s), 3.85 (3H, s), 3.84 (3H, s), 3.48 (2H, t,  $J = 7.0$  Hz), 3.07 (3H, s), 2.87 (2H, t,  $J = 6.5$  Hz) ppm.

**$^{13}\text{C}$  NMR** (125 MHz,  $\text{CDCl}_3$ ):  $\delta_{\text{C}}$  165.0, 151.8, 148.1, 131.6, 122.1, 110.6, 109.4, 56.2, 56.1, 48.5, 35.2, 27.6 ppm.

**HRESI-MS**  $m/z$   $[\text{M}+\text{H}]^+$  222.1138 (calcd for  $\text{C}_{12}\text{H}_{16}\text{NO}_3$ , 222.1132).

### 2.4.3 Cell culture methods

The human cervical cancer cell line, HeLa, was obtained from American Type culture collection (ATCC, USA), and the normal breast epithelial cell line MCF-10A from Elabscience, USA. HeLa cells were maintained in Dulbecco's modified eagle medium (DMEM, Sigma), and MCF-10A cells were maintained in MEGM (Mammary epithelial cell growth medium kit) Lonza and supplemented with 10% Fetal Bovine Serum (FBS, Himedia) and 1% antibiotic antimycotic solution 100X (with 10,000 units Penicillin, 10 mg Streptomycin and 25 µg Amphotericin B per mL in 0.9% normal saline-Himedia) and maintained at 5% CO<sub>2</sub> at 37°C in the incubator.

### 2.4.4 Cell viability assay

Cells were seeded in a 96 well plate at a seeding density of  $8 \times 10^3$  cells/well. After 24 hours of incubation, the compounds (phaeanthine, cycleanine, and *N*-methyl corydaldine) were added at different concentrations and incubated for 24 hours. After incubation, the compound containing medium was removed and washed with PBS, and MTT (3-[4,5-dimethylthiazol-2-yl]-2,5-diphenyltetrazolium) at a concentration of 0.5 mg/mL was added and kept in the dark for 2-4 hours. DMSO was added to dissolve the formazan crystals, and absorbance was measured at 570 nm in a multimode plate reader (Synergy H1, Biotek).

### 2.4.5 Molecular Docking

The X-ray crystal structure of the target proteins Akt/protein Kinase B(PDB:1O6L)<sup>46</sup>, MMP-2(1GEN), mTOR(4JSP), Survivin(1F3H), Caspase-9(2AR9), Caspase-8(4ZBW), p53(1TUP), PARP(5DSY) and STAT-3(6NJS) were obtained from the Protein Data Bank. The molecular docking is performed using Maestro to predict the binding modes against the active site pocket of the target protein.<sup>47</sup> Protein Preparation Wizard of Schrödinger suite of the program is used to prepare the protein for molecular docking. Then, Glide's receptor grid generation was used to generate a grid with a maximal size of 20 x 20 x 20 Å and 0.5 Å spacing. The molecular docking was performed using glide.<sup>48</sup>

### 2.4.6 Molecular Dynamics Simulation

All simulations were run with the OPLS-AA force field using the academic version of the MD simulation software, Desmond 6.9.<sup>49</sup> Desmond uses a specific neutral territory technique dubbed the midpoint approach to effectively take advantage of a high level of parallelism in the computation. We performed a 50 ns-long MD simulation of the system intending to analyze the Akt aberrations in an inhibitor-bound form of PHA. The system was initially set up by the system build panel and solvated in an orthorhombic box filled with water molecules. The system was then neutralized with the appropriate number of counter ions and salt concentration of 0.15 M, and a 10 buffer region was allowed between the protein-ligand complex and box sides. The systems were neutralised with Na<sup>+</sup> ions, and the overlapping water molecules were deleted. The system was exposed to local energy minimization utilising the limited memory Broyden Fletcher Goldfarb Shanno (LBFGS) algorithms and the hybrid steepest descent method. To produce simulation data for the post-simulation analyses, the system was relaxed using the constant NPT (number of atoms N, pressure P, and temperature T) ensemble condition. Using Nose-hoover thermostats and the Martina-Tobias-Klein barostat method, a constant temperature of 300 K and a stable atmospheric pressure of 1 atm were established for the duration of the simulation procedure. The final production MD was carried out for 50 ns for all systems, and the outcomes were examined using a simulated interaction diagram.

#### **2.4.7 Apoptotic assays**

Various assays were used to analyze the mode of cytotoxicity induced by the compound on HeLa cells. Acridine orange-ethidium bromide dual staining and APOPercentage were done to assess whether cells undergo apoptosis following the previously reported methods<sup>50</sup>, and the images were taken using Nikon-TS100 Inverted microscope. FITC annexin v is a sensitive probe for identifying apoptotic cells, binding to the negatively charged phosphatidyl serine. It was performed with FITC annexin V apoptosis detection kit (BD Pharmingen, Cat. No.-556547). The kit protocol was strictly followed to conduct the experiment accurately.

#### **2.4.8 Caspase fluorometric assays**

The expression of various caspases upon treatment with PHA was evaluated with caspase fluorometric assay kits (Biovision). The experiment was carried out as per the

manufacturer's protocol. HeLa cells were treated with PHA at two different concentrations (6  $\mu$ M and 15  $\mu$ M) for 24 hours; after the procedures, the fluorescence intensity was measured (Excitation: 400 nm and Emission: 505 nm) in a multimode plate reader. (Synergy H1, Biotek)

#### **2.4.9 Mitochondrial membrane potential assay**

Mitochondrial membrane potential was studied using a cationic dye, JC-1(5,5',6,6'-Tetrachloro-1,1',3,3'-tetraethyl-imidacarbocyanine iodide) (Sigma). The cells were seeded at a density of  $7 \times 10^3$  cells/well. PHA was added at lower concentrations of 5  $\mu$ M and 8  $\mu$ M. after 24 hours of incubation, cells were washed and incubated with JC-1(5  $\mu$ M) for 10 minutes. Cells were then observed under Nikon-TS100 Inverted microscope using Red and Green channel filters. The JC-1 aggregate/monomer ratio was calculated using Image J software.

#### **2.4.10 Cytochrome C release**

Cytosolic and mitochondrial proteins of the untreated control and treated cells were isolated using a previously reported method.<sup>51</sup> PHA was added at a concentration of 6  $\mu$ M and incubated for 12 hours. Fractionated proteins were subjected to western blot analysis, and mitochondrial and cytosolic cytochrome C expression in both control and treated sets were studied, keeping GAPDH as the internal control.<sup>52</sup> The density of each protein band was calculated using Image j software.

#### **2.4.11 DNA condensation and fragmentation studies**

The Condensation pattern of DNA induced by apoptosis was studied with Hoechst nuclear staining as previously reported.

##### DNA laddering

HeLa cells were seeded in T75 culture flasks. The treatment was given in two different concentrations 6  $\mu$ M and 15  $\mu$ M. The DNA was isolated using the Geneaid Genomic DNA mini kit (Geneaid, Cat. no- GB100), and the procedures were done per the kit protocol. The isolated DNA from treated cells and untreated control was run on 0.8% agarose gel to obtain the laddering pattern as previously reported. The image was captured in ChemiDoc instrument (Biorad).

### 2.4.12 Internalisation and fragmentation by SERS

SERS fingerprinting of the isolated DNA from PHA treated and untreated cells were performed by mixing the DNA with gold nanoparticles at 1:9 ratio, and SERS spectrum was collected using Raman spectroscopy (Witek, Germany). For this, 40 nm size gold nanoparticles were used as SERS substrates. SERS signals were acquired using a 633 nm laser with 5 mW power and 5 seconds integration time. The same substrate and instrumental parameters were also employed for the PHA internalization studies where the 1 mM PHA in methanol was mixed with gold nanoparticle (1:9 ratio) and SERS spectrum was collected. Further, PHA treated (6  $\mu$ M) and untreated HeLa cells seeded on a chamber slide were incubated with Gold nanoparticles for 10 minutes and SERS analysis was performed at different time points.

### 2.4.13 Colony formation assay

$1 \times 10^3$  cells/well were seeded in a 6 well plate. Compounds at two different concentrations (0.5  $\mu$ M and 1  $\mu$ M) were added after 24 hours of incubation. And the cells were allowed to form colonies for the next 9 days. After that, the colonies were visualized by staining with 0.3% crystal violet for 10 minutes and washing with PBS.<sup>53</sup> Images were captured using Nikon-TS100 Inverted microscope and processed, and colonies were counted using Image J software. Survival fraction was calculated with the formula<sup>54</sup>:

$$\text{Plating efficiency (PE)} = \frac{\text{No. of colonies counted}}{\text{No. of cells seeded}} \times 100$$

$$\text{Surviving fraction (SF)} = \frac{\text{PE of treated sample}}{\text{PE of control}} \times 100$$

### 2.4.14 Cell cycle assay

Cell cycle arrest induced by PHA was studied using BD cycletest<sup>TM</sup> Plus DNA kit (BD Pharmingen, Cat no.- 340242). All the procedures were conducted based on the kit protocol. The method involves dissolving the cell membrane lipids with a non-ionic detergent, digesting cellular RNA with enzyme, and stabilizing the nuclear chromatin. PI will bind to the isolated nuclei, and the flow cytometer analyzed the light emitted by stained cells.

The expression of some of the proteins involved in the cell cycle regulation was also evaluated by Western blot. PAGE was carried out based on the standard protocol. The isolated cell lysates from PHA treated and untreated control cells were subjected to PAGE to study the expression of Cyclin A2, Cyclin B1, CDK-2, and Cdc 25 with their corresponding antibodies (Cell signalling technology).

#### 2.4.15 Protein expression studies

Cells were seeded in T75 flasks and the compound at two concentrations (6  $\mu\text{M}$  & 15  $\mu\text{M}$ ) was added. After 24 hours of incubation, cell lysate was taken according to standard procedure using RIPA buffer and protease inhibitor cocktail. BCA protein assay kit (Thermo Scientific) was used to estimate the concentration of isolated protein, and western blotting was carried out to study the expression of various proteins. Image J software was used to get the band intensity of proteins. The expression of each protein was normalized with respect to the control and then with that of internal control  $\beta$ -actin.

#### 2.4.16 Apoptotic antibody array

The treated and untreated cell lysate were loaded on the apoptosis antibody array membrane (Abcam, Cat No.-ab134001) at equal concentrations. And all the procedures were conducted based on kit protocol. The signals were detected using a chemiluminescence imaging system (BIORAD ChemiDoc). The signal intensity for each antigen-specific antibody spot is proportional to the relative concentration of the antigen (protein) in the sample. Spot signal intensities were obtained with the help of densitometry software Image J. And the densitometric data were normalised with respect to the positive control of each membrane, and the normalization of the signals of the PHA treated lysate was done with respect to the spot on the membrane treated with lysate of untreated control cells. The relative differences in the protein expression of the treatment and control groups are obtained by comparing these signal intensities.

### 2.5 References

- (1) UICC.org. *Cervical cancer elimination*. [https://www.uicc.org/what-we-do/thematic-areas-work/cervical-cancer-elimination#\\_ftn2](https://www.uicc.org/what-we-do/thematic-areas-work/cervical-cancer-elimination#_ftn2) (accessed 2022-08-03).



- (2) Mukta Prabha, Akanksha Soni, K. P. A Review Article on Pushyanuga Churna in Stri Roga. *Univ. Res. Resour. J. Jayoti Vidyapeeth Women's Univ. Jaipur* **2018**, 1 (2), 71–75.
- (3) Suman Singh, K. Nishteswar, B. R. P. A Comprehensive Review on Therapeutic Potentials of Patha (Cissampelos Pareira Linn.) from Classical Texts of Ayurveda. *Res. Rev. A J. Pharmacogn.* **2017**, 17–35. <https://doi.org/10.5005/jp-journals-10059-0011>.
- (4) N P Rajith and V S Ramachandran. Ethnomedicines of Kurichyas , Kannur District , Western Ghats , Kerala. *Indian J. Nat. Prod. Resour.* **2010**, 1 (2), 249–253.
- (5) Yamuna C. V., Arthi I., Rajagopal P. L., Sajith Kumar P. N., Lithashabin P. K., A. A. K. Cyclea Peltata (Lam.) Hook.F. & Thomson: A Pharmacological Review. *World J. Pharm. Res.* **2020**, 9 (4), 265–273. <https://doi.org/10.20959/wjpr20204-17020>.
- (6) C Udhayavani & V S Ramachandran. Knowledge and Uses of Wild Edible Plants by Paniyas and Kurumbas of Western Nilgiris , Tamil Nadu. *Indian J. Nat. Prod. Resour.* **2013**, 4 (4), 412–418.
- (7) Sangeetha MS, Priyanga S, Hemalakshmi S, D. K. In Vivo Antidiabetic Potential of Cyclea Peltata in Streptozotocin Induced Diabetic Rats. *Asian J. Pharm. Clin. Res.* **2015**, 8 (1).
- (8) Meena J, S. S. K. Efficacy of Methanolic Extract of Cyclea Peltata as a Potent Anticancer Equivalent. *Eur. J. Environ. Ecol.* **2015**, 2 (2), 65–71.
- (9) Vijayan, F. P.; Rani, V. K. J.; Vineesh, V. R.; Sudha, K. S.; Michael, M. M.; Padikkala, J. Protective Effect of Cyclea Peltata Lam on Cisplatin-Induced Nephrotoxicity and Oxidative Damage. *J. Basic Clin. Physiol. Pharmacol.* **2007**, 18 (2), 101–114.
- (10) Shine, V. J.; Latha, P. G.; , Somasekharan Nair Rajam Suja, G. I.; Anuja; Raj, G.; Rajasekharan, S. N. Ameliorative Effect of Alkaloid Extract of Cyclea Peltata ( P Oir . ) Hook. f.& Thoms. Roots on APAP/CCl4 Induced Liver Toxicity in Wistar Rats and in Vitro Free Radical Scavenging Property. *Asian Pac. J. Trop. Biomed.* **2014**, 4 (2), 143–151. [https://doi.org/10.1016/S2221-1691\(14\)60223-9](https://doi.org/10.1016/S2221-1691(14)60223-9).
- (11) Abraham, J.; Thomas, T. D. Antibacterial Activity of Medicinal Plant Cyclea Peltata ( Lam ) Hooks & Thoms. *Asian Pacific J. Trop. Dis.* **2012**, 2, S280–S284. [https://doi.org/10.1016/S2222-1808\(12\)60166-2](https://doi.org/10.1016/S2222-1808(12)60166-2).
- (12) Darling, R.; Raja, A.; Jeeva, S.; Prakash, J. W.; Marimuthu, J. Antibacterial Activity of Selected Ethnomedicinal Plants from South India. *Asian Pac. J. Trop. Med.* **2011**, 4 (5), 375–378. [https://doi.org/10.1016/S1995-7645\(11\)60107-7](https://doi.org/10.1016/S1995-7645(11)60107-7).
- (13) Shine, V. J.; Latha, P. G.; Shyamal, S.; Suja, S. R.; Anuja, G. I.; Sini, S.; Pradeep, S.;

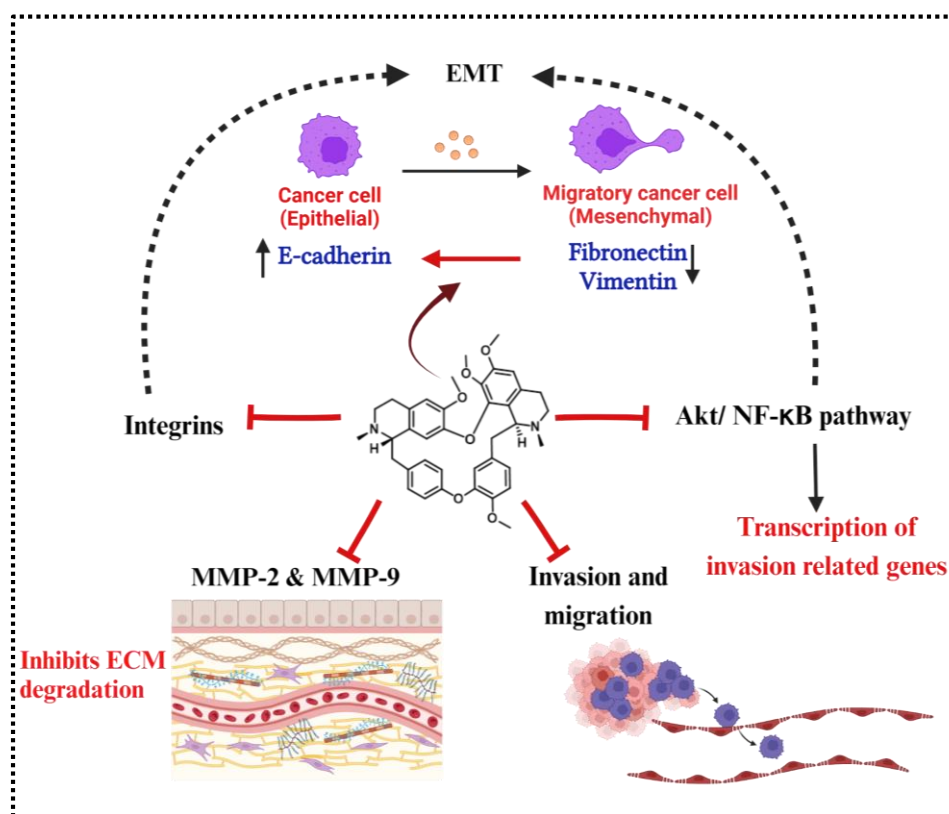
- Rajasekharan, S. Gastric Antisecretory and Antiulcer Activities of *Cyclea Peltata* ( Lam .) Hook . f . & Thoms . in Rats &. *J. Ethnopharmacol.* **2009**, *125*, 350–355. <https://doi.org/10.1016/j.jep.2009.04.039>.
- (14) Sivaraman, T.; Sreedevi, N. S.; Meenatchisundaram, S.; Vadivelan, R. Antitoxin Activity of Aqueous Extract of *Cyclea Peltata* Root against *Naja Naja* Venom. *Indian J. Pharmacol.* **2017**, *49* (4), 275–281. <https://doi.org/10.4103/ijp.IJP>.
- (15) Linn, C.; Lam, C.; Hook, F. Comparative Antipyretic and Analgesic Activities Of. *AYU (An Int. Q. J. Res. Ayurveda)* **2016**, *37* (1), 62–66. <https://doi.org/10.4103/ayu.AYU>.
- (16) Marshall, S. J.; Russell, P. F.; Wright, C. W.; Anderson, M. M.; Phillipson, J. D.; Kirby, G. C.; Warhurst, D. C.; Schiff, P. L. In Vitro Antiplasmodial, Antiamoebic, and Cytotoxic Activities of a Series of Bisbenzylisoquinoline Alkaloids. *Antimicrob. Agents Chemother.* **1994**, *38* (1), 96–103. <https://doi.org/10.1128/AAC.38.1.96>.
- (17) Cimanga Kanyanga, R.; Kikweta Munduku, C.; Nsaka Lumpu, S.; Tshodi Ehata, M.; Makila Bool-Miting, F.; Kambu Kabangu, O.; Mbamu Maya, B.; Cos, P.; Maes, L.; Vlietinck, A. J.; Tuentner, E.; Foubert, K.; Pieters, L. Isolation and Structure Elucidation of Two Antiprotozoal Bisbenzylisoquinoline Alkaloids from *Triclisia Gilletii* Stem Bark. *Phytochem. Lett.* **2018**, *28*, 19–23. <https://doi.org/10.1016/j.phytol.2018.09.008>.
- (18) Murebwayire, S.; Ingkaninan, K. *Triclisia Sacleuxii* ( Pierre ) Diels ( Menispermaceae ), a Potential Source of Acetylcholinesterase Inhibitors. *J. Pharm. Pharmacol.* **2009**, *61*, 103–107. <https://doi.org/10.1211/jpp/61.01.0014>.
- (19) Scheinmann, F.; Scriven, E. F. V.; Ogbeide, O. N. Cycleanine from *Synclisia Scabrida*: Conformational Information from the 1H NMR Spectrum at 300 MHz. *Phytochemistry* **1980**, *19* (8), 1837–1840. [https://doi.org/10.1016/S0031-9422\(00\)83824-8](https://doi.org/10.1016/S0031-9422(00)83824-8).
- (20) Ikram M, Said, Norizan A, A. Hamid. Ialifah Latif, L. B. D. and B. M. Y. 6,7-Dimethoxy-2-Methyl-3,4-Dihydro- Isoquinolin-1 (2H)-One. *Acta Crystallogr. Sect. E Struct. Reports* **2005**, *E61*, 0797–0798.
- (21) Ortega-forte, E.; Rovira, A.; Gandioso, A.; Bosch, M. COUPY Coumarins as Novel Mitochondria-Targeted Photodynamic Therapy Anticancer Agents. **2021**, *64*, 17209–17220. <https://doi.org/10.1021/acs.jmedchem.1c01254>.
- (22) Garrido, C.; Galluzzi, L.; Brunet, M.; Puig, P. E.; Didelot, C. Mechanisms of Cytochrome c Release from Mitochondria. *Cell Death Differ.* **2006**, *13*, 1423–1433. <https://doi.org/10.1038/sj.cdd.4401950>.
- (23) Malgorzata Baranska; Maciej Roman; Jan Cz. Dobrowolski; Hartwig Schulz; Rafal Baranski. Recent Advances in Raman Analysis of Plants: Alkaloids, Carotenoids, and

- Polyacetylenes. *Curr. Anal. Chem.* **2013**, *9* (1), 108–127. <https://doi.org/10.2174/1573411011309010108>.
- (24) Cañameres, M. V.; Pozzi, F.; Lombardi, J. R. Raman, SERS, and DFT Analysis of the Main Alkaloids Contained in Syrian Rue. *J. Phys. Chem. C* **2019**, *123*, 9262–9271. <https://doi.org/10.1021/acs.jpcc.9b01355>.
- (25) Zhang, W.; Zhao, Y.; Bai, X.; Wang, Y.; Zhao, D. The Orientation of Protoberberine Alkaloids and Their Binding Activities to Human Serum Albumin by Surface-Enhanced Raman Scattering. *Spectrochim. Acta - Part A Mol. Biomol. Spectrosc.* **2011**, *78* (3), 1105–1109. <https://doi.org/10.1016/j.saa.2010.12.061>.
- (26) Movasaghi, Z.; Rehman, S.; Rehman, I. U. Raman Spectroscopy of Biological Tissues. *Appl. Spectrosc. Rev.* **2007**, *42*, 493–541. <https://doi.org/10.1080/05704920701551530>.
- (27) Arya, J. S.; Joseph, M. M.; Sherin, D. R.; Nair, J. B.; Manojkumar, T. K.; Maiti, K. K. Exploring Mitochondria-Mediated Intrinsic Apoptosis by New Phytochemical Entities: An Explicit Observation of Cytochrome c Dynamics on Lung and Melanoma Cancer Cells. *J. Med. Chem.* **2019**, *62*, 8311–8329. <https://doi.org/10.1021/acs.jmedchem.9b01098>.
- (28) Diaz-moralli, S.; Tarrado-castellarnau, M.; Miranda, A.; Cascante, M. Targeting Cell Cycle Regulation in Cancer Therapy. *Pharmacol. Ther.* **2013**, *138*, 255–271. <https://doi.org/10.1016/j.pharmthera.2013.01.011>.
- (29) Cascales, H. S.; Burdova, K.; Middleton, A.; Kuzin, V.; Müllers, E.; Stoy, H.; Baranello, L.; Macurek, L.; Lindqvist, A. Cyclin A2 Localises in the Cytoplasm at the S / G2 Transition to Activate PLK1. *Life Sci. Alliances* **2021**, *4* (3), 1–15. <https://doi.org/10.26508/lsa.202000980>.
- (30) Choi, H. J.; Zhu, B. T. Critical Role of Cyclin B1/Cdc2 up-Regulation in the Induction of Mitotic Prometaphase Arrest in Human Breast Cancer Cells Treated with 2-Methoxyestradiol. *BBA - Mol. Cell Res.* **2012**, *1823* (8), 1306–1315. <https://doi.org/10.1016/j.bbamcr.2012.05.003>.
- (31) Ding, L.; Cao, J.; Lin, W.; Chen, H.; Xiong, X.; Ao, H.; Yu, M.; Lin, J.; Cui, Q. The Roles of Cyclin-Dependent Kinases in Cell-Cycle Progression and Therapeutic Strategies in Human Breast Cancer. *Int. J. Mol. Sci.* **2020**, *21* (1960), 1–28. <https://doi.org/10.3390/ijms21061960>.
- (32) Cho, Y.; Park, J. E.; Park, B. C.; Kim, J.; Jeong, D. G.; Park, S. G.; Cho, S. Cell Cycle-Dependent Cdc25C Phosphatase Determines Cell Survival by Regulating Apoptosis Signal-Regulating Kinase 1. *Cell Death Differ.* **2015**, *22*, 1605–1617. <https://doi.org/10.1038/cdd.2015.2>.

- (33) Johansson, M.; Persson, J. L. Cancer Therapy: Targeting Cell Cycle Regulators. *Anticancer. Agents Med. Chem.* **2008**, *8*, 723–731.
- (34) Livingstone, C. IGF2 and Cancer. *Endocr. Relat. Cancer* **2013**, *20* (6), 321–339. <https://doi.org/10.1530/ERC-13-0231>.
- (35) Weroha, S. J.; Haluska, P. IGF System in Cancer. *Endocrinol. Metab. Clin. North Am.* **2012**, *41* (2), 335–350. <https://doi.org/10.1016/j.ecl.2012.04.014>.IGF.
- (36) Eliopoulos, A. G.; Young, L. S. The Role of the CD40 Pathway in the Pathogenesis and Treatment of Cancer. *Curr. Opin. Pharmacol.* **2004**, *4* (4), 360–367. <https://doi.org/10.1016/j.coph.2004.02.008>.
- (37) Vonderheide, R. H. Prospect of Targeting the CD40 Pathway for Cancer Therapy. *Clin. Cancer Res.* **2007**, *13* (4), 1083–1088. <https://doi.org/10.1158/1078-0432.CCR-06-1893>.
- (38) Huang, X.; Wang, X. nan; Yuan, X. dong; Wu, W. yong; Lobie, P. E.; Wu, Z. XIAP Facilitates Breast and Colon Carcinoma Growth via Promotion of P62 Depletion through Ubiquitination-Dependent Proteasomal Degradation. *Oncogene* **2018**, *38* (9), 1448–1460. <https://doi.org/10.1038/s41388-018-0513-8>.
- (39) Bolomsky, A.; Vogler, M.; Köse, M. C.; Heckman, C. A.; Ehx, G.; Ludwig, H.; Caers, J. MCL-1 Inhibitors, Fast-Lane Development of a New Class of Anti-Cancer Agents. *J. Hematol. Oncol.* **2020**, *13* (1), 1–19. <https://doi.org/10.1186/s13045-020-01007-9>.
- (40) Wang, H.; Guo, M.; Wei, H.; Chen, Y. Targeting MCL-1 in Cancer: Current Status and Perspectives. *J. Hematol. Oncol.* **2021**, *14* (1), 1–18. <https://doi.org/10.1186/s13045-021-01079-1>.
- (41) Billen, L P, Shamas-Din, A.; Andrews, D. W. Bid : A Bax-like BH3 Protein. *Oncogene* **2009**, *27*, 93–104. <https://doi.org/10.1038/onc.2009.47>.
- (42) Xanthoudakis, S.; Sophie, R.; Rasper, D.; Hennessey, T.; Aubin, Y.; Cassady, R.; Tawa, P.; Ruel, R.; Rosen, A.; Nicholson, D. W. Hsp60 Accelerates the Maturation of Pro-Caspase-3 by Upstream Activator Proteases during Apoptosis. *EMBO J.* **1999**, *18* (8), 2049–2056. <https://doi.org/10.1093/emboj/18.8.2049>.
- (43) Du, C.; Fang, M.; Li, Y.; Li, L.; Wang, X. Smac , a Mitochondrial Protein That Promotes Cytochrome c – Dependent Caspase Activation by Eliminating IAP Inhibition. *Cell* **2000**, *102*, 33–42.
- (44) Yadav, V.; Sultana, S.; Yadav, J.; Saini, N. Gatifloxacin Induces S and G 2 -Phase Cell Cycle Arrest in Pancreatic Cancer Cells via P21 / P27 / P53. *PLoS One* **2012**, *7* (10), 1–12. <https://doi.org/10.1371/journal.pone.0047796>.

- (45) Patel, M. B.; Mishra, S. Isoquinoline Alkaloids from *Tinospora Cordifolia* Inhibit Rat Lens Aldose Reductase. *Phyther. Res.* **2012**, No. October 2011.
- (46) Yang, J.; Cron, P.; Good, V. M.; Thompson, V.; Hemmings, B. A.; Barford, D. Crystal Structure of an Activated Akt/Protein Kinase B Ternary Complex with GSK3-Peptide and AMP-PNP. *Nat. Struct. Biol.* **2002**, *9* (12), 940–944. <https://doi.org/10.1038/nsb870>.
- (47) Schrödinger Release 2022-2. Maestro, Schrödinger, LLC: New York 2022.
- (48) Friesner, R. A.; Murphy, R. B.; Repasky, M. P.; Frye, L. L.; Greenwood, J. R.; Halgren, T. A.; Sanschagrin, P. C.; Mainz, D. T. Extra Precision Glide: Docking and Scoring Incorporating a Model of Hydrophobic Enclosure for Protein-Ligand Complexes. *J. Med. Chem.* **2006**, *49* (21), 6177–6196. <https://doi.org/10.1021/jm051256o>.
- (49) D. E. Shaw Research. Maestro-Desmond Interoperability Tools, Schrödinger. D. E. Shaw Research: New York 2021.
- (50) Joseph, M. M.; Aravind, S. R.; George, S. K.; Pillai, K. R.; Mini, S.; Sreelekha, T. T. Galactoxyloglucan-Modified Nanocarriers of Doxorubicin for Improved Tumor-Targeted Drug Delivery with Minimal Toxicity. *J. Biomed. Nanotechnol.* **2014**, *10* (11), 3253–3268. <https://doi.org/10.1166/jbn.2014.1957>.
- (51) Dimauro, I.; Pearson, T.; Caporossi, D.; Jackson, M. J. A Simple Protocol for the Subcellular Fractionation of Skeletal Muscle Cells and Tissue. *BMC Res. Notes* **2012**, *5* (513).
- (52) Lu, X.; Costantini, T.; Lopez, N. E.; Wolf, P. L.; Hageny, A. M.; Putnam, J.; Eliceiri, B.; Coimbra, R. Vagal Nerve Stimulation Protects Cardiac Injury by Attenuating Mitochondrial Dysfunction in a Murine Burn Injury Model. *J. Cell. Mol. Med.* **2013**, *17* (5), 664–671. <https://doi.org/10.1111/jcmm.12049>.
- (53) Aswathy, M.; Banik, K.; Parama, D.; Sasikumar, P.; Harsha, C.; Joseph, A. G.; Sherin, D. R.; Thanathu, M. K.; Kunnumakkara, A. B.; Vasu, R. K. Exploring the Cytotoxic Effects of the Extracts and Bioactive Triterpenoids from *Dillenia Indica* against Oral Squamous Cell Carcinoma: A Scientific Interpretation and Validation of Indigenous Knowledge. *ACS Pharmacol. Transl. Sci.* **2021**, *4* (2), 834–847. <https://doi.org/10.1021/acsptsci.1c00011>.
- (54) Franken, N. A. P.; Rodermond, H. M.; Stap, J.; Haveman, J.; van Bree, C. Clonogenic Assay of Cells in Vitro. *Nat. Protoc.* **2006**, *1* (5), 2315–2319. <https://doi.org/10.1038/nprot.2006.339>.

## Mechanistic insights into the antimetastatic effects of phaeanthine in triple-negative breast cancer cell



### Abstract

Despite considerable advancements in cancer treatment, metastasis remains the predominant cause of cancer-related fatalities, contributing to over 90% of deaths associated with the disease. The preceding chapter of this thesis investigated the impact of Phaeanthine, a BBIQ alkaloid derived from *Cyclea peltata*, on cervical cancer cells. It was found to induce apoptosis and downregulate survival signaling by the treatment of phaeanthine. Based on this assessment, the current chapter delves into the evaluation of Phaeanthine's efficacy in curtailing cancer metastasis. The study focused on a highly metastatic model of triple-negative breast cancer cell line, MDA-MB-231. Results demonstrated that phaeanthine inhibited cell proliferation by inducing apoptosis, while also impeding cell migration and invasion at remarkably low concentrations. Additionally, Phaeanthine reversed the epithelial-mesenchymal transition (EMT) by downregulating

*mesenchymal marker proteins, major matrix metalloproteinases (MMPs), Integrins, and other regulatory proteins pivotal in the metastatic process. These findings resemble phaeanthine as a promising lead compound capable of influencing multiple pathways, thus effectively regulating cancer proliferation and metastasis.*

### **3A.1 Introduction**

A comprehensive approach to cancer therapy should focus on several physiological and biochemical processes that facilitate tumor growth. Hanahan and Weinberg proposed hallmarks of cancer, the six properties that are involved in the multistep process of tumor development.<sup>1</sup> Metastasis and angiogenesis are two such properties that can transform a tumor into a more malignant one.

Cancer metastasis is the progression of malignant cells originating from one part of the body to other distant organs. With metastasis being the deadliest form of cancer, a significant majority of patients succumb to the disease due to its aggressive nature. This phenomenon involves numerous biological processes where primary tumor cells obtain the ability to infiltrate deeper tissues, spread via the circulatory system (i.e. blood and lymphatic system), and finally, establish new colonies by initiating cell division at the distant site.<sup>2</sup> (Figure 3A.1) Metastasis results from a complex network of sequential events at the molecular level involving many steps, all these interactions are interlinked through a series of interactions and invasive processes as well as responses to specialized stimuli.<sup>3</sup>

The presence of dynamic changes in the metabolism of metastasizing cells contributes to their ability for the successful transition through the changing microenvironment of the metastatic cascade. One such adaptation is their metabolic changes, metastasizing cells undergo dynamic metabolic changes to cope up with the different microenvironment, while travelling through to various organs.<sup>4</sup> Thus, they exhibit the metabolic plasticity, in which they use one metabolite to fuel the various metabolic requirements of different steps of the metastatic cascade. As cancer progresses, metabolic plasticity allows cancer cells to undergo transition between glycolysis and oxidative phosphorylation in response to changing circumstances.<sup>5</sup> Alternatively, the circulating tumor cells display metabolic flexibility by using different metabolites to meet the same metabolic requirement imposed by a specific step of the metastatic cascade. So, in a tumor

microenvironment, both the metabolic plasticity and metabolic flexibility makes the cancer cells to thrive and to have metastasis.<sup>6</sup>

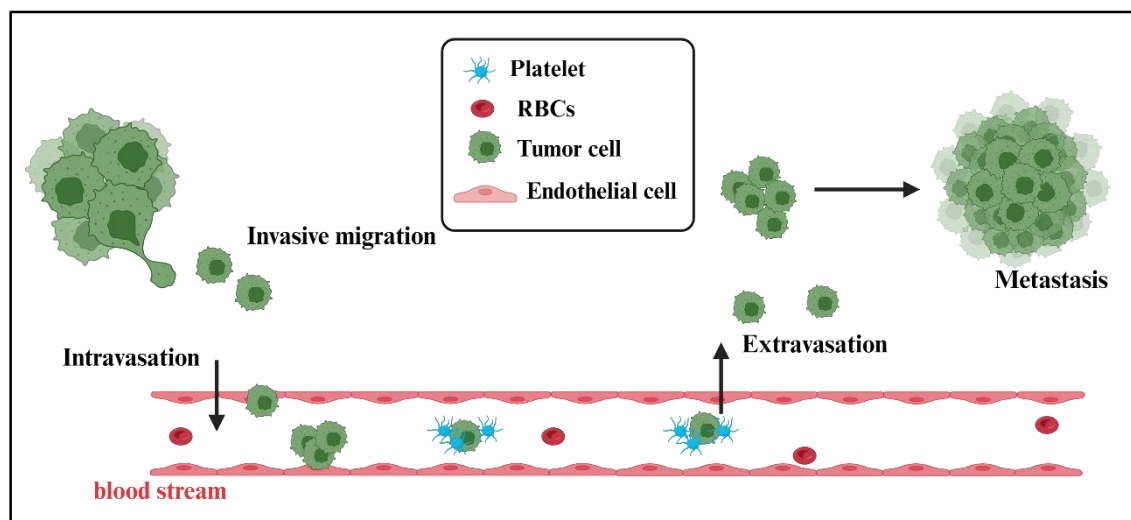


**Figure 3A.1.** The process of migration of cancer cells

Another special feature of the metastasizing cells is their ability to exhibit phenotypic plasticity, one such processes is epithelial-mesenchymal transition (EMT). This involves the loss of polarity of the epithelial cells and its cell-cell adhesion and they transform to mesenchymal one with the ability to migrate and invade. EMT is normally involved in many physiological processes such as during gastrulation, in several other developmental events and even in wound healing and it involves a continuum of ‘partial EMT’ state between the mesenchymal and epithelial endpoints.<sup>7</sup> EMT permits cancer cells to migrate, invade, and spread metastatically. At these sites, the cancer cells go through a reversible process called mesenchymal epithelial transition, or MET, to establish themselves in the new place.

The ability of cancer cells to undergo migration and invasion allows the neoplastic cells to enter the lymphatic and blood vessels for the dissemination into circulation and then start colonizing the distant organs. To migrate the cell body must undergo many modifications by changing its shape, and stiffness to interact with the surrounding tissue structures.

Metastasis research has a history spanning over a century, yet it remains the leading cause of cancer-related deaths. Challenges persist due to a scarcity of clinical trials addressing metastasis and a limited understanding of its biological mechanisms. Efforts to



design targeted therapies for metastatic cancer cells should consider the genetic and phenotypic distinctions between parental and metastatic/circulating cells. Presently, a diagnosis of metastatic cancer is often synonymous with a terminal prognosis. While preclinical evidence supports the preventability of metastasis, drug development faces obstacles from inadequate trial designs and therapeutic approaches. Advances in immunotherapy have enhanced survival in metastatic melanoma, and the introduction of novel androgen receptor inhibitors has prolonged survival in metastatic prostate cancer. However, the longevity of survival benefits in patients with metastatic breast cancer lacks consistent demonstration in long-term follow-ups.

The exploration of phytochemicals as potential agents for cancer and metastasis intervention holds significant promise, given their inherent compatibility with multiple agents. This distinctive characteristic permits a more in-depth investigation to unveil the comprehensive therapeutic potential they might offer. Among the plethora of phytochemicals, several have been extensively studied and demonstrated remarkable anticancer and antimetastatic activities.

Notable examples include apigenin, allicin,  $\alpha$ -carotene, baicalein, berberine, curcumin, wogonin, formononetin, as well as gambogic, ursolic, and ellagic acids. Additionally, papaya pectins, sulforaphane, and isothiocyanates have garnered attention for their compelling properties in the context of cancer and metastasis prevention.

This diverse array of phytochemicals presents a rich landscape for scientific exploration, with the potential to uncover novel opportunities for therapeutic interventions. As we delve into this chapter, our aim is to unravel the intricate mechanisms underlying the anticancer and antimetastatic effects of one such phytochemical, phaeanthine (PHA) in a metastatic model of TNBC using MDA-MB-231 cells.

### **3A.2 Results and Discussion**

The prime objective of this chapter was to study the effect of PHA as an anti-metastatic agent. We checked the anti-metastatic effect of the compound in HeLa cells itself, but the cells did not show a high metastatic nature, so, we further moved on with the highly metastatic model of TNBC cells, MDA-MB-231. Since there were no previous reports on the studies of PHA on MDA-MB-231, the cytotoxicity has been studied first to

assess the ability of the compound for induction of apoptosis or any other mode of cell death in the TNBC cells.

### 3A.2.1 Cytotoxicity induced by PHA in MDA-MB-231 cells

The cytotoxicity was analysed by MTT assay. The compound induced cell death at 24 hr incubation in MDA-MB-231 cells in a concentration dependent manner. And the  $IC_{50}$  was found to be  $13.3 \pm 1.07 \mu\text{M}$ . (Figure 3A.2) Since the compound showed better toxicity towards MDA-MB-231 cells, we further proceeded with some of the apoptotic assays to ensure the involvement of apoptosis in cell death.

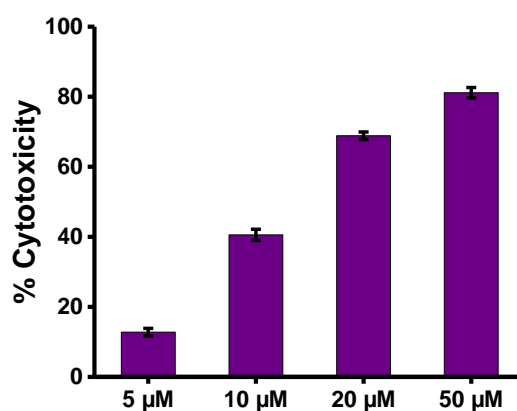


**Figure 3A.2.** Percentage of cytotoxicity induced by PHA in MDA-MB-231 cells (24 hr)

### 3A.2.2 Apoptosis induction by PHA

The live dead assay was employed to distinguish the dead cells from the live population, the assay employs dual staining with acridine orange and ethidium bromide, which will differently label the live and dead cell populations. The live cells will emit green fluorescence by uptaking acridine orange, while only the membrane-compromised dead cells will take up the ethidium bromide and appear as orange to red-colored cells. Here in the figure 3A.3. the treatment groups showed more orange to red colored cells as compared to the untreated control cells.

Nuclear condensation is a peculiar feature of apoptotic cells. The condensation pattern was studied by Hoechst nuclear staining. With 24 h of incubation with the compound, the cells showed more intensely fluoresced areas because of DNA condensation, while the DNA of the untreated cells showed uniformly stained DNA.

(Figure 3A.3.b) The PHA treatment also induced many morphological changes in the cell, including vacuole formation and membrane blebbing. (Figure 3A.3.c)

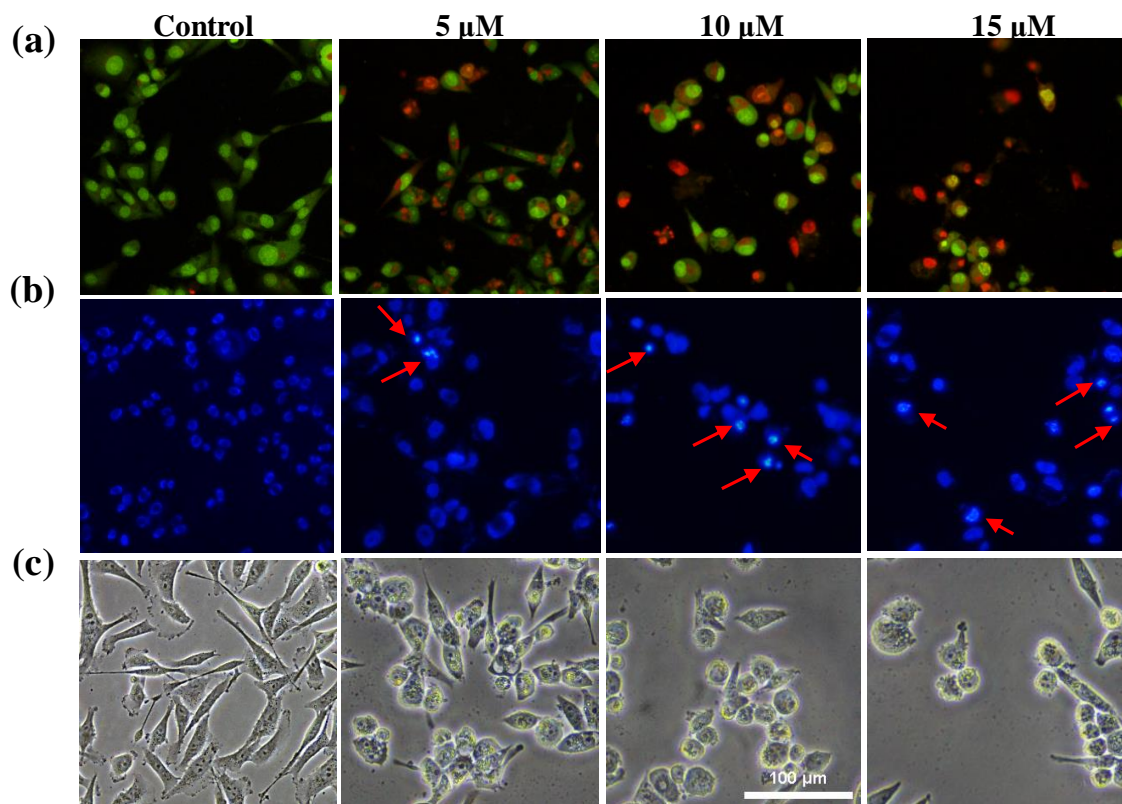


**Figure 3A.3.** Cell death induced by PHA (a) Live-dead dual staining, (b) Hoechst nuclear staining, red arrow indicates the DNA condensed areas and (c) brightfield images in MDA-MB-231 during 24 hr incubation. The scale bar indicates 100 μm.

### 3A.2.3 Annexin V apoptosis assay

Annexin V assay is a confirmatory assay to corroborate the involvement of apoptosis in the cell death. Under normal physiological conditions, the phosphatidyl serine (PS) residue of the phospholipid bilayer will be facing the cytosolic face, but upon receiving the apoptotic stimuli, the PS residue will flip to the extracellular side. Annexin V has a strong affinity for PS. So, with this principle, the apoptotic cells can be differentiated from live cells as well as from necrotic populations. Here, in the figure 3A.4.a, a higher percentage of cells in the apoptotic population is observed as compared to the control and necrotic population. The live cell population of the untreated control group was found to be 95.1 %, whereas the treated group reduced to around around 60 % and the cells in the

quadrat 2 indicating the late apoptotic stage showed a hike in the treatment group as compared to the control group.

### 3A.2.4 Caspase activation by PHA

The expression of major caspases was determined with the caspase fluorometric assays. The fluorescence intensity of the PHA treated cells showed a hike as compared to that of the control in the case of the executioner caspase 3 and initiator caspase 9. This result clearly depicts the intrinsic mode of apoptosis or the mitochondrial mediated apoptosis. In the case of caspase 9, the fluorescence intensity of treated groups showed almost a 1.5-fold increase as that of the control group, treatment also followed the same trend in caspase 3 fluorescence intensity. The treatment group showed an almost 4-fold hike in fluorescence as compared to the untreated control. (Figure 3A.4.b & c)

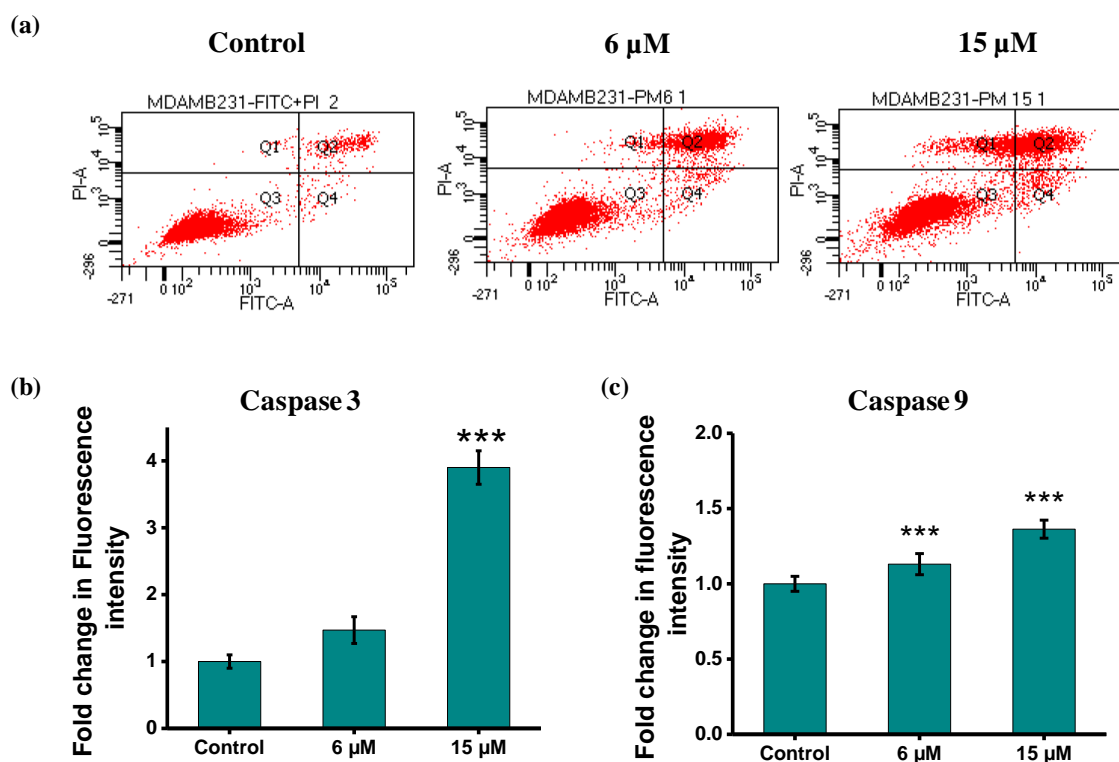


**Figure 3A.4.** (a) FITC-Annexin V apoptosis assay: MDA-MB-231 cells treated with 6 and 15 μM concentration of PHA to induce apoptosis, Caspase fluorometric assay- (b) caspase 3 and (c) caspase 9 expression with the treatment expressed as fold change in fluorescence intensity as compared to control.  $p < 0.001$  \*\*\* indicated the values are significant as compared to the control.

### 3A.2.5 Inhibition of clonogenic potential by PHA

To determine whether a single cell has the ability to self-renew into a colony of fifty or more cells, an *in vitro* method known as the colony forming (or clonogenic) experiment is frequently employed.<sup>8</sup> The compound is found to inhibit the colony forming ability of individual cancer cells at a very low concentration. Cells treated with 2 and 5  $\mu\text{M}$  concentrations of PHA showed a very limited number of colonies formed from an individual cancer cell. (Figure 3A.5.a) The survival fraction was also considerably reduced in the treatment group, which almost showed an 80 % fold reduction in the 5  $\mu\text{M}$  PHA treated group. (Figure 3A.5.b)

### 3A.2.6 Cell cycle arrest induced by PHA

Unusual regulation of the cell cycle is a prominent feature of cancer cells. Cell cycle control is one of the main regulatory systems of cell growth.<sup>9</sup> The compound PHA caused a cell cycle arrest, which was examined by flow cytometry. Following the cells' incubation with two distinct PHA concentrations, the DNA content in each cell cycle phase was examined. The DNA content of the cells in each phase clearly indicates an increased content in the G2 phase of cell cycle, with 36.2 % of cells at the G2 phase with a higher concentration of PHA as compared with only 15.8 % in the control group, while the cells at G1 phase is getting reduced with the higher concentration of PHA as 45.5 % cells as compared to 62.4 % cells in the control group. (Figure 3A.5.c & d)

### 3A.2.7 PHA inhibited migration and invasion of MDA-MB-231 cells

The processes like migration and invasion are of utmost importance in the process of metastatic cascade. They allow the tumor cells to disseminate into the lymphatic and blood circulatory system, circulate, and further proliferate and colonize at a distant organ where they actually originated.<sup>10</sup> Migration was initially studied with the help of the scrape-wound method or wound healing method. In the wound healing study, it is observed that the wound healing was hindered by the action of the PHA at 8 and 6  $\mu\text{M}$ . The percentage of wound closure was only 31 % at the 8  $\mu\text{M}$  concentration treated wounds, while the wounds of the control group showed complete healing at 48 hr incubation. (Figure 3A.6.a, b & c)

In the metastatic progression, tumor cells adhere initially to endothelial cells and the basement membrane before undergoing extravasation. This is followed by further

dissemination and secondary growth at a distant organ. The treatment with PHA during this process resulted in a notable reduction in adhered cells, specifically a 72% and 84% decrease observed in the 6  $\mu\text{M}$  and 8  $\mu\text{M}$  PHA-treated groups, respectively (Figure 3A.6.d & e).

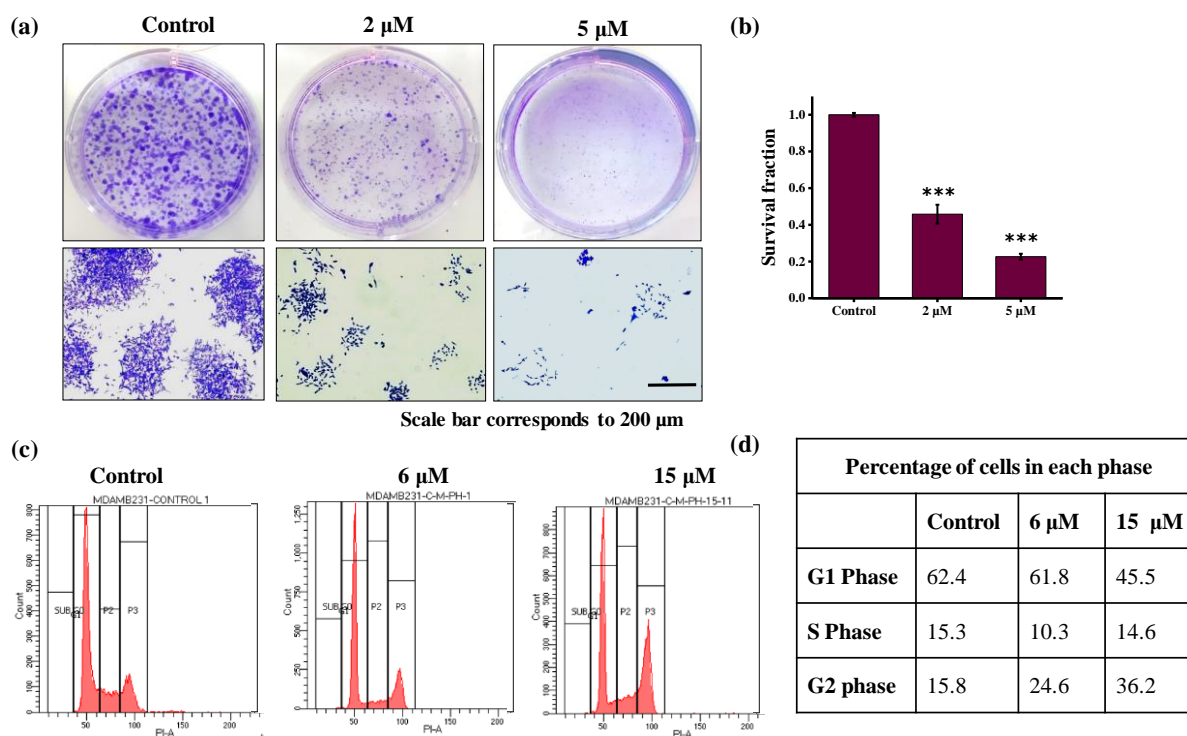


**Figure 3A.5.** (a) Clonogenic assay of MDA-MB-231 assessed with the PHA treatment. The scale bar indicates 200  $\mu\text{m}$ . (b) survival fraction of the colonies during the colony forming assay. (c) cell cycle analysis and (d) percentage of cells at each phase in cell cycle assay. p-value \*\*\*  $p < 0.001$  was considered to be significant as compared to the control.

Subsequently, the migratory inhibitory potential of PHA was validated through the transwell migration assay. The treatment group exhibited significantly fewer cells migrating through the transwell cell culture inserts compared to the untreated control group, demonstrating a reduction of nearly 61% and approximately 70% in the 6  $\mu\text{M}$  and 8  $\mu\text{M}$  PHA treatment groups, respectively (Figure 3A.6.f & g).

Likewise, the impact of PHA on the invasiveness of cancer cells was investigated using transwell cell culture inserts coated with matrigel, simulating the invasion process of metastasis. The matrigel-coated transwell serves as a barrier, mimicking the extracellular matrix that cancer cells must traverse to reach the chemically rich attractant medium on the lower side of the insert. The control group exhibited a higher number of invaded cells on

the lower side of matrigel-coated cell culture inserts, while the PHA-treated groups demonstrated a reduction in invaded cells compared to the untreated control group, particularly with an approximately 52% decrease in the 8  $\mu\text{M}$  concentration of PHA treatment group (Figure 3A.6.h & i).

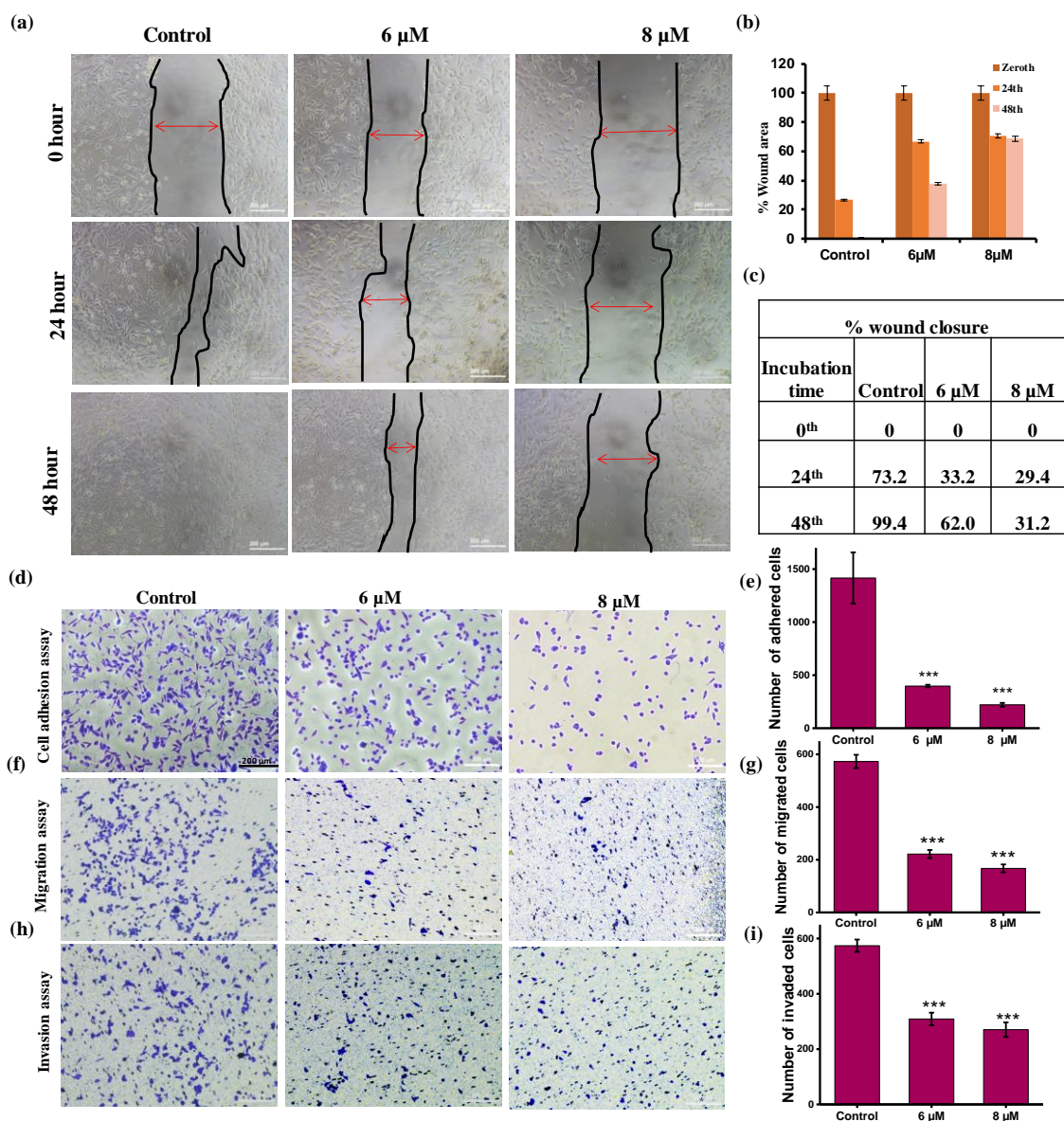


**Figure 3A.6.** (a) Wound healing assay in MDA-MB-231 cells for 24 h and 48 h of incubation with the compound, (b) and (c) % of wound area and wound closure changes with the treatment group (PHA- 6 & 8  $\mu\text{M}$ ) compared with control, (d) & (e) cell adhesion assay and the number of adhered cells, (f) & (g) migration assay of MDA-MB-231 cells using cell culture inserts and the number of migrated cells and (h) & (i) invasion assay of the MDA-MB-231 cells using matrigel coated transwell inserts and the number of invaded cells. The scale bar indicates 200  $\mu\text{m}$ . p-value \*\*\*  $p < 0.001$  was considered to be significant as compared to the control.

### 3A.2.8 PHA induced reversal of EMT

One of the defining characteristics of metastasis is the epithelial-mesenchymal transition (EMT), which is characterized by the redifferentiation of epithelial cells into mesenchymal ones, thereby altering the cellular phenotype to a malignant one.<sup>11</sup> The EMT always triggers the transition of cancer into malignant one, it enhances tumor stemness, chemoresistance, and migration of the tumor cells. The EMT process occurs when the equilibrium of expression of many transcriptional factors gets disrupted. There occurs an upregulation in the expression of mesenchymal markers like N-cadherin and a downregulation of the epithelial marker protein, E-cadherin.<sup>12</sup> There are a few reports on the mesenchymal type nature of MDA-MB-231 cells, it is a representative of the mesenchymal subtype of triple-negative breast cancer cell line.<sup>13,14</sup> So, the main interest was to evaluate the effect of the PHA on the epithelial-mesenchymal transitions, from the immunoblotting of the specific marker proteins. The expression of the mesenchymal marker was adversely affected upon the PHA treatment. Mesenchymal marker proteins like vimentin and N-cadherin expression got reduced, while the expression of epithelial marker protein, E-cadherin was getting upregulated. (Figure 3A.7) This exemplifies unequivocally that the PHA caused the EMT reversal, regulating the mesenchymal phenotype that is more susceptible to migration.

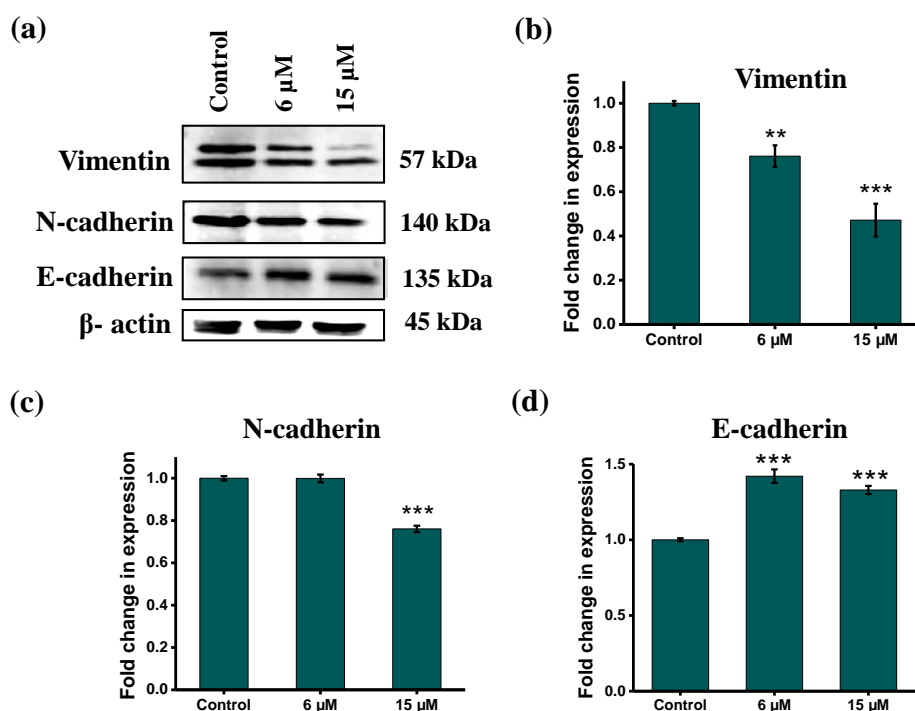




**Figure 3A.7.** (a) Immunoblot of mesenchymal and epithelial marker proteins, Fold change in the expression of (b) vimentin, (c) N-cadherin and (d) E-cadherin as compared to the control group. \*\*\* $p < 0.001$ , \*\* $p < 0.01$ , \* $p < 0.05$  were considered to be significant as compared to the control. No asterisk (\*) represents a non significant p value.

### 3A.2.9 PHA induced the downregulation of major integrins

Transmembrane glycoproteins with an  $\alpha$  and  $\beta$  subunit make up integrins. Certain integrin heterodimers can entirely change a cell's attributes by attaching themselves ideally to different extracellular matrix (ECM) proteins. Certain integrins play essential roles in the development of tumors and numerous events linked to cancer, including invasion, migration, survival, and proliferation.<sup>15</sup> The effect of PHA on the regulation of various integrins was analyzed by immunoblotting and could observe an adverse impact on the expression of these proteins viz., the expression of integrin  $\alpha 5$ , integrin  $\beta 5$ , and integrin  $\beta 3$  were downregulated. (Figure 3A.8) Integrin  $\alpha 5$  is frequently overexpressed in most tumors and is a key driver in the progression of cancer in many different types of cancer.

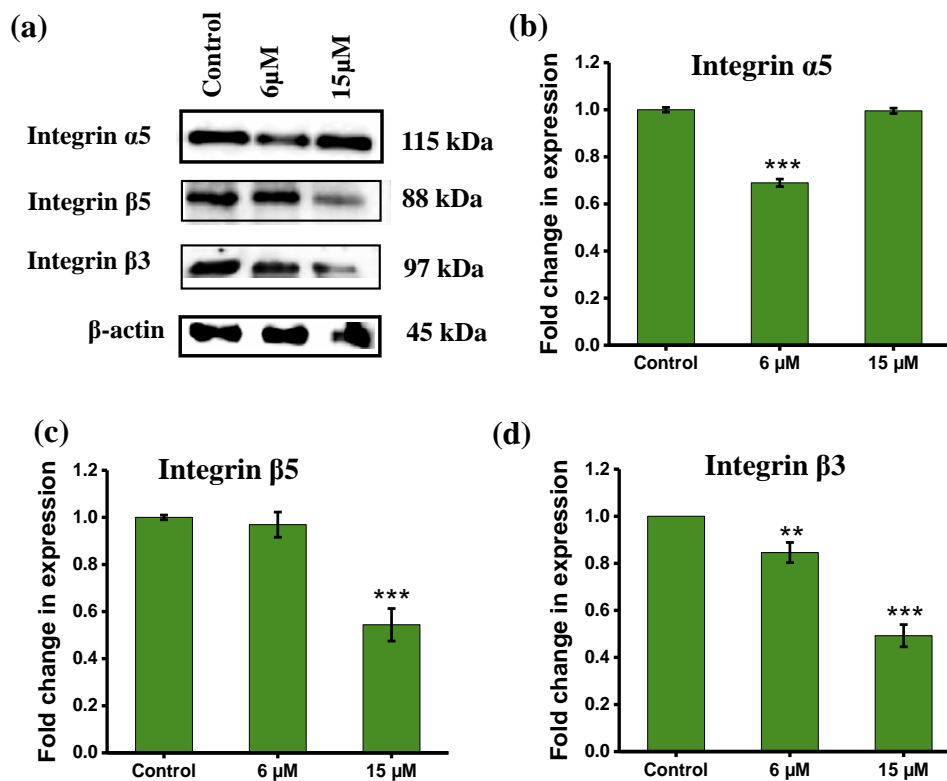


**Figure 3A.8.** (a) Immunoblot of major integrins involved in metastasis with PHA treatment, fold change in the expression of (b) Integrin  $\alpha 5$ , (c) Integrin  $\beta 5$ , and (d) Integrin  $\beta 3$  upon PHA treatment compared with that of the control group. \*\*\* $p < 0.001$ , \*\* $p < 0.01$ ,

were considered to be significant as compared to the control. No asterisk (\*) represents a non-significant p value.

Furthermore, in the residual metastatic deposits, the integrin subunit  $\alpha 5$  was upregulated in the absence of mesenchymal selectins from the host.<sup>16</sup> Integrin  $\beta 5$  has been discovered to mediate the transforming growth factor (TGF- $\beta$ ) induced EMT and enhance the carcinogenic potential of breast cancer cells. Additionally, it interacts with  $\beta$ -catenin, which ultimately aids in the progression of tumors. Elevated Integrin  $\beta 3$  expression in some cancer types is indicative of increased metastasis to lymph nodes or bone, as well as a lower patient survival rate. It has also been observed that this protein is linked to EMT and related processes.<sup>15</sup> Hence, by modulating the expression of these major integrins involved in various stages of metastasis, PHA can control the further spread and migration of cancer cells.

#### **3A.2.10 PHA modulated the expression of MMPs**

The matrix metalloproteinases (MMPs) also known as matrixins are a family of zinc-dependent endopeptidases. Their aberrant expression contributes to numerous pathological conditions and they are involved in the degradation of extracellular matrix. MMP-2 and MMP-9, also referred to as type IV collagenases or gelatinases, are the two main MMPs. Recent shards of evidence point to important roles for some MMPs in the development and spread of breast cancer.<sup>17</sup> Its activity and increased tumor metastasis are directly correlated because of its ECM degradation property. According to certain reports, MMPs stimulate the interaction between cancer cells and platelets and prevent the growth of immune response cells, which helps the circulating tumor cells evade the immune system.<sup>17-19</sup> From the expression studies using western blotting, the compound was found to be potent in inhibiting the expression of MMP-2 and MMP-9. (Figure 3A.9.a,b & c) The MMP-2 expression in the treatment group showed an almost 0.8-fold decrease as compared to that of the untreated control group. A similar trend is observed in the case of MMP-9, with almost 0.6-fold downregulation in the treatment group. Hence, PHA could adversely affect the expression of major MMPs thereby controlling the degradation of ECM and further metastatic cascade. The compound can be effectively used as an MMP-2 and MMP-9 inhibitor since targeting these gelatinases constitutes a new therapeutic strategy to efficaciously mitigate the metastasis of cancer.

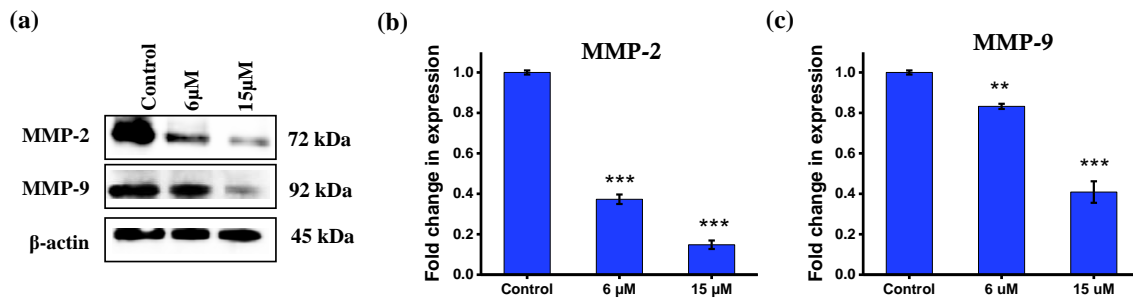


**Figure 3A.9.** (a) Immunoblot of major MMPs with PHA treatment, fold change in the expression of (b) MMP-2, and (c) MMP-9 upon PHA treatment compared with that of the control group. \*\*\* $p < 0.001$ , \*\* $p < 0.01$ , \* $p < 0.05$  were considered to be significant as compared to the control. No asterisk (\*) represents a non significant  $p$  value.

### 3A.2.11 PHA modulated the expression of major regulatory proteins

Metastasis comprises a highly organized cascade of events regulated by many regulatory proteins and transcriptional factors. Akt, HIF-1 $\alpha$ , and NF- $\kappa$ B are some of the major regulatory proteins involved in the dissemination, invasion, migration and finally colonizing of the cancer cells. The variations in the expression of these proteins with PHA treatment were studied via western blotting. And observed an adverse effect on the expression of these proteins with treatment. The hypoxic responses in the tumor microenvironment (TME) is mainly mediated by HIF-1 (hypoxia inducible factor), which is composed of HIF-1 $\alpha$  and HIF-1 $\beta$ . Their activation under hypoxic conditions will regulate metabolism, angiogenesis and invasion.<sup>20</sup> In cancer metastasis, HIF-1 regulated genes promote activation of VEGF to promote angiogenesis, and in addition its overexpression represses the expression of E-cadherin and thereby inducing invasion.<sup>20,21</sup> So, the downregulation of HIF-1 $\alpha$  with PHA treatment could be able to regulate the migration and invasion. Akt is implicated in the regulation of cell migration and invasion. The activated Akt can influence cytoskeletal dynamics and promotes the invasive behaviour of cancer cells facilitating their metastatic ability. And NF- $\kappa$ B can regulate the expression of genes involved in the immune responses, that can impart metastatic potential and it is implicated in the process of EMT for enhancing the cell motility and invasiveness. PHA treatment could downregulate the expression of these regulatory proteins, thereby controlling the migration and invasion of cancer cells. In the higher treatment group (15  $\mu$ M), a downregulation of almost half fold is observed for both Akt and NF- $\kappa$ B.<sup>22,23</sup> (Figure 3A.10)

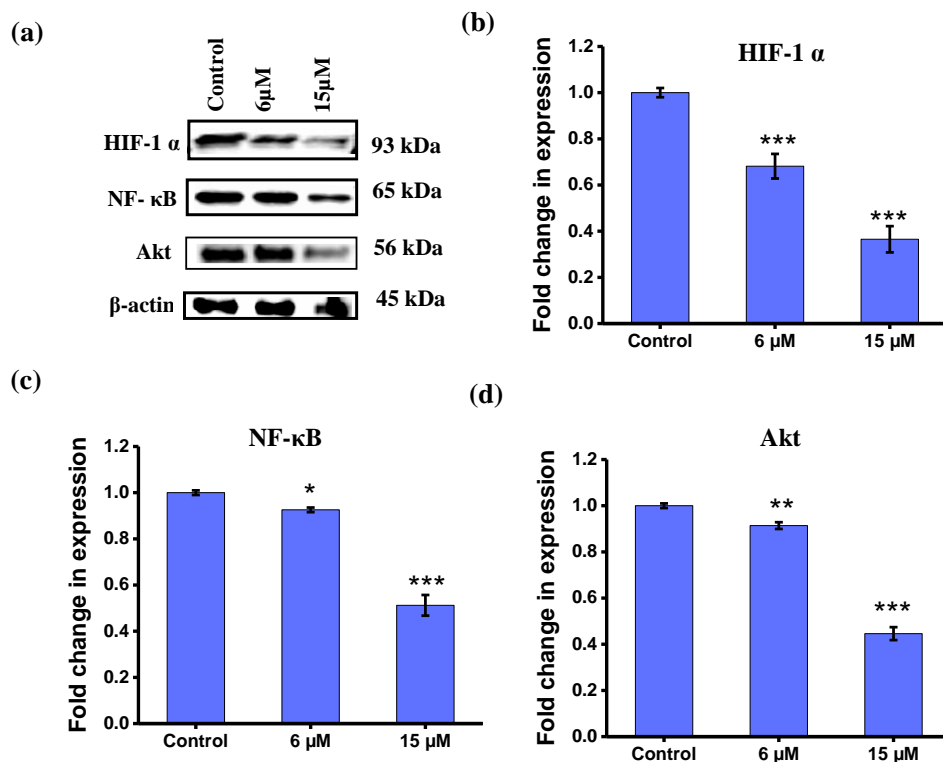


**Figure 3A.10.** (a) Immunoblot of major regulatory proteins of metastasis with PHA treatment, fold change in the expression of (b) HIF-1 $\alpha$ , (c) NF- $\kappa$ B and (d) Akt upon PHA treatment compared with that of the control group. \*\*\* $p < 0.001$ , \*\* $p < 0.01$ , \* $p < 0.05$  were considered to be significant as compared to the control.

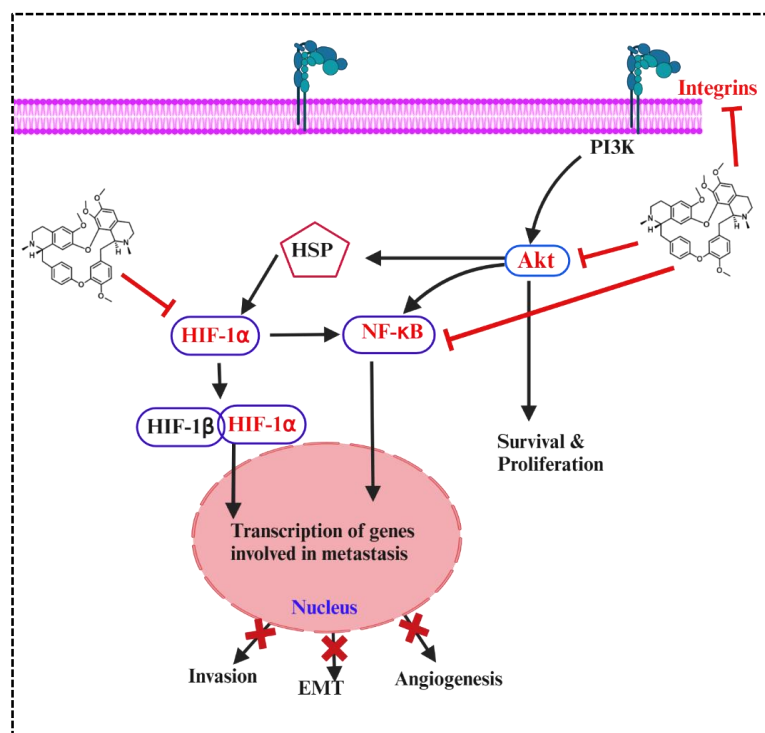


**Figure 3A.11.** Molecular targets of PHA in the metastatic events

### 3A.3 Conclusion

In conclusion, the anti-metastatic study employing PHA has yielded promising and impactful effect on MDA-MB-231 cells. Through meticulous investigation, it was demonstrated that PHA significantly hinders metastasis in MDA-MB-231 cells. The experimental results emphasize PHA's efficacy in inhibiting critical processes such as migration, invasion and EMT thereby mitigating the potential spread of cancer cells.

Furthermore, the study illuminated the underlying molecular mechanisms by which PHA exerts its anti-metastatic effects. Notably, by modulating the expression of mesenchymal marker proteins *N*-cadherin and vimentin, major MMPs, Integrins, Akt, NF- $\kappa$ B and HIF-1 $\alpha$ . These mechanistic insights contribute to our understanding of the intricate interplay between PHA and metastatic pathways.

While these results are promising, further investigations, including in vivo studies and clinical trials, are necessary to validate the translational potential of PHA as a safe and effective anti-metastatic agent. This research contributes to the growing body of evidence supporting the exploration of natural products for their anti-cancer properties and holds promise for advancing therapeutic strategies in the realm of metastatic cancer treatment.

### 3A.4 Experimental Section

#### 3A.4.1 Cell culture methods

The human triple negative breast cancer cell, MDA-MB-231 was obtained from ATCC and maintained in Dulbecco's modified eagle medium (DMEM, Sigma), and supplemented with 10% Fetal Bovine Serum (FBS, Himedia) and 1% antibiotic antimycotic solution 100X (with 10,000 units Penicillin, 10 mg Streptomycin and 25  $\mu$ g Amphotericin B per mL in 0.9% normal saline-Himedia) and maintained at 5% CO<sub>2</sub> at 37°C in the incubator.

#### 3A.4.2 Cytotoxicity assays

The MDA-MB-231 cells were seeded in 96 well plate for 24 h and after the incubation compound PHA at different concentrations was added and incubated for 24 h. after the desired incubation time, MTT dissolved in HBSS was added to each well for 2-4 h and the formazan crystals were dissolved in 100  $\mu$ L of DMSO by removing the MTT solution. The absorbance was measured at 570 nm in a multimode plate reader.

### 3A.4.3 Apoptotic assays

The cells were seeded in 96 well plate, after 24 h of incubation, compound at three different concentrations (5, 10 and 15  $\mu\text{M}$ ) were added. With 24 h incubation of the compound, Live dead assay, Hoechst nuclear staining were performed by adding the specified dyes. And the images were taken in a fluorescent microscope. For live dead staining, acridine orange and ethidium bromide were added.

### 3A.4.4 Annexin V apoptosis assay

FITC annexin v is a sensitive probe for identifying apoptotic cells, binding to the negatively charged phosphatidyl serine. It was performed with FITC annexin V apoptosis detection kit (BD Pharmingen, Cat. No.- 556547). The kit protocol was strictly followed to conduct the experiment accurately.

### 3A.4.5 Caspase fluorometric assay

The expression of various caspases upon treatment with phaeanthine was evaluated with caspase fluorometric assay kits (Abcam). The experiment was carried out as per the manufacturer's protocol. MDA-MB-231 cells seeded in 6 well plates were treated with PHA at two different concentrations (6  $\mu\text{M}$  and 15  $\mu\text{M}$ ) for 24 hours; after the procedures, the fluorescence intensity was measured (Excitation: 400 nm and Emission: 505 nm) in a multimode plate reader. (Synergy H1, Biotek)

### 3A.4.6 Colony formation assay

Cells were seeded at a density of  $1 \times 10^3$  cells per well in a 6-well plate. After 24 hours of incubation, compounds at two distinct concentrations (2  $\mu\text{M}$  and 5  $\mu\text{M}$ ) were introduced, and the cells were permitted to develop colonies over the subsequent 9 days. Following this incubation period, colonies were visualized through staining with 0.3% crystal violet for 10 minutes, followed by washing with PBS. Imaging was conducted using a Nikon-TS100 Inverted microscope, and the captured images were processed. Colony quantification was performed using Image J software. The survival fraction was computed utilizing the formula:

$$\text{Plating efficiency (PE)} = \frac{\text{No. of colonies counted}}{\text{No. of cells seeded}} \times 100$$

$$\text{Surviving fraction (SF)} = \frac{\text{PE of treated sample}}{\text{PE of control}} \times 100$$

### 3A.4.7 Cell cycle analysis

Cell cycle arrest induced by phaeanthine was studied using BD cycletest Plus DNA kit (B D Pharmingen, Cat no.- 340242). All the procedures were conducted based on the kit protocol. The method involves dissolving the cell membrane lipids with a non-ionic detergent, digesting cellular RNA with enzyme, and stabilizing the nuclear chromatin. PI will bind to the isolated nuclei, and the flow cytometer analyzed the light emitted by stained cells.

### 3A.4.8 Wound healing assay

Cells were seeded in a 96-well plate at a seeding density of  $10 \times 10^4$  cells per well. Wounds were created in each well by carefully scratching with a 200  $\mu\text{L}$  pipette tip. Various concentrations of compounds were then applied, and images were captured at regular intervals to monitor the wound healing progress. The treated group was subsequently compared to the untreated control to assess the impact of the compounds on the observed wound closure. The wound area was evaluated with the help of ImageJ software and the wound closure was calculated by the formula:

$$\text{Wound closure \%} = \frac{A_{t=0} - A_{t=\Delta h}}{A_{t=0}}$$

Where,  $A_{t=0}$  – Area of the wound at zeroth hour

$A_{t=\Delta h}$  – Area of the wound at specified time interval

### 3A.4.9 Adhesion, Migration and Invasion assays

In the cell adhesion assay, cells were initially seeded in a 6-well plate and allowed to incubate for 24 hours. After this incubation period, compounds were introduced at concentrations of 6 and 8  $\mu\text{M}$ . The following day, 48-well plates were coated with 100  $\mu\text{L}$  of diluted matrigel. Once gelled, trypsinized cells from both the untreated and treated groups were added to the matrigel-coated wells and incubated for 4 hours. The cells were subsequently fixed using 70% methanol, stained with a 0.3% crystal violet solution, and images were captured for analysis.<sup>24</sup>

The transwell migration and invasion assays utilized cell culture inserts of 8.0  $\mu\text{m}$  pore size. These inserts created a barrier between two distinct media compartments, where the lower portion contained either conditioned medium or serum-containing medium, and the inside of the insert housed cells in serum-free medium, separated by a porous membrane. In the invasion assay, the upper side of the insert was coated with diluted matrigel. Cells were introduced into the serum-free medium, and after 24 hours of incubation, they migrated through the pores towards the serum-containing medium. Following the specified incubation period, the inserts were fixed, stained, and subjected to image capture. Subsequent calculations were performed using Image J software.<sup>25</sup>

#### **3A.4.10 Protein Expression Studies**

Cells were seeded in T75 flasks and the compound at two concentrations (6  $\mu\text{M}$  & 15  $\mu\text{M}$ ) was added. After 24 hours of incubation, cell lysate was taken according to standard procedure using RIPA buffer and protease inhibitor cocktail. BCA protein assay kit (Thermo Scientific) was used to estimate the concentration of isolated protein, and western blotting was carried out to study the expression of various proteins. Image J software was used to get the band intensity of proteins. The expression of each protein was normalized with respect to the control and then with that of the internal control  $\beta$ -actin.





---

## Mechanistic insights into the anti-angiogenic effects of Phaeanthine in EA.hy926 cells

---

### Abstract

*The study explores the antiangiogenic properties of Phaeanthine, a phyto molecule previously identified for its inhibitory effects on the proliferation and migration of cancer cells, as detailed in preceding chapters. The investigation specifically delves into Phaeanthine's impact on angiogenesis, a pivotal process in tumor progression. Through meticulous analysis, it is revealed that Phaeanthine effectively inhibits angiogenesis by controlling the migration, invasion, and tube formation of EA.hy926 endothelial cells. The findings shed light on the intricate mechanisms through which Phaeanthine intervenes in key aspects of endothelial cell behavior, ultimately disrupting the formation of new blood vessels. This research not only highlights Phaeanthine's potential as an inhibitor of angiogenesis but also underscores its significance in the broader context of developing therapeutic strategies for cancer treatment.*

### 3B.1 Introduction

Angiogenesis refers to the formation of new blood vessels within a tumor. This process is a crucial aspect of tumor growth and progression. Tumor development requires a continuous supply of oxygen and nutrients to sustain their rapid proliferation. When the size of a tumor reaches a point where its existing blood supply becomes inadequate, angiogenesis is triggered as a means to establish new blood vessels.<sup>26</sup> Understanding and manipulating the angiogenic process in cancer have become important avenues of research, offering potential insights into developing more effective and targeted cancer therapies.

In 1970, Folkman proposed the theory that suppressing vascular proliferation contributes to an anti-tumor effect, regulating the enlargement and spread of the tumor mass.<sup>27</sup> Angiogenesis, a highly regulated process, involves a delicate balance of pro- and anti-angiogenic signals, encompassing integrins, cytokines, angiopoietins, oxygen-sensing agents, junctional molecules, and endogenous inhibitors. This intricate orchestration plays a pivotal role in over 50 different disease states, with its dysregulation linked to conditions like cancer, psoriasis, and various eye diseases.

The sustenance and growth of tumors depend on a continuous supply of nutrition and oxygen. Tumors unable to surpass a size of 1-2 mm without encountering central necrosis highlight the significance of angiogenesis. The genetic adaptability of neoplasms often involves the activation of genes enhancing invasion and metastasis, crucially involving the induction of local small blood vessels.

Angiogenesis encompasses a series of intricate and multistep processes, involving the extravasation of plasma proteins, degradation of the extracellular matrix, migration, and proliferation of endothelial cells, culminating in the formation of capillary tubes that facilitate the supply of oxygen and essential nutrients. In normal tissues, vascular senescence is maintained by the prevalence of angiogenesis inhibitors, which outweigh the stimuli favoring angiogenesis. However, in diseased conditions or tumor-associated scenarios, the initiation of angiogenesis occurs when the angiogenic stimuli surpass the endogenous inhibitors.<sup>28</sup>

Neoplasms possess the capacity to produce or induce the secretion of numerous angiogenic inducers, including vascular endothelial growth factor (VEGF), angiopoietins, transforming growth factors (TGF), platelet-derived growth factors (PDGF), tumor necrosis factor- $\alpha$  (TNF- $\alpha$ ), interleukins, and members of the fibroblast growth factor (FGF) family.<sup>29</sup> Hypoxia acts as a stimulus for these proteins, initiating the sprouting of endothelial cords. This sprouting results in the formation of abundant yet immature networks of thin, endothelial-lined channels, crucial for facilitating sufficient oxygenation for the tumor.

The activated endothelial cells exhibit accelerated proliferation and release proteolytic enzymes that aid in the digestion of the basement membrane and extracellular matrix (ECM), facilitating cell invasion. Distinct alterations in endothelial-integrin interactions enable the migration of capillary sprouts across the dynamic extracellular environment. Subsequent to migration, the endothelial cells undergo canalization and stabilization, recruiting additional support cells such as pericytes and smooth muscle cells. The recruitment of circulatory hematopoietic precursors to angiogenic sites results in the formation of tortuous, dilated neovasculature, contributing to tumor growth and dissemination.<sup>30</sup> (Figure 3B.1)

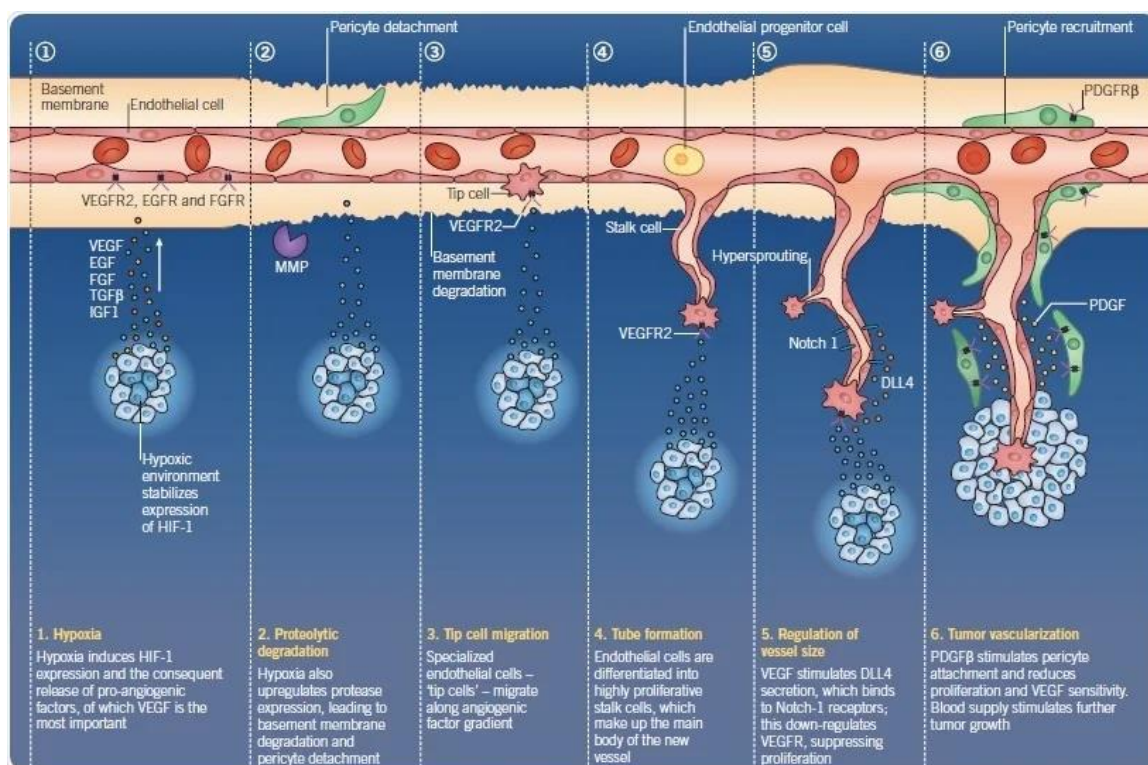


**Figure 3B.1.** The process of angiogenesis. Image credit: Tocris Bioscience

Subsequently, a multitude of drugs has been developed to regulate neovascularization or angiogenesis. Antiangiogenic medications like sunitinib, bevacizumab, ranibizumab, and ponatinib have proven effective by inhibiting key regulatory proteins such as VEGF, basic fibroblast growth factor (b-FGF), and their respective receptors. Despite their success, these drugs are linked to diverse side effects, encompassing hypertension, gastrointestinal perforations, and the possibility of physiological harm to patients. Therefore, there is a pressing need to identify novel drug candidates capable of inhibiting angiogenesis with minimal side effects and adverse reactions. Natural products emerge as promising leads in this context.<sup>31</sup>

Numerous natural product-derived anti-angiogenic agents are undergoing clinical trials. For instance, squalamine, an aminosterol discovered in the tissues of the dogfish shark, and Combretastatin A-4 phosphate, a prodrug derived from combretastatin A-4, show tremendous potential as antiangiogenic agents. In a 2020 study by Chen K. *et al.*, the antiangiogenic potential of 240 compounds was investigated using a transgenic zebrafish line with fluorescent blood vessels. Among these compounds, dihydromunduletone, deoxysappanone B 7,4'-Dimethyl Ether (DeoxB 7,4), Mundoserone, ononetin, and pomiferin were identified as having potential anti-angiogenic activity during zebrafish embryogenesis.<sup>32</sup>

Therefore, agents derived from natural products exhibit considerable potential in inhibiting angiogenesis. The primary objective of this chapter is to analyze the antiangiogenic effect of the molecule of interest, PHA, previously explored in preceding chapters. Considering this in mind, the human umbilical vein cell line, EA.hy926 cell line was chosen for the study, which was established by fusing primary human umbilical vein cells with a thioguanine-resistant clone of A549 by exposure to polyethylene glycol (PEG). This cell line has been widely used in the angiogenesis related and vascular studies in place of HUVEC.<sup>33</sup>

### 3B.2 Results and Discussion

The prime objective of this study was to investigate the efficacy of Phaeanthine as an anti-angiogenic agent. The wound healing assay, migration and invasion using the transwell inserts and the tube formation assays were performed to evaluate the antiangiogenic potential of PHA in EA.hy926 cells.

#### 3B.2.1 Cytotoxicity evaluation of PHA

The cytotoxicity induced by the PHA was evaluated by MTT assay, as previously reported. After 24 h of incubation with compound, the results were taken. It indicates PHA was safe upto a higher concentration and at 20  $\mu\text{M}$  concentration the cytotoxicity was only 21 % and the  $\text{IC}_{50}$  was found to be  $34.4 \pm 0.9 \mu\text{M}$ . (Figure 3B.1)

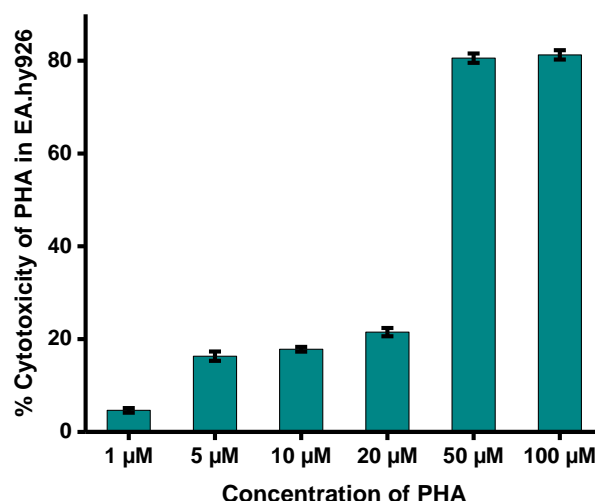


**Figure 3B.2.** Cytotoxicity (%) induced by PHA in EA.hy926 cells at 24h incubation

### 3B.2.2 Effect of PHA on Wound healing in EA.hy926 cells

The wound healing assay stands as a widely employed *in vitro* technique for investigating endothelial cell migration and invasion.<sup>34</sup> In the untreated group, nearly complete wound closure was observed, signifying robust healing. Conversely, the PHA-treated groups exhibited varying degrees of impairment in wound closure, ranging from partial to minimal. Notably, the group treated with the lowest concentration of PHA (2  $\mu\text{M}$ ) displayed only around half of the wound area covered, whereas the highest treatment group, subjected to an 8  $\mu\text{M}$  concentration, demonstrated only 19% wound closure after 24 hours of incubation. These results underscore the inhibitory effect of PHA on endothelial cell migration and highlight its potential in modulating wound healing processes. (Figure 3B.3.a & b)

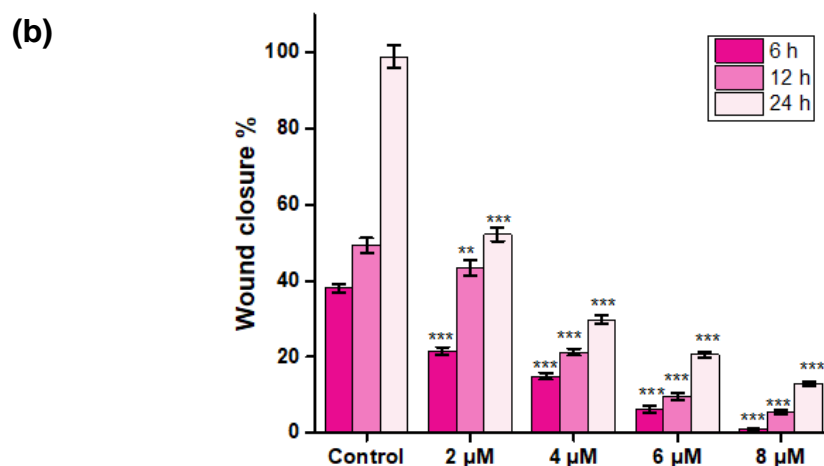
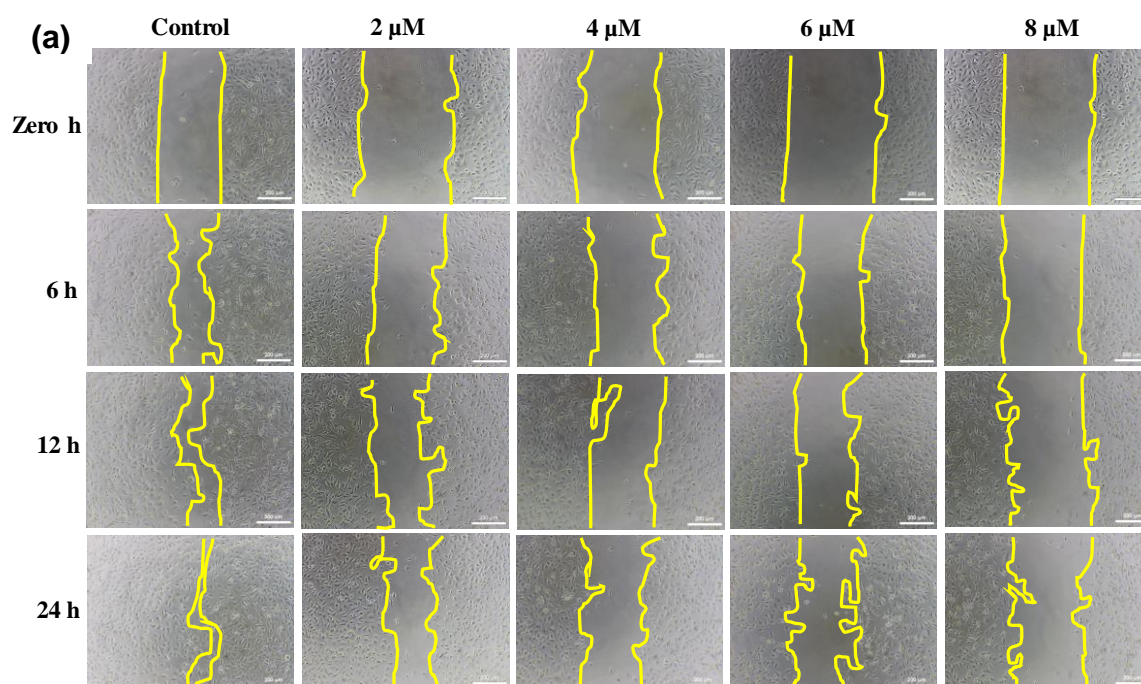


**Figure 3B.3.** (a) Wound healing assay in EA.hy926 endothelial cells, with the PHA treatment. The wounds were treated with 2,4,6 and 8  $\mu\text{M}$  of PHA and observed at regular intervals. The scale bar indicates 200  $\mu\text{m}$ . (b) Wound closure percentage on PHA treatment compared with untreated control.

### 3B.2.3 Effect of PHA on Migration and invasion of endothelial cells

Migration and invasion are integral processes in angiogenesis. Key antiangiogenic agents have been identified for their ability to impede the migration and invasion of endothelial cells, thereby modulating the development of new blood vessels.<sup>35</sup> The potential of PHA to inhibit these pivotal processes was investigated in EA.hy926 cells using transwell cell culture inserts. The treated groups exhibited a significantly reduced rate of both migrated and invaded cells compared to the untreated control. Specifically, the group exposed to a higher concentration (6  $\mu\text{M}$ ) demonstrated minimal migration, mirroring the observed trend in invasion. Consequently, the compound displays a heightened efficacy in suppressing the migration and invasion of endothelial cells, particularly at a substantially lower concentration. (Figure 3B.4.a, b, & c)

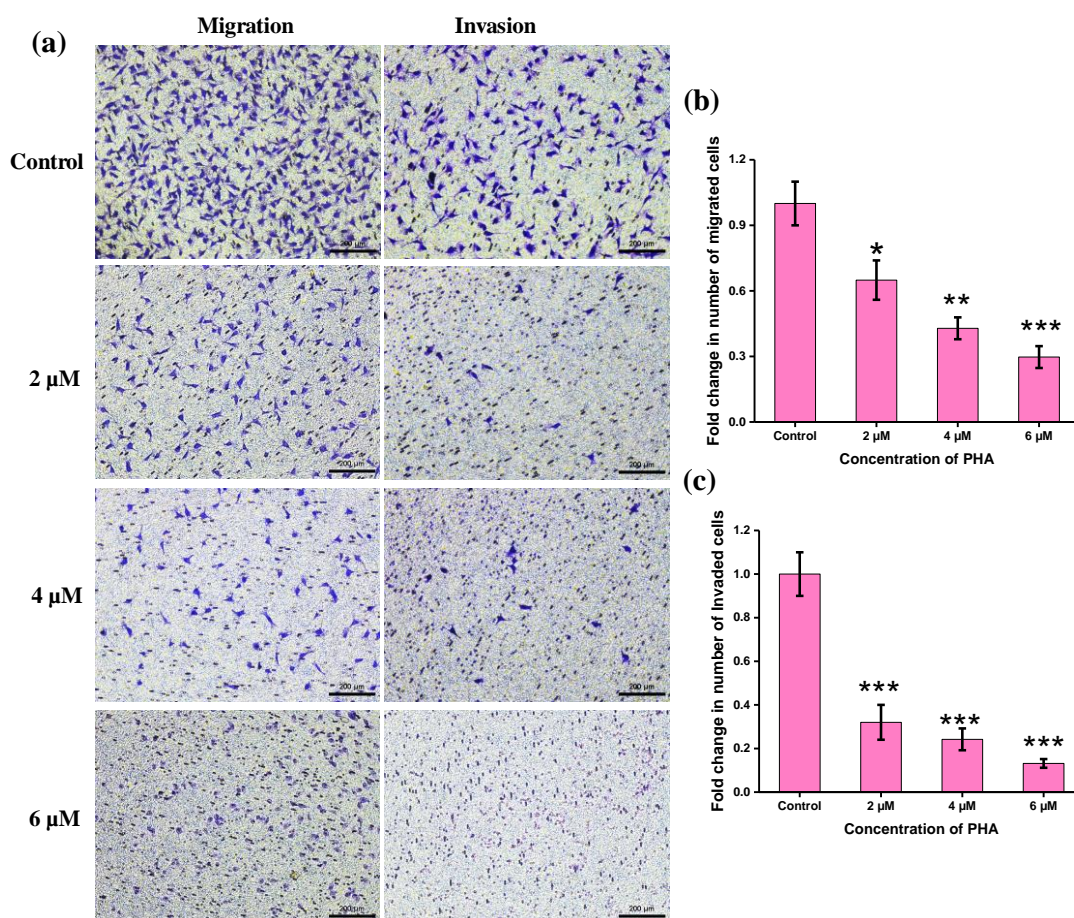


**Figure 3B.4.** (a) Migration and invasion assay using cell culture inserts, with treatments with PHA. The scale bar indicates 200  $\mu\text{m}$ . (b) Fold change in number of migrated cells compared with control, and (c) fold change in the invaded cells in the treatment compared with control. The experiments were conducted in triplicates and the graphical value represents average  $\pm$  SD, and \*\*\* indicates  $p$  value  $<0.001$ , considered as significant when compared to the control.

### 3B.2.4 Effect of PHA on Tube formation of endothelial cells

The tube formation assay serves as a rapid and quantitative method to assess the antiangiogenic impact of a drug molecule. Endothelial cells undergo differentiation, giving rise to tube-like structures when cultured on a matrix of basement membrane or in matrigel. These structures consist of lumens surrounded by endothelial cells interconnected through junctional complexes.<sup>36</sup> As a subsequent step in assessing the antiangiogenic potential of PHA, effort was taken to evaluate the impact on the tube formation ability of endothelial cells. Surprisingly, even at minimal concentrations (2, 4, and 6  $\mu\text{M}$ ), PHA significantly impeded tube formation. Parameters such as the number of nodes, junctions, and total tube length were markedly reduced, demonstrating this effect at concentrations as low as 2  $\mu\text{M}$  of PHA. The calculation of the number of nodes was performed using Image J software, revealing a remarkable 77% and 97% reduction in the number of nodes formed during tube formation at 2 and 4  $\mu\text{M}$  concentrations of PHA, respectively. (Figure 3B.5.a & b)

Similarly, in the case of junctions formed, a substantial 76% and 97% reduction was observed compared to the untreated control group at 2 and 4  $\mu\text{M}$  concentrations of PHA, respectively. Additionally, when assessing the total tube length, a consistent trend emerged, showcasing a 47%, 72%, and 81% reduction in tube length at 2, 4, and 6  $\mu\text{M}$  concentrations of PHA. The  $p$ -value  $< 0.005$  in comparison to the untreated control indicates a highly significant value. (Figure 3B.5.c & d) Consequently, the compound has proven to be a potent candidate for inhibiting tube formation and, consequently, angiogenesis.



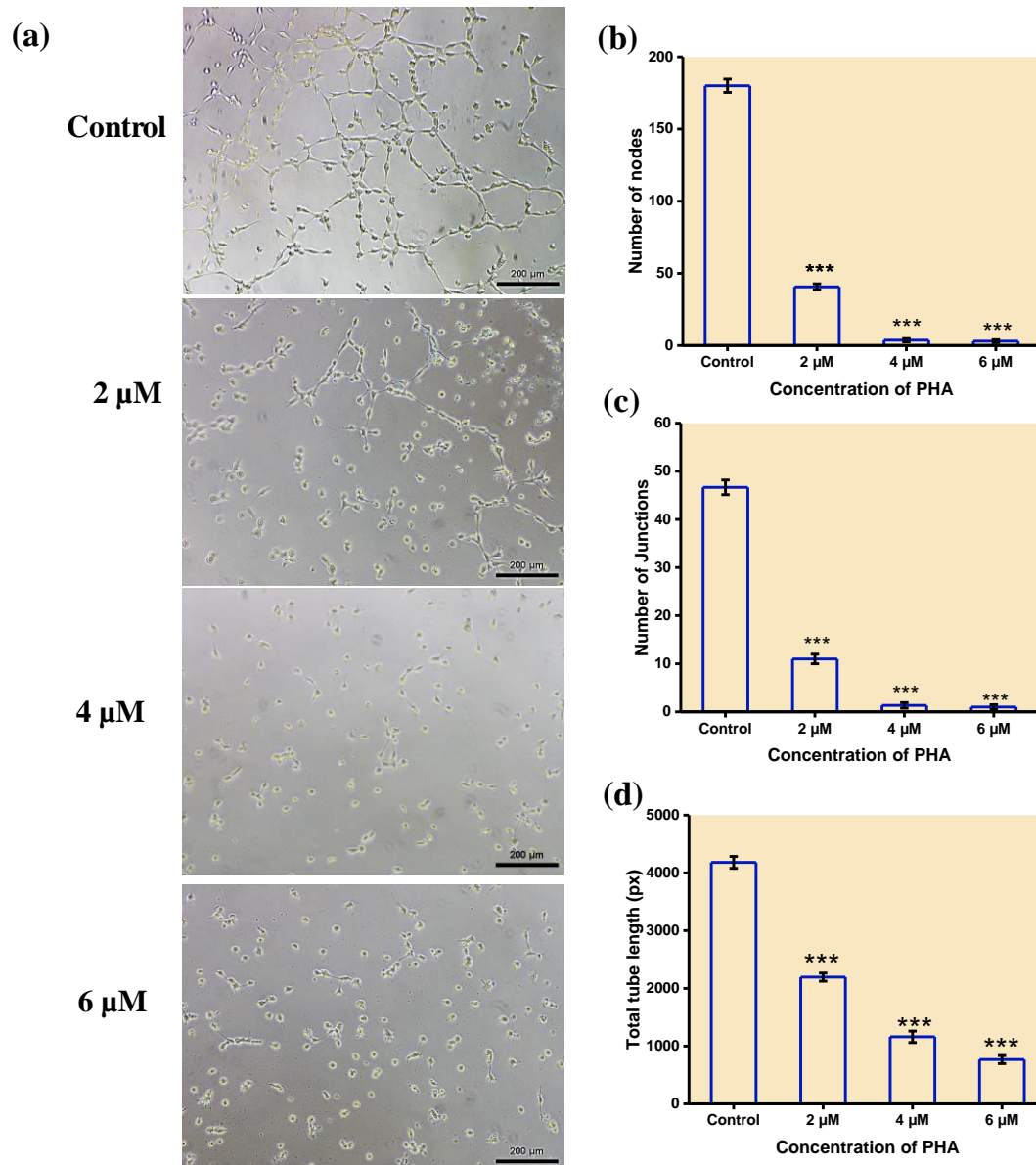


**Figure 3B.5.** (a) Tube formation assay in EA.hy926 cells in untreated and treated groups, treatment with PHA reduced the tube formation in endothelial cells in a concentration-dependent manner, (b) number of nodes formed during the assay, (c) number of junctions and (d) total length of the tube showed a reduction in the treatment groups. The scale bar indicates 200  $\mu\text{m}$ . The experiments were conducted in triplicates and the graphical value represents average  $\pm$  SD, and \*\*\* indicates  $p$  value  $<0.001$ , considered as significant when compared to the control.

### 3B.3 Conclusion

In conclusion, the antiangiogenic study of the compound, PHA isolated from *Cyclea peltata* on EA.hy926 endothelial cells revealed significant inhibitory effects across multiple crucial processes. The compound demonstrated notable suppression of wound healing, migration, invasion, and tube formation at a very low concentration when compared to its IC<sub>50</sub> value. These findings underscore its potential as a potent antiangiogenic agent, suggesting a promising avenue for further exploration in the development of therapeutic strategies targeting angiogenesis-related cancer therapy. The comprehensive impact observed across various aspects of endothelial cell behavior positions phaeanthine as a compelling candidate for future investigations and potential therapeutic applications in the modulation of angiogenesis. Overall, the study not only sheds light on the inhibitory potential of the natural compound, PHA but also provides a foundation for future research endeavors aimed at understanding its mechanisms and translating these findings into clinically relevant strategies.

### 3B.4 Experimental Section

#### 3B.4.1 Cell culture methods

The human umbilical vein cell line, EA.hy926 cell line was obtained from ATCC and maintained in Dulbecco's modified eagle medium-high glucose (DMEM, Sigma), and supplemented with 10% Fetal Bovine Serum (FBS, Himedia) and 1% antibiotic antimycotic solution 100X (with 10,000 units Penicillin, 10 mg Streptomycin and 25 µg Amphotericin B per mL in 0.9% normal saline-Himedia) and maintained at 5% CO<sub>2</sub> at 37°C in the incubator.

#### 3B.4.2 Cytotoxicity assays

The EA.hy926 cells were seeded in 96 well plate for 24 h and after the incubation compound PHA at different concentrations was added and incubated for 24 h. after the desired incubation time, MTT dissolved in HBSS was added to each well for 2-4 h and the formazan crystals were dissolved in 100 µL of DMSO by removing the MTT solution. The absorbance was measured at 570 nm in a multimode plate reader.

### 3B.4.3 Wound healing assay

Cells were seeded in a 96-well plate at a seeding density of  $10 \times 10^4$  cells per well. Wounds were created in each well by carefully scratching with a 200  $\mu\text{L}$  pipette tip. Various concentrations of compounds were then added, and images were captured at regular intervals to monitor the wound healing progress. The treated group was subsequently compared to the untreated control to assess the impact of the compounds on the observed wound closure. The wound area was evaluated with the help of ImageJ software and the wound closure was calculated by the formula:

$$\text{Wound closure \%} = \frac{A_{t=0} - A_{t=\Delta h}}{A_{t=0}}$$

Where,  $A_{t=0}$  – Area of the wound at zeroth hour

$A_{t=\Delta h}$  – Area of the wound at specified time interval

### 3B.4.4 Migration and Invasion assay

The transwell migration and invasion assays utilized cell culture inserts of 8.0  $\mu\text{m}$  pore size. These inserts created a barrier between two distinct media compartments, where the lower portion contained serum-containing medium, and the inside of the insert cell suspension in serum-free medium, separated by a porous membrane. In the invasion assay, the inner side of the insert was coated with diluted matrigel. Cells were introduced into the serum-free medium, and after 24 hours of incubation, they migrated through the pores towards the serum-containing medium. Following the specified incubation period, the inserts were fixed, stained, and subjected to image capture. Subsequent calculations were performed using Image J software.<sup>25</sup>

### 3B.4.5 Tube formation assay

To investigate the anti-angiogenic impact of PHA, the tube formation study was conducted using EA.hy926 cells. In a 96-well plate, 25  $\mu\text{L}$  of Matrigel was applied to each well and left to solidify at  $37^\circ\text{C}$ . The cells were trypsinized, resuspended in serum-free media, and then added to the Matrigel-precoated wells at a seeding density of  $1 \times 10^4$  cells per well.

Following a 12-hour incubation period, images were captured, and the data were subjected to analysis using Image J software.<sup>33,37</sup>

### References of 3A & 3A

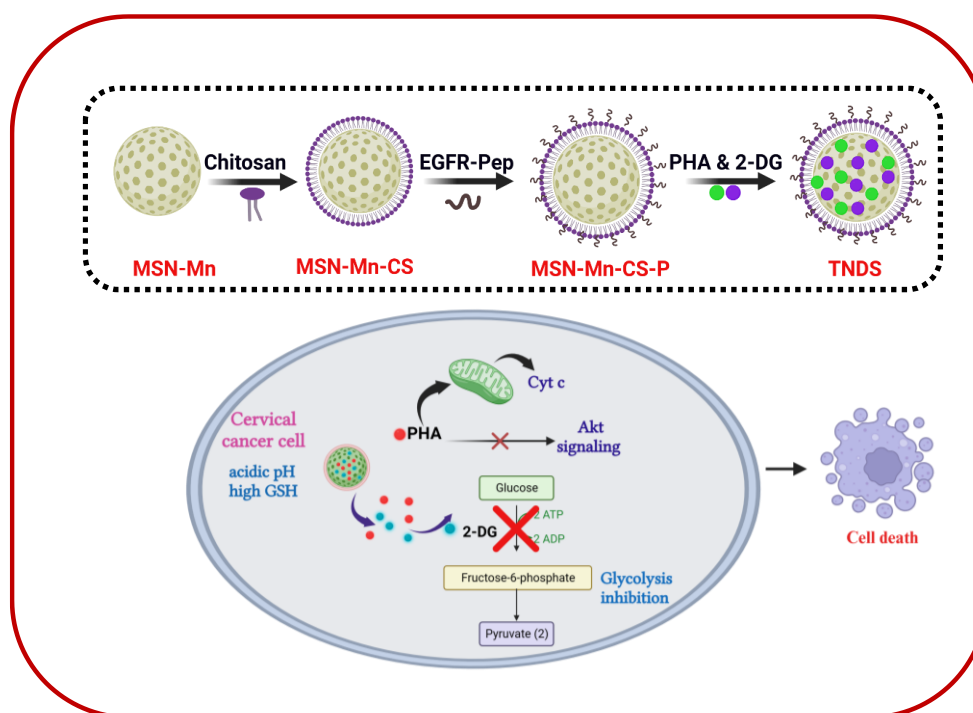
- (1) Douglas Hanahan and Robert A. Weinberg. The Hallmarks of Cancer. *Cell* **2000**, *100* (7), 57–70. [https://doi.org/10.1016/S0092-8674\(00\)81683-9](https://doi.org/10.1016/S0092-8674(00)81683-9).
- (2) Gerstberger, S.; Jiang, Q.; Ganesh, K. Metastasis. *Cell* **2023**, *186*. <https://doi.org/10.1016/j.cell.2023.03.003>.
- (3) Ganguly, K. K.; Pal, S.; Moulik, S.; Chatterjee, A. Integrins and Metastasis. *Cell Adh. Migr.* **2013**, *7* (3), 251–261.
- (4) Bergers, G.; Fendt, S.-M. The Metabolism of Cancer Cells during Metastasis. *Nat. Rev. Cancer* **2021**, *21* (March), 162–180. <https://doi.org/10.1038/s41568-020-00320-2>.
- (5) Al-Masri, M.; Paliotti, K.; Tran, R.; Halaoui, R.; Lelarge, V.; Chatterjee, S.; Wang, L. T.; Moraes, C.; McCaffrey, L. Architectural Control of Metabolic Plasticity in Epithelial Cancer Cells. *Commun. Biol.* **2021**, *4* (371), 1–16. <https://doi.org/10.1038/s42003-021-01899-4>.
- (6) Xie, Y.; Ma, S.; Tong, M. Metabolic Plasticity of Cancer Stem Cells in Response to Microenvironmental Cues. *Cancers (Basel)*. **2022**, *14* (21), 1–14. <https://doi.org/10.3390/cancers14215345>.
- (7) Ganesh, K.; Massagué, J. Targeting Metastatic Cancer. *Nat. Med.* **2021**, *27* (January), 34–44. <https://doi.org/10.1038/s41591-020-01195-4>.
- (8) Rajendran, V.; Jain, M. V. In Vitro Tumorigenic Assay: Colony Forming Assay for Cancer Stem Cells. In *Cancer Stem Cells: Methods and Protocols, Methods in Molecular Biology*; 2018; Vol. 1692, pp 89–95. <https://doi.org/10.1007/978-1-4939-7401-6>.
- (9) Matthews, H. K.; Bertoli, C.; Bruin, R. A. M. Cell Cycle Control in Cancer. *Nat. Rev. Mol. Cell Biol.* **2021**, *23*, 74–88. <https://doi.org/10.1038/s41580-021-00404-3>.
- (10) Friedl, P.; Wolf, K. TUMOUR-CELL INVASION AND MIGRATION : DIVERSITY AND ESCAPE MECHANISMS. *Nat. Rev. Cancer* **2003**, *3* (May), 362–374. <https://doi.org/10.1038/nrc1075>.
- (11) Kozak, J.; Forma, A.; Czezelewski, M.; Kozyra, P.; Sitarz, M.; Baj, J. Inhibition or Reversal of the Epithelial-Mesenchymal Transition in Gastric Cancer : Pharmacological Approaches. *Int. J. Mol. Sci.* **2021**, *22* (277), 1.23.

- (12) Loh, C.-Y.; Chai, J. Y.; Tang, T. F.; Wong, W. F.; Sethi, G.; Shanmugham, M. K.; Chong, P. P.; Looi, C. Y. The E-Cadherin and N-Cadherin Switch in Epithelial-to-Mesenchymal Transition: Signaling, Therapeutic Implications, and Challenges. *Cells* **2019**, *8* (1118), 1–33.
- (13) Yin, K. B. *The Mesenchymal-Like Phenotype of the MDA-MB-231 Cell Line. Breast Cancer - Focusing Tumor Microenvironment, Stem Cells and Metastasis*, Prof. Mehm.; 2011.
- (14) Liu, S.; Dong, Y.; Wang, Y.; Hu, P.; Wang, J.; Yi, R. Pristimerin Exerts Antitumor Activity against MDA-MB-231 Triple-Negative Breast Cancer Cells by Reversing of Epithelial-Mesenchymal Transition via Downregulation of Integrin  $\beta 3$ . *Biomed. J.* **2021**, *44* (6), S84–S92. <https://doi.org/10.1016/j.bj.2020.07.004>.
- (15) Pan, B.; Guo, J.; Liao, Q.; Zhao, Y.  $\beta 1$  and  $\beta 3$  Integrins in Breast, Prostate and Pancreatic Cancer: A Novel Implication (Review). *Oncol. Lett.* **2018**, *15*, 5412–5416. <https://doi.org/10.3892/ol.2018.8076>.
- (16) Kemper, M.; Schiecke, A.; Maar, H.; Nikulin, S.; Poloznikov, A.; Galatenko, V.; Tachezy, M.; Gebauer, F.; Lange, T.; Riecken, K.; Tonevitsky, A.; Aigner, A.; Izbicki, J.; Schumacher, U.; Wicklein, D. Integrin Alpha-V Is an Important Driver in Pancreatic Adenocarcinoma Progression. *J. Exp. Clin. Cancer Res.* **2021**, *40* (214), 1–19.
- (17) Duffy, M. J.; Maguire, T. M.; Hill, A.; McDermott, E.; O’Higgins, N. Metalloproteinases: Role in Breast Carcinogenesis, Invasion and Metastasis. *Breast Cancer Res.* **2000**, *2* (4), 252–257. <https://doi.org/10.1186/bcr65>.
- (18) Kleiner, D. E.; Stetler-Stevenson, W. G. Matrix Metalloproteinases and Metastasis. *Cancer Chemother. Pharmacol. Suppl.* **1999**, *43*, 42–51. <https://doi.org/10.1007/s002800051097>.
- (19) Yoon, S. O.; Park, S. J.; Yun, C. H.; Chung, A. S. Roles of Matrix Metalloproteinases in Tumor Metastasis and Angiogenesis. *J. Biochem. Mol. Biol.* **2003**, *36* (1), 128–137. <https://doi.org/10.5483/bmbrep.2003.36.1.128>.
- (20) Yang, M.; Wu, K. TWIST Activation by Hypoxia Inducible Factor-1 (HIF-1): Implications in Metastasis and Development. *cell cycle* **2008**, *7* (14), 2090–2096. <https://doi.org/10.4161/cc.7.14.6324>.
- (21) Rankin, E. B.; Giaccia, A. J. Hypoxic Control of Metastasis. *Science* (80-. ). **2016**, *352* (6282), 175–180.
- (22) Huber, M. A.; Azoitei, N.; Baumann, B.; Grünert, S.; Sommer, A.; Pehamberger, H.; Kraut, N.; Beug, H.; Wirth, T. NF- $\kappa$ B Is Essential for Epithelial-Mesenchymal Transition and Metastasis in a Model of Breast Cancer Progression. *Journal Clin. Invest.* **2004**, *114* (4), 569–581. <https://doi.org/10.1172/JCI200421358>.

- (23) Kilic-eren, M.; Boylu, T.; Tabor, V. Targeting PI3K / Akt Represses Hypoxia Inducible Factor-1  $\alpha$  Activation and Sensitizes Rhabdomyosarcoma and Ewing ' s Sarcoma Cells for Apoptosis. *Cancer Cell Int.* **2013**, *13* (36), 1–8.
- (24) Johanning, G. L.; Lin, T. Y. Unsaturated Fatty Acid Effects on Human Breast Cancer Cell Adhesion. *Nutr. Cancer* **1995**, *24* (1), 57–66. <https://doi.org/10.1080/01635589509514393>.
- (25) Kramer, N.; Walzl, A.; Unger, C.; Rosner, M.; Krupitza, G.; Hengstschla, M. In Vitro Cell Migration and Invasion Assays. *Mutat. Res. Mutat. Res.* **2013**, *752*, 10–24. <https://doi.org/10.1016/j.mrrev.2012.08.001>.
- (26) Ramjiawan, R. R.; Griffioen, A. W.; Duda, D. G. Anti-Angiogenesis for Cancer Revisited: Is There a Role for Combinations with Immunotherapy? *Angiogenesis* **2017**, *20* (2), 185–204. <https://doi.org/10.1007/s10456-017-9552-y>.
- (27) Li, J. ping; Zhao, F. li; Yuan, Y.; Sun, T. ting; Zhu, L.; Zhang, W. you; Liu, M. xiang. Studies on Anti-Angiogenesis of Ginsenoside Structure Modification HRG in Vitro. *Biochem. Biophys. Res. Commun.* **2017**, *492* (3), 391–396. <https://doi.org/10.1016/j.bbrc.2017.08.090>.
- (28) Detmar, M. Tumor Angiogenesis. *J. Investig. Dermatology Symp. Proc.* **2000**, *5*, 20–23.
- (29) Gatne, D.; Addepalli, V. Overview of Angiogenesis Inhibitors. In *Biochemical Basis and Therapeutic Implications of Angiogenesis. Advances in Biochemistry in Health and Disease*; Springer, New York, 2013; pp 499–520. <https://doi.org/10.1007/978-1-4614-5857-9>.
- (30) Neal, C. P.; Berry, D. P.; Doucas, H.; Manson, M. M.; Steward, W.; Garcea, G. Clinical Aspects of Natural Anti-Angiogenic Drugs. *Curr. Drug Targets* **2006**, *7*, 371–383.
- (31) Ma, J.; Waxman, D. J. Combination of Antiangiogenesis with Chemotherapy for More Effective Cancer Treatment. *Mol. Cancer Ther.* **2008**, *7* (12), 3670–3684. <https://doi.org/10.1158/1535-7163.MCT-08-0715>.
- (32) Chen, K.; Fan, Y.; Gu, J.; Han, Z.; Zeng, H.; Mao, C.; Wang, C. In Vivo Screening of Natural Products Against Angiogenesis and Mechanisms of Anti-Angiogenic Activity of Deoxysappanone B 7 , 4 ' -Dimethyl Ether. *Drug Des. Devel. Ther.* **2020**, *14*, 3069–3078.
- (33) Lu, H.; Li, X.; Zhang, J.; Shi, H.; Zhu, X.; He, X. Effects of Cordycepin on HepG2 and EA.Hy926 Cells: Potential Antiproliferative, Antimetastatic and Anti-Angiogenic Effects on Hepatocellular Carcinoma. *Oncol. Lett.* **2014**, *7* (5), 1556–1562. <https://doi.org/10.3892/ol.2014.1965>.

- (34) Wang, X.; Decker, C. C.; Zechner, L.; Krstin, S.; Wink, M. In Vitro Wound Healing of Tumor Cells : Inhibition of Cell Migration by Selected Cytotoxic Alkaloids. *BMC Pharmacol. Toxicol.* **2019**, *20* (4), 1–12.
- (35) Lamalice, L.; Le Boeuf, F.; Huot, J. Endothelial Cell Migration during Angiogenesis. *Circ. Res.* **2007**, *100* (6), 782–794. <https://doi.org/10.1161/01.RES.0000259593.07661.1e>.
- (36) DeCicco-Skinner, K. L.; Henry, G. H.; Cataisson, C.; Tabib, T.; Curtis Gwilliam, J.; Watson, N. J.; Bullwinkle, E. M.; Falkenburg, L.; O’Neill, R. C.; Morin, A.; Wiest, J. S. Endothelial Cell Tube Formation Assay for the in Vitro Study of Angiogenesis. *J. Vis. Exp.* **2014**, *10* (91), 1–8. <https://doi.org/10.3791/51312>.
- (37) Yu, F.; Fu, R.; Liu, L.; Wang, X.; Wu, T.; Shen, W.; Gui, Z.; Mo, X.; Fang, B.; Xia, L. Leptin-Induced Angiogenesis of EA.HY926 Endothelial Cells via the Akt and Wnt Signaling Pathways in Vitro and in Vivo. *Front. Pharmacol.* **2019**, *10* (OCT), 1–15. <https://doi.org/10.3389/fphar.2019.01275>.

## Development of MSN-based nano delivery system for the combination therapy of phaeanthine & 2-deoxy-D-glucose against cervical cancer cells



### Abstract

The progress and breakthroughs in nanotechnology have positioned nanoparticle-based drug delivery systems as a promising strategy for overcoming challenges associated with conventional therapies. Herein, a synergistic assessment carried out with the blend of Phaeanthine and the glycolytic inhibitor 2-deoxy D-glucose (2-DG), co-loaded in a chitosan-coated MSN-Mn nano delivery system targeting to cervical cancer HeLa cells. The nanoconstruct was coupled with a small peptide substrate of EGFR-targeting hexapeptide sequence, LARLLT, to impart the targetability towards overexpressed receptor protein, EGFR in HeLa cells. The nanostruct found safer for normal cells as its drug release response prevailed in tumor cells only, where the acidic pH enhances the swelling of the chitosan and the high GSH concentration favors imparted the degradation of bonds stabilizing the MSN-Mn. The choice of 2-DG was deliberate, aiming to amplify



*the therapeutic efficacy by inhibiting cellular glycolysis. On the other hand, PHA operates by regulating the Akt signaling pathway to induce mitochondria-mediated apoptosis. The synergistic interplay between PHA and 2-DG was evaluated through a series of cytotoxicity assays with various combinations, and the resulting data were analyzed using compusyn software. The effectiveness of the drug coloaded nanoconstruct was assessed through various assays, revealing its ability to induce glycolytic inhibition, apoptosis, and inhibition on proliferation of HeLa cells.*

#### **4.1 Introduction**

Cervical cancer constitutes a significant portion of the global cancer burden for women, ranking as the fourth most prevalent cancer among women worldwide. Low and middle-income countries bear the majority of this burden, with approximately 84% of global cervical cancer cases and 88% of related deaths occurring in nations with a low human development index.<sup>1</sup> In India, according to Globocan 2020, cervical cancer stands as the second leading cancer among women. The treatment approaches for invasive cervical cancer are stratified based on the cancer stage. Locally advanced cervical cancer is typically addressed through a combination of surgery, chemotherapy, and radiotherapy, involving external beam radiation therapy and brachytherapy. In 2021, the FDA approved pembrolizumab (Keytruda) in conjunction with chemotherapy for advanced cervical cancer. This drug impedes the binding of PD-1, a protein on cytotoxic T-cells, to the PD-L1 protein expressed on certain cancer cells, reactivating T cells to target cancer cells.<sup>2</sup> Despite advancements, reports highlight various side effects associated with medications used for cervical cancer treatment, including increased fatigue and nausea, decreased white blood cell counts, and skin issues like rashes and blisters, along with severe lung problems. Consequently, there is an urgent need for the development of more effective therapeutics with fewer side effects and lower costs to address this life-threatening condition.

In this regard, the natural product could be a promising lead, in the presiding chapters, the role of phaeanthine as an anticancer lead to cure cervical cancer has been explored, it can act by regulating multiple pathways like inducing apoptosis, inhibiting the proliferative signalling, inhibiting the migration, and invasion, thereby controlling the metastasis, also it can control the neovascularization or angiogenesis at a low concentration. Another potent drug molecule 2-deoxy d-glucose (2-DG), which is an glycolytic inhibitor,

is widely used as an anticancer drug and used in combination with other drugs to treat varying types of cancers. 2-DG can competitively inhibit the uptake of glucose and inside the cell, it will inhibit the glycolytic pathway. With the kinase action of hexokinase 2-DG will be converted to 2-DG-6-phosphate leading to the inhibition of glycolysis, thereby affecting ATP production.<sup>3</sup>

In recent decades, there has been an extraordinary surge in nanomedicine research, particularly in the realm of cancer treatment. Researchers have made significant strides in creating a diverse range of nanomedicines, broadly categorized as metal nanoparticles, inorganic nanoparticles, metal-organic frameworks, polymer nanoparticles, exosomal nanoparticles, and more. These groundbreaking discoveries have paved the way for innovative treatment approaches that depart from traditional methods.<sup>4</sup> The widespread integration of nanomedicine in oncology can be largely attributed to its unique characteristics, such as protecting drug molecules from enzymatic and mechanical degradation, facilitating prolonged drug release, overcoming biological barriers for effective delivery, and achieving targeting specificity for site-specific drug delivery. Additionally, nanosystems offer the advantage of enabling multidrug delivery, further enhancing their therapeutic potential.<sup>4</sup> (Figure 4.1) Currently, at least 15 cancer nanomedicines are approved globally and more than 80 novel cancer nanomedicines are being evaluated in over 200 clinical trials.<sup>5</sup>

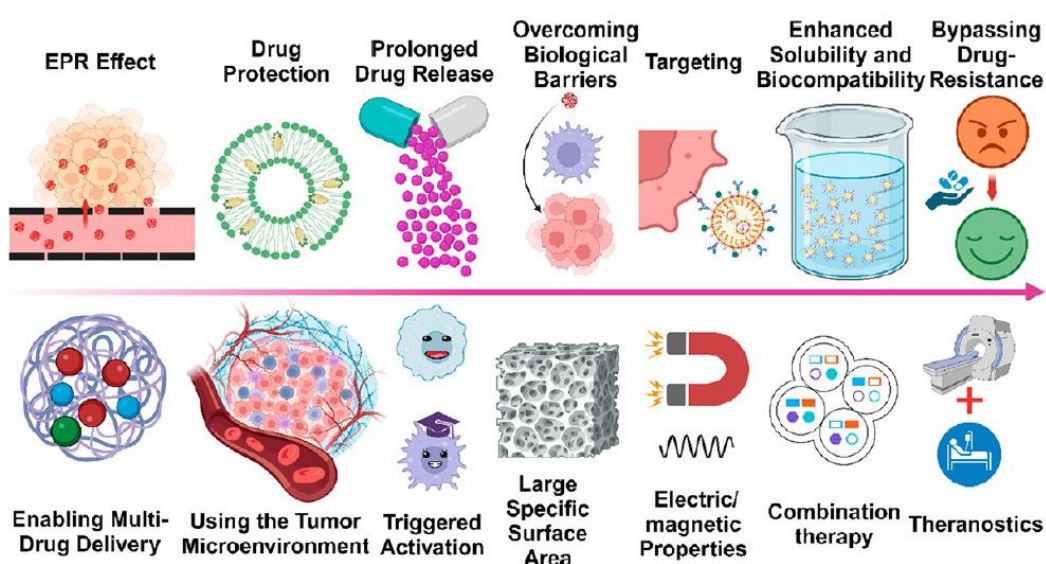


**Figure 4.1.** Scheme illustrating the multifaceted advantages of nanomedicine in cancer therapy. (*ACS Appl. Nano Mater.* 2023, [doi.org/10.1021/acsnm.3c04487](https://doi.org/10.1021/acsnm.3c04487))

The system is envisioned to comprise a nanoscale delivery platform designed for specific tumor targeting and efficient cargo transfer. This nanosystem should exhibit controlled release triggered by various stimuli, such as temperature, pH, light, among others. An ideal drug delivery system should possess certain attributes, including: i) sufficient stability to prevent premature cargo release; ii) biocompatibility; iii) target-specific accumulation; iv) favorable biodegradation profile; and v) cost-effective synthetic feasibility for scaling up in pre-clinical and clinical applications.<sup>6</sup> However, even with the desired criteria, versatile nanoparticles (NPs) face challenges in successfully delivering cargos. In this context, mesoporous silica nanoparticles (MSN) have gained attention in nano-drug delivery due to their characteristics, such as tunable pore size with high volume and large surface area for effective cargo loading, straightforward fabrication methods, and unique immune-stimulatory potential. Despite these advantages, the physiologically inert nature of the Si-O-Si network in MSN poses a challenge for biodegradation. Introducing inorganic metal species like iron, calcium, and manganese promotes selective degradation of the MSN network in the tumor microenvironment (TME), facilitating renal clearance. Additionally, sealing MSN pores with pH-sensitive biopolymers, such as chitosan, proves to be a sensible approach to prevent premature drug release.<sup>7</sup>

This chapter aimed to innovate a synergistic therapeutic strategy by augmenting the potency of established PHA through a combined regimen with the glycolytic inhibitor 2-DG. The efficacy of this combination was evaluated and subsequently encapsulated within a cancer cell-specific, self-degradable MSN-Mn nanocarrier system. This nanoconstruct was further adorned with an EGFR-targeting hexapeptide, specifically designed for heightened affinity to cervical cancer cells to make it a targeted nano delivery system (TNDS). The selective internalization of this construct occurred through receptor-mediated endocytosis, triggered by the acidic pH and elevated reductive GSH environment, resulting in the degradation of the nanocarrier and the release of the therapeutic payload within the cancer cells. The cargo promptly initiates the activation of mitochondria-mediated chemotherapy via PHA, coupled with the inhibition of glycolysis induced by 2-DG. The consequential reduction in cellular energy production generated a starvation effect, dismantling the resistance mechanisms of cancer cells. Notably, this approach selectively eradicated cancer cells while sparing normal ones. The incorporation of the 2-DG-mediated energy deprivation and PHA-induced chemotherapy orchestrated a potent anticancer synergy. This strategic combination, facilitated by a self-degradable and cancer-targeting

nanocarrier, heralds a paradigm shift in the landscape of combination therapy, promising significant advancements in scientific and therapeutic realms. (Scheme 4.1)

## 4.2 Results and Discussion

The initial phase, investigation was focused on identifying a synergistic pairing of two pivotal compounds, namely PHA and 2-deoxy D-glucose (2-DG), with the overarching objective of devising an efficient nano-delivery system for drug administration. Synergy in pharmacology denotes a scenario where the combined impact of multiple substances surpasses the sum of their individual effects, while antagonistic effects arise when the collective impact is less than the cumulative effect of the individual components. The selection of PHA and 2-DG was motivated by the anticipation that their combined actions could yield heightened therapeutic outcomes. PHA, the molecule, whose chemotherapeutic attributes against cervical cancer cells was explored in the previous chapter, and 2-DG, acknowledged for its interference with glucose metabolism, manifested an intriguing synergy that could be exploited for refined drug delivery. The exploration of synergy between these compounds encompassed a series of experiments to evaluate their collective effects on specific cellular processes and biological pathways. Within the realm of drug delivery, a synergistic amalgamation offers manifold advantages, such as augmenting therapeutic efficacy, diminishing individual dosage requirements, mitigating adverse effects, and enhancing overall patient outcomes. Conversely, an antagonistic effect has the potential to curtail the effectiveness of the treatment or lead to unintended repercussions. To validate these hypotheses, we embarked on the optimization of suitable and effective synergistic combinations.

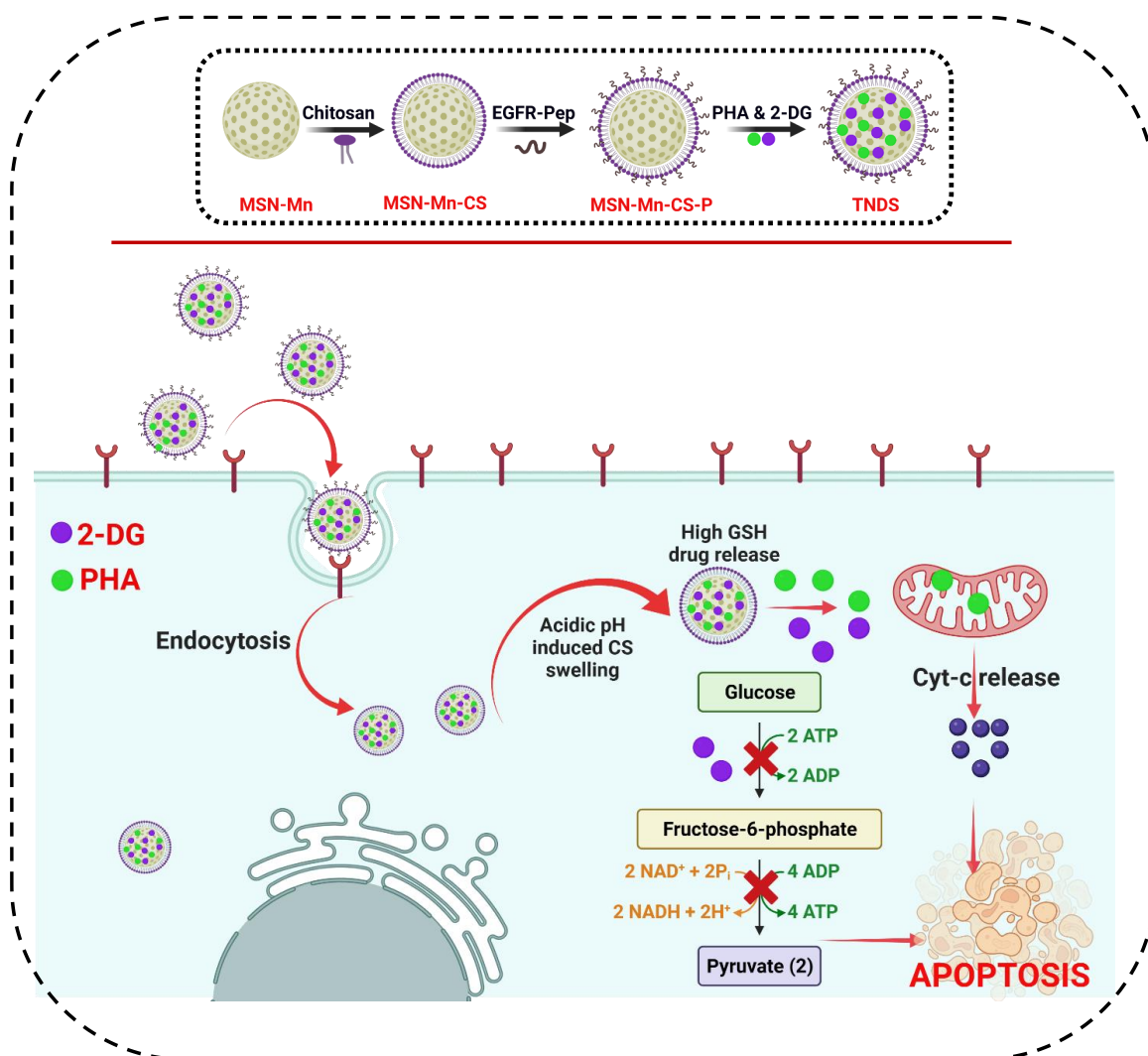
### 4.2.1 Cytotoxicity of PHA and 2-DG

Cytotoxicity evaluation of PHA and 2-DG was carried out on HeLa cells for an incubation period of 24 h by MTT assay. From the results, it is observed that the  $IC_{50}$  of PHA and 2-DG was  $8.1 \pm 0.04 \mu\text{M}$  and  $18.1 \pm 0.2 \text{ mM}$  respectively. 2-DG always has toxicity at mM concentrations.<sup>8</sup> (Figure 4.2 a & b)

### 4.2.2 Establishing the synergistic combination of PHA & 2-DG

The effective action against cancer cells resulting from the synergistic combination of two drug molecules was determined using the Chou-Talalay method, also known as the combination index method, facilitated by Compusyn software. Multiple combinations of

the two drugs were tested in MTT assays, including ratios of 1:2, 1:4, 1:1, and 1:5. Cytotoxicity values obtained from these assays were subjected to Compusyn software to elucidate the specific type of interaction between the compound ratios. (Figure 4.2.c)



**Scheme 4.1.** Schematic representation of the fabrication of cervical cancer targeting nano delivery system and its mechanistic evaluation

The selected concentrations for the study spanned a wide range, starting from the minimum concentration of both drugs to a higher concentration relative to the  $IC_{50}$  of each compound. This range extended from 1  $\mu$ M for PHA to 10  $\mu$ M, and similarly, from 2 mM to 25 mM for 2-DG. The analysis yielded combination index (CI) values, which were then used to determine the nature of the interaction. A  $CI > 1$  indicated antagonism,  $CI < 1$  signified synergism, and  $CI = 1$  denoted an additive effect.

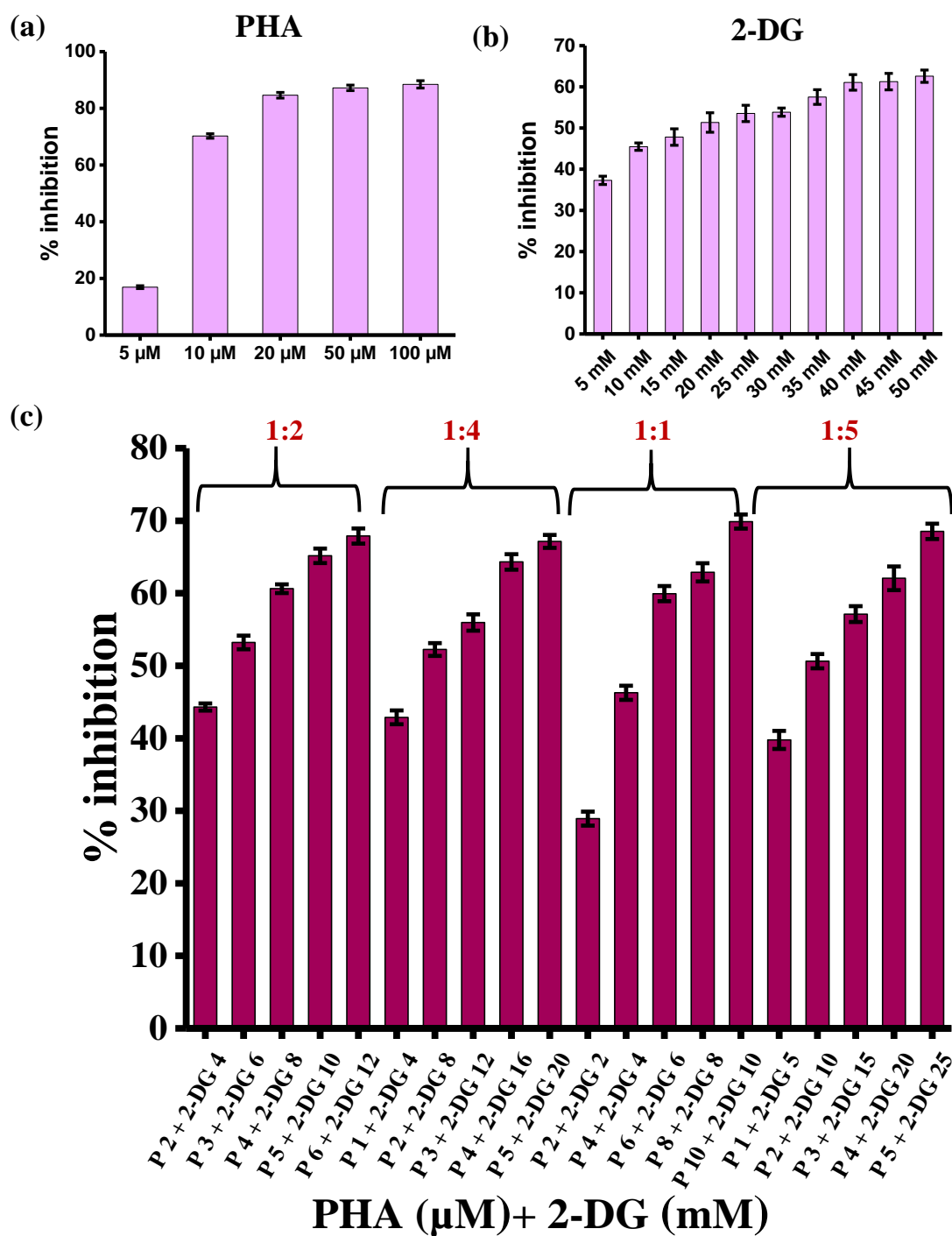


**Figure 4.2.** The cytotoxicity induced by (a) PHA and (b) 2-deoxy-D-glucose (2-DG) in a concentration-dependent manner in HeLa cells at 24 h incubation and (c) cytotoxicity of various ratios 1:2, 1:4, 1:1, and 1:5 ratio of PHA and 2-DG respectively in HeLa cells.

**Table 4.1.** CI values of various combinations of PHA with 2-DG against HeLa cells

Combination ratio	PHA ( $\mu\text{M}$ )	2-DG (mM)	Total Dose	Fa	CI Value
1:4	1	4	5	0.429	0.74973
	2	8	10	0.523	0.73193
	3	12	15	0.56	0.82944
	4	16	20	0.643	0.5793
	5	20	25	0.671	0.57593
1:1	2	2	4	0.289	1.42712
	4	4	8	0.463	0.7469
	6	6	12	0.599	0.44084
	8	8	16	0.629	0.47717
	10	10	20	0.699	0.35922
1:5	1	5	6	0.398	1.17723
	2	10	12	0.506	1.01724
	3	15	18	0.571	0.92789
	4	20	24	0.621	0.83621
	5	25	30	0.685	0.61625
1:2	2	4	6	0.443	0.73496
	3	6	9	0.532	0.57421
	4	8	12	0.606	0.44547
	5	10	15	0.652	0.39339
	6	12	18	0.679	0.38221

The findings from the analysis report table (Table 4.1.) indicate that the 1:2 combination yielded superior results compared to other combinations. Combinations 5:10 and 6:12 demonstrated a robust synergistic effect, with CI values below 0.4 at very low concentrations in comparison to their respective  $\text{IC}_{50}$  values. Consequently, the combination with lower concentrations of compounds (5:10, i.e., 5  $\mu\text{M}$  PHA and 10 mM 2-DG) was selected for further studies to achieve efficient toxicity against cancer cells. In the combination index plot (Figure 4.3.b), all the combinations of the 1:2 ratio were below  $\text{CI}=1$ , indicating a strong synergism.

In the dose-effect curve, the fraction of cells affected was plotted against the dose of the individual drugs and in combination (Figure 4.3.a). Notably, the combination of PHA and 2-DG exhibited a higher fraction affected compared to the individual drug doses. The isobologram of the 1:2 combination ratio revealed that the effects of the combination were positioned to the left of the hypotenuse, or in other words, the points were below the additivity line, suggesting a synergistic combination. This isobologram serves as a visual representation of the drug interaction. (Fig.4.3.d) In summary, the parameters derived from the Chou-Talalay analysis of synergism using CompuSyn software suggest a strong synergism between the two drugs, PHA and 2-DG, at a 1:2 ratio.

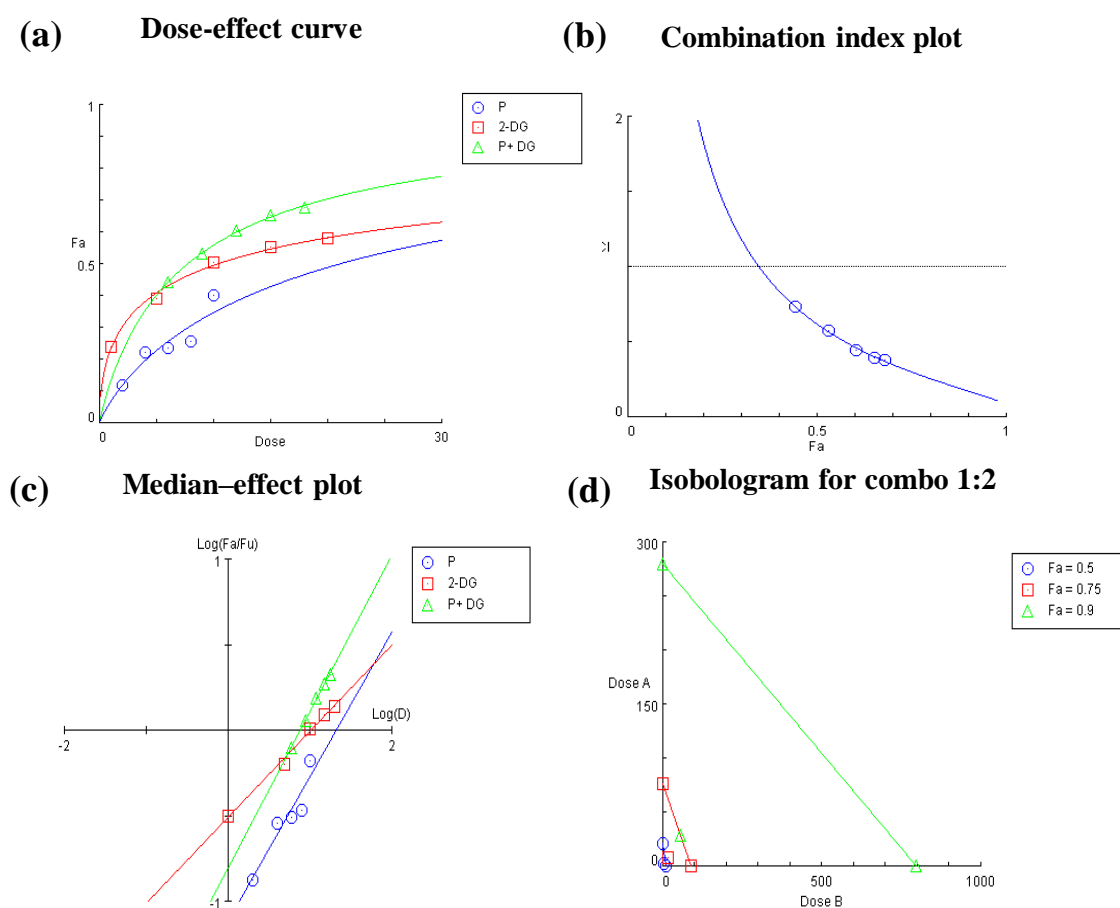


**Figure 4.3.** CompuSyn analysis of 1:2 combinations of PHA to 2-DG in HeLa cells (a) dose-effect curve, (b) combination index plot of the different combinations, (c) Median-effect plot and (d) isobologram for the combination.



### 4.2.3 Fabrication of chitosan coated MSN-Mn nanoparticle for pH responsive synergic release of PHA and 2-DG.

The method chosen for delivering the cargo comprising the synergistic combination of PHA and 2-DG drugs was the utilization of mesoporous silica nanoparticles (MSN). These nanoparticles were meticulously synthesized through a sol-gel procedure, employing tetraethyl orthosilicate (TEOS), cetyltrimethylammonium bromide (CTAB), and L-arginine.<sup>9</sup> To augment the biodegradability of the silica particles, an in-situ metal doping strategy involving manganese (Mn) was implemented.<sup>7</sup> In this process, Mn was introduced in between to disrupt the robust Si-O bonds, incorporating itself between these bonds and rendering them more susceptible to cleavage inside the tumor where the GSH concentration is higher. Following the synthesis, the nanoparticles underwent amino functionalization with (3-aminopropyl)triethoxysilane (APTES) to facilitate the effective binding of the chitosan (CS) group. The subsequent step involved coating the MSN-Mn with chitosan,<sup>10</sup> a polysaccharide derived from chitin, for a pH-dependent release mechanism. (Figure 4.4.a) This specialized coating was specifically engineered to facilitate the secure liberation of cargo at designated locations within the tumor microenvironment, distinguished by its acidic pH. The pH-responsive release mechanism imparts a precise and regulated drug release, thereby augmenting the therapeutic effectiveness of the synergistic combination of drugs. The constructed system underwent characterization through diverse methods, including Transmission Electron Microscopy (TEM). The TEM analysis provided insight into the size of the MSN-Mn, indicating a size distribution ranging between 70 and 90 nm.

Furthermore, Energy Dispersive X-ray Spectroscopy (EDX) analysis was employed to scrutinize the elemental composition of the sample at a nanometer scale. The outcomes of the EDX analysis not only validated the presence of manganese (Mn) but also, via elemental mapping, elucidated the presence of elements like silicon, oxygen, and manganese within the sample. These findings collectively validate the successful incorporation of manganese into the MSN system, as indicated by the comprehensive data obtained from TEM and EDX analyses. DLS analysis was conducted to examine the size distribution of nanoparticles in a suspended state (Figure 4.5.a) from the results, size of the particles in MSN-Mn was found to be around 110 to 120 nm and with Chitosan coating the size was found to increase a bit with an average value of 150 nm. The PDI values of the samples also showed lower values, indicating a predominantly uniform particle size within

the sample. The MSN-Mn nanoparticle showed PDI value of 0.201, while the chitosan coated nanoparticles was 0.111. The values close to 0.1 indicates its uniformity of size distribution suggests more consistent nanoparticle for drug delivery applications (Figure 4.5.b). Additionally, the surface zeta potential illustrated the successful coating of chitosan (CS) over the MSN-Mn nanoparticles. The negative  $\zeta$  potential of MSN-Mn ( $-21.2 \pm 1.5$  mV) transitioned to a positive value upon functionalization with APTES ( $+27.8 \pm 2$  mV). Moreover, the chitosan-coated MSN-Mn exhibited a higher  $\zeta$  potential of  $40 \pm 1.7$  mV, attributed to the presence of amino groups on the surface of the coated nanoparticles (Figure 4.5.c).

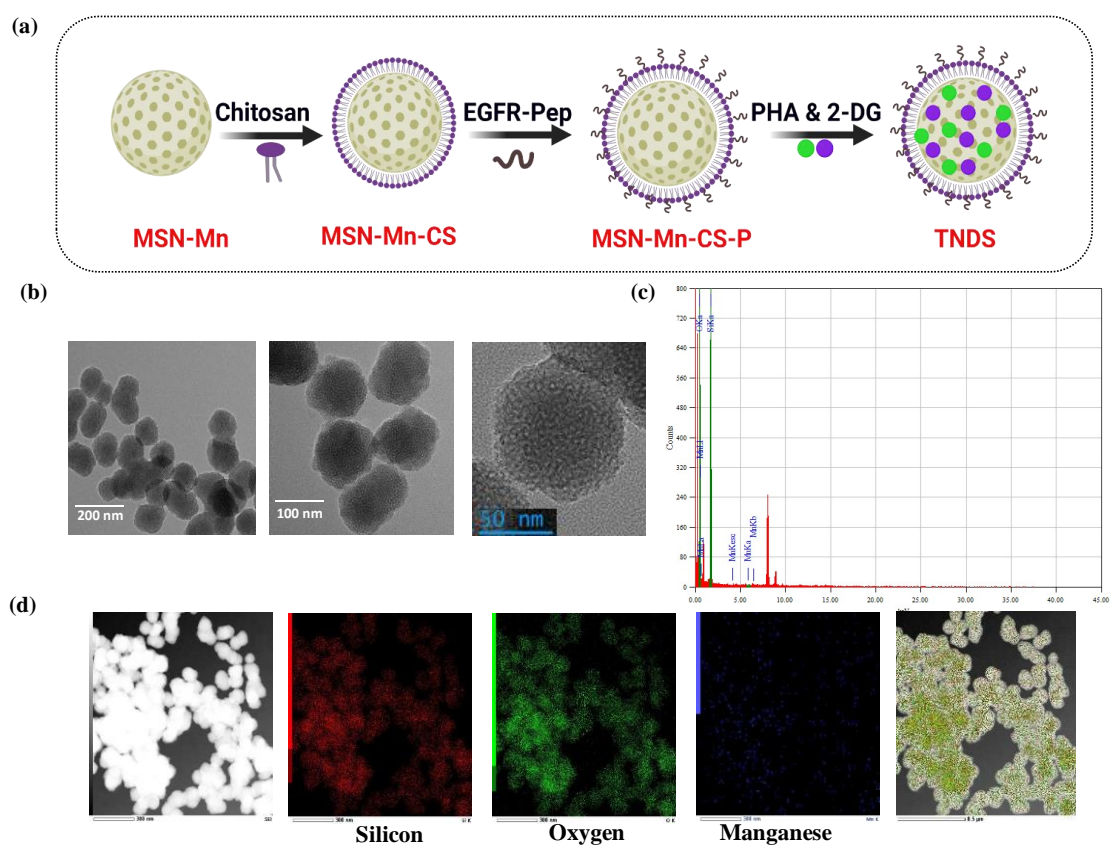


**Figure 4.4.** (a) Scheme for the synthesis of TNDS, Characterisation of the synthesized MSN-Mn (b) TEM images of MSN-Mn, (c) EDX analysis of MSN-Mn and (d) elemental mapping indicating the successful doping of Mn into the MSN system.

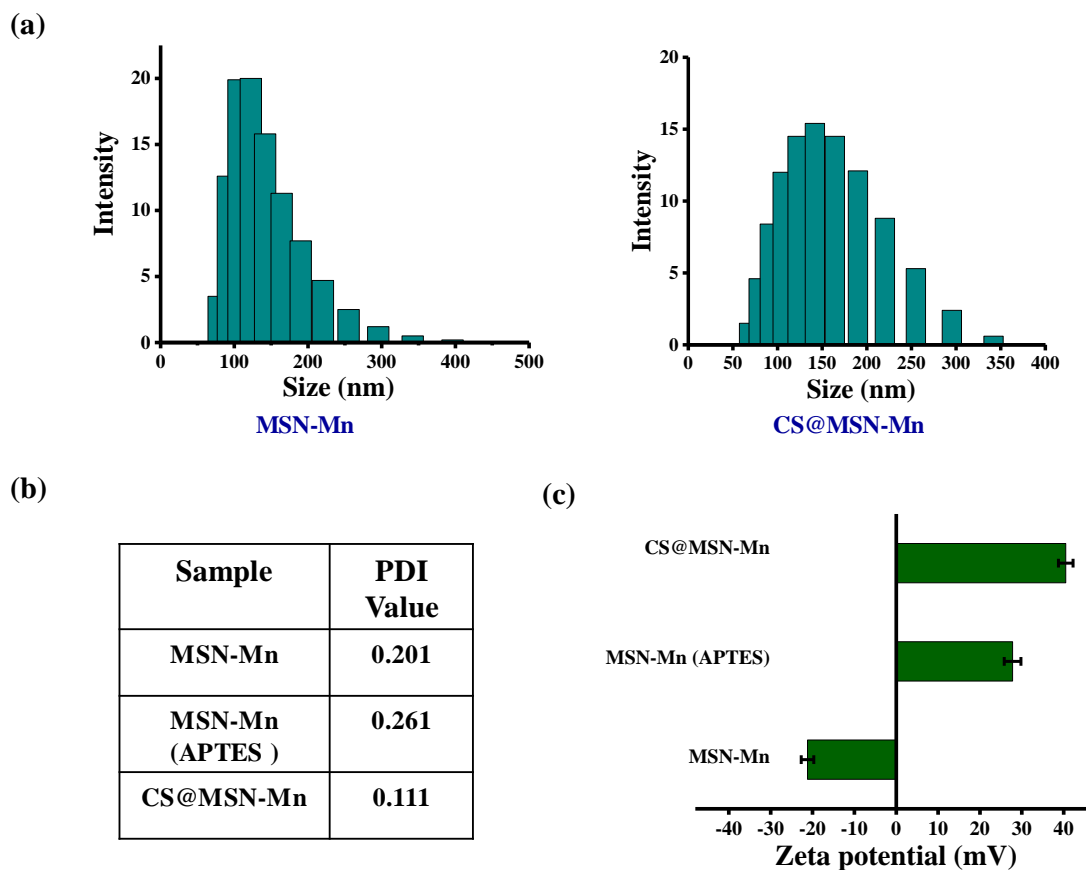


**Figure 4.5.** (a) DLS analysis of the synthesized nanoparticles, (b) polydispersity index (PDI) values, and (c) surface zeta potential of MSN-Mn, APTES functionalized MSN-Mn and CS coated MSN-Mn

#### 4.2.4 Synthesis of EGFR targeting peptide- LARLLT by SPPS

For the construction of a nano-carrier system specifically targeted towards the cancer cell, a targeting moiety is appended that will specifically bind to the respective receptors overexpressed on the tumor cells. Substantiated by literature findings, the epidermal growth factor receptor (EGFR) was identified as being overexpressed in cervical cancers.<sup>11–14</sup> The initial phase involved an assessment of EGFR expression in HeLa, a cervical cancer cell line, and the comparison with the expression in the normal non-tumorigenic cell, MCF-10A, revealed a noteworthy overexpression of EGFR in HeLa cells (Figure 4.6.a). Subsequently, the approach focused on identifying an apt peptide sequence that could selectively target the EGFR receptor. Notably, the selected hexapeptide sequence LARLLT emerged as a specific targeting agent for EGFR.<sup>15–17</sup> Consequently, the synthesis of this peptide sequence, LARLLT, was undertaken using the solid-phase peptide synthesis

(SPPS) method using Fmoc chemistry. (Figure 4.6.b & 4.6.c) This strategic progression aims to enhance the specificity of the nanosystem by incorporating a targeting moiety tailored to the overexpressed EGFR in cervical cancer cells. The synthesized peptide was characterised by HRMS and NMR spectroscopy.

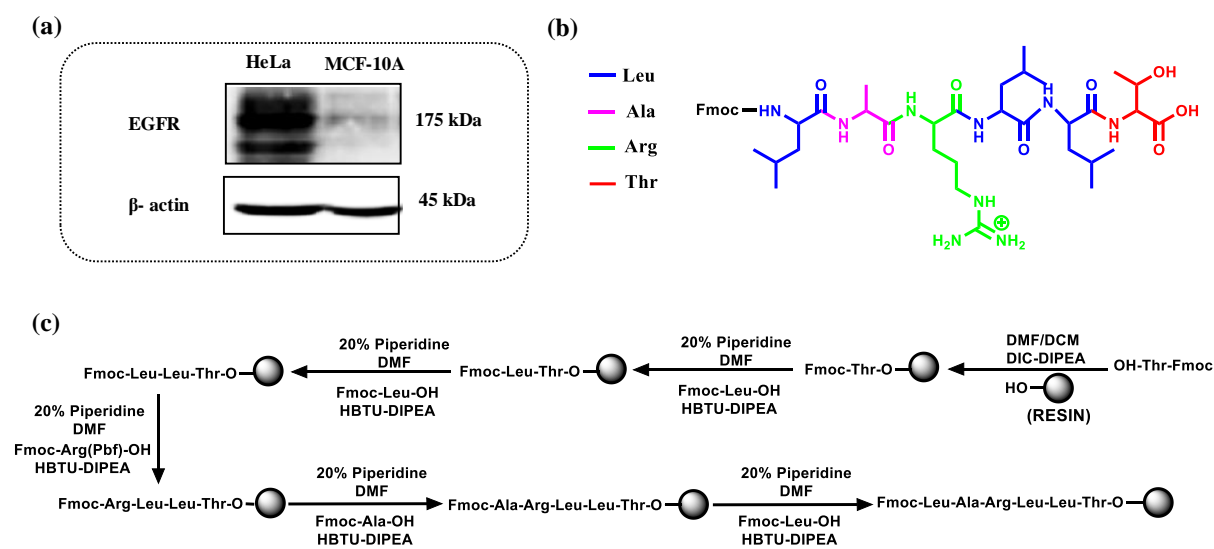


**Figure 4.6.** (a) Expression of EGFR in cervical cancer cell, HeLa and its expression is compared with that of a nontumorigenic cell, MCF-10A, (b) Hexapeptide sequence-LARLLT (targeting EGFR receptor) and (c) scheme for the synthesis of the hexasequence peptide by SPPS method.

#### 4.2.5 Targetability of the synthesized peptide in cervical cancer cell

To check the effectiveness and targetability of the synthesized peptide sequence, it was conjugated with the fluorescent dye Rhodamine B (*EGFR-P@Rho B*). The internalization of this construct was observed after a 1-hour of incubation in HeLa cells exhibiting a prominent fluorescence fluorescing from the cellular milieu. This observation indicates that the rhodamine-conjugated peptide specifically targeted the receptor protein of interest. Moreover, the targeting efficiency of the peptide was compared with that of a normal cell line, MCF-10A, which demonstrated minimal expression of EGFR. Notably, *EGFR-P@Rho B* did not exhibit any fluorescence in MCF-10A, underscoring its specific targeting to cells expressing the receptor of interest. (Figure 4.9)

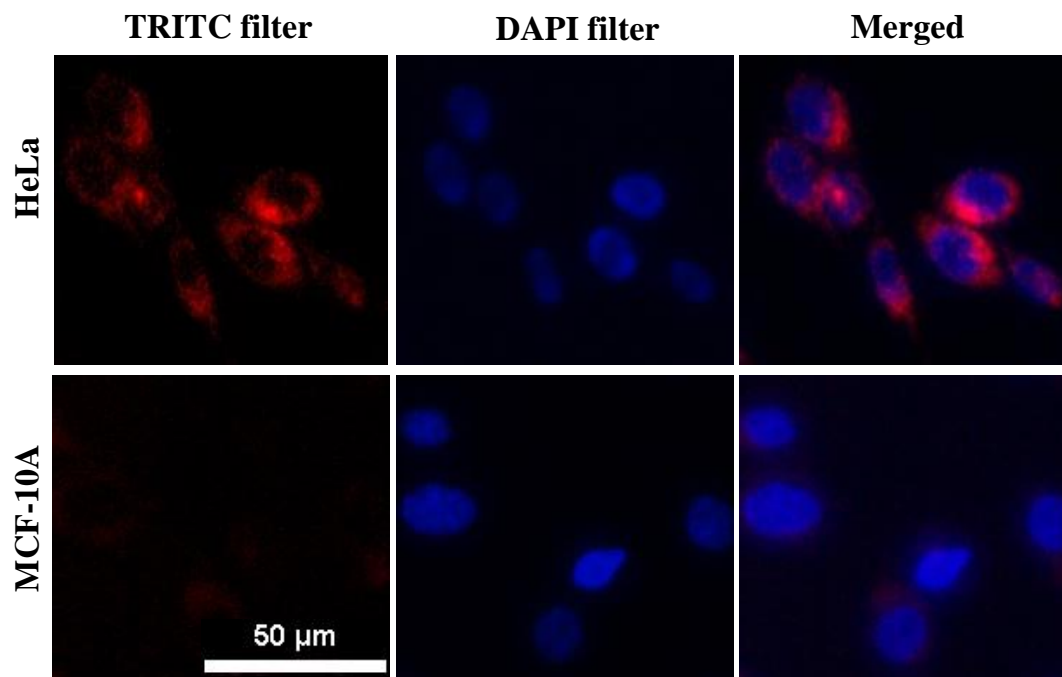


**Figure 4.9.** Targetability of EGFR targeting peptide conjugated with rhodamine B (*EGFR-P@Rho B*) in HeLa cells and MCF-10A cells after 1 h of incubation. The scale bar indicates 50  $\mu\text{m}$ .

#### 4.2.6 Drug loading and cellular internalization assessment of the targeted nanodelivery system (TNDS)

To investigate the drug loading and internalization of the newly developed targeted nanodrug delivery system (TNDS), rhodamine B (RhoB) was employed as a fluorescent molecular probe within the system. RhoB, a widely recognized fluorescent dye belonging to the xanthene family, exhibits an absorption peak at 546 nm and an emission peak at 567 nm. The primary objective was to examine the loading and internalization processes through fluorescence analysis.<sup>18,19</sup>

In the absorption spectrum, a comparison among the absorbance of mesoporous silica nanoparticles doped with manganese (MSN-Mn) alone, aminopropyltriethoxysilane (APTES) functionalized MSN-Mn, chitosan (CS) coated MSN-Mn (CS@MSN-Mn), and the RhoB-loaded CS@MSN-Mn revealed a modest increase in absorption at 546 nm, indicative of RhoB presence (Figure 4.10.a). To validate the RhoB loading, the emission spectrum was scrutinized. A significant surge in the 567 nm region was observed in the RhoB-loaded nanosystem when compared with other groups, aligning with the

characteristics of the standard RhoB (Figure 4.10.b). With successful confirmation of drug loading, the subsequent focus shifted to analyzing the internalization of the drug-loaded nanoparticles.

Prior to internalization studies, the nanoparticles were conjugated with a target specific peptide substrate *w.r.t.*, EGFR receptor (EGFR@CS@MSN-Mn), rendering the entire system ready to deliver the cargo into cancer cells. This system, loaded with RhoB, was denoted as (EGFR@CS@MSN-Mn-RhoB). Internalization studies were conducted in HeLa cells, known for their overexpression of epidermal growth factor receptor (EGFR) receptors on the cell surface. The TNDS, conjugated with an EGFR-targeting peptide, demonstrated directed delivery toward cancer cells. The internalization process was observed through fluorescence intensity, particularly in the TRITC filter, owing to the fluorescence emitted by RhoB from 1 hour onwards.

The internalization of the developed nanosystem was conclusively affirmed in HeLa cells, with observable fluorescence intensity after 1 hour of introducing the nanosystem. Nanoparticles at concentrations of 50 and 100  $\mu\text{g/mL}$  were employed for internalization studies, both exhibiting emitted fluorescence intensity. This further substantiates the efficiency and effectiveness of the synthesized nanosystem.

#### **4.2.7 Evaluating the pH and GSH responsive release of cargo from the TNDS by surface-enhanced Raman spectroscopy (SERS) modality**

The efficacy of the engineered nanosystem was investigated under pH and glutathione (GSH) responsive conditions. Within the acidic tumor microenvironment, the chitosan coating of the mesoporous silica nanoparticles doped with manganese (MSN-Mn) undergoes swelling, leading to the exposure of MSN-Mn. Subsequently, the elevated GSH concentrations within the tumor milieu induce the degradation of the MSN bonds incorporated with inorganic Mn. The degradation of MSN-Mn induced by GSH operates through a redox reaction involving the Mn-O bonds and intracellular GSH in tumor cells. The breakdown of -Mn-O- in MSN-Mn utilizes two GSH molecules, contributing to the depletion of GSH in tumor cells and disrupting the redox balance within them.<sup>20</sup> This degradation process facilitates the release of drug molecules within the system. The pH and

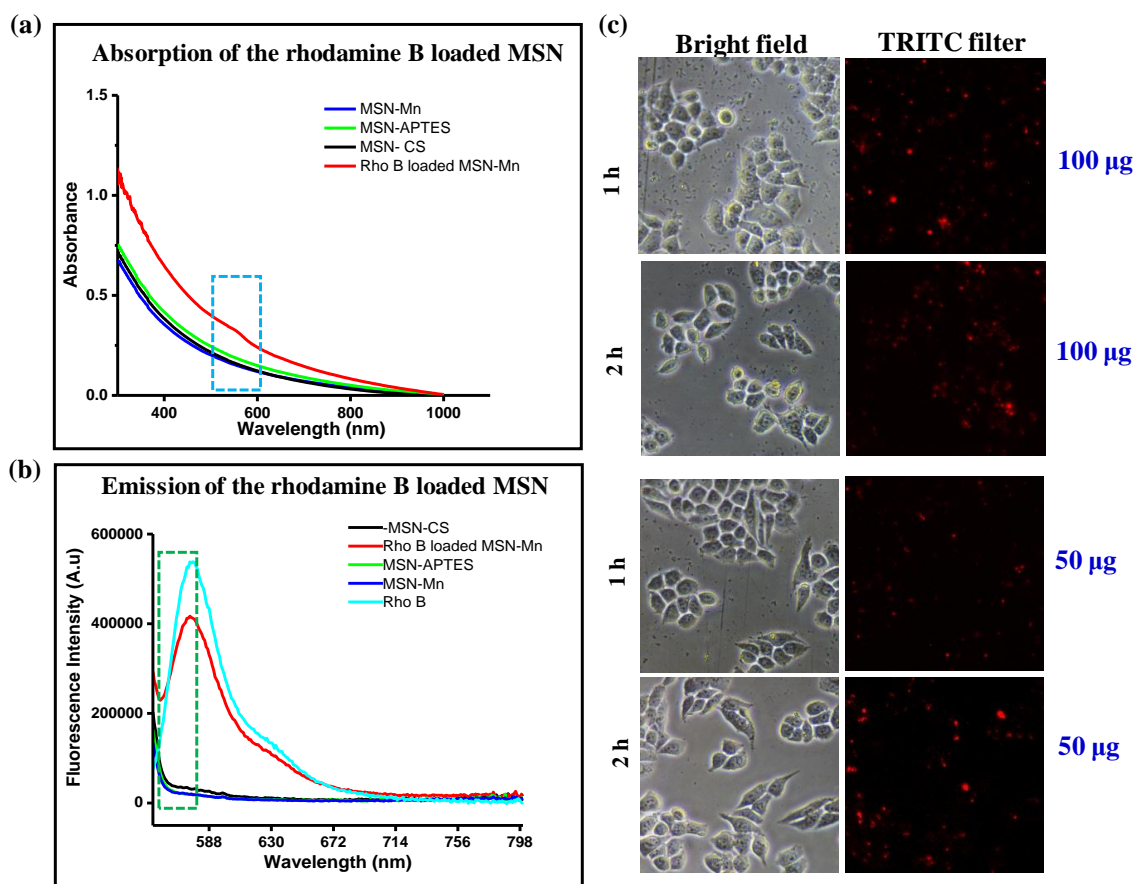


**Figure 4.10.** (a) Absorption spectrum of Rhodamine B loaded CS@MSN-Mn, compared with bare nanosystems without drug (b) emission spectrum comparing the drug loading by the nanosystem, and (c) internalization of the rhodamine B loaded nanosystem (EGFR@CS@MSN-Mn-RhoB) in HeLa cells showing fluorescence, after 1 h of incubation, indicating the internalization.

GSH responsive drug release phenomenon was meticulously monitored using surface-enhanced Raman spectroscopy (SERS) with 633 nm laser of confocal Raman microscope using colloidal gold nanoparticles (AuNPs: 40-45 nm) as SERS substrate, with a focus on the distinctive Raman peaks associated with phaeanthine (PHA) and 2-deoxy D-glucose (2-DG). Initially, the Raman spectrum of bare nanoparticles was acquired, revealing the absence of discernible peaks. However, chitosan-coated MSN-Mn and the peptide-conjugated system exhibited specific peaks at  $254\text{ cm}^{-1}$  and from  $1535\text{--}1582\text{ cm}^{-1}$ . PHA was characterized with the signature Raman peaks at  $990\text{--}1000\text{ cm}^{-1}$  and  $1590\text{ cm}^{-1}$  corresponding to aromatic ring vibrations, while 2-DG possessed with signature peaks at  $1021\text{ cm}^{-1}$  corresponding to C-H in plane bonding and  $1245\text{ cm}^{-1}$  corresponding to bending vibration of  $\text{CH}_2\text{OH}$ .<sup>21</sup>

In the drug co-loaded TNDS (EGFR@CS@MSN-Mn-PHA+2-DG), the characteristic Raman peaks of the two compounds were not visible, indicating proper encapsulation within the chitosan-coated MSN-Mn nanoparticle (Figure 4.11.b). To investigate pH-responsive drug release at varying concentrations of GSH and pH 7.4, compound-specific peaks at 1590, 990, and 1021  $\text{cm}^{-1}$  were observed at higher GSH concentrations compared to lower concentrations. In an acidic pH (pH 5.5), compound-specific peaks were more abundant compared to higher pH (Figure 4.11.c and d), indicating initiation of drug release in an acidic pH and higher GSH concentration, characteristic of the tumor microenvironment.

The time-dependent release of drugs at pH 5.5 and a higher GSH concentration (3 mM) at 37°C revealed compound-specific peaks at 1590, 990, and 1021  $\text{cm}^{-1}$  from half an hour onwards, intensifying after 1 hour of incubation. These results demonstrate the pH and GSH responsive release of cargo from the nanoconstruct, emphasizing that drug release initiates only in the tumor site where conditions favor the release within the tumor microenvironment.

#### 4.2.8 Cytotoxicity evaluation of the TNDS

The cytotoxicity assessment of the nanoconstruct containing co-loaded drugs, EGFR@CS@MSN-Mn-PHA+2-DG, was conducted on HeLa cells using the MTT assay. The obtained results were compared with those of the nanoparticle alone (CS@MSN-Mn & EGFR@CS@MSN-Mn) and the constructs loaded with each individual drug (EGFR@CS@MSN-Mn-PHA & EGFR@CS@MSN-Mn-2-DG) at an equivalent concentration of the synergistic combinative ratio. The findings suggest that the drug co-loaded system, EGFR@CS@MSN-Mn-PHA+2-DG, exhibits superior cytotoxicity against HeLa cells compared to the individual drug-loaded systems as reflected by the percentage of cytotoxicity at 24 hours of incubation. This indicates the predominant synergistic effect of the drug combination within the nanosystem. Consequently, this system has been demonstrated to be a more favorable option than individual drugs loaded at the same concentration. (Figure 4.12)



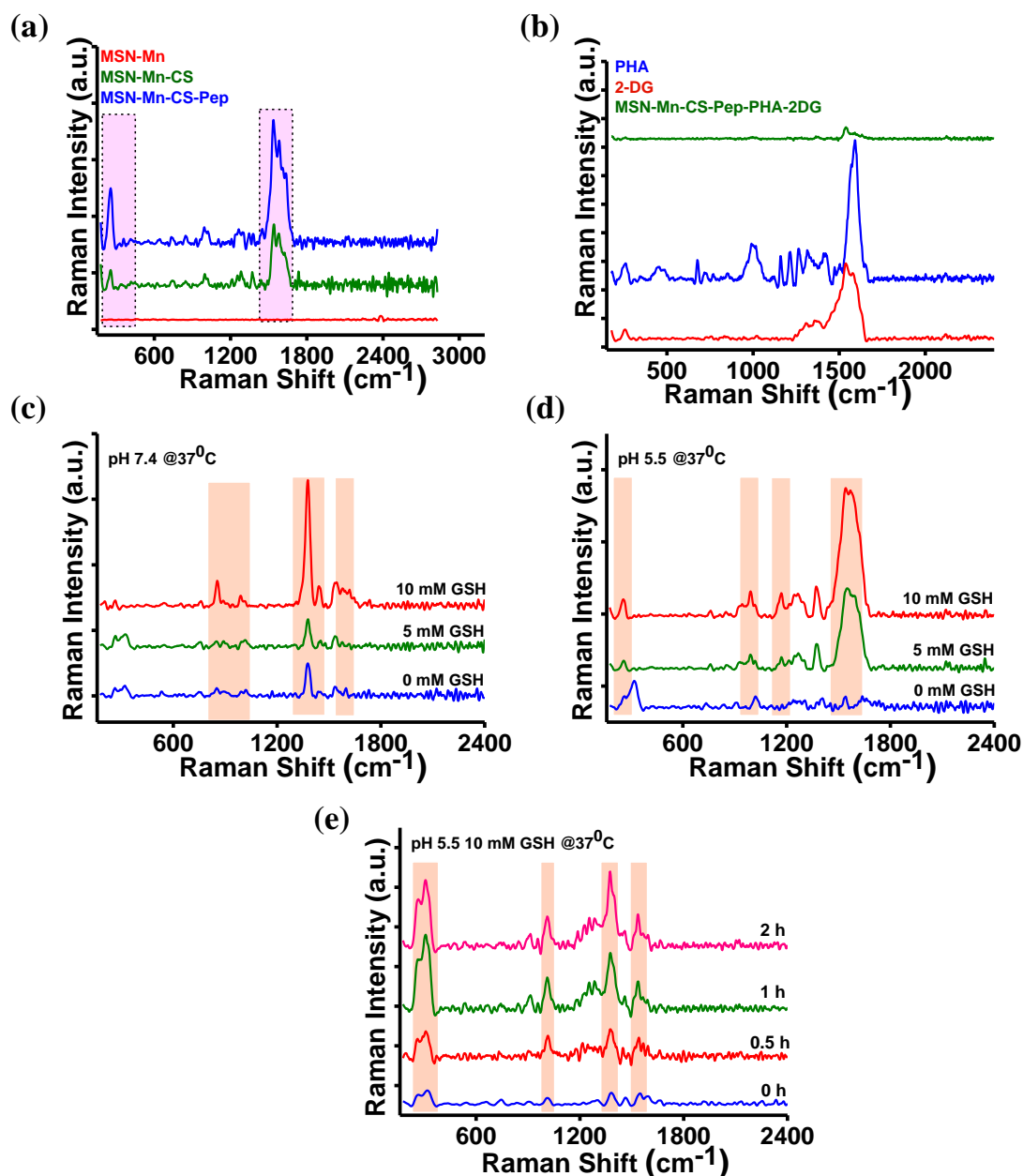


**Figure 4.11.** Drug release monitored by Raman spectroscopy (a) raman intensity graph comparing the bare nanoparticles without drug, (b) Raman peaks of the drugs alone, PHA and 2-DG and it is compared with drug co-loaded nanosystem, The release of drugs were studied at *in vitro* system at (c) pH 7.4 and (d) pH 5.5 at 37 °C at varying concentrations of GSH and (e) At conditions of acidic pH- pH 5.5 and 3 mM GSH concentration, the drug release from the nanosystem was monitored in a time dependent manner upto 2 h.

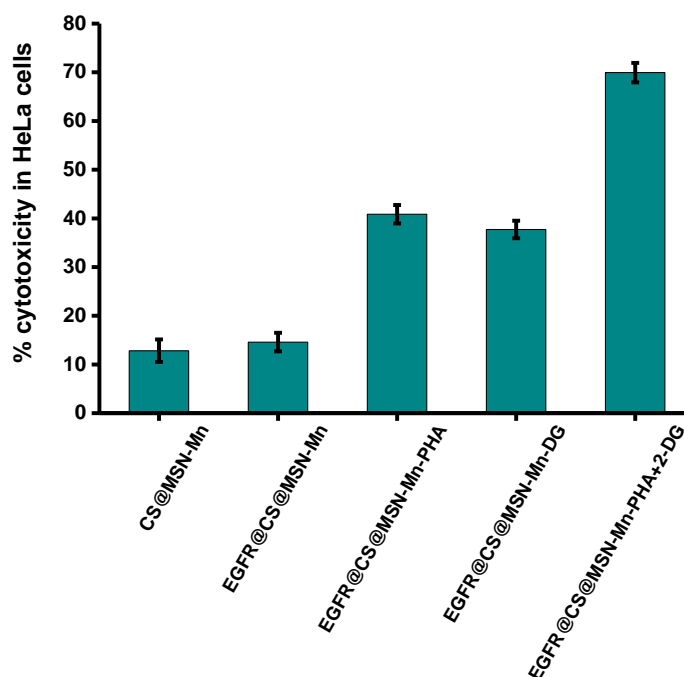


**Figure 4.12.** Cytotoxicity induced by the nanoconstruct in HeLa cells at 24 h incubation

#### 4.2.9 Apoptosis inducing potential of the TNDS

Next, the apoptosis inducing potential of the nanoconstructs were studied by live-dead assay and the nuclear condensation was studied with Hoechst nuclear staining in HeLa cells after 24 h of incubation with the treatment groups. In the live-dead assay, the orange to red colored cells were observed in more number in case of the drug co-loaded system, EGFR@CS@MSN-Mn-PHA+2-DG, with the membrane damage and cell death induced by the action of the compounds, the ethidium bromide dye, entered the cells, and gave orange to red colored fluorescence, while in the case of the individual drug loaded systems, EGFR@CS@MSN-Mn-PHA & EGFR@CS@MSN-Mn-2-DG, the early apoptotic cells were observed, with the presence of light orange colored nuclei in the centre of cells. while the bare systems without drugs did not exhibit any cell death, only the acridine orange dye was absorbed into the cells giving green fluorescence. (Figure 4.13.a).

The nuclear condensation induced by the action of the TNDS was also evaluated with the help of Hoechst nuclear staining. Nuclear condensation and subsequent fragmentation of DNA are key events in the process of apoptosis, the Hoechst dye will specifically bind with the DNA and fluoresce in DAPI filter, the condensed DNA will give a intense fluorescence upon binding with the dye. So, the condensation induced by the

compound was evaluated by identifying intensely fluoresced areas as compared to the other areas. From the results it is clear that, the drug co-loaded system, EGFR@CS@MSN-Mn-PHA+2-DG showed more intensely stained areas indicated more condensed areas, as compared to the individually drug loaded systems, EGFR@CS@MSN-Mn-PHA & EGFR@CS@MSN-Mn-2-DG. This results again proves the efficiency of the constructed nanosystem in targeting and inducing cell death in cervical cancer cell, HeLa specifically. (Figure 4.13.b)

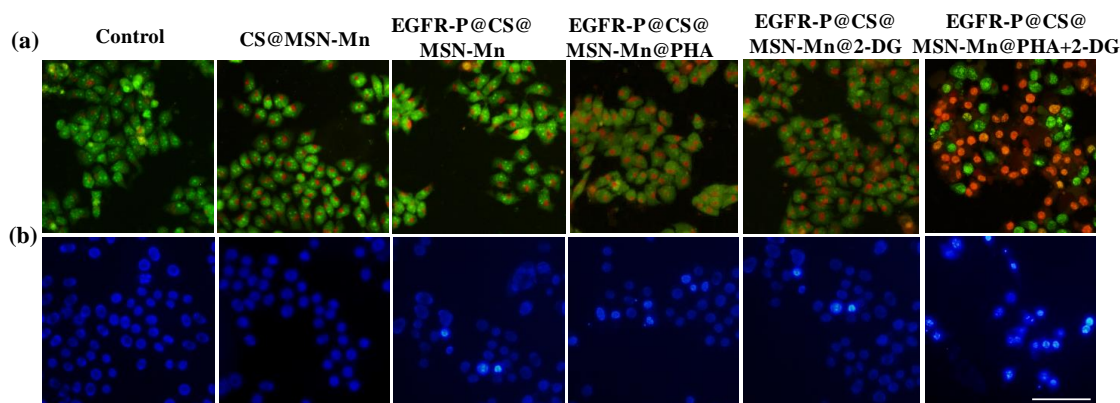


**Figure 4.13** (a) Live- dead assay and (b)Hoechst nuclear staining assay of the nanoparticles in HeLa cells for 24 h incubation. The scale bar indicates 100  $\mu\text{m}$ .

#### 4.2.10 Glycolytic inhibition and alterations induced by the TNDS

2-DG is an anti-cancer drug entity, which can alter the glycolytic pathway and induce the cell death by starving the cancer cells by depriving it with the inhibited production of ATP. 2-DG will be taken up the GLUT transporters of the cancer cells, in a rate greater than that of normal cells, since the energy need of the cancer cells are very high. Inside the cell, the 2-DG will compete with glucose for the active site of hexokinase enzymes and will be converted to 2-DG-6- phosphate. This will get accumulated in the cancer cells and thereby hindering the process of glycolysis, which will further culminate in the ATP depletion process. So, the next strategy employed was to analyse how the nanoconstruct co-loaded with PHA and 2-DG are efficient in exhibiting the traits induced by 2-DG. So, the initial step was to evaluate the changes in ATP generated in cells. From the results, it is clear that the co-loaded system EGFR@CS@MSN-Mn-PHA+2-DG was very efficient in depriving the cancer cell with ATP and finally lead to cell death, the 2-DG loaded EGFR@CS@MSN-Mn-2-DG, was also found to induce a pause on the ATP production as compared to the other treatment and control groups. (Figure 4.14.a. ) Next

step was to analyse the activity of one of the key enzymes involved in glycolysis. It catalyzes the sixth step of glycolysis by converting glyceraldehyde-3-phosphate to 1,3-bisphosphoglycerate, which is crucial step in the energy production of cells. The construct treatment with EGFR@CS@MSN-Mn-PHA+2-DG, lead to a decreased activity of GAPDH, than that of the 2-DG loaded construct (EGFR@CS@MSN-Mn-2-DG). (Figure 4.14.b) Clearly indicating the synergistic action enhances the efficiency of the drug co-loaded construct. Therefore, the system was found to be more efficient in inducing energy starvation by reducing the action of a regulatory enzyme of glycolysis, ie, GAPDH activity, and also, by controlling the ATP production of the cells.

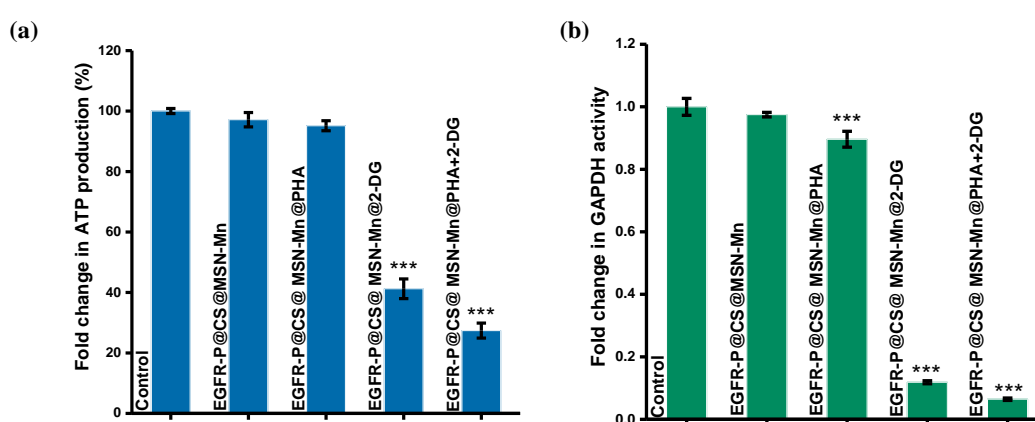


Figure 4.14. (a) Fold change (%) in the ATP production was studied with the nanoparticle treatment in HeLa cells and (b) the fold change in the GAPDH activity induced by the treatment groups.

### 4.3 Conclusion

In conclusion, a synergistic combination of the bisbenzylisoquinoline alkaloid, phaeanthine, in conjunction with the glycolytic inhibitor, 2-DG, demonstrated an enhanced cytotoxicity against HeLa cells at significantly lower concentrations compared to their individual  $IC_{50}$  values. This potent combination was encapsulated within a cancer cell-specific degradable targeted nano delivery system (TNDS), comprised of MSN-Mn coated with chitosan, designed to augment therapeutic efficacy. Furthermore, the system was functionalized with an EGFR-targeted hexapeptide to facilitate cancer cell specific localization, ensuring targeted entry while sparing normal cells. The TNDS degradation mechanism, based on reductive GSH and acidic pH, ensured the selective release of the cargo in the cellular milieu. Upon receptor-mediated endocytosis and exposure to the acidic

intracellular environment, chitosan-induced swelling revealed MSN-Mn nanoparticles co-loaded with the synergistic drugs. The elevated concentration of intratumoral glutathione (GSH) triggered the degradation of chemical bonds in MSN-Mn, leading to the controlled release of Phaeanthine and 2-DG. This orchestrated release mechanism initiated their respective cellular pathways, inducing apoptotic cell death. The TNDS efficacy in promoting apoptosis and glycolytic inhibition was comprehensively assessed through diverse assays. Consequently, this developed targeted nano delivery platform not only amplified the therapeutic potency of Phaeanthine but also facilitated targeted delivery when co-loaded with 2-DG, presenting a promising strategy for advancing cancer treatment modalities.

## **4.4 Experimental Section**

### **4.4.1 Synthesis of MSN-Mn and APTES functionalization of the nanoparticle**

About 473 mg of hexadecyltrimethylammonium bromide (CTAB) was dissolved in 100 mL of Milli-Q water (12 mM) and stirred at 500 rpm until the CTAB was dissolved completely. Followed by the addition of 2.3 mL TEOS along with 105 mg  $\text{MnSO}_4 \cdot 2\text{H}_2\text{O}$  and stirred for a while for the complete dilution. After that, 84 mg of L-Arg-HCl (0.04 %) was immediately added and stirred at 80 °C for 24 h. After the required time, the nanoparticle was collected by centrifugation at 12,000 rpm for 20 minutes. Followed by washing with ethanol three times and centrifuging to remove any traces of CTAB present in it. The CTAB free nanoparticle was dissolved in MilliQ water and 1 mL APTES was added and stirred again for 24 h for the amino functionalization of the nanoparticles.

### **4.4.2 Chitosan coating of the MSN-Mn**

0.6 % w/v solution of chitosan was prepared in 10 % v/v aqueous acetic acid and the pH was adjusted to 6.0 using 1M NaOH solution. The dried MSN-Mn were added to the chitosan solution with the help of magnetic stirring to prepare 0.5 % w/v suspension of MSN-Mn in chitosan solution. The suspension was stirred at room temperature for 48 h. after the specified incubation time, the excess unbound chitosan was removed by centrifugation at 6842 X g for 15 minutes. The washed chitosan coated MSN-Mn was dried in vacuum by keeping it in desiccator and the powder was stored in 4 °C.

#### 4.4.3 Synthesis of EGFR targeting peptide-LARLLT by SPPS

The EGFR receptor-targeting hexapeptide sequence was synthesized using Solid Phase Peptide Synthesis (SPPS) with HMPB-MBHA resin as the solid support. Initially, 200 mg of HMPB-MBHA resin was weighed and allowed to swell in DCM for approximately 30 minutes. After swelling, the DCM was removed, and the resin was washed with DMF (3 x 3 mL). The activation of the last amino acid, Thr, was initiated by weighing 452 mg of Fmoc-Thr (tBu)-OH, activating it under N<sub>2</sub> conditions for 1 hour in an ice bath (10 mL of DCM, 225 µL of DIC). Following activation, the reaction mixture was concentrated in a rotary evaporator, dissolved in 5 mL DMF, and 0.098 mL DIPEA before being added to the swelled resin. The reaction was left in a shaker at 300 rpm for 16-24 hours. Subsequently, the reaction mixture underwent washing with DMF (3 x 3 mL) to eliminate unbound amino acids, and the protective Fmoc group at the amino terminal was cleaved using 20% piperidine for 1 hour. This process was repeated for the other amino acids in the sequence, including Fmoc-Leu-OH (151 mg), Fmoc-D-Arg(Pbf)-OH (276 mg), and Fmoc-Ala-OH (133 mg), to bind the sequence to the solid resin support. After completing the reaction, unreacted reagents were removed with DMF, followed by Dichloromethane (DCM) (3 x 5 mL) and finally by hexane (1 x 3 mL). The peptide was detached from the resin support by treating it with 5% trifluoroacetic acid (TFA) in DCM.<sup>22-24</sup> The resulting peptide was concentrated using a rotary evaporator and precipitated in diethyl ether to obtain a pure form. The structure of the synthesized peptide was confirmed through <sup>1</sup>H NMR and HRMS analysis.

Subsequently, the Fmoc-protected peptide was conjugated to the amino group of the chitosan coating of MSN-Mn via EDC-NHS coupling. EDC (1-ethyl-3-(3-dimethylaminopropyl) carbodiimide) and NHS (N-hydroxysuccinimide) were utilized as coupling agents to activate the carboxyl groups of the peptide and form an amide bond with the amine groups of the chitosan. Equal volumes of 25 mM EDC and NHS were added to the peptide solution dissolved in DMSO + water. The mixture was activated under reduced conditions of N<sub>2</sub> for 1.5 hours at 0 – 4 °C. The activated peptide was then introduced to the nanoparticle suspension (Chitosan-coated MSN-Mn) and stirred for approximately 6 hours at room temperature. The peptide-bound nanoparticles were collected via centrifugation, washed with MilliQ water, and stored at 4 °C.

#### 4.4.4 Rhodamine B conjugation with the peptide sequence

In order to study the targetability of the synthesized peptide, it was conjugated with fluorescent dye, Rhodamine B. First step is the activation of RhoB, weigh 30 mg of RhoB and dissolved in 5 mL of DCM/DMF mixture, to which added 5 equivalent of DIC (111  $\mu$ L) and 5 equivalent of HoBt (96 mg). This mixture was stirred for about 1 h at 0°C under argon purged condition. After the required incubation time, the reaction mixture was concentrated in rotary evaporator and dried in vacuum pump. And the internalization studies were performed with RhoB conjugated peptide.

#### 4.4.5 Drug loading and internalization

The loading of drugs, both individually and in combination, was carried out within the pores of MSN-Mn. The chitosan-coated MSN-Mn was solubilized in PBS with a slightly acidic pH of 5.5. At this acidic pH, chitosan underwent swelling, and after a period, drugs at specific concentrations were introduced and stirred for 24 hours. Following the designated incubation time, the drug-loaded nanoparticles were harvested through centrifugation, washed with MilliQ water, and then stored. To investigate the internalization of the nanoconstruct, the nanoparticles were loaded with RhoB. Targetability and internalization studies were conducted in HeLa cells.

#### 4.4.6 Cytotoxicity and synergy combination evaluation

The cytotoxicity of individual drugs, as well as various combinations, was assessed using the MTT assay. Different ratios of the two drugs were chosen, some falling below and others exceeding the IC<sub>50</sub> values of both compounds. The identification of a synergistic combination was determined through the application of the Chou-Talalay method, utilizing Compusyn software. This involved analyzing cytotoxicity values obtained from experiments involving diverse combinations and ratios of the two drugs.

#### 4.4.7 Apoptotic evaluation

Apoptosis inducing potential of the synthesized nanoconstruct was evaluated with the help of live-dead dual staining assay, utilizing the two fluorescent dyes, acridine orange and ethidium bromide, which can differently label the live and dead cell population differently. The cells were seeded in a 96 well plate at  $8 \times 10^3$  cells /well. After 24 h the

treatment groups were added and again incubated for 24 h. after the specified time, the dyes were added and images were captured in a fluorescent microscope.

Likewise, the nuclear condensation induced by the treatment was studied by Hoechst nuclear staining with hoeschst dye, which will specify binds to DNA and fluorescence was obtained in the DAPI filter.

#### 4.4.8 Glycolytic inhibition analysis

In order to study the role of 2-DG in the cell death induced by the nanoconstruct, the glycolytic intervention was studied by evaluating the expression of GAPDH and the total ATP generated. GAPDH assay was performed with GAPDH Activity Assay Kit (MAK277) from Sigma. And the ATP production was studied with ATP Kit (Invitrogen cat.no. A22066 ). All the procedures were done in accordance with the kit protocol from the manufacturer.

#### 4.5 References

- (1) Mayadev, J. S.; Ke, G.; Mahantshetty, U.; Pereira, M. D.; Tarnawski, R.; Toita, T. Global Challenges of Radiotherapy for the Treatment of Locally Advanced Cervical Cancer. *Int. J. Gynecol. cancer* **2022**, 32, 436–445. <https://doi.org/10.1136/ijgc-2021-003001>.
- (2) Food and Drug administration. *FDA approves pembrolizumab combination for the first-line treatment of cervical cancer*. [https://www.fda.gov/drugs/resources-information-approved-drugs/fda-approves-pembrolizumab-combination-first-line-treatment-cervical-cancer#:~:text=On October 13%2C2021%2C the Food and Drug Administration,PD-L1 %28CPS  \$\geq\$ 1%29%2C as determined by an FDA-appro](https://www.fda.gov/drugs/resources-information-approved-drugs/fda-approves-pembrolizumab-combination-first-line-treatment-cervical-cancer#:~:text=On%20October%2013%2C2021%2C%20the%20Food%20and%20Drug%20Administration,PD-L1%20CPS%20%26gt;=1%29%2C%20as%20determined%20by%20an%20FDA-appro).
- (3) Zhang, D.; Li, J.; Wang, F.; Hu, J.; Wang, S.; Sun, Y. 2-Deoxy-D-Glucose Targeting of Glucose Metabolism in Cancer Cells as a Potential Therapy. *Cancer Lett.* **2014**, 355 (2), 176–183. <https://doi.org/10.1016/j.canlet.2014.09.003>.
- (4) Wang, C.; Zhang, S. Advantages of Nanomedicine in Cancer Therapy : A Review. *ACS Appl. Nano Mater.* **2023**. <https://doi.org/10.1021/acsanm.3c04487>.
- (5) Fan, D.; Cao, Y.; Cao, M.; Wang, Y.; Cao, Y.; Gong, T. Nanomedicine in Cancer



- Therapy. *Signal Transduct. Target. Ther.* **2023**, *8* (293), 1–34. <https://doi.org/10.1038/s41392-023-01536-y>.
- (6) Tang, F.; Li, L.; Chen, D. Mesoporous Silica Nanoparticles: Synthesis, Biocompatibility and Drug Delivery. *Adv. Mater.* **2012**, *24* (12), 1504–1534. <https://doi.org/10.1002/adma.201104763>.
- (7) Joseph, M. M.; Ramya, A. N.; Vijayan, V. M.; Nair, J. B.; Bastian, B. T.; Pillai, R. K.; Therakathinal, S. T.; Maiti, K. K. Targeted Theranostic Nano Vehicle Endorsed with Self-Destruction and Immunostimulatory Features to Circumvent Drug Resistance and Wipe-out Tumor Reinitiating Cancer Stem Cells. *Small* **2020**, *16*, 2003309(1-17).
- (8) Nik Nur Syazni Nik Mohamed Kamal; Aziz, F. A. A.; Tan, W.-N.; Fauzi, A. N.; Lim, V. Mechanistic Actions between Garcinia Atroviridis Essential Oil and D-Deoxy-D-Glucose in Cultured PANC-1 HUMAN Pancreatic Cancer Cells. *Molecules* **2021**, *26* (3518), 1–23.
- (9) Yokoi, T.; Sakamoto, Y.; Terasaki, O.; Kubota, Y.; Okubo, T.; Tatsumi, T. Periodic Arrangement of Silica Nanospheres Assisted by Amino Acids. *J. Am. Chem. Soc.* **2006**, *128* (42), 13664–13665. <https://doi.org/10.1021/ja065071y>.
- (10) Buchman, J. T.; Elmer, W. H.; Ma, C.; Landy, K. M.; White, J. C.; Haynes, C. L. Chitosan-Coated Mesoporous Silica Nanoparticle Treatment of Citrullus Lanatus (Watermelon): Enhanced Fungal Disease Suppression and Modulated Expression of Stress-Related Genes. *ACS Sustain. Chem. Eng.* **2019**, *7* (24), 19649–19659. <https://doi.org/10.1021/acssuschemeng.9b04800>.
- (11) Tian, W.; Huang, M.; Qin, Q.; Chen, Q.; Fang, K. Prognostic Impact of Epidermal Growth Factor Receptor Overexpression in Patients with Cervical Cancer : A Meta-Analysis. *PLoS One* **2016**, *11* (7), 1–13. <https://doi.org/10.1371/journal.pone.0158787>.
- (12) Schrevel, M.; Gorter, A.; Kolkman-uljee, S. M.; Trimbos, J. B. M. Z.; Fleuren, G. J.; Jordanova, E. S. Molecular Mechanisms of Epidermal Growth Factor Receptor Overexpression in Patients with Cervical Cancer. *Mod. Pathol.* **2011**, *24*, 720–728. <https://doi.org/10.1038/modpathol.2010.239>.

- (13) Nicholson, R. I.; Gee, J. M. W.; Harper, M. E. EGFR and Cancer Prognosis. *Eur. J. Cancer* **2001**, *37*, 9–15.
- (14) Soonthornthum, T.; Joste, N.; Lomo, L.; Muller, C.; Rutledge, T.; Verschraegen, C. Epidermal Growth Factor Receptor as a Biomarker for Cervical Cancer. *Ann. Oncol.* **2011**, *22* (10), 2166–2178. <https://doi.org/10.1093/annonc/mdq723>.
- (15) Williams, T. M.; Sable, R.; Singh, S.; Vicente, M. G. H.; Jois, S. D. Peptide Ligands for Targeting the Extracellular Domain of EGFR : Comparison between Linear and Cyclic Peptides. *Chem. Biol. Drug Des.* **2018**, *91*, 605–619. <https://doi.org/10.1111/cbdd.13125>.
- (16) Fontenot, K. R.; Ongarora, B. G.; Leblanc, L. E.; Zhou, Z.; Jois, S. D.; Vicente, M. G. H. Targeting of the Epidermal Growth Factor Receptor with Mesoporphyrin IX-Peptide Conjugates. *J. Porphyr. Phthalocyanines* **2016**, *20*, 1–15. <https://doi.org/10.1142/S1088424616500115>.
- (17) Mayr, J.; Hager, S.; Koblmüller, B.; Klose, M. H. M.; Holste, K.; Fischer, B.; Pelivan, K.; Berger, W.; Heffeter, P.; Kowol, C. R.; Keppler, B. K. EGFR - Targeting Peptide - Coupled Platinum ( IV ) Complexes. *J. Biol. Inorg. Chem.* **2017**, *22*, 591–603. <https://doi.org/10.1007/s00775-017-1450-7>.
- (18) Bar, N.; Chowdhury, P. A Brief Review on Advances in Rhodamine B Based Chromic Materials and Their Prospects. *ACS Appl. Electron. Mater.* **2022**, *4* (8), 3749–3771. <https://doi.org/10.1021/acsaelm.2c00107>.
- (19) Kathiravan, A.; Anbazhagan, V.; Jhonsi, M. A.; Renganathan, R. Fluorescence Quenching of Xanthene Dyes by TiO<sub>2</sub>. *Zeitschrift fur Phys. Chemie* **2007**, *221* (7), 941–948. <https://doi.org/10.1524/zpch.2007.221.7.941>.
- (20) Tang, H.; Li, C.; Zhang, Y.; Zheng, H.; Cheng, Y.; Zhu, J.; Chen, X.; Zhu, Z.; Piao, J. G.; Li, F. Targeted Manganese Doped Silica Nano GSH-Cleaner for Treatment of Liver Cancer by Destroying the Intracellular Redox Homeostasis. *Theranostics* **2020**, *10* (21), 9865–9887. <https://doi.org/10.7150/thno.46771>.
- (21) Suvarna, S.; Das, U.; Sunil, K. C.; Mishra, S.; Sudarshan, M.; Saha, K. Das; Dey, S.; Chakraborty, A.; Narayana, Y. Synthesis of a Novel Glucose Capped Gold Nanoparticle as a Better Theranostic Candidate. *PLoS One* **2017**, *12* (6), 1–15.

- <https://doi.org/10.1371/journal.pone.0178202>.
- (22) Saranya, G.; Joseph, M. M.; Karunakaran, V.; Nair, J. B.; Saritha, V. N.; Veena, V. S.; Sujathan, K.; Ajayaghosh, A.; Maiti, K. K. Enzyme-Driven Switchable Fluorescence-SERS Diagnostic Nanococktail for the Multiplex Detection of Lung Cancer Biomarkers. *ACS Appl. Mater. Interfaces* **2018**, *10* (45), 38807–38818. <https://doi.org/10.1021/acsami.8b15583>.
- (23) Nair, J. B.; Joseph, M. M.; Arya, J. S.; Sreedevi, P.; Sujai, P. T.; Maiti, K. K. Elucidating a Thermoresponsive Multimodal Photo-Chemotherapeutic Nanodelivery Vehicle to Overcome the Barriers of Doxorubicin Therapy. *ACS Appl. Mater. Interfaces* **2020**, *12* (39), 43365–43379. <https://doi.org/10.1021/acsami.0c08762>.
- (24) Arya, J. S.; Joseph, M. M.; Murali, V. P.; Vidyalekshmi, M. S.; Maiti, K. K. Targeted Delivery Polymeric Nanosystem Reinforced by Synergism of Embilin and RPI-1 for Therapeutics of Pancreatic Cancer. *ACS Appl. Nano Mater.* **2022**, *5* (12), 18622–18636. <https://doi.org/10.1021/acsanm.2c04400>.

## ABSTRACT

Name of the Student: Ms. ALISHA VALSAN C. Registration No.: 10BB18A39030  
Faculty of Study: Biological Sciences Year of Submission: 2024  
AcSIR academic center/CSIR Lab: CSIR-National Institute for Interdisciplinary Science and Technology (CSIR-NIIST), TVM, Kerala  
Name of the Supervisor: Dr. K.V. Radhakrishnan Co-supervisor: Dr. Nisha P.  
Title of the thesis: Exploring the anticancer potential of bisbenzylisoquinoline alkaloid-phaeanthine and its targeted delivery through a nanocarrier system

Cancer remains one of the most formidable challenges to human health, exerting a significant global burden with its diverse and complex nature. As conventional cancer therapies often pose limitations, there has been an increasing exploration of alternative treatment strategies, including the utilization of natural products with inherent anti-cancer properties. **Chapter 1** presents a comprehensive review of bisbenzylisoquinoline alkaloids (BBIQ) as a potent anticancer agent, emphasizing their pivotal role in drug development. Many BBIQ alkaloids are currently under clinical trials for various cancer types, making them promising candidates for cancer treatment.

**Chapter 2** includes exploring the anticancer potential of a BBIQ alkaloid isolated from *Cyclea peltata*, Phaeanthine (PHA), which induced mitochondrial mediated apoptosis in cervical cancer cell, HeLa. PHA induced the release of cyt c into cytosol, thereby initiating the caspase cascade. Surface-enhanced Raman scattering (SERS) modality used to evaluate the PHA internalization and DNA fragmentation as a novel strategy. PHA also could downregulate the proliferative signalling mechanism by downregulating Akt pathway. The anti-metastatic and anti-angiogenic potential of PHA was explored in **Chapter 3**. The anti-metastatic studies was carried in a highly metastatic model of TNBC, MDA-MB-231 and PHA induced the reversal of EMT by downregulating the expression of mesenchymal marker proteins, N-cadherin and vimentin. Also it could downregulate the major MMPs and integrins involved in the metastatic cascade. PHA found to pose a challenge for the migration and invasion of cancer cells and also it regulated the key regulators like, HIF-1 $\alpha$ , NF- $\kappa$ B and Akt. The antiangiogenic studies was evaluated in EA.hy926 cell, PHA inhibited the wound closure, migration and invasion at a very low concentration as compared to its IC<sub>50</sub> value. It also reduced the tube forming ability of the endothelial cells by inhibiting the number of nodes and junctions formed even at 2 and 4  $\mu$ M of PHA.

**Chapter 4** delves into the strategies adopted in improving the efficiency and targetability of PHA by incorporating it into a nanodelivery system composed of chitosan coated MSN-Mn. PHA was co-loaded with another drug molecule, 2-deoxy-D-glucose (2-DG) to improve the therapeutic efficacy of the nanoconstruct. The nanoconstruct was conjugated with a EGFR targeting hexapeptide sequence for the targeted delivery of the nanosystem into the EGFR overexpressing cervical cancer cells. the targeted nanodelivery system (TNDS) was effective and it will release the drug molecules only when it is incorporated into tumor cells, where the acidic pH and high GSH level will induce the chitosan swelling and initiate the MSN-Mn degradation, thereby releasing drug molecules. The efficacy of the targeted nanodelivery system (TNDS) was evaluated by its effect in inhibiting the glycolytic pathway and also in inducing apoptosis. Herein, this work sets the stage for delving into the multifaceted landscape of natural product-based drug treatments for cancer. The intricate interplay between nature's pharmacy and cancer therapeutics unfolds as a promising avenue for the advancement of novel treatment modalities with the potential to revolutionize the field of oncology.

## List of Publications

### Emanating from the thesis

1. A. Valsan, M.T. Meenu, V.P. Murali, B. Malgija, A.G. Joseph, P. Nisha, K.V. Radhakrishnan\*, K.K. Maiti\*, Exploration of Phaeanthine: A Bisbenzylisoquinoline Alkaloid Induces Anticancer Effect in Cervical Cancer Cells Involving Mitochondria-Mediated Apoptosis, *ACS Omega*. 8 (2023) 14799–14813.  
<https://doi.org/10.1021/acsomega.3c01023>
2. A. Valsan, Shamjith S, K.V. Radhakrishnan and K.K. Maiti, Development of MSN-based nano delivery system for the combination chemotherapy of phaeanthine & 2-DG against cervical cancer cells. (Manuscript under preparation)
3. A. Valsan, V.P. Murali, K.V. Radhakrishnan and K.K. Maiti, Mechanistic insights into the antimetastatic effects of phaeanthine in triple-negative breast cancer cell, MDA MB 231. (Manuscript under preparation)

### Not related to Thesis

1. Sharathna P., Alisha V., Sasikumar P., Vijayan Ajesh, Ayisha F., Shibi I.G., Sivan V.V., Maiti Kaustabh Kumar, Lankalapalli Ravi S., Radhakrishnan K.V., Mirabijalones S-W, rotenoids from rhizomes of white *Mirabilis jalapa* Linn. and their cell proliferative studies, *Phytochemistry Letters*, Volume 44, 2021, Pages 178-184, ISSN 1874-3900, <https://doi.org/10.1016/j.phytol.2021.06.017>.
2. Omanakuttan, V.K.; Valsan, A.; Hopf, H.; John, J. Palladium Catalyzed Ring-Opening of Diazabicyclic Olefins with 4-Halo-1,3-Dicarbonyl Compounds: Accessing 3(2H)-Furanone-Appended Cyclopentenes. *Organics* **2023**, 4, 70-85.  
<https://doi.org/10.3390/org4010006>
3. C. P. Irfana Jesin, V. R. Padma Priya, R. Kataria, V. Alisha, P. S. Vimalkumar, A. G. Joseph, G. C. Nandi, A One-Pot Tandem Synthesis of Sulfoximine-Based Urea From Organic Acid via Curtius Rearrangement . *ChemistrySelect* 2022, 7, e202202898.  
<https://doi.org/10.1002/slct.202202898>

## Conference Presentations

1. **Alisha Valsan**, Meenu M T, K. V. Radhakrishnan, Kaustabh Kumar Maiti. Phaeanthine, a bisbenzylisoquinoline alkaloid isolated from *Cyclea peltata* induces mitochondria mediated apoptosis in cervical cancer cell line, HeLa. At 5<sup>th</sup> International Conference on Nutraceuticals and Chronic diseases (INCD 2022) held from 7-9 October 2022, at Department of Zoology, University of Delhi. (**Best Oral Presentation award- Doctoral Session**)
2. **Alisha Valsan**, Meenu M T, K. V. Radhakrishnan, Kaustabh Kumar Maiti. Phaeanthine, a bisbenzylisoquinoline alkaloid isolated from *Cyclea peltata* induces mitochondria mediated apoptosis in cervical cancer cell line, HeLa At International Seminar on Plant chemistry, Gene prospecting and Clinical Biology, Organized by Kerala Academy of Sciences at Mar Ivanios College, Thiruvananthapuram, on November 10<sup>th</sup> and 11<sup>th</sup> 2022 (**Best Paper presentation award**)
3. **Alisha Valsan**, Greeshma Gopalan, K. V. Radhakrishnan. Phytochemical evaluation and antiurolithiatic activity of *Rotula aquatica* Lour. An International seminar on Phytochemistry organized by college of Pharmaceutical Sciences, Govt. Medical college, Thiruvananthapuram on 29<sup>th</sup> & 30<sup>th</sup> March 2019. (**Best Poster award**)
4. **Alisha Valsan**, Greeshma Gopalan, K. V. Radhakrishnan. Phytochemical evaluation and antiurolithiatic activity of *Rotula aquatica* Lour. Fourth International conference for Nutraceuticals and Chronic diseases. September 23-25 (INCD 2019) at IIT Guwahati. (Poster)
5. **Alisha Valsan**, Vishnu K Omanakuttan, K.V. Radhakrishnan, Unveiling the phytochemical constituents of *Pandanus odoratissimus* L. from ayurvedic system of medicine, in the International Ayurveda Seminar held during March 12-19, 2021, organised in connection with the Fourth Global Ayurveda Festival- Virtual Conference & Expo. (Poster presentation)

# Exploration of Phaeanthine: A Bisbenzylisoquinoline Alkaloid Induces Anticancer Effect in Cervical Cancer Cells Involving Mitochondria-Mediated Apoptosis

Alisha Valsan, Murugan Thulasi Meenu, Vishnu Priya Murali, Beutline Malgija, Anuja Gracy Joseph, Prakasan Nisha, Kokkuvayil Vasu Radhakrishnan,\* and Kaustabh Kumar Maiti\*



Cite This: *ACS Omega* 2023, 8, 14799–14813



Read Online

ACCESS |



Metrics & More

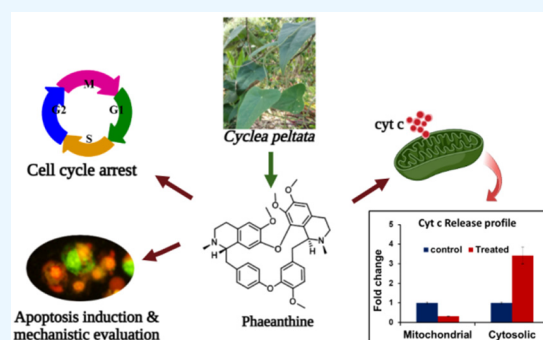


Article Recommendations



Supporting Information

**ABSTRACT:** Natural-product-based pharmacophores possess considerably more structural diversity, attractive physicochemical features, and relatively less toxicity than synthesized drug entities. In this context, our studies on phaeanthine, a bisbenzylisoquinoline alkaloid isolated from the rhizomes of *Cyclea peltata* (Lam) Hook.f & Thoms., showed selective cytotoxicity toward cervical cancer cells (HeLa) with an  $IC_{50}$  of  $8.11 \pm 0.04 \mu\text{M}$ . Subsequent investigation with in silico molecular docking of phaeanthine displayed preferential binding to the antiapoptotic protein Akt as reflected by a docking score of  $-5.023$ . Interestingly, the follow-up in vitro assessment of the compound correlated with mitochondria-mediated apoptosis specifically by downregulating the expression of Akt and p-Akt, including other antiapoptotic proteins Mcl-1, IGF-2, and XIAP. In the complementary in vitro assessment, mitochondrial membrane polarization and dynamics of intercellular cytochrome *c* validated the intrinsic mechanism of the apoptotic phenomenon. To the best of our knowledge, this is the first comprehensive anticancer profiling study of phaeanthine against HeLa cells.



## INTRODUCTION

Cancer is the second leading cause of death globally, with an approximate number of 10 million deaths in 2020 alone, and cervical cancer is the fourth most prevalent cancer worldwide, claiming one life every 2 min. It is also the leading cause of death in women cancer patients in 42 countries.<sup>1</sup> However, cervical cancer can be prevented by an early diagnosis because it takes a long time to become metastatic. Due to this reason, developing more affordable therapeutic entities can greatly help in fighting this disease.

In ancient India, traditional medicines involved ayurvedic formulations developed from plants and herbs. With advancements in technology and knowledge, these formulations have been replaced by more precise and accurate treatment strategies using bioactive molecules. So, natural products and their synthetically modified derivatives occupy a significant role in the current pharmacopeia.

For this work, we have chosen a plant that is frequently used in traditional systems but hitherto unexplored for its anticancer activity. *Cyclea peltata* (Lam) Hook.f & Thoms. belongs to the family Menispermaceae. The plant is known as Rajapata in Sanskrit and is reputedly a well-known drug quoted in most of the ancient ayurvedic classics like Charak Samhita (1000BC), Sushruta Samhita (1000BC), and Ashtangahridaya (6AD). It has been widely used in many ayurvedic formulations like Pushyanuga churna for overall wellness of a women's

reproductive system and for treating many female reproductive disorders.<sup>2,3</sup> The plant enables excess water stagnation with uterine tumors, ovarian cysts, and leucorrhea to decrease.<sup>2</sup> The plant is also traditionally used by tribal communities in India to treat diarrhea, wounds, and certain skin diseases.<sup>4–6</sup> The plant is known to possess many pharmacological properties, including antidiabetic, anticancer potential at an extract level,<sup>7,8</sup> nephroprotective activity,<sup>9</sup> hepatoprotective potential,<sup>10</sup> antibacterial activity,<sup>11,12</sup> gastric antisecretory, and antiulcer property.<sup>13</sup> Additionally, *C. peltata* root extract is effective in neutralizing the venom of *Naja naja*<sup>14</sup> and also shows significant antipyretic and analgesic activity,<sup>15</sup> and the ethyl acetate extract is shown to have anti-inflammatory potential. In Swiss albino rats, the methanolic extract of the plant reduced DAL-induced tumor development.<sup>8</sup> So, based on the available literature, it is clear that the plant possesses antitumor potential, but an in-depth evaluation of the key phytomolecule, phaeanthine, is lacking. Phaeanthine is a type of benzylisoquinoline alkaloid that

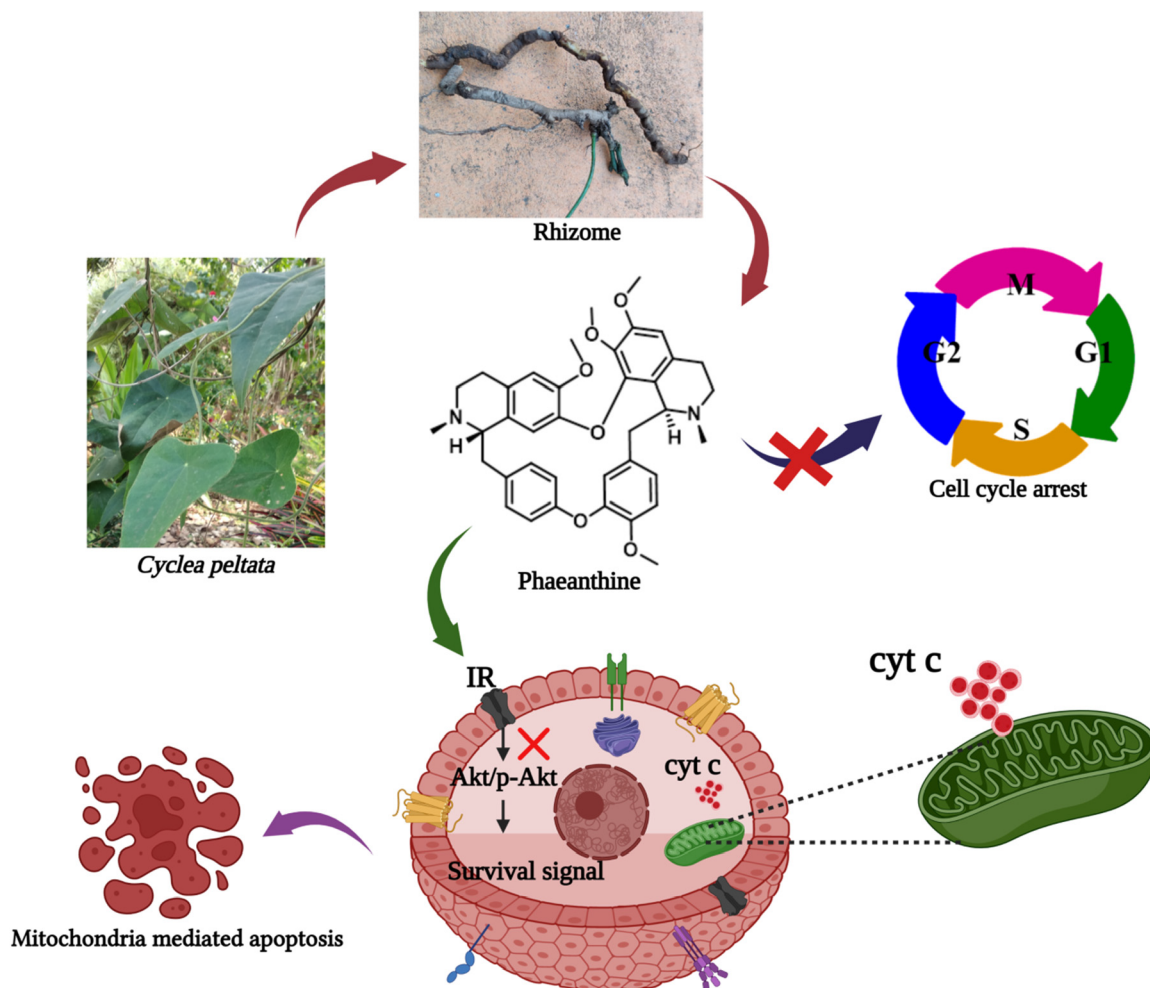
Received: February 15, 2023

Accepted: March 30, 2023

Published: April 10, 2023



## Scheme 1. Phaeanthine Downregulates Akt Signaling Pathway and Induces Mitochondria-Mediated Cell Death



includes narcotics such as codeine and morphine, muscle relaxants such as papaverine and (+)-tubocurarine, antimicrobials such as sanguinarine and berberine, and anticancer agent noscapine, among others. Phaeanthine has not been explored much in terms of its anticancer potential. Some other activities are reported for the compound, such as antiplasmodial activity,<sup>16</sup> antiprotozoal activity,<sup>17</sup> and acetylcholinesterase inhibitory potential.<sup>18</sup>

Considering the reports, we investigated the effect of phytomolecules isolated from the plant on anticancer profiling with a focus on the most common cancer of the female reproductive system, i.e., cervical cancer. We isolated the major phytomolecules from *C. peltata* rhizomes and examined the anticancer potential in the present investigation. The acetone and ethanolic extract of the plant yielded mainly three compounds, phaeanthine, cycleanine, and *N*-methylcorydaldine. Initially, all three compounds were screened for antiproliferative potential against cervical cancer cells, HeLa, among which phaeanthine was found to have appealing cytotoxicity features. In silico examination of phaeanthine demonstrated an excellent binding affinity with the proliferative protein Akt, compared to the other eight protein codes. Subsequently, the anticancer potential of phaeanthine has been evaluated with downstream in vitro assays to assess its ability to induce apoptosis, including FITC annexin V, caspase assays, and DNA fragmentation. Furthermore, clonogenic assay

and changes in mitochondrial membrane potential were also performed. As a novel insight, surface-enhanced Raman spectroscopy (SERS) was employed to scrutinize DNA fragmentation by identifying the signature Raman fingerprint of the phosphate backbone. Moreover, phaeanthine exhibited intrinsic mitochondria-mediated apoptosis and resulted in the downregulation of the expression of proliferative protein Akt and its phosphorylated form, p-Akt, and other antiapoptotic proteins Mcl-1 and XIAP (Scheme 1). To the best of our knowledge, this is the first report on the anticancer potential of phaeanthine against cervical cancer cells; HeLa cells and their apoptotic induction through mitochondria-mediated intrinsic pathway were also established.

## RESULTS AND DISCUSSION

**Extraction, Isolation, and Characterization of Phytomolecules from *Cyclea peltata* Rhizomes.** The collected *C. peltata* rhizome was subjected to sequential extraction by hexane, acetone, ethanol, and water (Figure S1). Since the acetone and ethanol extract responded to Dragendorff's test, we adopted a detailed acid–base extraction procedure. We isolated 3 compounds from the plant extract, which included 2 DBBI (dibenzylisoquinoline) alkaloids. The compounds were identified as phaeanthine (80 mg, 0.004% yield), cycleanine (50 mg, 0.0025% yield), and *N*-methylcorydaldine (30 mg, 0.0015% yield) (Figure 1) based on extensive characterization



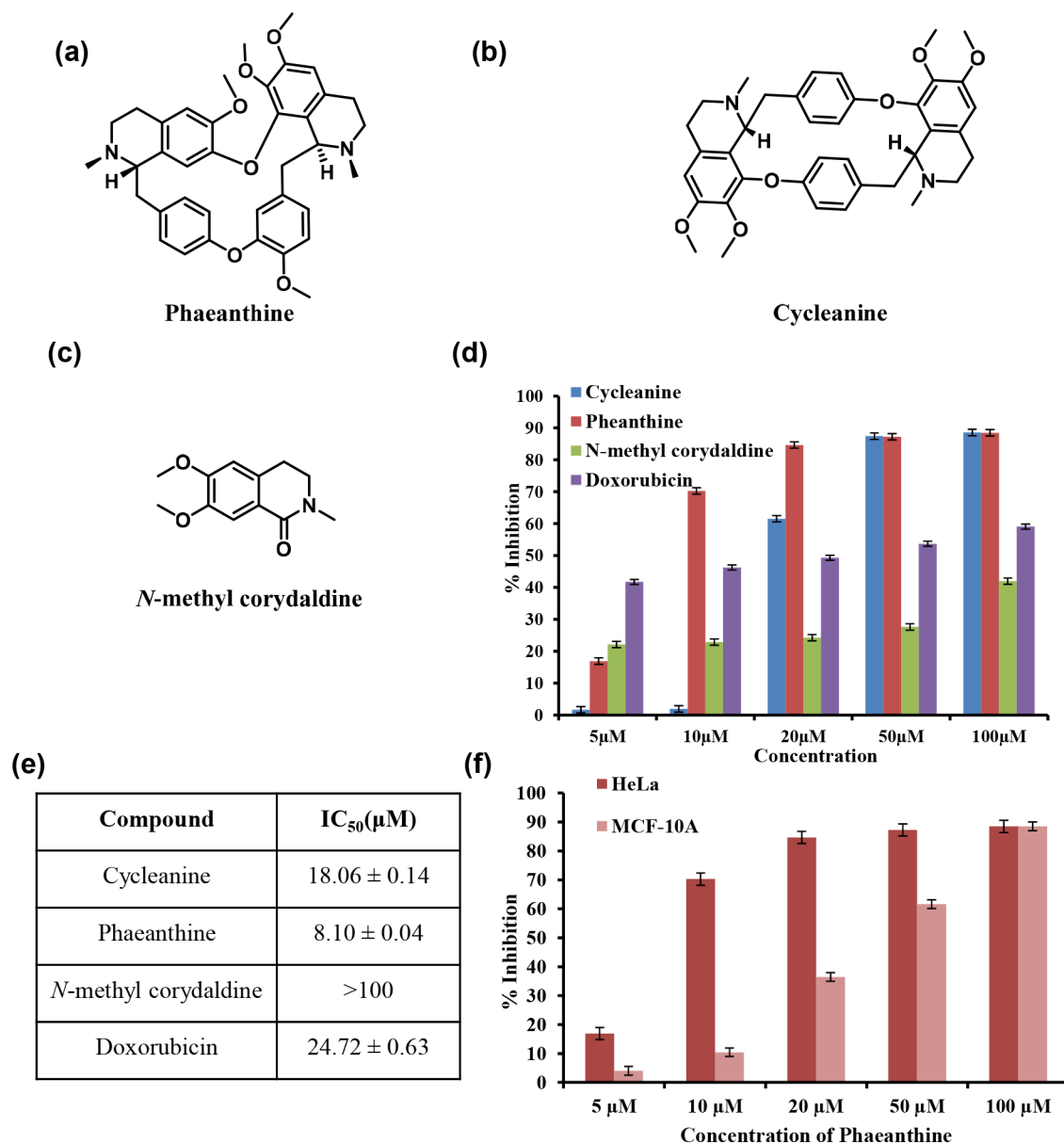


**Figure 1.** Chemical structure of the isolated compounds from *Cyclea peltata* rhizome: (a) phaeanthine, (b) cycleanine, (c) *N*-methylcorydaldine. (d) Percent inhibition on proliferation of the compounds in HeLa cells, (e) their IC<sub>50</sub> (μM) in HeLa cells for 24 h incubation, and (f) comparative % of inhibition of phaeanthine on HeLa cells and MCF-10A (nontumorigenic cell) cells for 24 h of incubation.

using the NMR technique (<sup>1</sup>H, <sup>13</sup>C, 2D) and HRMS analysis, which were in good agreement with the reported data<sup>17,19,20</sup> (Figures S2–S22).

**Primary Cytotoxicity Screening of Isolated Phytomolecules.** Preliminary selection based on the cytotoxicity of the three isolated compounds was evaluated by MTT (3-[4,5-dimethylthiazol-2-yl]-2,5-diphenyltetrazolium) assay in HeLa cells. Among the three compounds, phaeanthine showed a promising antiproliferative potential with an IC<sub>50</sub> value of 8.11 ± 0.04 μM at 24 h, whereas cycleanine showed an IC<sub>50</sub> value of 18.06 ± 0.14 μM. Although, *N*-methylcorydaldine did not show much toxicity even when concentration was increased to 100 μM (Figure 1d,e). Since phaeanthine exhibited pronounced inhibitory potential against HeLa cells at a lower concentration, we checked its toxicity against a normal nontumorigenic breast epithelial cell line, MCF-10A. To our pleasant surprise, phaeanthine did not show toxicity up to a moderate

concentration, and its IC<sub>50</sub> was found to be 36.33 ± 0.14 μM; thus the compound is not toxic up to a higher concentration. (Figure 1f). Therefore, we extended the downstream in vitro studies with phaeanthine as a potential phytomolecule.

**Computational Screening of Phaeanthine.** Next, we extended the screening strategy by employing computational tools where molecular docking was conducted with the selected proteins (Akt, MMP-2, mTOR, Survivin, caspase-9, caspase-8, p53, PARP, and STAT-3) involved in the apoptotic mechanism. Molecular docking studies among these proteins exhibited good binding affinity of phaeanthine with the target Akt, possessing a docking score of −5.023 compared to other target proteins (Table S2 and Figures S24–S32). Hence, Akt was chosen for further molecular dynamic simulation studies. In the binding interaction between Akt and phaeanthine, we observed that Thr162 donated hydrogen atoms to the ligand, leading to the formation of a H-bond with a distance of 2.31 Å. Apart from

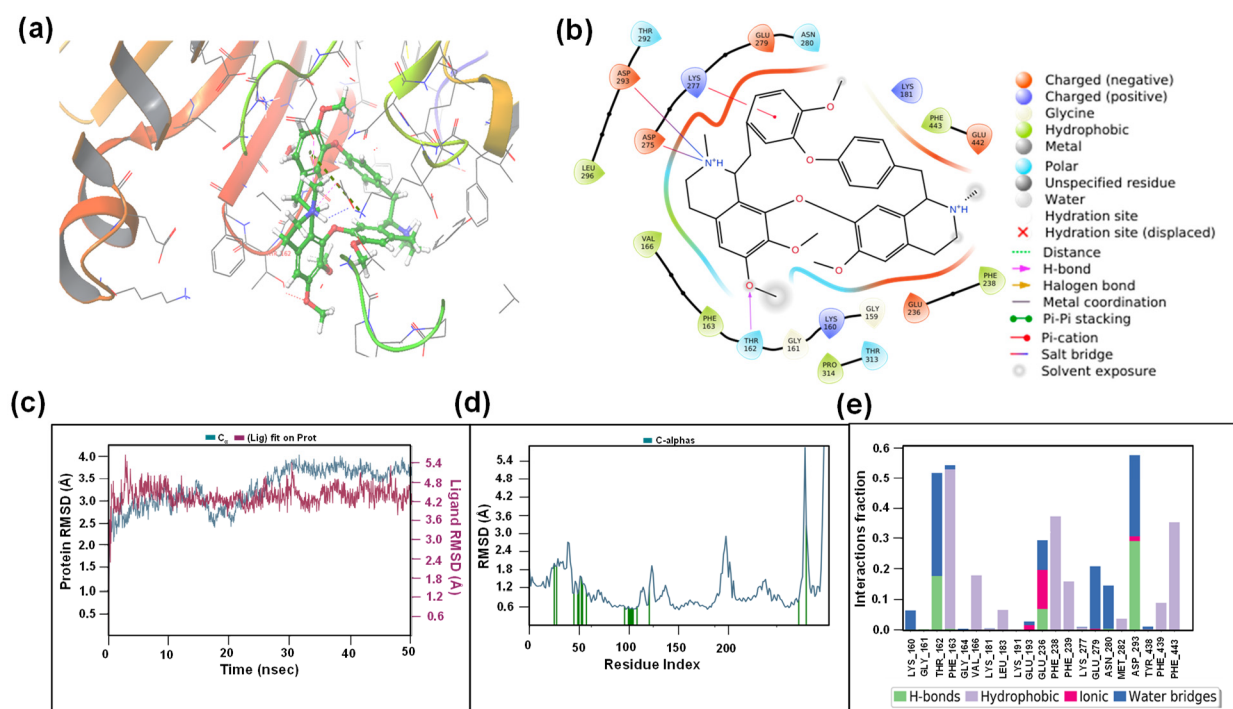


**Figure 2.** (a,b) Interaction of phaeanthine with Akt; results from MD simulation. (c) RMSD plot of Akt and phaeanthine complex; (d) RMSF plot of the protein. The green vertical line shows the residues interacting with the ligand. (e) Interactions between Akt and phaeanthine over the 50 ns simulation time.

hydrogen bonds,  $\pi$ -cation interaction and salt bridges were also observed, which may contribute to the complex's stability. The intermolecular  $\pi$ -cation interaction was formed by the interaction of a cation from Lys277 with the polarizable  $\pi$  electron cloud of an aromatic ring in phaeanthine (Figure 2a,b).

**Molecular Dynamics Simulation of Akt–Phaeanthine Complex.** To assess the stability and conformational flexibility of the Akt–phaeanthine complex, molecular dynamics simulation was performed using Desmond (academic version) of Schrödinger Suite for 50 ns under the OPLS-2005 force field. The root mean square deviation (RMSD), which gives insights into the conformational stability of the complex, was calculated throughout the 50 ns simulation time. The RMSD plot shows that the protein and protein–ligand complexes were stable until the end of the trajectory (Figure 2c). Similarly, the root mean square fluctuation (RMSF) parameter to assess flexibility was also calculated, in which minor fluctuations of the residues were found, and the residues at the N-terminal region were more fluctuated (Figure 2d). In order to further decipher the changes in the position of the ligand atoms, the ligand RMSF was calculated, which showed minor fluctuations in ligand atoms. The H-bond interactions formed by the residue Thr162 were also confirmed by protein–ligand contacts in the MD simulation (Figure 2e). The  $\pi$ -cation hydrophobic contacts which formed over the simulation time with the residues Phe163, Val166, Phe238, Phe239, Phe439, and Phe443 could also contribute to its stability. Ionic interactions, which do not involve a hydrogen bond, were also observed with the residues Glu193, Glu236, and Asp293. Apart from these interactions, water bridges involving hydrogen-bonded interactions mediated by water molecules were observed. Overall, this suggests the stability of the Akt–phaeanthine complex with the collaborative role of hydrogen bonding, hydrophobic interactions, and salt bridges.

**Apoptotic Evaluation of Phaeanthine.** First we employed a live–dead dual staining assay to differentiate the apoptotic cells where the fluorescent dyes (acridine orange and ethidium bromide) would label the viable and dead cells differently. HeLa cells were treated with phaeanthine, which showed redder to orange-colored cells than the control (green fluorescence) in a concentration-dependent manner (Figure 3a). Next, APOP staining of cells was carried out to distinguish the apoptotic cells from healthy ones, where the dead cells resembled a pink color due to membrane damage by the treatment of phaeanthine. At the same time, the untreated control did not show pink-colored cells (Figure 3b).

To corroborate the apoptosis-driven cell death by phaeanthine, we also investigated the FITC annexin V apoptosis assay. HeLa cells were treated with two different concentrations of phaeanthine (6 and 15  $\mu$ M), where the percentage of apoptotic cells showed a considerable hike in the treated cells compared to that of the control. As shown in Figure 3c, the percentage of apoptotic cells in the untreated control was 11.6%, which increased to 65.5% in cells treated with 6  $\mu$ M and 93.4% in 15  $\mu$ M phaeanthine-treated cells (Figure 3c).

**Evaluation of Caspase-Mediated Apoptosis.** Cysteine–aspartic proteases or caspases regulate the cell death pathways involving mitochondria. We have studied the expression of caspase-3, -8, and -9 by fluorometric assays. The expression of executioner caspase-3 upon treatment with phaeanthine (15  $\mu$ M) showed a hike of 2.6-fold fluorescence intensity compared to that of untreated cells. Likewise, in the case of caspase-9, cells treated with a higher concentration of compound (15  $\mu$ M) showed a similar pattern with approximately 2.3-fold increases in the fluorescence intensity compared to that with the control. But in case of caspase-8, a notable decrease in the fluorescence intensity was observed in the treated cells. At a 6  $\mu$ M concentration of phaeanthine, there was a 2.25-fold decrease,

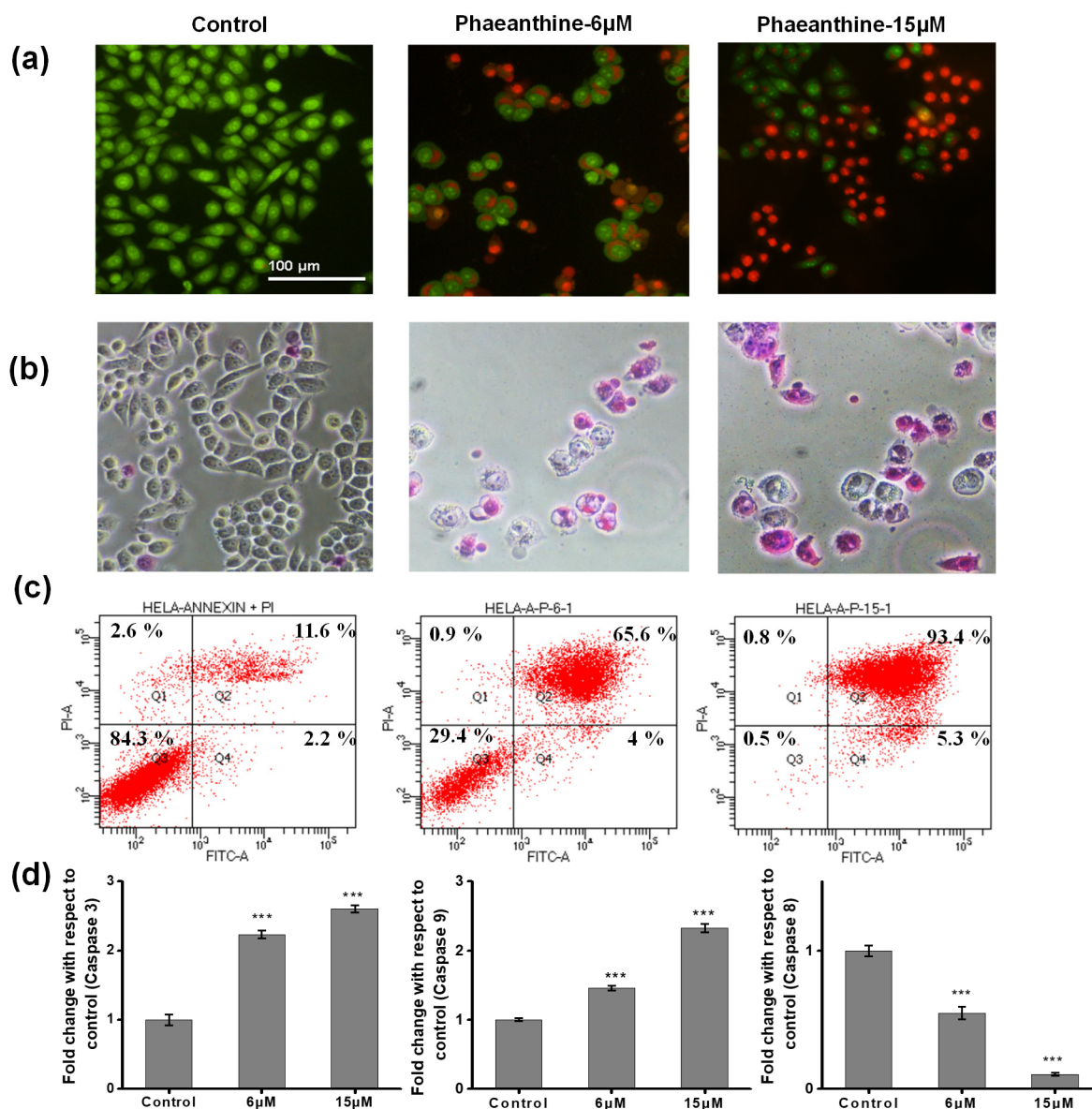


**Figure 3.** Phaeanthine-induced apoptosis in HeLa cells. HeLa cells were treated/untreated with 6 and 15  $\mu$ M concentrations for 24 h to perform (a) acridine orange–ethidium bromide dual staining assay, (b) APOP staining assay, (c) Annexin V apoptosis assay, (d) caspase fluorometric assay. The assays were carried out in triplicates, and the data are expressed as mean  $\pm$  SD; \*\*\* $p$  < 0.001, \* $p$  < 0.05 were considered to be significant as compared to the control.

and at a higher (15  $\mu$ M) concentration, a decrease in the fluorescence intensity (8.72-fold) compared to that of the control was observed (Figure 3d). The upregulation of caspase-9 and downregulation of caspase-8 substantiated the intrinsic or mitochondria-mediated apoptosis involved in the treatment of phaeanthine in HeLa cells.

**Assessment of Mitochondrial Membrane Potential Induced by Phaeanthine.** A decrease in the mitochondrial membrane potential (MMP) could be considered a marker event in the early stages of apoptosis.<sup>21</sup> JC-1 is a cationic dye that can form aggregates at a high membrane potential in the mitochondrial matrix. This polymerization will yield red emission. But in mitochondrial membrane-compromised cells or an apoptotic cell, the MMP is very low. At this low MMP, JC-1 cannot form an aggregate and will be retained as a monomer and yield green fluorescence. So, this aggregate/monomer ratio can be used as a parameter to study apoptosis in cancer cells. The

apoptotic cells will show a lower red/green or aggregate/monomer ratio. HeLa cells were treated with 5 and 8  $\mu$ M phaeanthine for 24 h of incubation, which showed a higher green fluorescence than red, indicating the JC-1 was retained as a monomer (Figure S33). The aggregate/monomer ratio is reduced compared to that of the untreated cells. The untreated cells showed an aggregate/monomer ratio of  $2.6034 \pm 0.30$ . In contrast, treated cells at 5  $\mu$ M concentration were  $0.2830 \pm 0.03$ , and at 8  $\mu$ M, phaeanthine treated cells have  $0.2013 \pm 0.05$  ratios (Figure 4a). The decrease in the aggregate/monomer ratio indicates the JC-1 aggregate formation is hindered upon the treatment by the depolymerization of membrane potential.

**Evaluation of Cytochrome *c* (cyt *c*) Dynamics by Phaeanthine.** The extent of the intrinsic apoptotic pathway was well understood by the dynamics of cyt *c*, which triggers the mitochondria-dependent apoptosis pathways. The cyt *c* is located in normal healthy cells' inner mitochondrial membrane

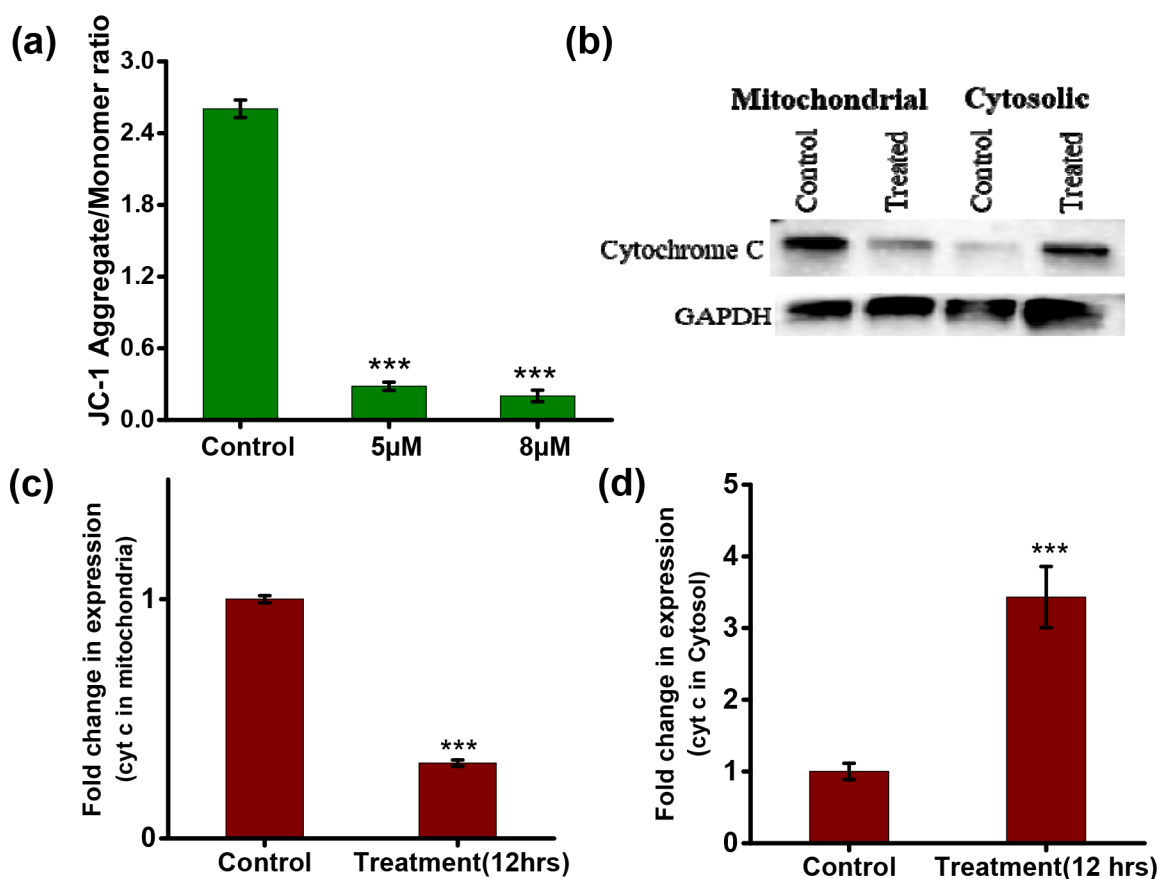


**Figure 4.** (a) Mitochondrial membrane potential evaluated by JC-1 dye: JC-1 aggregate/monomer ratio decreases with treatment at concentrations of 5 and 8  $\mu$ M phaeanthine. (b) Blot of mitochondrial and cytosolic cytochrome *c*. (c) Expression of mitochondrial cytochrome *c* in control versus phaeanthine-treated cells. (d) Expression of cytosolic cytochrome *c* in control versus phaeanthine-treated cells. The assays were carried out in triplicates, and the data are expressed as mean  $\pm$  SD; \*\*\* $p$  < 0.001, \* $p$  < 0.05 were considered significant compared to the control.

space. Upon receiving apoptotic stimuli, the outer membrane gets permeabilized and releases cyt *c* to the cytosol. So, the release of cyt *c* is a noticeable change during apoptosis, or it represents mitochondria's involvement in apoptotic cell death.<sup>22</sup> We checked the expression of mitochondrial and cytosolic cyt *c* and compared their expression between phaeanthine-treated and untreated cells (Figure 4b). The results depicted the release of cyt *c* into the cytosol from mitochondria since the treated group showed an upregulation in cytosolic cyt *c* (Figure 4d). Also, downregulated mitochondrial cytochrome *c* protein expression was compared to that of the control group (Figure 4c).

**Phaeanthine-Induced DNA Condensation and DNA Fragmentation.** DNA condensation and subsequent fragmentation is a hallmark of apoptosis. Therefore, the condensation pattern of DNA was studied using a Hoechst nuclear staining assay. The nuclei of the untreated cells appeared round and uniformly stained, while the phaeanthine-treated cells showed intensely stained areas because of DNA condensation (Figure 5a).

We further carried out agarose gel electrophoresis to confirm the DNA fragmentation pattern. The isolated DNA demonstrated a laddering pattern in the cells treated with a higher concentration of phaeanthine (Figure 5b).

**Cellular Internalization and DNA Fragmentation by SERS Modality.** For further insights, we investigated Raman fingerprints of phaeanthine through surface-enhanced Raman scattering (SERS) spectral analysis (Figure 5d). Cellular

internalization of phaeanthine was tracked in a time-dependent manner in HeLa cells. Cells were treated with phaeanthine (6  $\mu$ M) to monitor intracellular Raman fingerprints of phaeanthine with the 633 nm laser of a confocal Raman microscope using colloidal gold nanoparticles (AuNPs: 40–45 nm) as the SERS substrate. After 1 h, we observed the signature peaks of phaeanthine at 1000 and 1590  $\text{cm}^{-1}$  (aromatic ring vibrations),<sup>23,24</sup> 1160  $\text{cm}^{-1}$ , and 1212  $\text{cm}^{-1}$  (trisubstituted amine C–N stretch).<sup>25</sup> Similarly, distinct peak patterns were observed at around 2 h onward until 4 h, but after 8 h, the phaeanthine peaks decreased substantially, which may be due to its cellular metabolic decomposition.

Next, the isolated DNA from the phaeanthine-treated and the untreated cells was mixed with AuNPs, and SERS fingerprints were assessed. We identified the signature Raman peaks associated with various molecular vibrations from DNA, which were perfectly aligned with the reported literature.<sup>26,27</sup> The DNA signature peaks from 746 to 800  $\text{cm}^{-1}$ , including the ring breathing mode of pyrimidines, phosphodiester bond vibrations, especially –O–P–O stretching, as well as deoxyribose and phosphodiester bond peaks at 870 to 900  $\text{cm}^{-1}$  and aromatic ring vibrations at 1002  $\text{cm}^{-1}$  were found to be less intensified in the treated samples (Figure 5c). A similar effect was observed for 1177/1180  $\text{cm}^{-1}$  cytosine/guanine and 1303  $\text{cm}^{-1}$  adenine, cytosine peaks, and DNA mode vibrations peaks at 1573–1577  $\text{cm}^{-1}$ . We could observe enhanced peak intensity at 1620–1660  $\text{cm}^{-1}$  in higher dosage (15  $\mu$ M) of phaeanthine-treated cellular DNA, indicating the base-pairing interactions and base-stacking

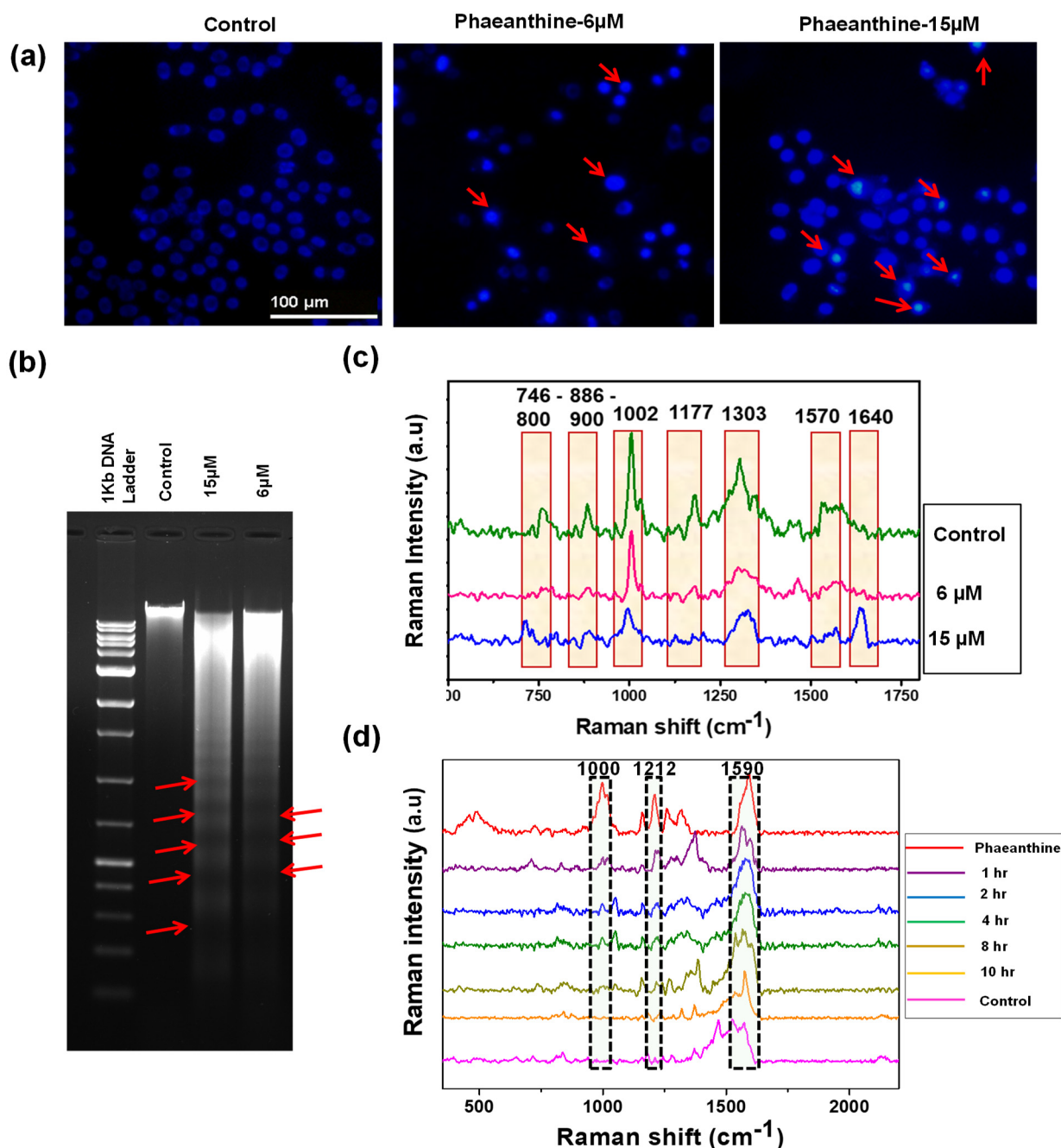


**Figure 5.** Nuclear fragmentation and condensation induced by phaeanthine: (a) Hoechst nuclear staining, (b) DNA laddering by AGE, (c) SERS analysis of DNA fragmentation, and (d) internalization of phaeanthine ( $6 \mu\text{M}$ ) into cells monitored using SERS.

effects due to H-bond formation. This may be due to DNA fragmentation associated with the base-pairing regions, leading to the generation of the particular SERS peaks in the treated sample. Thus, the SERS analysis reconfirms the apoptosis-associated DNA fragmentation in the phaeanthine treated samples.

**Inhibition of Clonogenic Potential by Phaeanthine in HeLa Cells.** Next, we investigated the inhibitory potential of phaeanthine in the colony-forming capacity of HeLa cells. The compound at  $0.5$  and  $1 \mu\text{M}$  effectively inhibited the clonogenic potential of HeLa cells. The survival fraction was substantially reduced in  $1 \mu\text{M}$  phaeanthine-treated colonies compared to that in the control colonies (Figure 6b). A very high clonogenic inhibitory potential at a significantly lower concentration ( $1$

$\mu\text{M}$ ) reflects the inhibitory ability of the compound in a dose-dependent manner (Figure 6a).

**Induction of Cell Cycle Arrest by Phaeanthine.** Flow cytometric analysis to investigate the cell cycle distribution was performed to further explore the mechanism of action of phaeanthine. Malignancies are characterized by a dysregulation of the cell cycle, which allows them to proliferate uncontrollably. Many clinically used drugs are known to induce cell cycle arrest, thereby controlling tumor growth.<sup>28</sup> We have monitored the effect of phaeanthine in regulating the cell cycle pattern upon treatment with  $6$  and  $15 \mu\text{M}$  concentrations for  $24$  h of incubation. The percentage of cells at the G1 phase decreased to  $51$  and  $41.2\%$ , respectively, compared to that of the untreated control ( $59.1\%$ ). The treated cells also showed an upsurge in the

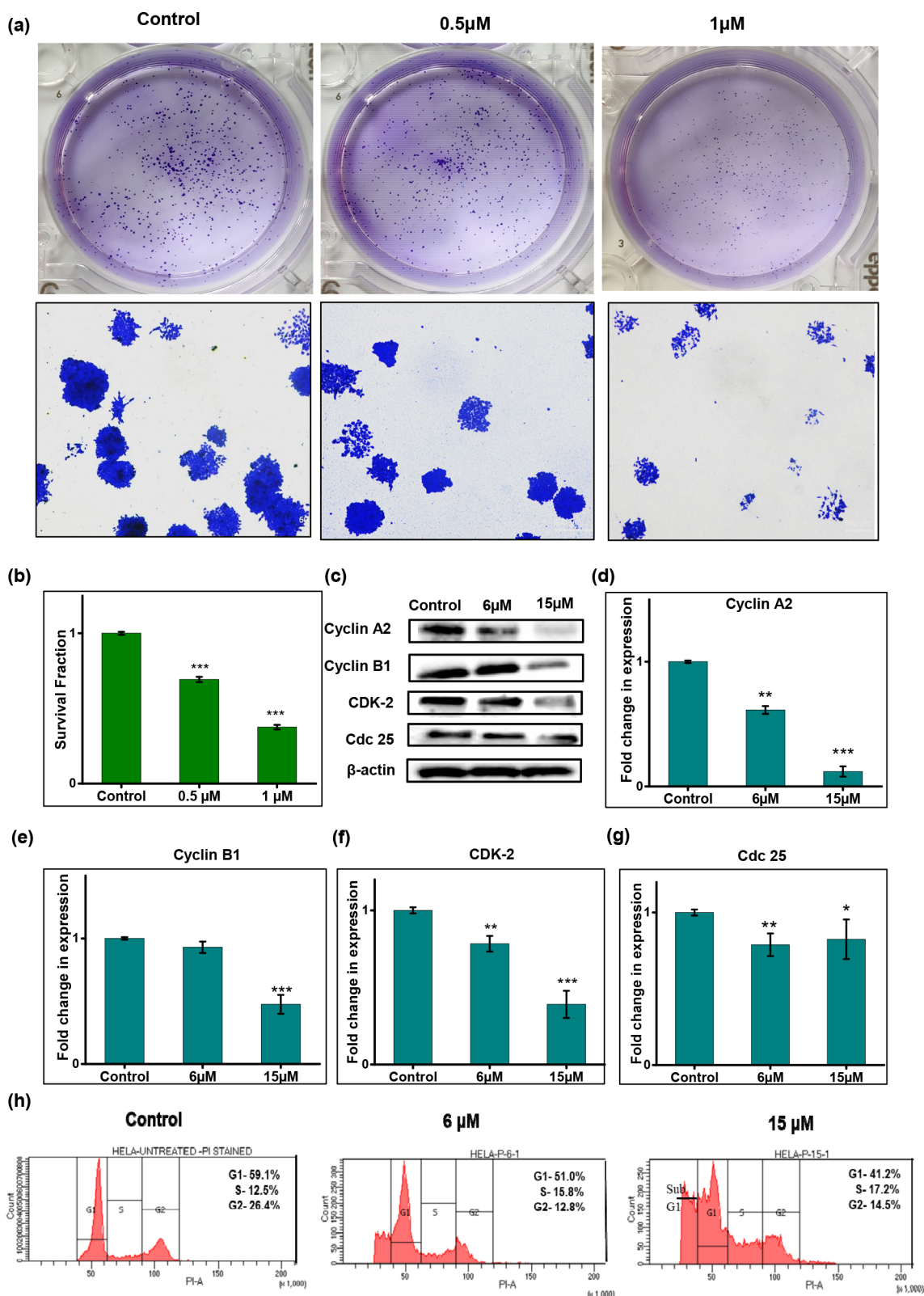


**Figure 6.** (a) Colony formation assay. (b) Survival fraction of the colonies. (c) Blot of cell cycle proteins. Expression of (d) cyclin A2, (e) cyclin B1, (f) CDK-2, and (g) Cdc 25. (h) Cell cycle assay: control denotes the untreated cells. The assays were carried out in triplicates, and the data are expressed as mean  $\pm$  SD; \*\*\* $p < 0.001$ , \*\* $p < 0.01$ , \* $p < 0.05$  were considered to be significant as compared to the control. No asterisk (\*) represents a nonsignificant  $p$  value.

cells at the sub-G1 phase in a dose-dependent manner, indicating the apoptotic population of cells upon treatment (Figure 6h). Further, we checked the expression of some of the

key regulator proteins involved in the cell cycle regulation. Western blot analysis of various proteins such as cyclin A2, cyclin B1, CDK 2, and Cdc25c was also carried out (Figure 6c).

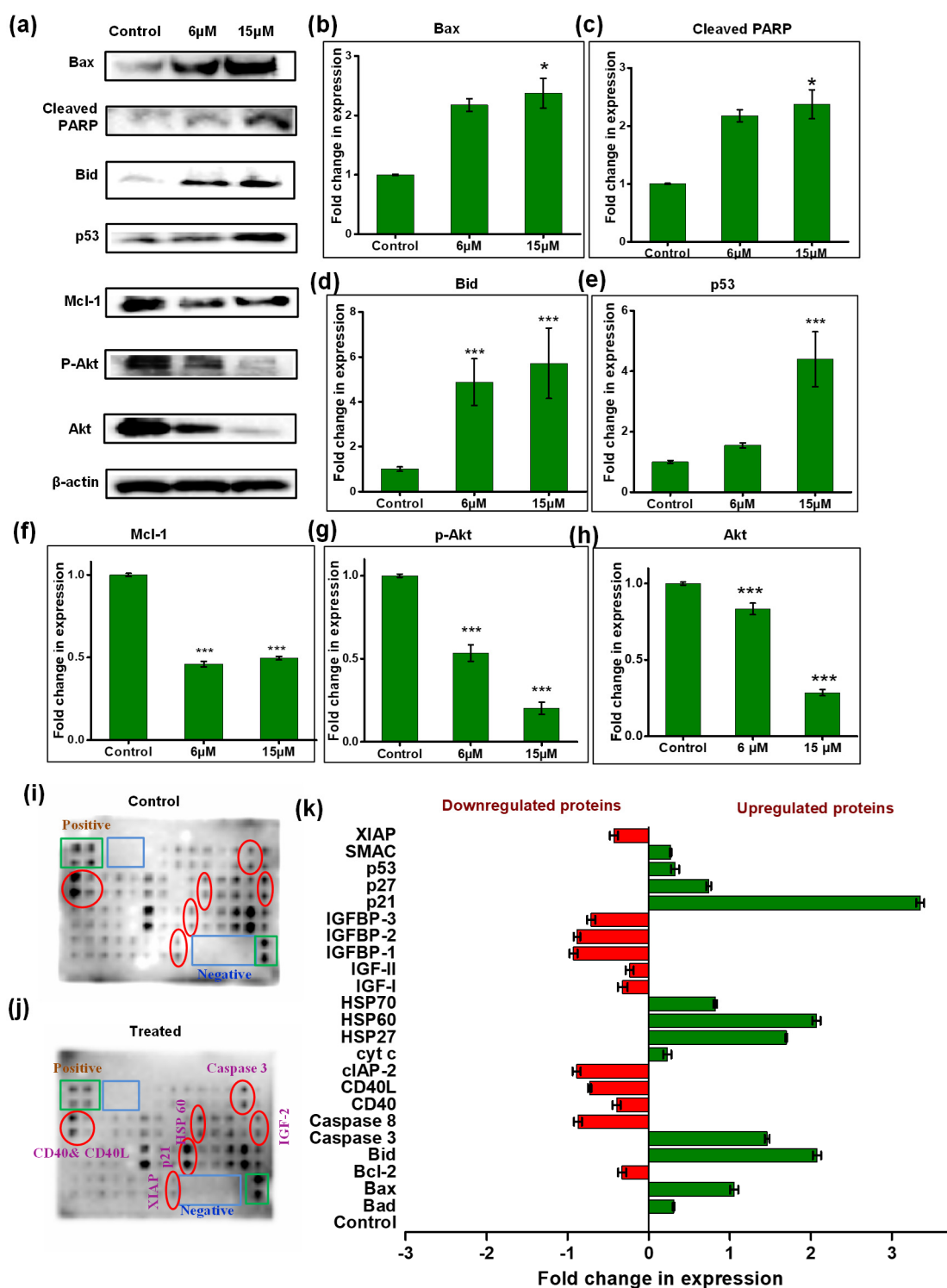


**Figure 7.** (a) Blot of apoptotic proteins. Fold change in expression of (b) Bax, (c) cleaved PARP, (d) Bid, (e) p53, (f) Mcl-1, (g) p-Akt, and (h) Akt. Apoptotic antibody array membrane analysis on HeLa cells: (i) untreated control and (j) treatment with phaeanthine at a concentration of 8  $\mu$ M for 24 h incubation and (k) fold change in expression of proteins in apoptotic array membrane treated by phaeanthine. The red color bars indicate downregulated, and the green represents upregulated proteins; the graph represents values as control intensity (1) subtracted from the normalized value of each protein. The assays were carried out in triplicates and the data are expressed as mean  $\pm$  SD; \*\*\* $p$  < 0.001, \* $p$  < 0.05 were considered significant compared to the control, and no asterisk (\*) represents a nonsignificant  $p$  value.

A significant reduction in the expression of cyclins was observed, indicating the downregulation of cell cycle proteins, thereby arresting the cell cycle to prevent the proliferation of the cancer cells. Cyclin A2 is in a strategic position to control a large part of the cell cycle because of its presence during S, G2, and

early mitosis.<sup>29</sup> Cells with repressed cyclin B1/Cdc2 activity are more likely to remain in the G2 phase, whereas cells with upregulated cyclin B1/Cdc2 activity are more likely to enter and complete mitosis.<sup>30</sup> So, the cyclin B1 downregulation will allow the cancer cells to remain in the G2 phase and arrest its entry to

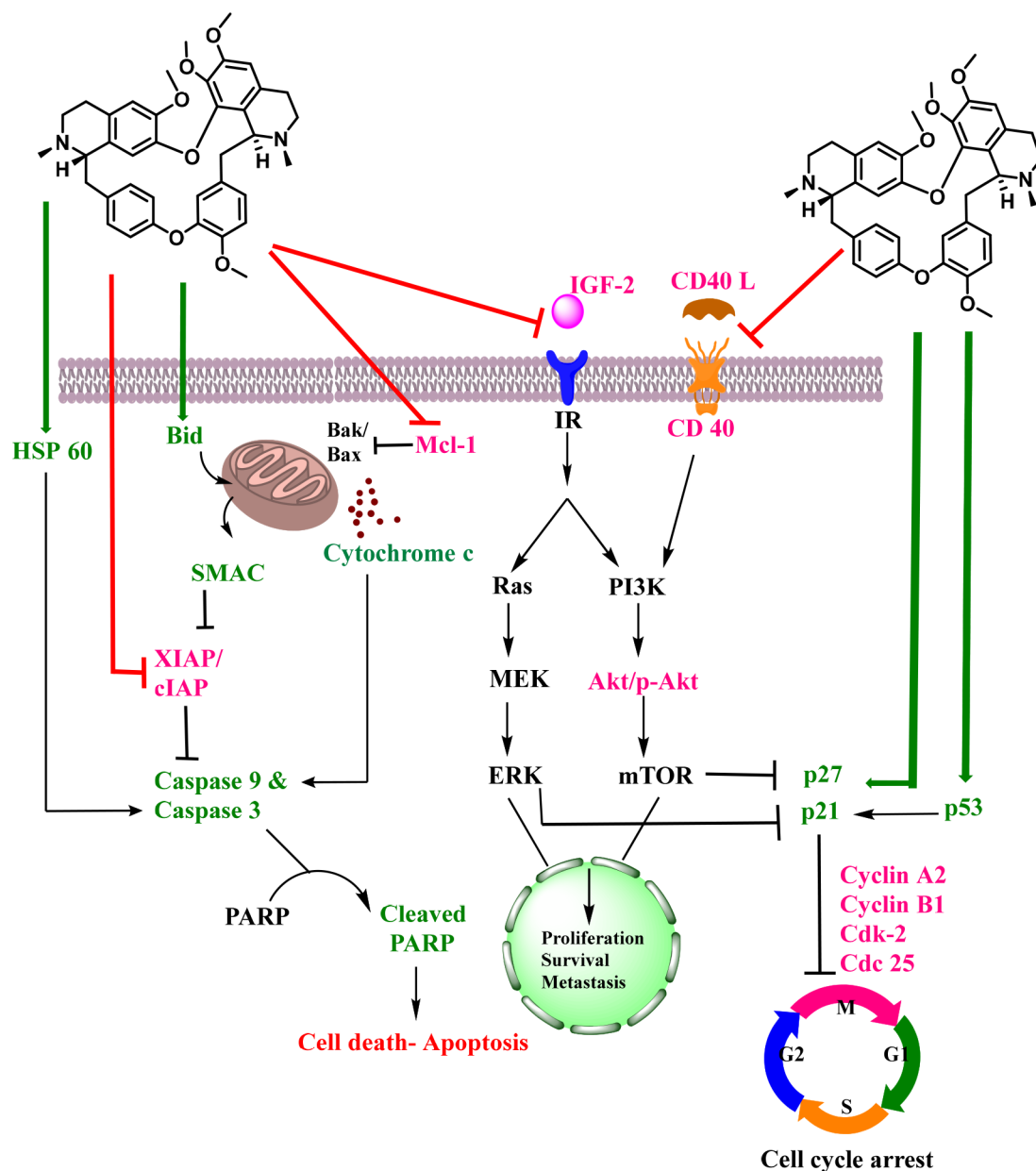


**Figure 8.** Proposed mechanism of action of phaeanthine. Red arrows indicate inhibition, and green arrows represent activation of proteins. Green colored and magenta colored entries represent experimentally validated proteins that are upregulated and downregulated, respectively, while the black colored entries are not currently evaluated.

mitosis for proliferation. CDK2 helps in the S phase to G2 phase transition by binding to cyclin E and cyclin A during the initial and terminating stages of the S phase.<sup>31</sup> Cdc25c is involved in the G2/M transition in cell cycle.<sup>32</sup> From the Western blotting of these proteins, we could observe the downregulation of all four proteins involved in the cell cycle regulation (Figure 6d–g). The results also indicate a possible chance of arrest at the G2 phase of the cell cycle, thereby regulating the proliferation of cells. Phaeanthine can control the cell cycle progression by downregulating the expression of crucial regulators such as cyclins and CDKs. Targeting cell cycle regulators always makes a better therapeutic strategy.<sup>33</sup>

**Phaeanthine-Modulated Expression of Various Proteins Involved in Apoptosis.** The promising apoptosis-inducing potential of phaeanthine encouraged us to investigate the expression of major proteins involved in the apoptotic

pathway. Western blot analysis (Figure 7a) and human apoptosis antibody array membrane assay (Figure 7i,j) were performed to evaluate the expression of key players in the apoptosis pathways. The array membrane comprises antibodies of 43 key proteins involved in the process of cell death via apoptosis. The expression studies finally revealed the alteration of various proteins. The proteins involved in promoting apoptosis, such as Bax, cleaved PARP, Bid, p53, caspase-3, p21, Hsp60, and p27, were upregulated. Treatment with phaeanthine downregulated some of the antiapoptotic proteins such as Akt, p-Akt, Mcl-1, CD40, IGF-2, and XIAP (Figure 7k). Bax and Bid are proapoptotic proteins, and the activation of caspases and p53 promotes the apoptotic pathway. High levels of IGF-2 were found to be associated with an increased risk of developing cancer.<sup>34</sup> By downregulating the expression of IGF-2, phaeanthine inhibits the binding of IGF-2 to the insulin



receptor, thereby downregulating the Ras and Akt pathway, which ultimately inhibits the survival, proliferation, invasion, and angiogenesis of cancer cells.<sup>35</sup> The regulation of Akt signaling is an important phenomenon in cancer control. We observed a downregulation in the expression of total Akt and its phosphorylated form p-Akt, thereby inhibiting PI3K/Akt signaling for survival and proliferation with phaeanthine treatment. CD40 is overexpressed in a wide variety of carcinomas; even a higher level of expression is observed in cervical carcinomas.<sup>36</sup> Activation of CD40 by CD40L results in the proliferation of cancer cells by upregulating MAPK, NF- $\kappa$ B, and JNK pathways.<sup>37</sup> So, phaeanthine-mediated downregulation of CD40 revealed an evident inhibition of the proliferative cells. X-linked inhibitor of apoptosis protein (XIAP) expression is observed to be elevated in cases of malignancies by inhibiting the activation of caspase-3 and -9 and inhibiting apoptosis-mediated cell death.<sup>38</sup> Phaeanthine induced a downregulation of XIAP, which indicates the activation of initiator and executioner caspases, thereby initiating the cellular apoptotic death mechanism. We observed a decrease in the expression of Mcl-1 protein with the treatment; Mcl-1 is usually found to inhibit the oligomerization of Bak and Bax and inhibits the release of cytochrome *c* from the mitochondrial membrane.<sup>39</sup> So, its downregulation will initiate apoptosis. Therefore, targeting Mcl-1 is a new strategy for cancer therapy.<sup>40</sup>

Bid is a proapoptotic protein which cleaves on activation and moves into the mitochondria to induce mitochondrial membrane permeabilization. This process is achieved by the oligomerization of Bax and Bak and, thus, the release of cyt *c* out of mitochondria.<sup>41</sup> Hsp60 plays a role in caspase-3 activation by functioning as a chaperone and promoting the protease-sensitive state of pro-caspase-3.<sup>42</sup> SMAC is another mitochondrial protein along with cyt *c* that gets released into the cytosol upon receiving the death signal. SMAC eradicates the action of IAPs (inhibitor of apoptosis proteins) and activates the caspase activation cascade with the help of cyt *c* and Apaf.<sup>43</sup> So, the upregulation of these proteins, namely, Bid, Hsp60, SMAC, and cyt *c*, specifies the involvement of mitochondria-mediated apoptosis in cancer cell death. Apart from these, the expression of proteins such as p21, p27, and p53 were also elevated. These proteins are involved in cell cycle arrest and regulation,<sup>44</sup> thereby controlling the tumors' further growth. From the above data, a mechanism has been proposed for cell death in HeLa cells by phaeanthine (Figure 8).

## CONCLUSION

In summary, we have successfully isolated three major alkaloids from the rhizome of *Cyclea peltata*, namely, phaeanthine, cycleanine, and *N*-methylcorydaldine. Among the three, phaeanthine showed its highest potency in inhibiting cervical cancer cell proliferation. The selected compound, phaeanthine, was found safer for the nontumorigenic cell line, MCF-10A, especially at a moderate concentration, which was adequate for apoptotic induction in HeLa cells. In silico studies of the phaeanthine revealed its good binding affinity with the antiapoptotic and proliferative protein Akt, reflecting a docking score of  $-5.023$ . The in silico data were well complemented with in vitro assessment which confirmed mitochondria-mediated apoptosis by downregulating the expression of total Akt and its phosphorylated form, p-Akt, including other antiapoptotic proteins such as Mcl-1, IGF-2, and XIAP. Furthermore, mitochondrial depolymerization and the release of cytochrome *c* into the cytosol resembled the mitochondria-mediated cell

death by the treatment of phaeanthine. As a new insight, the SERS fingerprint of phaeanthine was utilized to track cellular internalization and investigated apoptotic events by Raman fingerprint analysis of cellular DNA and other biomolecules. Finally, the phaeanthine triggered cell cycle arrest through downregulation of the expression of major regulatory proteins involved in cell cycle progression was studied, as well. To the best of our knowledge, this is the first report on the detailed in vitro anticancer studies of phaeanthine, and its inhibition on the Akt signaling pathway demonstrated in HeLa cells. These results can help in developing a better treatment strategy for cervical cancer from phaeanthine, a natural pharmacophore.

## EXPERIMENTAL SECTION

**General Experimental Procedures.** All chemicals and solvents were purchased from Sigma-Aldrich, Merck, and Spectrochem and used without further purification. Analytical TLC was performed on a Merck 60 F<sub>254</sub> silica gel plate (0.25 mm thickness), and visualization was done with UV light (254 and 365 nm). Column chromatography was performed on Merck 60 silica gel (60–120 or 100–200 mesh). The 1D and 2D NMR spectra were recorded on a Bruker ADVANCE 500 MHz, using MeOD and CDCl<sub>3</sub> as solvents, and the chemical shifts were expressed in parts per million relative to the TMS peak. The melting point was recorded on a Leica DM 2500 P optical transmission microscope equipped with a wide zoom camera and Mettler Toledo hot stage. The HRESIMS data were recorded at 60,000 resolutions using Thermo Scientific Exactive mass spectrometer. Specific rotation was measured on JASCO P-2000 polarimeter. HPLC of the compound phaeanthine was done on Shimadzu HPLC-LC 20A series (in C18 column, conditions: 0.25% acetic acid in water and methanol in the ratio 1:1, 145 kgf pressure and flow rate: 1.0 mL/min) and showed a purity of >98%.

**Extraction, Isolation, and Characterization of Phyto-molecules.** *Collection of Plant Material.* *Cyclea peltata* rhizomes were collected from Wayanad, Kerala, India. A voucher specimen of the plant was deposited in the herbarium repository of M.S. Swaminathan Research Foundation (MSSRF), Kerala, India, with voucher number M.S.S.H. 2709.

*Extraction and Isolation Procedure of C. peltata.* The rhizomes of *Cyclea peltata* were thoroughly cleaned and dried in a hot air oven maintained at 50 °C for 3 days. Approximately 2 kg of the plant material was coarsely crushed and subjected to repeated extraction using hexane, acetone, ethanol, and water, yielding 5 g of hexane extract, 20 g of acetone extract, 200 g of ethanol extract, and 10 g of water extract. Since the acetone and ethanol extract showed a positive result for Dragendorff's test for alkaloids, we adopted a detailed acid–base extraction procedure<sup>45</sup> to isolate the benzyloquinoline alkaloids from the ethanol extract, and the fractions were subjected to silica column chromatography to isolate the compounds.

**Cell Culture Methods.** The human cervical cancer cell line, HeLa, was obtained from American Type culture collection (ATCC, USA), and the normal breast epithelial cell line MCF-10A from Elabscience, USA. HeLa cells were maintained in Dulbecco's modified eagle medium (DMEM, Sigma), and MCF-10A cells were maintained in MEGM (mammary epithelial cell growth medium kit) Lonza and supplemented with 10% fetal bovine serum (FBS, Himedia) and 1% antibiotic antimycotic solution 100 $\times$  (with 10,000 units penicillin, 10 mg of streptomycin, and 25  $\mu$ g of amphotericin B per mL in 0.9%

normal saline, Himedia) and maintained at 5% CO<sub>2</sub> at 37 °C in the incubator.

**Cell Viability Assay.** Cells were seeded in a 96-well plate at a seeding density of  $8 \times 10^3$  cells/well. After 24 h of incubation, the compounds (phaeanthine, cycleanine, and *N*-methylcorydaldine) were added at different concentrations and incubated for 24 h. After incubation, the compound containing medium was removed and washed with PBS, and MTT (3-[4,5-dimethylthiazol-2-yl]-2,5-diphenyltetrazolium) at a concentration of 0.5 mg/mL was added and kept in the dark for 2–4 h. DMSO was added to dissolve the formazan crystals, and absorbance was measured at 570 nm in a multimode plate reader (Synergy H1, Biotek).

**Molecular Docking.** The X-ray crystal structure of the target proteins Akt/protein kinase B (PDB: 1O6L),<sup>46</sup> MMP-2 (1GEN), mTOR (4JSP), Survivin (1F3H), caspase-9 (2AR9), caspase-8 (4ZBW), p53 (1TUP), PARP (5DSY), and STAT-3 (6NJS) were obtained from the Protein Data Bank. The molecular docking is performed using Maestro to predict the binding modes against the active site pocket of the target protein.<sup>47</sup> Protein Preparation Wizard of the Schrödinger suite of the program is used to prepare the protein for molecular docking. Then Glide's receptor grid generation was used to generate a grid with a maximal size of  $20 \times 20 \times 20$  and 0.5 Å spacing. The molecular docking was performed using glide.<sup>48</sup>

**Molecular Dynamics Simulation.** All simulations were run with the OPLS-AA force field using the academic version of the MD simulation software, Desmond 6.9.<sup>49</sup> Desmond uses a specific neutral territory technique dubbed the midpoint approach to effectively take advantage of a high level of parallelism in the computation. We performed a 50 ns long MD simulation of the system intending to analyze the Akt aberrations in an inhibitor-bound form of phaeanthine. The system was initially set up by the system build panel and solvated in an orthorhombic box filled with water molecules. The system was then neutralized with the appropriate number of counterions and salt concentration of 0.15 M, and a 10 buffer region was allowed between the protein–ligand complex and box sides. The systems were neutralized with Na<sup>+</sup> ions, and the overlapping water molecules were deleted. The system was exposed to local energy minimization utilizing the limited memory Broyden Fletcher Goldfarb Shanno (LBFGS) algorithms and the hybrid steepest descent method. To produce simulation data for the postsimulation analyses, the system was relaxed using the constant *NPT* (number of atoms *N*, pressure *P*, and temperature *T*) ensemble condition. Using Nosé-Hoover thermostats and the Martina-Tobias-Klein barostat method, a constant temperature of 300 K and a stable atmospheric pressure of 1 atm were established for the duration of the simulation procedure. The final production MD was carried out for 50 ns for all systems, and the outcomes were examined using a simulated interaction diagram.

**Apoptotic Assays.** Various assays were used to analyze the mode of cytotoxicity induced by the compound on HeLa cells. Acridine orange–ethidium bromide dual staining and APO percentage were done to assess whether cells undergo apoptosis following the previously reported methods,<sup>50</sup> and the images were taken using a Nikon-TS100 inverted microscope. FITC Annexin V is a sensitive probe for identifying apoptotic cells, binding to the negatively charged phosphatidyl serine. It was performed with a FITC Annexin V apoptosis detection kit (BD Pharmingen, Cat. No. 556547). The kit protocol was strictly followed to conduct the experiment accurately.

**Caspase Fluorometric Assays.** The expression of various caspases upon treatment with phaeanthine was evaluated with caspase fluorometric assay kits (Biovision). The experiment was carried out as per the manufacturer's protocol. HeLa cells were treated with phaeanthine at two different concentrations (6 and 15 μM) for 24 h; after the procedures, the fluorescence intensity was measured (excitation: 400 nm and emission: 505 nm) in a multimode plate reader (Synergy H1, Biotek).

**Mitochondrial Membrane Potential Assay.** Mitochondrial membrane potential was studied using a cationic dye, JC-1 (5,5',6,6'-tetrachloro-1,1',3,3'-tetraethylimidocarbocyanine iodide) (Sigma). The cells were seeded at a density of  $7 \times 10^3$  cells/well. Phaeanthine was added at lower concentrations of 5 and 8 μM. After 24 h of incubation, cells were washed and incubated with JC-1 (5 μM) for 10 min. Cells were then observed under a Nikon-TS100 inverted microscope using red and green channel filters. The JC-1 aggregate/monomer ratio was calculated using ImageJ software.

**Cytochrome *c* Release.** Cytosolic and mitochondrial proteins of the untreated control and treated cells were isolated using a previously reported method.<sup>51</sup> Phaeanthine was added at a concentration of 6 μM and incubated for 12 h. Fractionated proteins were subjected to Western blot analysis, and mitochondrial and cytosolic cytochrome *c* expression in both control and treated sets were studied, keeping GAPDH as the internal control.<sup>52</sup> The density of each protein band was calculated using ImageJ software.

**DNA Condensation and Fragmentation Studies.** The condensation pattern of DNA induced by apoptosis was studied with Hoechst nuclear staining as previously reported.

**DNA Laddering.** HeLa cells were seeded in T75 culture flasks. The treatment was given in two different concentrations of 6 and 15 μM. The DNA was isolated using the Geneaid genomic DNA mini kit (Geneaid, cat. no. GB100), and the procedures were done per the kit protocol. The isolated DNA from treated cells and untreated control was run on 0.8% agarose gel to obtain the laddering pattern as previously reported. The image was captured with a ChemiDoc instrument (Biorad).

**Internalization and Fragmentation by SERS.** SERS fingerprinting of the isolated DNA from phaeanthine treated and untreated cells were performed by mixing the DNA with gold nanoparticles at 1:9 ratio, and a SERS spectrum was collected using a Raman spectroscope (Witek, Germany). For this, 40 nm sized gold nanoparticles were used as the SERS substrates. SERS signals were accrued using a 633 nm laser with 5 mW power and 5 s integration time. The same substrate and instrumental parameters were also employed for the phaeanthine internalization studies where the 1 mM phaeanthine in methanol was mixed with gold nanoparticles (1:9 ratio) and the SERS spectrum was collected. Further, phaeanthine-treated (6 μM) and untreated HeLa cells seeded on a chamber slide were incubated with gold nanoparticles for 10 min, and SERS analysis was performed at different time points.

**Colony Formation Assay.** First,  $1 \times 10^3$  cells/well were seeded in a 6-well plate. Compounds at two different concentrations (0.5 and 1 μM) were added after 24 h of incubation, and the cells were allowed to form colonies for the next 9 days. After that, the colonies were visualized by staining with 0.3% crystal violet for 10 min and washing with PBS.<sup>53</sup> Images were captured using a Nikon-TS100 inverted microscope and processed, and colonies were counted using ImageJ software. Survival fraction was calculated with the following formula:<sup>54</sup>

$$\text{plating efficiency (PE)} = \frac{\text{no. of colonies counted}}{\text{no. of cells seeded}} \times 100$$

$$\text{surviving fraction (SF)} = \frac{\text{PE of treated sample}}{\text{PE of control}} \times 100$$

**Cell Cycle Assay.** Cell cycle arrest induced by phaeanthine was studied using BD cycletest plus DNA kit (BD Pharmingen, cat. no. 340242). All procedures were conducted based on the kit protocol. The method involves dissolving the cell membrane lipids with a nonionic detergent, digesting cellular RNA with enzyme, and stabilizing the nuclear chromatin. PI will bind to the isolated nuclei, and the flow cytometer analyzes the light emitted by stained cells.

The expression of some of the proteins involved in the cell cycle regulation was also evaluated by Western blot. PAGE was carried out based on the standard protocol. The isolated cell lysates from phaeanthine-treated and untreated control cells were subjected to PAGE to study the expression of cyclin A2, cyclin B1, CDK-2, and Cdc 25 with their corresponding antibodies (cell signaling technology).

**Protein Expression Studies.** Cells were seeded in T75 flasks and the compound at two concentrations (6 and 15  $\mu\text{M}$ ) was added. After 24 h of incubation, cell lysate was taken according to standard procedure using RIPA buffer and protease inhibitor cocktail. BCA protein assay kit (Thermo Scientific) was used to estimate the concentration of isolated protein, and Western blotting was carried out to study the expression of various proteins. ImageJ software was used to get the band intensity of proteins. The expression of each protein was normalized with respect to the control and then with that of internal control  $\beta$ -actin.

**Apoptotic Antibody Array.** The treated and untreated cell lysate were loaded on the apoptosis antibody array membrane (Abcam, cat. no. ab134001) at equal concentrations, and all procedures were conducted based on kit protocol. The signals were detected using a chemiluminescence imaging system (BIORAD ChemiDoc). The signal intensity for each antigen-specific antibody spot is proportional to the relative concentration of the antigen (protein) in the sample. Spot signal intensities were obtained with the help of ImageJ densitometry software. The densitometric data were normalized with respect to the positive control of each membrane, and the normalization of the signals of the phaeanthine-treated lysate was done with respect to the spot on the membrane treated with lysate of untreated control cells. The relative differences in the protein expression of the treatment and control groups are obtained by comparing these signal intensities.

## ■ ASSOCIATED CONTENT

### SI Supporting Information

The Supporting Information is available free of charge at <https://pubs.acs.org/doi/10.1021/acsomega.3c01023>.

Isolation scheme, characterization of the isolated phytomolecules by NMR spectroscopic data, results of preliminary screening of the isolated compounds by MTT assay in HeLa, HPLC chromatogram of phaeanthine showing 98% purity, molecular docking data of the compound phaeanthine with various proteins and their interaction and the image of JC-1 mitochondrial membrane potential assay (PDF)

## ■ AUTHOR INFORMATION

### Corresponding Authors

**Kaustabh Kumar Maiti** – Chemical Sciences and Technology Division, CSIR-National Institute for Interdisciplinary Science and Technology (CSIR-NIIST), Thiruvananthapuram 695019, India; Academy of Scientific and Innovative Research (AcSIR), Ghaziabad 201002, India; [orcid.org/0000-0003-3368-6929](https://orcid.org/0000-0003-3368-6929); Email: [kkmaiti@niist.res.in](mailto:kkmaiti@niist.res.in)

**Kokkuvayil Vasu Radhakrishnan** – Chemical Sciences and Technology Division, CSIR-National Institute for Interdisciplinary Science and Technology (CSIR-NIIST), Thiruvananthapuram 695019, India; Academy of Scientific and Innovative Research (AcSIR), Ghaziabad 201002, India; [orcid.org/0000-0001-8909-3175](https://orcid.org/0000-0001-8909-3175); Email: [radhu2005@gmail.com](mailto:radhu2005@gmail.com)

### Authors

**Alisha Valsan** – Chemical Sciences and Technology Division, CSIR-National Institute for Interdisciplinary Science and Technology (CSIR-NIIST), Thiruvananthapuram 695019, India; Academy of Scientific and Innovative Research (AcSIR), Ghaziabad 201002, India; [orcid.org/0000-0002-8719-7138](https://orcid.org/0000-0002-8719-7138)

**Murugan Thulasi Meenu** – Chemical Sciences and Technology Division, CSIR-National Institute for Interdisciplinary Science and Technology (CSIR-NIIST), Thiruvananthapuram 695019, India; Academy of Scientific and Innovative Research (AcSIR), Ghaziabad 201002, India; [orcid.org/0000-0002-1532-496X](https://orcid.org/0000-0002-1532-496X)

**Vishnu Priya Murali** – Chemical Sciences and Technology Division, CSIR-National Institute for Interdisciplinary Science and Technology (CSIR-NIIST), Thiruvananthapuram 695019, India; [orcid.org/0000-0003-0759-991X](https://orcid.org/0000-0003-0759-991X)

**Beutline Malgija** – MCC-MRF Innovation Park, Madras Christain College, Chennai 600059, India

**Anuja Gracy Joseph** – Chemical Sciences and Technology Division, CSIR-National Institute for Interdisciplinary Science and Technology (CSIR-NIIST), Thiruvananthapuram 695019, India; Academy of Scientific and Innovative Research (AcSIR), Ghaziabad 201002, India; [orcid.org/0000-0002-7115-4889](https://orcid.org/0000-0002-7115-4889)

**Prakasan Nisha** – Academy of Scientific and Innovative Research (AcSIR), Ghaziabad 201002, India; Agroprocessing and Technology Division, CSIR-National Institute for Interdisciplinary Science and Technology (CSIR-NIIST), Thiruvananthapuram 695019, India

Complete contact information is available at:

<https://pubs.acs.org/10.1021/acsomega.3c01023>

### Author Contributions

The manuscript was written through the contributions of all authors.

### Notes

The authors declare no competing financial interest.

## ■ ACKNOWLEDGMENTS

K.K.M. thanks the Council of Scientific and Industrial Research (CSIR), Govt. of India, and Indian Council of Medical Research (ICMR), Govt. of India (No. 5/4-5/3/01/DHR/NEURO/2020-NCD-I and Accounting Code: RFC NO(P-67) NCD/Ad-hoc/220/2021-22), for research funding. AcSIR Ph.D. student A.V. (31/038(0580)/2019-EMR-I) acknowledges CSIR, New

Delhi, for financial assistance in the form of a fellowship, and M.M.T. thanks UGC for the research fellowship. V.P.M. acknowledges DHR young scientist program (R.12014/22/2021) for the funding provided. The help rendered by Mr. Vimalkumar PS for HPLC quantification is also acknowledged.

## ABBREVIATIONS

AGE, agarose gel electrophoresis; Apaf, apoptotic protease activating factor-1; Bax, BCL-2 associated X protein; Bid, BH3 interacting domain death agonist; CD40, cluster of differentiation 40; Cdc25c, cell division cycle 25c; CDK, cyclin-dependent kinases; cyt *c*, cytochrome *c*; DBBI, dibenzyl isouquinoline; DMEM, Dulbecco's modified Eagle's medium; DMSO, dimethyl sulfoxide; FBS, fetal bovine serum; FITC, fluorescein isothiocyanate; HSP60, heat shock protein 60; IC<sub>50</sub>, half-maximal inhibitory concentration; IGF-2, insulin-like growth factor-2; JNK, c-Jun N-terminal kinase; MAPK, mitogen-activated protein kinase; Mcl-1, myeloid cell leukemia-1; MEGM, mammary epithelial cell growth medium; MMP, mitochondrial membrane potential; MTT, 3-[4,5-dimethylthiazol-2-yl]-2,5-diphenyltetrazolium; NF- $\kappa$ B, nuclear factor kappa B; PAGE, polyacrylamide gel electrophoresis; PARP, poly-ADP ribose polymerase; PBS, phosphate-buffered saline; PI, propidium iodide; SERS, surface-enhanced Raman spectroscopy; SMAC, second mitochondria-derived activator of caspase; XIAP, X-linked inhibitor of apoptosis protein

## REFERENCES

- (1) UICC.org. *Cervical cancer elimination*; [https://www.uicc.org/what-we-do/thematic-areas-work/cervical-cancer-elimination#\\_ftn2](https://www.uicc.org/what-we-do/thematic-areas-work/cervical-cancer-elimination#_ftn2) (accessed 2022-08-03).
- (2) Prabha, Mukta; Akanksha Soni, K. P. A Review Article on Pushyanuga Churna in Stri Roga. *Univ. Res. Resour. J. Jayoti Vidyapeeth Women's Univ. Jaipur* **2018**, *1* (2), 71–75.
- (3) Suman Singh, K.; Nishteswar, B. R. P. A Comprehensive Review on Therapeutic Potentials of Patha (Cissampelos Pareira Linn.) from Classical Texts of Ayurveda. *Res. Rev. A J. Pharmacogn.* **2017**, 17–35.
- (4) Rajith, N. P.; Ramachandran, V. S. Ethnomedicines of Kurichyas, Kannur District, Western Ghats, Kerala. *Indian J. Nat. Prod. Resour.* **2010**, *1* (2), 249–253.
- (5) Yamuna, C. V.; Arthi, I.; Rajagopal, P. L.; Sajith Kumar, P. N.; Lithashabin, P. K.; Cyclea Peltata, A. A. K. A Pharmacological Review. *World J. Pharm. Res.* **2020**, *9* (4), 265–273.
- (6) Udhayavani, C.; Ramachandran, V. S. Knowledge and Uses of Wild Edible Plants by Paniyas and Kurumbas of Western Nilgiris, Tamil Nadu. *Indian J. Nat. Prod. Resour.* **2013**, *4* (4), 412–418.
- (7) Sangeetha, M. S.; Priyanga, S.; Hemalakshmi, S.; D, K. In Vivo Antidiabetic Potential of Cyclea Peltata in Streptozotocin Induced Diabetic Rats. *Asian J. Pharm. Clin. Res.* **2015**, *8* (1), 103108
- (8) Meena J, S. S. K. Efficacy of Methanolic Extract of Cyclea Peltata as a Potent Anticancer Equivalent. *Eur. J. Environ. Ecol.* **2015**, *2* (2), 65–71.
- (9) Vijayan, F. P.; Rani, V. K. J.; Vineesh, V. R.; Sudha, K. S.; Michael, M. M.; Padikkala, J. Protective Effect of Cyclea Peltata Lam on Cisplatin-Induced Nephrotoxicity and Oxidative Damage. *J. Basic Clin. Physiol. Pharmacol.* **2007**, *18* (2), 101–114.
- (10) Shine, V. J.; Latha, P. G.; Somasekharan Nair Rajam Suja, G. I.; Anuja, Raj, G.; Rajasekharan, S. N. Ameliorative Effect of Alkaloid Extract of Cyclea Peltata (P. Oir.) Hook. f. & Thoms. Roots on APAP/CCl4 Induced Liver Toxicity in Wistar Rats and in Vitro Free Radical Scavenging Property. *Asian Pac. J. Trop. Biomed.* **2014**, *4* (2), 143–151.
- (11) Abraham, J.; Thomas, T. D. Antibacterial Activity of Medicinal Plant Cyclea Peltata (Lam) Hooks & Thoms. *Asian Pacific J. Trop. Dis.* **2012**, *2*, S280–S284.
- (12) Darling, R.; Raja, A.; Jeeva, S.; Prakash, J. W.; Marimuthu, J. Antibacterial Activity of Selected Ethnomedicinal Plants from South India. *Asian Pac. J. Trop. Med.* **2011**, *4* (5), 375–378.
- (13) Shine, V. J.; Latha, P. G.; Shyamal, S.; Suja, S. R.; Anuja, G. I.; Sini, S.; Pradeep, S.; Rajasekharan, S. Gastric Antisecretory and Antiulcer Activities of Cyclea Peltata (Lam.) Hook. f. & Thoms. in Rats. *J. Ethnopharmacol.* **2009**, *125*, 350–355.
- (14) Sivaraman, T.; Sreedevi, N. S.; Meenatchisundaram, S.; Vadivelan, R. Antitoxin Activity of Aqueous Extract of Cyclea Peltata Root against Naja Naja Venom. *Indian J. Pharmacol.* **2017**, *49* (4), 275–281.
- (15) Singh, S.; Nishteswar, K.; Patel, B.; Nariya, M. Comparative Antipyretic and Analgesic Activities Of Cissampelos pareira Linn. and Cyclea peltata (Lam.) Hook. F. & Thomas. *AYU (An Int. Q. J. Res. Ayurveda)* **2016**, *37* (1), 62–66.
- (16) Marshall, S. J.; Russell, P. F.; Wright, C. W.; Anderson, M. M.; Phillipson, J. D.; Kirby, G. C.; Warhurst, D. C.; Schiff, P. L. In Vitro Antiplasmodial, Antiamoebic, and Cytotoxic Activities of a Series of Bisbenzylisoquinoline Alkaloids. *Antimicrob. Agents Chemother.* **1994**, *38* (1), 96–103.
- (17) Cimanga Kanyanga, R.; Kikweta Munduku, C.; Nsaka Lumpu, S.; Tshodi Ehata, M.; Makila Bool-Miting, F.; Kambu Kabangu, O.; Mbamu Maya, B.; Cos, P.; Maes, L.; Vlietinck, A. J.; Tuentler, E.; Foubert, K.; Pieters, L. Isolation and Structure Elucidation of Two Antiprotozoal Bisbenzylisoquinoline Alkaloids from Trichlisia Gillettii Stem Bark. *Phytochem. Lett.* **2018**, *28*, 19–23.
- (18) Murebwayire, S.; Ingkaninan, K.; Changwijit, K.; Frederich, M.; Duez, P. Triclisia Sacleuxii (Pierre) Diels (Menispermaceae), a Potential Source of Acetylcholinesterase Inhibitors. *J. Pharm. Pharmacol.* **2009**, *61*, 103–107.
- (19) Scheinmann, F.; Scriven, E. F. V.; Ogbeide, O. N. Cyclicanin from Synclisia Scabrida: Conformational Information from the 1H NMR Spectrum at 300 MHz. *Phytochemistry* **1980**, *19* (8), 1837–1840.
- (20) Said, I. M.; Hamid, N. A. A.; Latif, J.; Din, L. B.; Yamin, B. M. 6,7-Dimethoxy-2-Methyl-3,4-Dihydro- Isoquinolin-1 (2H)-One. *Acta Crystallogr. Sect. E Struct. Reports* **2005**, *61*, o797–o798.
- (21) Ortega-Forte, E.; Rovira, A.; Gandioso, A.; Bonelli, J.; Bosch, M.; Ruiz, J.; Marchan, V. COUPY Coumarins as Novel Mitochondria-Targeted Photodynamic Therapy Anticancer Agents. *J. Med. Chem.* **2021**, *64*, 17209–17220.
- (22) Garrido, C.; Galluzzi, L.; Brunet, M.; Puig, P E; Didelot, C.; Kroemer, G Mechanisms of Cytochrome c Release from Mitochondria. *Cell Death Differ.* **2006**, *13*, 1423–1433.
- (23) Baranska, M.; Roman, M.; Cz. Dobrowolski, J.; Schulz, H.; Baranski, R. Recent Advances in Raman Analysis of Plants: Alkaloids, Carotenoids, and Polyacetylenes. *Curr. Anal. Chem.* **2013**, *9* (1), 108–127.
- (24) Cañamares, M. V.; Pozzi, F.; Lombardi, J. R. Raman, SERS, and DFT Analysis of the Main Alkaloids Contained in Syrian Rue. *J. Phys. Chem. C* **2019**, *123*, 9262–9271.
- (25) Zhang, W.; Zhao, Y.; Bai, X.; Wang, Y.; Zhao, D. The Orientation of Protoberberine Alkaloids and Their Binding Activities to Human Serum Albumin by Surface-Enhanced Raman Scattering. *Spectrochim. Acta - Part A Mol. Biomol. Spectrosc.* **2011**, *78* (3), 1105–1109.
- (26) Movasaghi, Z.; Rehman, S.; Rehman, I. U. Raman Spectroscopy of Biological Tissues. *Appl. Spectrosc. Rev.* **2007**, *42*, 493–541.
- (27) Arya, J. S.; Joseph, M. M.; Sherin, D. R.; Nair, J. B.; Manojkumar, T. K.; Maiti, K. K. Exploring Mitochondria-Mediated Intrinsic Apoptosis by New Phytochemical Entities: An Explicit Observation of Cytochrome c Dynamics on Lung and Melanoma Cancer Cells. *J. Med. Chem.* **2019**, *62*, 8311–8329.
- (28) Diaz-moralli, S.; Tarrado-castellarnau, M.; Miranda, A.; Cascante, M. Targeting Cell Cycle Regulation in Cancer Therapy. *Pharmacol. Ther.* **2013**, *138*, 255–271.
- (29) Silva Cascales, H.; Burdova, K.; Middleton, A.; Kuzin, V.; Mullers, E.; Stoy, H.; Baranello, L.; Macurek, L.; Lindqvist, A. Cyclin A2 Localises in the Cytoplasm at the S/G2 Transition to Activate PLK1. *Life Sci. Alliances* **2021**, *4* (3), e202000980.

- (30) Choi, H. J.; Zhu, B. T. Critical Role of Cyclin B1/Cdc2 up-Regulation in the Induction of Mitotic Prometaphase Arrest in Human Breast Cancer Cells Treated with 2-Methoxyestradiol. *BBA - Mol. Cell Res.* **2012**, *1823* (8), 1306–1315.
- (31) Ding, L.; Cao, J.; Lin, W.; Chen, H.; Xiong, X.; Ao, H.; Yu, M.; Lin, J.; Cui, Q. The Roles of Cyclin-Dependent Kinases in Cell-Cycle Progression and Therapeutic Strategies in Human Breast Cancer. *Int. J. Mol. Sci.* **2020**, *21* (6), 1960.
- (32) Cho, Y.; Park, J. E.; Park, B. C.; Kim, J.; Jeong, D. G.; Park, S. G.; Cho, S. Cell Cycle-Dependent Cdc25C Phosphatase Determines Cell Survival by Regulating Apoptosis Signal-Regulating Kinase 1. *Cell Death Differ.* **2015**, *22*, 1605–1617.
- (33) Johansson, M.; Persson, J. L. Cancer Therapy: Targeting Cell Cycle Regulators. *Anticancer. Agents Med. Chem.* **2008**, *8*, 723–731.
- (34) Livingstone, C. IGF2 and Cancer. *Endocr. Relat. Cancer* **2013**, *20* (6), R321–R339.
- (35) Weroha, S. J.; Haluska, P. IGF System in Cancer. *Endocrinol. Metab. Clin. North Am.* **2012**, *41* (2), 335–350.
- (36) Eliopoulos, A. G.; Young, L. S. The Role of the CD40 Pathway in the Pathogenesis and Treatment of Cancer. *Curr. Opin. Pharmacol.* **2004**, *4* (4), 360–367.
- (37) Vonderheide, R. H. Prospect of Targeting the CD40 Pathway for Cancer Therapy. *Clin. Cancer Res.* **2007**, *13* (4), 1083–1088.
- (38) Huang, X.; Wang, X.-n.; Yuan, X.-d.; Wu, W.-y.; Lobie, P. E.; Wu, Z. XIAP Facilitates Breast and Colon Carcinoma Growth via Promotion of P62 Depletion through Ubiquitination-Dependent Proteasomal Degradation. *Oncogene* **2019**, *38* (9), 1448–1460.
- (39) Bolomsky, A.; Vogler, M.; Köse, M. C.; Heckman, C. A.; Ehx, G.; Ludwig, H.; Caers, J. MCL-1 Inhibitors, Fast-Lane Development of a New Class of Anti-Cancer Agents. *J. Hematol. Oncol.* **2020**, *13* (1), 1–19.
- (40) Wang, H.; Guo, M.; Wei, H.; Chen, Y. Targeting MCL-1 in Cancer: Current Status and Perspectives. *J. Hematol. Oncol.* **2021**, *14* (1), 1–18.
- (41) Billen, L. P.; Shamas-Din, A.; Andrews, D. W. Bid: A Bax-like BH3 Protein. *Oncogene* **2008**, *27*, S93–S104.
- (42) Xanthoudakis, S.; Sophie, R.; Rasper, D.; Hennessey, T.; Aubin, Y.; Cassidy, R.; Tawa, P.; Ruel, R.; Rosen, A.; Nicholson, D. W. Hsp60 Accelerates the Maturation of Pro-Caspase-3 by Upstream Activator Proteases during Apoptosis. *EMBO J.* **1999**, *18* (8), 2049–2056.
- (43) Du, C.; Fang, M.; Li, Y.; Li, L.; Wang, X. Smac, a Mitochondrial Protein That Promotes Cytochrome c - Dependent Caspase Activation by Eliminating IAP Inhibition. *Cell* **2000**, *102*, 33–42.
- (44) Yadav, V.; Sultana, S.; Yadav, J.; Saini, N. Gatifloxacin Induces S and G 2 -Phase Cell Cycle Arrest in Pancreatic Cancer Cells via P21/P27/P53. *PLoS One* **2012**, *7* (10), e47796.
- (45) Patel, M. B.; Mishra, S. Isoquinoline Alkaloids from *Tinospora Cordifolia* Inhibit Rat Lens Aldose Reductase. *Phyther. Res.* **2012**, *26* (9), 1342.
- (46) Yang, J.; Cron, P.; Good, V. M.; Thompson, V.; Hemmings, B. A.; Barford, D. Crystal Structure of an Activated Akt/Protein Kinase B Ternary Complex with GSK3-Peptide and AMP-PNP. *Nat. Struct. Biol.* **2002**, *9* (12), 940–944.
- (47) *Schrödinger Release 2022-2*; Maestro, Schrödinger, LLC: New York, 2022.
- (48) Friesner, R. A.; Murphy, R. B.; Repasky, M. P.; Frye, L. L.; Greenwood, J. R.; Halgren, T. A.; Sanschagrin, P. C.; Mainz, D. T. Extra Precision Glide: Docking and Scoring Incorporating a Model of Hydrophobic Enclosure for Protein-Ligand Complexes. *J. Med. Chem.* **2006**, *49* (21), 6177–6196.
- (49) *Maestro-Desmond Interoperability Tools*, Schrödinger; D. E. Shaw Research: New York, 2021.
- (50) Joseph, M. M.; Aravind, S. R.; George, S. K.; Pillai, K. R.; Mini, S.; Sreelekha, T. T. Galactoxyloglucan-Modified Nanocarriers of Doxorubicin for Improved Tumor-Targeted Drug Delivery with Minimal Toxicity. *J. Biomed. Nanotechnol.* **2014**, *10* (11), 3253–3268.
- (51) Dimauro, I.; Pearson, T.; Caporossi, D.; Jackson, M. J. A Simple Protocol for the Subcellular Fractionation of Skeletal Muscle Cells and Tissue. *BMC Res. Notes* **2012**, *5* (1), 513.
- (52) Lu, X.; Costantini, T.; Lopez, N. E.; Wolf, P. L.; Hageny, A. M.; Putnam, J.; Eliceiri, B.; Coimbra, R. Vagal Nerve Stimulation Protects Cardiac Injury by Attenuating Mitochondrial Dysfunction in a Murine Burn Injury Model. *J. Cell. Mol. Med.* **2013**, *17* (5), 664–671.
- (53) Aswathy, M.; Banik, K.; Parama, D.; Sasikumar, P.; Harsha, C.; Joseph, A. G.; Sherin, D. R.; Thanathu, M. K.; Kunnumakkara, A. B.; Vasu, R. K. Exploring the Cytotoxic Effects of the Extracts and Bioactive Triterpenoids from *Dillenia Indica* against Oral Squamous Cell Carcinoma: A Scientific Interpretation and Validation of Indigenous Knowledge. *ACS Pharmacol. Transl. Sci.* **2021**, *4* (2), 834–847.
- (54) Franken, N. A. P.; Rodermond, H. M.; Stap, J.; Haveman, J.; van Bree, C. Clonogenic Assay of Cells in Vitro. *Nat. Protoc.* **2006**, *1* (5), 2315–2319.

## Recommended by ACS

### Isolation, Structural Elucidation of a New Triterpenoid from the Roots of *Jasminum sambac* (L.) Ait. with Potent Cytotoxicity against MCF-7 Cell Lines

Olagoke Zacchaeus Olatunde, Canzhong Lu, *et al.*

APRIL 12, 2023  
ACS OMEGA

READ 

### Characterization of Cooked Nonglutinous Rice Cultivars Based on Flavor Volatiles and Their Change during Storage

Keishi Yamashita, Tomohiro Uchimura, *et al.*

APRIL 12, 2023  
ACS OMEGA

READ 

### Synthesis of Carlactone Derivatives to Develop a Novel Inhibitor of Strigolactone Biosynthesis

Kojiro Kawada, Shinsaku Ito, *et al.*

APRIL 05, 2023  
ACS OMEGA

READ 

### Formation of L1<sub>0</sub> Ordering in FeNi by Mechanical Alloying and Field-Assisted Heat Treatment: Synchrotron XRD Studies

Shuvam Mandal, Suddhasatwa Basu, *et al.*

APRIL 10, 2023  
ACS OMEGA

READ 

Get More Suggestions >